

**Development of novel image analysis
approaches for seaweed discrimination –
Species level study using field
spectroscopy and UAV multispectral
remote sensing**

Sadhvi Selvaraj

A thesis submitted to Auckland University of
Technology in fulfilment of the requirements for the
degree of Doctor of Philosophy (PhD)

2021

School of Science

Faculty of Health and Environmental Sciences

Abstract

Seaweeds play important roles in coastal ecosystems such as providing habitat, feeding grounds and improving water quality. It is crucial to map their distribution to quantify biodiversity and assess changes over time especially due to invasive species. The seaweed *Undaria pinnatifida* (Harvey) Suringar, native to north-western Asia, is one of the top 100 invasive species in the world and has become established across much of New Zealand (NZ), competing and co-existing with native seaweed species. Remote sensing is an efficient tool for mapping since current seaweed mapping practices in NZ such as snorkelling and SCUBA surveys can be time-consuming and do not cover large extents. Despite the invasive nature of *U. pinnatifida*, there was no spectral information available that would assist in remote sensing surveys in NZ.

A hyperspectral library of common NZ native and invasive seaweed species was created to identify the key wavelengths that discriminated NZ seaweed species at both inter- and intra- taxonomic levels. The hyperspectral data of the native and invasive seaweed species collected from field survey were subjected to two supervised classification methods - Partial Least Square Discriminant Analysis (PLS-DA) for wavelength selection/classification and random forest for validating the wavelengths from PLS-DA. The seaweeds were separable at broad taxonomic level (red, green and brown seaweeds) with accuracies > 85% using PLS-DA. Some of the influential wavelengths identified were consistent with pigment absorption peaks unique to red and brown seaweeds. *U. pinnatifida* differed from native browns in the visible (574 nm) and near-infrared (716 – 721, 750 nm) region of the electromagnetic spectrum and the classification accuracies were 97.7% and 90.7% using random forest and PLS-DA, respectively.

Variations in season or location may affect the spectral reflectance which in turn would affect the accuracy of mapping aquatic and terrestrial vegetation from remote sensing surveys. Such variations are widely studied in terrestrial plants compared to seaweeds. The hyperspectral data of the two commonly found New Zealand native seaweed species, *Ecklonia radiata* (C. Agardh) J. Agardh. and *Carpophyllum maschalocarpum* (Turner) Grev from four locations across four seasons were used to analyse spatial and seasonal effects on their spectral reflectance values using mixed-effects modelling. The modelling showed that season affects spectral reflectance of the seaweed species across the four locations, specifically in summer, which is likely due to the higher rates of photosynthesis.

There are many studies on the effect of depth and turbidity on seaweeds at broad taxonomic level globally. However, a detailed study on the depth and turbidity effects on seaweeds in New Zealand at broad taxonomic and species level is lacking. The hyperspectral data of the two seaweed species, *U. pinnatifida* and *E. radiata*, at five depths and two turbidity levels were used in two different models for different purposes. Mixed-effects modelling that was used to understand the effect of depth and turbidity on the spectral reflectance values of the seaweed species showed depth significantly affected the spectral reflectance of the seaweed species compared to turbidity. Random forest model was used to assess the feasibility to discriminate the two seaweed species from each other across different depths within a turbidity level. Two sets of wavelengths were used as explanatory variables to assess the suitability of bands for discrimination – wavelengths that discriminated *U. pinnatifida* from rest of the brown seaweed species and wavelengths that matched the Micasense RedEdge-m sensor. This comparison would help understand if existing multispectral sensors would suffice or if it would be better to customise the sensor for the application. The former set of wavelengths (574, 716-718, 720-721, 750 nm) discriminated the two seaweed species

from each other better with accuracy in the range of 57 – 87% and the accuracy increased with the depth. The overall accuracy of the discrimination of the two seaweed species from multispectral data was better at flight height of 30m (63%, kappa = 0.45) compared to that at flight height of 10m (60%, kappa = 0.38).

This is the first study on the spectral variability of seaweeds due to season and location, globally. This research is a significant step towards mapping common habitat forming NZ native and invasive seaweed species using remote sensing. This study identified key wavelengths for discriminating emerged seaweeds (out of water) at species level using robust discriminatory models developed. A novel image pre-processing technique that reduced noise was implemented before image classification. The study is also the first to use 5-band multispectral UAV data to classify two submerged spectrally similar invasive and native brown seaweed species of New Zealand.

Table of Contents

| | |
|--|-----|
| Abstract..... | i |
| Table of Contents | iv |
| List of Figures..... | vii |
| List of Tables..... | xi |
| Attestation of authorship | xiv |
| Co-Authored Works | xv |
| Acknowledgements | xvi |
| Chapter 1. Introduction | 1 |
| 1.1 Introduction to <i>Undaria pinnatifida</i> | 2 |
| 1.1.1 Distribution of <i>U. pinnatifida</i> in New Zealand | 2 |
| 1.1.2 Biology of <i>U. pinnatifida</i> | 3 |
| 1.1.2.1 Morphology and growth..... | 3 |
| 1.1.2.2 Reproduction by dispersal mechanism..... | 4 |
| 1.1.2.3 Mortality..... | 5 |
| 1.1.3 Ecology of <i>U. pinnatifida</i> in New Zealand | 5 |
| 1.1.3.1 Interaction with conspecifics and other species | 5 |
| 1.1.3.2 <i>U. pinnatifida</i> - environment relationship | 6 |
| 1.1.4 Economic importance of <i>U. pinnatifida</i> | 7 |
| 1.2 Concepts of Remote Sensing | 7 |
| 1.2.1 Electromagnetic Spectrum | 7 |
| 1.2.2 Types of resolution in remote sensing..... | 9 |
| 1.2.3 Image classification techniques..... | 12 |
| 1.3 Remote sensing for seaweed mapping..... | 13 |
| 1.3.1 Spectral signature of plants | 13 |
| 1.3.2 Spectral signature of seaweed | 14 |
| 1.3.3 Challenges of mapping submerged/emerged seaweeds from remote sensing data..... | 16 |
| 1.4 Discrimination of seaweeds | 18 |
| 1.4.1 Spectral data analysis techniques | 19 |
| 1.4.2 Image classification approach for seaweed mapping..... | 21 |
| 1.5 Remote Sensing scale of mapping emerged/submerged seaweed | 24 |
| 1.5.1 UAV seaweed mapping..... | 26 |
| 1.5.2 Challenges of processing UAV borne multispectral images..... | 26 |
| 1.6 Rationale and significance of the study | 28 |

| | | |
|--|---|----|
| 1.7 | Research questions..... | 29 |
| 1.8 | Thesis structure | 29 |
| Chapter 2. Discrimination of common New Zealand native seaweeds from the invasive <i>Undaria pinnatifida</i> using hyperspectral data | | 31 |
| 2.1 | Introduction..... | 32 |
| 2.2 | Materials and Methods..... | 35 |
| 2.2.1 | Seaweed collection and spectral measurements..... | 35 |
| 2.2.2 | Data analysis | 38 |
| 2.2.2.1 | Pre-processing..... | 40 |
| 2.2.2.2 | Discrimination of common seaweeds at a broad taxonomic level | 40 |
| 2.2.2.3 | Discrimination of <i>Undaria pinnatifida</i> from native seaweed species.... | 41 |
| 2.3 | Results..... | 42 |
| 2.3.1 | Discrimination between seaweed taxa (brown, green and red) and influential wavelengths..... | 43 |
| 2.3.2 | Classification of <i>Undaria pinnatifida</i> relative to New Zealand native seaweed species..... | 46 |
| 2.4 | Discussion..... | 49 |
| 2.5 | Conclusions..... | 53 |
| Chapter 3. Effects of location and season on seaweed spectral signatures..... | | 54 |
| 3.1 | Introduction..... | 55 |
| 3.2 | Materials and Methods..... | 56 |
| 3.2.1 | Seaweed collection and spectral measurements..... | 56 |
| 3.2.2 | Data analysis | 57 |
| 3.2.2.1 | Data pre-processing..... | 57 |
| 3.2.2.2 | Qualitative separation of seaweed species | 58 |
| 3.2.2.3 | Spatial and seasonal variability in spectral reflectance..... | 58 |
| 3.3 | Results..... | 59 |
| 3.3.1 | Data pre-processing and PCA | 59 |
| 3.3.2 | Spatial and seasonal variation on the spectral reflectance of <i>Carpophyllum maschalocarpum</i> using linear mixed modelling | 60 |
| 3.3.2.1 | Variables contributing to PC1 | 60 |
| 3.3.2.2 | Effect of season and location on PC1 | 60 |
| 3.3.3 | Spatial and seasonal variation on the spectral reflectance of <i>Ecklonia radiata</i> using linear mixed modelling..... | 62 |
| 3.3.3.1 | Important variables contributing to components PC1 and PC2 | 63 |
| 3.3.3.2 | Effect of season and location on PC1 | 63 |
| 3.4 | Discussion..... | 64 |

| | |
|--|-----|
| Chapter 4. Discrimination of <i>Undaria pinnatifida</i> from <i>Ecklonia radiata</i> using multispectral unmanned aerial vehicle (UAV) image and hyperspectral data: Role of depth and turbidity | 67 |
| 4.1 Introduction..... | 67 |
| 4.2 Materials and Methods..... | 71 |
| 4.2.1 Spectral data collection and processing | 71 |
| 4.2.2 UAV data collection and image processing | 78 |
| 4.2.3 Data analysis | 86 |
| 4.2.3.1 Field spectroscopy - sun glint removal and data pre-processing | 86 |
| 4.2.3.2 Effect of depth and turbidity on the spectral reflectance of <i>Undaria pinnatifida</i> and <i>Ecklonia radiata</i> | 86 |
| 4.2.3.3 Discrimination of <i>Undaria pinnatifida</i> from <i>Ecklonia radiata</i> at various depth and turbidity levels using field spectroscopy data | 87 |
| 4.2.3.4 Discrimination of <i>Undaria pinnatifida</i> from <i>Ecklonia radiata</i> at various depth levels within a turbidity level using UAV-collected multispectral data ... | 89 |
| 4.2.3.5 Application: Classifying <i>U. pinnatifida</i> and <i>E. radiata</i> along rocky reef using high spatial resolution RedEdge multispectral data | 95 |
| 4.3 Results..... | 96 |
| 4.3.1 Glint removal and data pre-processing..... | 96 |
| 4.3.2 UAV data collection and image processing | 98 |
| 4.3.3 Effect of depth and turbidity on the spectral reflectance of <i>Undaria pinnatifida</i> | 103 |
| 4.3.4 Effect of depth and turbidity on the spectral reflectance of <i>Ecklonia radiata</i> | 105 |
| 4.3.5 Discrimination of <i>Undaria pinnatifida</i> from <i>Ecklonia radiata</i> at various depth and turbidity levels using field spectroscopy data | 106 |
| 4.3.6 Discrimination of <i>Undaria pinnatifida</i> from <i>Ecklonia radiata</i> at various depth and turbidity levels using UAV-collected multispectral data | 109 |
| 4.3.7 Application: Classifying <i>Undaria pinnatifida</i> and <i>Ecklonia radiata</i> along rocky reef using high spatial resolution Rededge-m multispectral UAV data | 116 |
| 4.4 Discussion..... | 122 |
| Chapter 5. Conclusion..... | 126 |
| 5.1 Insights from the study..... | 126 |
| 5.2 Future research..... | 129 |
| 5.3 Summary | 132 |
| References..... | 133 |
| Appendix A. Chapter 2 Appendices..... | 147 |
| Appendix B. Chapter 3 Appendices..... | 148 |
| Appendix C. Chapter 4 Appendices..... | 151 |

List of Figures

| | |
|--|----|
| Figure 1: Location of <i>U. pinnatifida</i> and the year it was first observed in brackets. Adapted from Russell et al., (2007). | 3 |
| Figure 2: The life cycle of <i>U. pinnatifida</i> . Adapted from (White et al., 2014). | 5 |
| Figure 3: Electromagnetic Spectrum..... | 8 |
| Figure 4: Interaction between the electromagnetic spectrum and aquatic environment...9 | |
| Figure 5: Typical spectral reflectance curve of a green leaf..... | 14 |
| Figure 6: The North Island sites were mainly located near Auckland, in the Hauraki Gulf in the east and one off the western coast. The South Island sites were in Pelorus sound in Marlborough Sounds. | 36 |
| Figure 7: Seaweed species, <i>Xiphophora chondrophylla</i> , <i>Carpophyllum maschalocarpum</i> and <i>Pterocladia lucida</i> (left to right), placed against a black mat for measurement of spectral reflectance to minimise any background noise | 37 |
| Figure 8: Reflectance spectra of all the common New Zealand seaweed species used in this study grouped at a broad taxa level - brown, red and green..... | 43 |
| Figure 9: The graph shows the influential wavelengths that discriminate each seaweed taxon (brown seaweed taxa represented in black, green seaweed taxa represented by white and red seaweed taxa represented by grey) from the other two taxa.. | 44 |
| Figure 10: Performace statistics of external validation of models built using PLS-DA and random forest techniques..... | 44 |
| Figure 11: Multidimensional Scaling (MDS) plot using a proximity matrix of n=110 individuals from the between-taxa random forest classification model for brown, green and red seaweeds. X- and Y- axes are first and second dimension, respectively, in 109 (n-1) dimensional cartesian space..... | 45 |
| Figure 12: Influential wavelengths discriminating <i>Undaria pinnatifida</i> from other seaweed species in each of the four PLS-DA models..... | 47 |
| Figure 13: Multidimensional Scaling plots of two class random forest models. | 48 |
| Figure 14: Principal component analysis of <i>Ecklonia radiata</i> and <i>Carpophyllum</i> <i>maschalocarpum</i> showing the separation of the two seaweed species | 60 |
| Figure 15: (A) Model predictions plot with two standard deviations (and 95% confidence interval) of PC1 for <i>Carpophyllum maschalocarpum</i> in different locations within each season | 62 |
| Figure 16: Panoramic shot of depth experiment setup..... | 73 |
| Figure 17: STS-VIS spectroradiometer used for collecting hyperspectral data over the depth experiment. | 73 |
| Figure 18: Seaweed sample collection, UAV data collection and experiment location. 77 | |
| Figure 19: UAV setup including Micasense RedEdge-m sensor on the base, DLS sensor with GPS unit on top of Phantom 4 Pro. Known reflectance panel (bottom right). Photo credit: Graham Hinchliffe. | 81 |
| Figure 20: Step 1 in seaweed classification from UAV multispectral data | 94 |
| Figure 21: Step 2 in seaweed classification of UAV multispectral data..... | 94 |

| | |
|--|-----|
| Figure 22: Raw (blue) and glint corrected (orange) spectral reflectance values of <i>U. pinnatifida</i> at five depth and two turbidity levels. SD – Secchi depth..... | 97 |
| Figure 23: Standardised spectral reflectance values of <i>U. pinnatifida</i> at five depth and two turbidity levels. SD – Secchi depth. | 98 |
| Figure 24: In the depth experiment, <i>E. radiata</i> on the base plate immersed in water at <10cm depth was captured in five spectral bands by Rededge-m sensor on Phantom 4 Pro at FH of 10m. | 100 |
| Figure 25: Individual spectral bands of <i>E. radiata</i> at <10cm water depth captured on Phantom 4 Pro at FH of 10m. | 100 |
| Figure 26: (A) Direct geo-referenced images of the rocky reef at FH of 30m showing glint in the top half of the images, (B) direct georeferenced images with additional tie points to match the locations, reordered to remove glint and mosaicked as a single image | 101 |
| Figure 27: Photo centres automatically plotted from image metadata (represented in yellow), plotted photo centre manually adjusted to represent true <i>U. pinnatifida</i> locations by comparing with UAV's RGB photos (represented in red). | 102 |
| Figure 28: Adjusted <i>U. pinnatifida</i> locations 6 and 7 on the multispectral mosaic (left) compared to RGB photos (right) with snorkeller in the centre of each photo. . | 103 |
| Figure 29: Variables contributing to PC1 for <i>Undaria pinnatifida</i> | 103 |
| Figure 30: Model predictions plot with two standard deviations (and 95% confidence interval) of PC1 for <i>Undaria pinnatifida</i> at different Secchi depth levels (m) within each water depth level (m)..... | 105 |
| Figure 31: Raw hyperspectral reflectance values (top) and Rededge-m resampled spectral reflectance values (bottom) of <i>E. radiata</i> and <i>U. pinnatifida</i> . Index numbers 1, 2, 3, 4 and 5 on the x-axis refer to blue, green, red, NIR and rededge, respectively (bottom). | 107 |
| Figure 32: Comparison of the overall accuracy of random forest model classification using two types of datasets for two turbidity levels across all depths.. | 108 |
| Figure 33: Screenshot of classified images of three different <i>E. radiata</i> individuals at 10cm below water surface..... | 110 |
| Figure 34: Screenshot of classified images of three different <i>U. pinnatifida</i> individuals at 1m below water surface..... | 111 |
| Figure 35: Classification accuracy assessment of <i>U. pinnatifida</i> at five depth levels and two spatial scales..... | 113 |
| Figure 36: Classification accuracy assessment of <i>Ecklonia radiata</i> and <i>Undaria pinnatifida</i> collated across depth levels at two spatial scales.. | 115 |
| Figure 37: Collated classification accuracy assessment of both seaweed species at all depth levels combined at two spatial scales. | 115 |
| Figure 38: (A) True colour RGB image of a section of the AOI, (B) False colour composite enhancing vegetation of the same area. | 118 |
| Figure 39: (A) True colour RGB image of a section of the AOI with the land area masked (in black), (B) standardised RGB image of the same area with the land masked (in red)..... | 119 |

| | |
|---|-----|
| Figure 40: Rocky reef classification. Classification of <i>U. pinnatifida</i> is in red and that of <i>E. radiata</i> is in green..... | 120 |
| Figure 41: Screenshot of classification of <i>U. pinnatifida</i> (red) and <i>E. radiata</i> (green) within a buffer of 20cm radius (black circle) at 20 validation locations in the rocky reef | 121 |
| Figure A-1: PCA plots of seaweed grouping at (A) taxa level, (B) grouping of seaweed species within brown, (C) within green and (D) within red using standardised data | 147 |
| Figure B-1: Seaweed sample locations in Hauraki Gulf, North Island, NZ | 148 |
| Figure B-2: Variables contributing to variance in PC1 for <i>Carpophyllum maschalocarpum</i> in percentage..... | 149 |
| Figure B-3: Variables contributing to variance in PC1 for <i>Ecklonia radiata</i> in percentage | 149 |
| Figure B-4: (A) Model predictions plot with two standard deviations (and 95% confidence interval) of PC1 for <i>Ecklonia radiata</i> in different locations within each season..... | 150 |
| Figure C-1: Adjusted <i>U. pinnatifida</i> locations 1 and 2 on the multispectral mosaic (left) compared to RGB photos (right) with snorkeller in the centre of each photo. . | 151 |
| Figure C-2: Adjusted <i>U. pinnatifida</i> locations 3, 4 and 5 on the multispectral mosaic (left) compared to RGB photos (right) with snorkeller in the centre of each photo..... | 152 |
| Figure C-3: Adjusted <i>U. pinnatifida</i> locations 8 and 9 on the multispectral mosaic (left) compared to RGB photos (right) with snorkeller in the centre of each photo. . | 152 |
| Figure C-4: Adjusted <i>U. pinnatifida</i> locations 10 and 11 on the multispectral mosaic (left) compared to RGB photos (right) with snorkeller in the centre of each photo..... | 152 |
| Figure C-5: Adjusted <i>U. pinnatifida</i> locations 12 to 16 on the multispectral mosaic (top left) compared to RGB photos (bottom and right) with snorkeller in the centre of each photo. | 153 |
| Figure C-6: Adjusted <i>U. pinnatifida</i> locations 17 to 20 on the multispectral mosaic (top left) compared to RGB photos (bottom and right) with snorkeller in the centre of each photo. | 154 |
| Figure C-7: Variables contributing to PC1 of <i>Ecklonia radiata</i> | 154 |
| Figure C-8: Model predictions plot with two standard deviations (and 95% confidence interval) of PC1 for <i>Ecklonia radiata</i> at different Secchi depth levels (m) within each water depth level (m) | 155 |
| Figure C-9: Comparison of the overall accuracy of random forest model classification using two types of datasets for two turbidity and five depth levels..... | 159 |
| Figure C-10: Screenshot of classified images of three different <i>E. radiata</i> individuals at 10cm below water surface..... | 170 |
| Figure C-11: Classification of <i>E. radiata</i> at 10cm water depth from images captured at FH of 10m (top) and FH of 30m (bottom)..... | 184 |

| | |
|---|-----|
| Figure C-12: Classification of <i>E. radiata</i> at 50cm water depth from images captured at FH of 10m (top) and FH of 30m (bottom).. | 185 |
| Figure C-13: Classification of <i>E. radiata</i> at 1m water depth from images captured at FH of 10m (top) and FH of 30m (bottom).. | 186 |
| Figure C-14: Classification of <i>E. radiata</i> at 1.5m water depth from images captured at FH of 10m (top) and FH of 30m (bottom).. | 187 |
| Figure C-15: Classification of <i>E. radiata</i> at 2m water depth from images captured at FH of 10m (top) and FH of 30m (bottom).. | 188 |
| Figure C-16: Classification of <i>U. pinnatifida</i> at 10cm water depth from images captured at FH of 10m (top) and FH of 30m (bottom).. | 189 |
| Figure C-17: Classification of <i>U. pinnatifida</i> at 50cm water depth from images captured at FH of 10m (top) and FH of 30m (bottom).. | 190 |
| Figure C-18: Classification of <i>U. pinnatifida</i> at 1m water depth from images captured at FH of 10m (top) and FH of 30m (bottom).. | 191 |
| Figure C-19: Classification of <i>U. pinnatifida</i> at 1.5m water depth from images captured at FH of 10m (top) and FH of 30m (bottom).. | 192 |
| Figure C-20: Classification of <i>U. pinnatifida</i> at 2m water depth from images captured at FH of 10m (top) and FH of 30m (bottom).. | 193 |

List of Tables

| | |
|---|-----|
| Table 1: Summary of sensor characteristics (Corporation; Ünsalan & Boyer, 2011) | 12 |
| Table 2: Causes for variability in spectral reflectance at leaf scale and canopy scale (Blackburn, 2007; Mulla, 2013)..... | 13 |
| Table 3: Spectral characteristics of pigments present in seaweed groups (Casal et al., 2012) | 15 |
| Table 4: Spectral data analysis techniques..... | 20 |
| Table 5: A literature review of some of the image classification approaches relevant to the study.. | 22 |
| Table 6: Model performance statistics from external validation using both random forest and PLS-DA techniques. Acc is accuracy, Sens is sensitivity, Spec is specificity, K is kappa, ncomp is the number of components selected for PLS-DA models and UP is <i>U. pinnatifida</i> | 49 |
| Table 7: Random forest model calibration parameter settings and performance statistics. | 49 |
| Table 8: Information on sample, sea state and sky condition | 75 |
| Table 9: Rededge-m specifications (Micasense, 2020)..... | 79 |
| Table 10: UAV data collection identifiers | 81 |
| Table 11: Various models used in mixed-effects modelling to test the significance of each term | 87 |
| Table 12: Spectral data description | 89 |
| Table 13: Likelihood ratio test of models explaining difference in spectral signatures of <i>U. pinnatifida</i> across four locations and four seasons..... | 104 |
| Table 14: Parameter settings for each of the random forest models across all depths within a turbidity level.. | 108 |
| | |
| Table B-1: Description of locations where the seaweed individuals were collected... | 148 |
| Table B-2: Various models used in mixed-effects modelling to test the significance of each term | 149 |
| Table C-1: Likelihood ratio test of models explaining difference in spectral signatures of <i>E. radiata</i> across four locations and four seasons | 155 |
| Table C-2: Parameter settings for each of the random forest models at each depth within a turbidity level.. | 156 |
| Table C-3: Random forest model classification statistics for discriminating two seaweed species at each depth with two turbidity levels utilising dataset A. ... | 157 |
| Table C-4: Random forest model classification statistics for discriminating two seaweed species at each depth with two turbidity levels utilising dataset B. ... | 158 |
| Table C-5: Collated accuracy assessment of <i>E. radiata</i> at a depth of 10 cm from the water surface.. | 160 |

| | |
|---|-----|
| Table C-6: Collated accuracy assessment of <i>E. radiata</i> at a depth of 50 cm from the water surface.. | 161 |
| Table C-7: Collated accuracy assessment of <i>E. radiata</i> at a depth of 100 cm from the water surface.. | 162 |
| Table C-8: Collated accuracy assessment of <i>E. radiata</i> at a depth of 150 cm from the water surface.. | 163 |
| Table C-9: Collated accuracy assessment of <i>E. radiata</i> at a depth of 200 cm from the water surface.. | 164 |
| Table C-10: Collated accuracy assessment of <i>U. pinnatifida</i> at a depth of 10 cm from the water surface.. | 165 |
| Table C-11: Collated accuracy assessment of <i>U. pinnatifida</i> at a depth of 50 cm from the water surface.. | 166 |
| Table C-12: Collated accuracy assessment of <i>U. pinnatifida</i> at a depth of 100 cm from the water surface.. | 167 |
| Table C-13: Collated accuracy assessment of <i>U. pinnatifida</i> at a depth of 150 cm from the water surface.. | 168 |
| Table C-14: Collated accuracy assessment of <i>U. pinnatifida</i> at a depth of 200 cm from the water surface.. | 169 |
| Table C-15: Collated accuracy assessment of <i>E. radiata</i> at a depth of 10cm from the water surface.. | 171 |
| Table C-16: Collated accuracy assessment of <i>E. radiata</i> at a depth of 50cm from the water surface.. | 172 |
| Table C-17: Collated accuracy assessment of <i>E. radiata</i> at a depth of 100cm from the water surface.. | 173 |
| Table C-18: Collated accuracy assessment of <i>E. radiata</i> at a depth of 150cm from the water surface.. | 174 |
| Table C-19: Collated accuracy assessment of <i>E. radiata</i> at a depth of 200cm from the water surface.. | 175 |
| Table C-20: Collated accuracy assessment of <i>U. pinnatifida</i> at a depth of 10cm from the water surface.. | 176 |
| Table C-21: Collated accuracy assessment of <i>U. pinnatifida</i> at a depth of 50cm from the water surface.. | 177 |
| Table C-22: Collated accuracy assessment of <i>U. pinnatifida</i> at a depth of 100cm from the water surface.. | 178 |
| Table C-23: Collated accuracy assessment of <i>U. pinnatifida</i> at a depth of 150cm from the water surface.. | 179 |
| Table C-24: Collated accuracy assessment of <i>U. pinnatifida</i> at a depth of 200cm from the water surface.. | 180 |
| Table C-25: Collated classification accuracy assessment of <i>E. radiata</i> at all depths.. | 181 |
| Table C-26: Collated classification accuracy assessment of <i>E. radiata</i> at all depths excluding 1.5 and 2m.. | 181 |
| Table C-27: Collated classification accuracy assessment of <i>U. pinnatifida</i> at all depths.. | 182 |

| | |
|--|-----|
| Table C-28: Collated classification accuracy assessment of <i>U. pinnatifida</i> at all depths excluding 1.5m and 2m..... | 182 |
| Table C-29: Collated accuracy assessment of classification of both seaweed species at depths 10cm, 50cm and 1m from images collected at a flight height of 10m.. | 183 |
| Table C-30: Collated accuracy assessment of classification of both seaweed species at depths 10cm, 50cm and 1m from images collected at a flight height of 30m.. | 183 |

Attestation of authorship

I hereby declare that this submission is my work and that, to the best of my knowledge and belief, it contains no material previously written or published by another person, nor material that to a substantial extent has been submitted for the award of any other degree or diploma of a university or other institute of higher learning.

Sadhvi Selvaraj

29th May 2021

Co-Authored Works

| | |
|---|---|
| Chapter 2 Selvaraj, S., Case, B.S., and White, W. L. (2021) "Discrimination of common New Zealand native seaweeds from the invasive <i>Undaria pinnatifida</i> using hyperspectral data," <i>Journal of Applied Remote Sensing</i> 15(2), 024501. https://doi.org/10.1117/1.JRS.15.024501 | Selvaraj 80%, Case 10%, White 10% |
| Chapter 3 Selvaraj S, Case BS and White WL (2021) Effects of Location and Season on Seaweed Spectral Signatures. <i>Front. Ecol. Evol.</i> 9:581852. doi: 10.3389/fevo.2021.581852 | Selvaraj 80%, Case 10%, White 10% |

Sadhvi Selvaraj

Dr Bradley Case

Professor Lindsey White

Acknowledgements

I would like to thank and extend my sincere gratitude to the following people who have been part of my PhD journey one way or the other:

Professor Lindsey White and Associate Professor Barbara Bollard for encouraging me to pursue this research into UAV remote sensing after carefully considering my skills.

Professor Lindsey White and Dr. Brad Case, my amazing supervisory team, for constant support throughout the journey. Together they brought different perspectives, expertise and aspects into this research that helped with experiment design, data analysis, crafting good manuscripts and eventually shape up the thesis. I hope I have done justice to the time and effort they invested in me!

Dr. Andrew Fletcher who was part of the initial supervisory team for his support and input into some of the experimental designs.

Glen Farrington from Sanford for organising field visit to collect UAV data of their mussel farms.

Dr. Jenny Pannell for being the extra pair of eyes on my first manuscript and providing detailed comments.

Dr. Martin Bader for pointing me in the right direction for some of the data analysis in Chapter 2.

Kim Ollivier from Ollivier & Co for pointing me in the right direction for direct georeferencing of UAV images.

Evan Brown for all his help in the field keeping us safe, well-informed of the weather forecast for data collection and Adam Slater for his help in the field with seaweed collection along with Evan.

My parents, Komathi and Selvaraj, for supporting me immensely both in Auckland and India when I needed it.

Graham Hinchliffe, my partner-in-crime, for his support both in the field in UAV operations and at home. I have had valuable research discussions with him over the PhD years and we reaped mutual benefit from both our research.

Reeva, my little munchkin, for being a much needed welcome distraction.

My friends, Shona and Dila for their love and support and especially taking Reeva off my hands when I needed more time on my research. My friends from AUT, Shweta, Loretta and Mansi for being my emotional support and laugh medicine for all things PhD and otherwise!

Chapter 1. Introduction

Aquatic ecosystems are home to diverse flora and fauna that depend on each other to ensure the stability and biodiversity of the system (Krecker, 1939). Submerged aquatic vegetation, which includes both vascular plants and seaweeds, is an ecologically and economically significant part of aquatic ecosystems due to their multifaceted role in both freshwater and coastal ecosystems. This vegetation provides habitat (Cacabelos et al., 2010; Pallas et al., 2006), feeding grounds for various organisms (Lorentsen et al., 2004; Persson et al., 2012), improves water clarity, filters nutrients and runoff, helps settle sediment in water (Cho et al., 2012), is a source of raw materials for alginate extraction and provides kelp fishery (Vásquez et al., 2014) and prevents coastal erosion (Hu et al., 2015).

Imbalances in ecosystems affect the effective functioning of the ecosystem. For example, invasive species may affect the local biodiversity (Aneece & Epstein, 2016), growth of undesirable seaweeds like filamentous *Cladophora* in dense mats due to eutrophication disrupts the benthic flora/fauna by reducing dissolved oxygen and pH levels in lakes/rivers and the recreational value of the nearshore plummets (Flynn & Chapra, 2014; Wezernak & Lyzenga, 1975). Other effects of imbalanced ecosystem also include the disappearance of kelp forests possibly due to invasive non-native species like *U. pinnatifida* (Russell et al., 2007), large grazers like sea urchin (Perreault et al., 2014), mesograzers (Davenport & Anderson, 2007), pollution (Smith, 2000), increase in seawater temperature associated with El Nino events (Deysher, 1993) and harmful fishing practices (Christie et al., 1998). Therefore, increasing knowledge on the distribution and composition of New Zealand seaweed communities offers several benefits including biosecurity, ecological and commercial considerations.

The kelp species, *U. pinnatifida*, is a seaweed native to Japan that has invaded and established in numerous temperate coastal habitats around the globe (Morelissen et al., 2016). It is one of only two seaweeds listed in the top 100 most invasive species of the world (Lowe et al., 2000). It spreads mainly by fouling on boat hulls (MPI, 2016). It can form dense stands underwater, potentially competing for light and space and leading to the exclusion or displacement of native plant and animal species (MPI, 2016). However, since 2010 the New Zealand Ministry for Primary Industries Biosecurity unit has allowed harvesting of *U. pinnatifida* from artificial structures (such as mussel farms) as well as farming in already heavily infested areas. Although conventional surveying methods employing SCUBA diving can provide high accuracy and resolution, it is very expensive, time-consuming, inaccessible in certain parts of the ocean and requires extensive human power to cover long stretches of coastline (Flynn & Chapra, 2014; Vahtmäe et al., 2006). Remote sensing (RS) has the potential to be a valuable, efficient and low-cost tool to monitor seaweed communities and provide detailed information from surrounding areas over time (Dehouck et al., 2012). Therefore, a remote sensing approach for *U. pinnatifida* detection could have management and commercial opportunities. Remote sensing is the measurement of specific parts of the electromagnetic energy absorbed, transmitted, reflected or scattered by the various features on the earth surface. A detailed explanation of remote sensing related to vegetation both terrestrial and aquatic are in section 1.3.

1.1 Introduction to *Undaria pinnatifida*

1.1.1 Distribution of *U. pinnatifida* in New Zealand

U. pinnatifida is an invasive species of kelp that has established in temperate coastal habitats around the world (Morelissen et al., 2016) and is one of the least studied invasive seaweed species (Jiménez et al., 2015). It was first recorded in Wellington

Harbour in New Zealand in 1987 (Hay, 1990) and has since been found in various ports along the east coast of North and South Island (Figure 1).

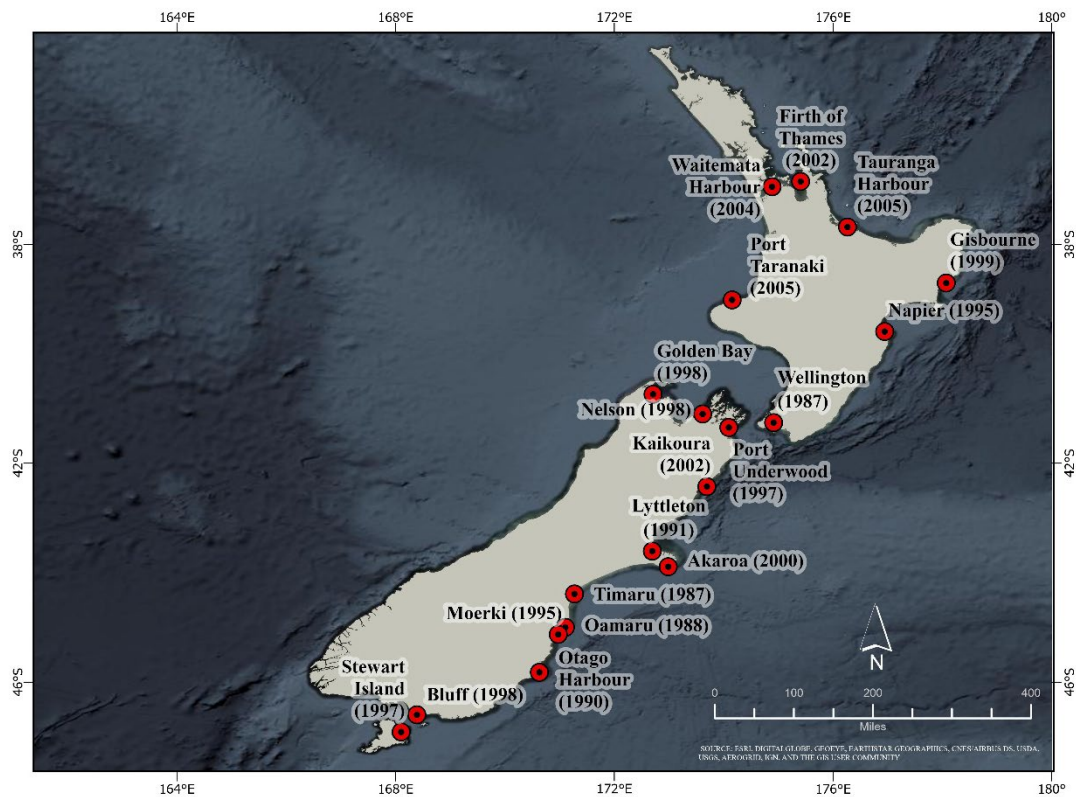


Figure 1: Location of *U. pinnatifida* and the year it was first observed in brackets. Adapted from Russell et al., (2007).

1.1.2 Biology of *U. pinnatifida*

1.1.2.1 Morphology and growth

U. pinnatifida has a holdfast, stipe, blade, midrib and sporophyll on the mature plant (Figure 2). In New Zealand, it reaches lengths of 1-2m, midrib width of 1-3cm and blades about 50-80 cm (Hay, 1990). Dean and Hurd (2007) investigated *U. pinnatifida* in Otago Harbour, New Zealand and inferred average sporophyte lengths increased from around 30 cm in May to roughly 2.5 times that length from July to September and then started decreasing in October and November. The stipe was on average 15 cm long. Chen (2012) inferred that the maximum growth of *U. pinnatifida* in Marlborough Sounds, New Zealand was in November.

1.1.2.2 Reproduction by dispersal mechanism

U. pinnatifida is an annual seaweed and has two life stages; sporophyte stage (macroscopic) and gametophyte stage (microscopic) (Thompson & Schiel, 2012). The spores of *U. pinnatifida* remain viable for many days and are usually dispersed short distances in the order of 100m (Forrest et al., 2000). Reproduction (spore release) of *U. pinnatifida* takes place in autumn and a large number of juvenile sporophytes were found in winter and spring. When the day length increased, sporophyll started forming in *U. pinnatifida* in spring (Chen, 2012). However, they spread further as spores in ballast water in recreational and commercial vessels (MPI, 2016); fragments or whole plants can drift up to 10km (Sanderson, 1997). Sometimes, they also spread from mussel farms to the nearby shores if the receiving coastal site is appropriate (James & Shears, 2016a).

Asexual zoospores (Figure 2) are released by the mature sporophyll of *U. pinnatifida* in millions, these drift until they find a suitable substrate to attach to (Hay & Gibbs, 1996). Once settled these zoospores germinate into female and male gametophytes (Parsons, 1995). While the egg produced by female gametophyte remains in place, the sperm produced by male gametophyte is mobile and fertilizes the egg which later develops into sporophytes (Parsons, 1995).

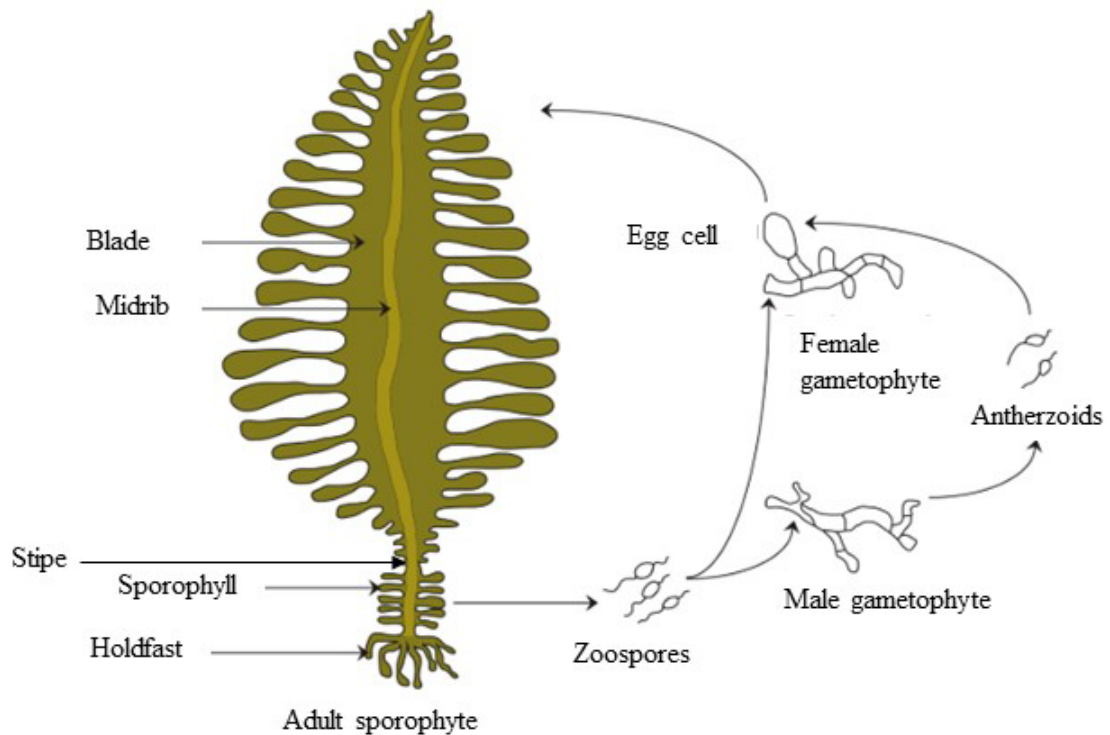


Figure 2: The life cycle of *U. pinnatifida*. Adapted from (White et al., 2014).

1.1.2.3 Mortality

In Japan, mature *U. pinnatifida* degenerate and new sporophytes establish themselves in late summer/early autumn. However, in New Zealand sporophytes are present throughout the year presumably due to the narrow range of annual sea temperature compared to Japanese and Korean coastal waters (Hay & Villouta, 1993). Various stages of the life cycle of *U. pinnatifida* depends on sea surface temperature (Saito, 1975).

1.1.3 Ecology of *U. pinnatifida* in New Zealand

1.1.3.1 Interaction with conspecifics and other species

Along the Otago coastline, Russell et al (2007) found that in wave-dominated shores *U. pinnatifida* extends into *Lessonia variegata* and *Marginariella boryana* zones; in deeper sheltered subtidal areas they invaded *Macrocystis pyrifera* forests and competed with *Ecklonia radiata* and *Landsburgia quercifolia*. A detailed account of seaweed growing and competing with *U. pinnatifida* is given in Parsons (1995). If the coast is

teeming with native algal species, recruitment of *U. pinnatifida* is unlikely unless there is a disturbance to the native population (Morelissen et al., 2016) due to their low competitive ability (Thompson and Schiel, 2012).

Thompson and Schiel (2012) found the following from their study: maximum recruitment of *U. pinnatifida* occurred where there was no mature *U. pinnatifida* canopy and where the substratum was dominated by coralline turf (*Corallina officinalis*); *U. pinnatifida* recruitment occurred during spring; when *U. pinnatifida* die off in summer other native alga like *Carpophyllum maschalocarpum* occupy the space and recruitment of *U. pinnatifida* in these areas again is less likely; no recruitment of *U. pinnatifida* on a thin encrusting form of coralline algae and recruitment is less likely on brown alga *Halopteris congesta*.

1.1.3.2 *U. pinnatifida* - environment relationship

U. pinnatifida occurs throughout temperate regions where the maximum temperatures range between 13.5 ° – 29.5 ° C and minimum temperatures range between 0.1 ° – 15.5 ° C (James et al., 2015). It is found in low intertidal to subtidal depths of 15m in sheltered to exposed coastal environments (MPI, 2016). A recent study by James and Shears (2016b) in New Zealand revealed *U. pinnatifida* was found at high densities at 0-3 m below mean low water in the shallow subtidal or very low intertidal zone. *U. pinnatifida* readily attached themselves to manmade structures or floating objects in harbours or boat hulls (MPI, 2016) compared to a natural coastal environment.

According to James and Shears (2016b) *U. pinnatifida* thrives in aquaculture sites like mussel farms as the competition from other seaweed species is less likely and due to absence of herbivorous grazers. They have also found that mussel farms enable the longer annual presence of *U. pinnatifida* due to sporophytes suspended in shallow waters with good light levels and no tidal variation with enhanced water flow. James

and Shears (2016b) suggests it is likely that *U. pinnatifida* is more prevalent in waters with high clarity and greater water motion. It was observed mostly in the top two metres of water and declined with depth.

1.1.4 Economic importance of *U. pinnatifida*

U. pinnatifida is an invasive seaweed and has a high economic value to it. White et al. (2014) outline the importance of *U. pinnatifida* in industrial applications such as soap, toothpaste, animal feed, fertilizer and fuel. They also mention the incorporation of the two main natural bioactive compounds, fucoidan and fucoxanthin from *U. pinnatifida*, in food and nutraceuticals has increased significantly over the years. Global estimate of the wholesale value of *U. pinnatifida* and products made from it is between 1.6 – 2.2 billion US dollars (White & Wilson, 2015). In New Zealand, *U. pinnatifida* has been used for producing food and fucoidan products, feeding Paua, manufacturing seasonings, other innovative products and organic fertilizers (White & White, 2020). By harvesting it from heavily infested areas, the ecological impact is reduced, and revenue generated. Waikaitu Ltd in NZ has collaborated with mussel farms to hand-harvest *U. pinnatifida* from mussel lines to turn invasive pest species into organic fertilisers (White & White, 2020). These farm owners go through a manual, expensive and time-consuming process of physically driving a boat to check each mussel line in the farms to estimate *U. pinnatifida* yield. With UAV remote sensing, much of the operational cost associated with manpower and boat time can be reduced and also enable accurate estimation of biomass.

1.2 Concepts of Remote Sensing

1.2.1 Electromagnetic Spectrum

All matter above absolute zero (K) radiates electromagnetic waves of various wavelengths. Electromagnetic (EM) spectrum is the collation of this entire range of wavelengths from gamma to radio waves (Figure 3).

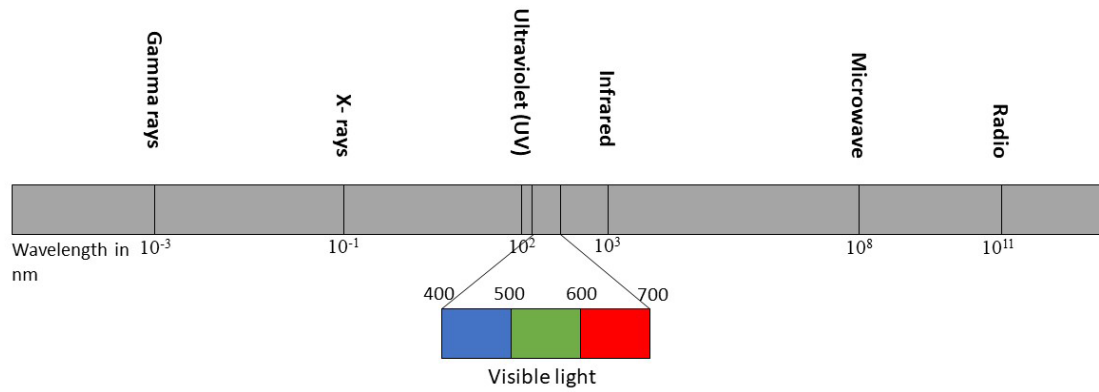


Figure 3: Electromagnetic Spectrum

The optical range of the spectrum extends from X-rays through to far-infrared. The visible part of the spectrum consists of blue, green and red (400 to 700nm) and near infra-red (NIR) region is between 700 – 2500nm. The EM spectrum interacts differently with a variety of features on the Earth's surface and atmosphere, especially the aquatic environment (Figure 4) since water absorbs energy at wavelengths beyond 700nm.

EM energy incident (E_i) on earth interacts with various features and gets reflected (E_r), absorbed (E_a) and transmitted (E_t):

$$E_i = E_r + E_a + E_t \text{ (Lillesand et al., 2004)}$$

Different features on earth reflect incident energy at varying levels and a sensor detects this reflected energy across the EM spectrum as spectral reflectance (SR) or spectral signature. SR is the proportion of reflected energy (upwelling radiance) to incident energy (downwelling irradiance).

There are two types of remote sensing: passive and active. Passive sensors record the electromagnetic radiation that is reflected or emitted from the earth (Jensen, 2016). Sun is the main source of EM radiation in passive remote sensing system. Most earth observation satellites used for, but not limited to, emergency response, precision agriculture, land use/land cover, forestry, geology applications, bathymetry mapping,

aquatic habitat mapping use passive remote sensing. Active sensors use their source of energy which is mostly in the microwave region of the EM spectrum and records the energy reflected from the feature of interest (EarthData, 2020). Some of the applications of active sensors include detecting wind speed and direction, creating elevation models, measuring temperature/humidity/cloud composition.

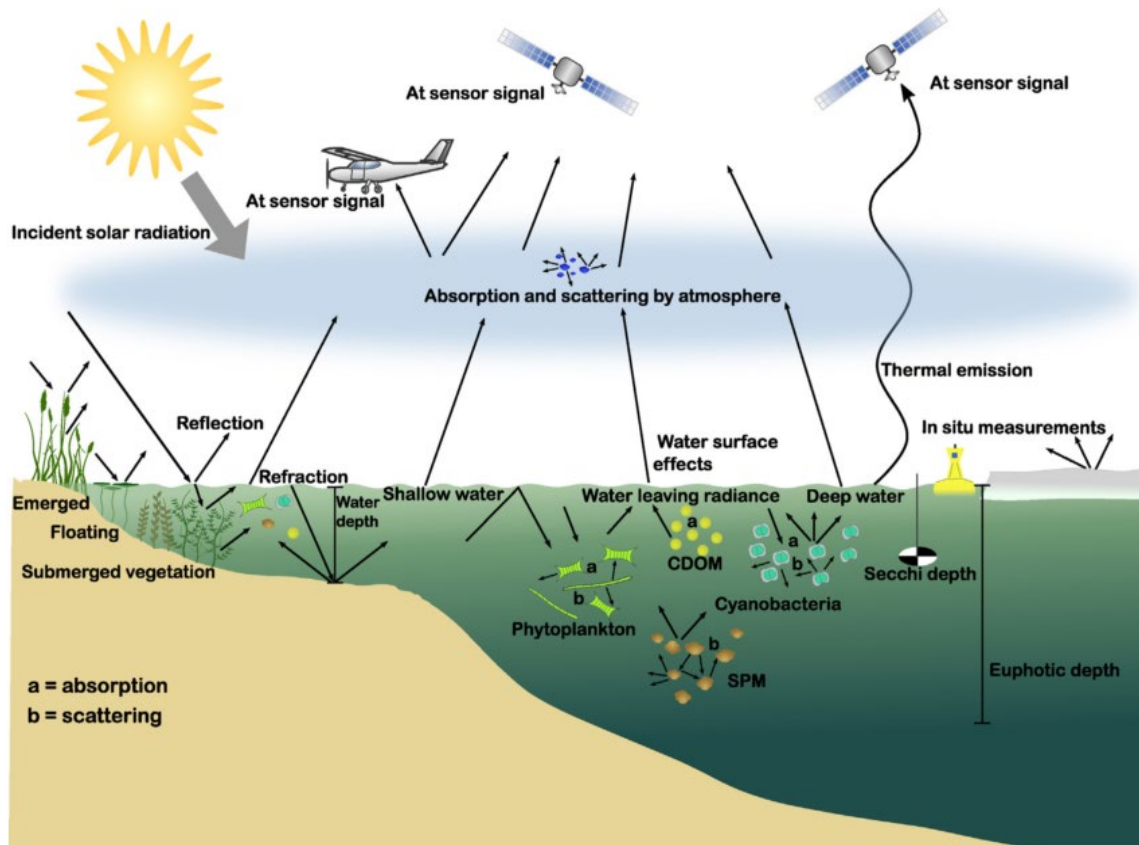


Figure 4: Interaction between the electromagnetic spectrum and aquatic environment. Reprinted from *Remote sensing for lake research and monitoring – Recent advances* (p 108), by Dörnhöfer & Oppelt, 2016. Elsevier. Copyright (2020) by Katja Dörnhöfer and Natascha Oppelt. Reprinted with permission.

1.2.2 Types of resolution in remote sensing

A remotely sensed image is assessed based on four different types of resolution. The type of resolutions needed depends on the application that it is used for.

i) Spatial resolution

A measure of the smallest angular or linear separation between two objects that can be resolved by remote sensing (Jensen, 2016). Pixels are normally represented on computer screens and in hard-copy images as rectangles with length and width (Jensen, 2016).

ii) Spectral resolution

The number and dimension (size) of wavelength intervals (bands) in the EM spectrum to which a remote sensing instrument is sensitive (Jensen, 2016). For example, a remote sensing sensor with four spectral bands (red, green blue, infra-red) of bandwidth 60nm each is considered to have low spectral resolution compared to a sensor with 10 spectral bands of bandwidth 10nm each. The following are some of the passive sensors with different spectral resolutions:

Multispectral

Multispectral sensors record energy in multiple bands of EM spectrum. They typically have four or more wavelength bands. Most satellites have multispectral sensors with broad wavelength bands. Ünsalan and Boyer (2011) provides a detailed understanding of spatial and spectral resolution and revisit times of some of the earth observation/commercial satellites in the past and the present (Table 1).

Hyperspectral

Hyperspectral sensors have hundreds of contiguous bands of narrow bandwidth. These narrow bandwidths are sensitive to various biochemical and biophysical constituents found in plants species and most of them identified are in the near infrared (NIR) and shortwave infrared (SWIR) region of electromagnetic radiation (George et al., 2014; Ollinger, 2011). Hyperion is the first hyperspectral sensor in space onboard the Earth

Observing-1 satellite. It can resolve 220 spectral bands (400 to 2500 nm) with a 30 m spatial resolution (USGS, 2017).

Field Spectroradiometer

Field spectroradiometers are handheld devices that measure the intensity of radiation reflected from a target over several wavelengths. These are calibrated against a standard reflectance panel such as Spectralon® to calculate reflectance values. These instruments are usually of very high resolution, for example, an STS-VIS mini spectroradiometer has a wavelength range of 350-800nm with a spectral resolution of 3nm whereas an ASD Handheld spectroradiometer (ASDInc., 2017) has a wavelength range of 325 – 1025nm with a spectral resolution of 3nm.

iii) Temporal resolution

Temporal resolution refers to how often and when the sensor records imagery of a particular area (Jensen, 2016).

iv) Radiometric resolution

Radiometric resolution can be described as the sensitivity of a remote sensing detector to differences in signal strength as it records the radiant flux reflected, emitted or backscattered from the terrain (Jensen, 2016).

Table 1: Summary of sensor characteristics (Satellite Imaging Corporation; Ünsalan and Boyer, 2011)

| Sensor | Spatial Resolution Corporation | Spectral range (nm) | Revisit interval (days) |
|-----------|-----------------------------------|------------------------|-------------------------|
| Landsat | 15 | 450 – 2350 | 16 |
| SPOT | 2.5 | 500 – 1750 | 5 |
| IRS | 5 | 500 – 1700 | 5 |
| IKONOS | 1 | 450 – 850 | 3 |
| QuickBird | 0.61 | 450 – 900 | 3 |
| FORMOSAT | 2 | 450 – 900 | 1 |
| CARTOSAT | 2.5 | N/A | 5 |
| WorldView | 0.46 | 400 – 1040 | 1.1 |
| ALOS | 2.5 | 420 – 890 | 2 |
| GeoEye | 0.41 | 450 – 900 | 3 |
| Airborne | 1 to 25 | 420 - 14000 | N/A |
| Pleiades | 0.5 | 430 – 950 | Daily |

1.2.3 Image classification techniques

Remotely sensed images can be classified using three types of classification techniques – visual, unsupervised and supervised. Visual interpretation is a manual, time-consuming technique that requires extensive knowledge from the interpreter.

Unsupervised classification technique classifies a remotely sensed image based on user-defined parameters such as the number of classes and iterations of the algorithm. This technique requires less time to process since it does not require a training dataset for classification. Supervised classification technique uses training dataset to classify images. The training dataset is a collection of spectral data of various features obtained from a remotely sensed image by an expert.

1.3 Remote sensing for seaweed mapping

1.3.1 Spectral signature of plants

Green plants have a unique spectral characteristic where they have low reflectance in the visible region and high reflectance in NIR which is exploited to create spectral indices for mapping, monitoring and managing vegetation (Giri et al., 2007). The green leaf absorbs light in the blue and red region due to the presence of pigments, reflects light in the green region of the spectrum and the peak reflectance in NIR is a result of leaf density and canopy structure effects (Figure 5). Spectral reflectance of plants varies primarily due to pigment composition (Kieleck et al., 2001). However, there are also other causes of variability in the plant signal (Table 2).

Table 2: Causes for variability in spectral reflectance at leaf scale and canopy scale (Blackburn, 2007; Mulla, 2013)

| Leaf level | Canopy level |
|-------------------------|--|
| Internal structure | Variation in the number of leaf layers |
| Surface characteristics | Orientation |
| Moisture content | Canopy to ground coverage ratio |
| | Areas of shadow |

Other causes of spectral variability in plant signals are physiological status of vegetation, physiological stress and mixing of water with plant signal, in the case of submerged/emerged aquatic vegetation, reduces the reflected radiation in near to mid-infrared region due to strong water absorption (Silva et al., 2008).

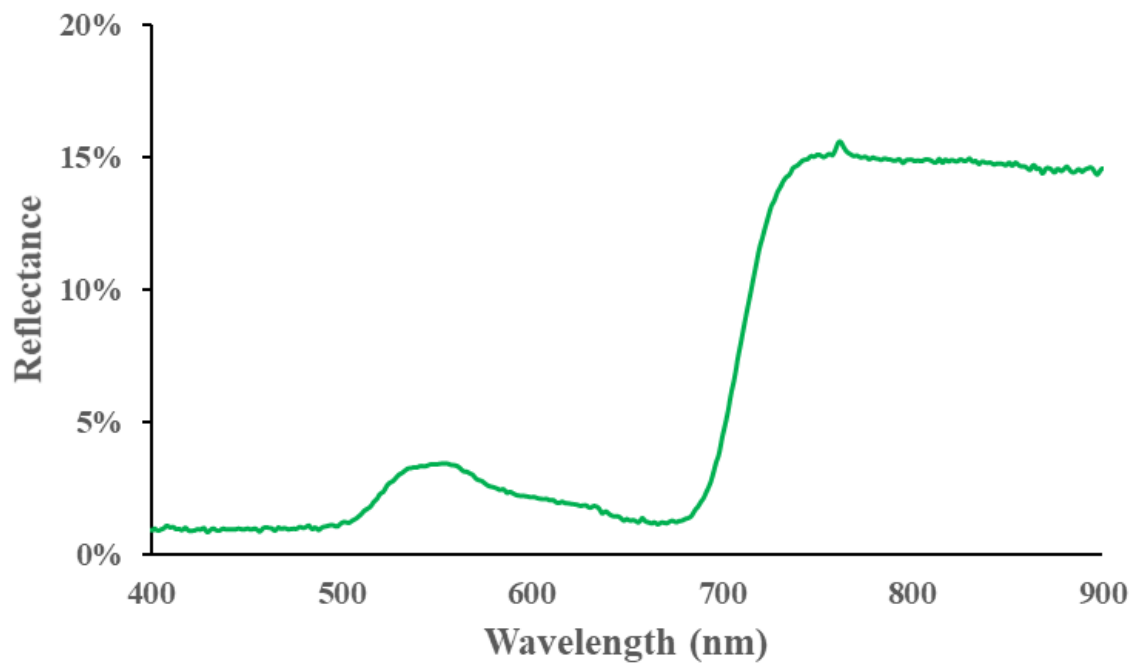


Figure 5: Typical spectral reflectance curve of a green leaf

1.3.2 Spectral signature of seaweed

Seaweeds are macroscopic algae subdivided into three groups – Chlorophyta (green), Phaeophyceae (brown) and Rhodophyta (red). All three groups show differences in pigment composition (Table 3). Their spectral reflectance characteristics are similar to those of terrestrial plants and so are the factors affecting the spectral signatures of seaweeds. However, Kotta et al (2014) suggest that differences in seaweed canopy orientation only marginally contributes to absolute spectral reflectance values. Pigment composition (Kieleck et al., 2001) and leaf structure (Cho et al., 2012) affect the visible and NIR region of the spectral signature of seaweed, respectively.

Reflectance properties of a species of marine vegetation can vary spatially and seasonally (Fyfe, 2003). There is little information on reflectance properties of a single marine vegetation species across different seasons (Casal et al., 2013). Researchers who have mapped eelgrass in shallow waters of Canada (O'Neill et al., 2011), discriminated invasive *Caulerpa* seaweed species from native species in the Mediterranean (Kišević et al., 2011) and mapped seaweeds in Baltic Sea (Kotta et al., 2014) have all recommended

more research on reflectance properties of individual species across different seasons and locations. This would support mapping applicability across different region and seasons, accurate characterisation of the discriminating spectral features of the species in question or true representation of training dataset for spectral library classification approach.

Table 3: Spectral characteristics of pigments present in seaweed groups (Casal et al., 2012)

| Seaweed group | Pigments present | Absorption peak (nm) |
|-------------------------------------|--------------------|----------------------|
| Chlorophyta (Green seaweed) | Chlorophyll-a | 435, 675 |
| | Chlorophyll-b | 480, 650 |
| | β -Carotene | 427, 449, 475 |
| Phaeophyceae (Brown seaweed) | Chlorophyll-a | 435, 675 |
| | Chlorophyll-c | 460, 633 |
| | Fucoxanthin | 426, 449, 465 |
| Rhodophyta (Red seaweed) | Chlorophyll-a | 435, 675 |
| | β -Carotene | 427, 449, 475 |
| | α -carotene | 423, 444, 475 |
| | Biliprotein | |
| | Phycoerythrin | 543, 568 |
| | Phycocyanin | 553, 618 |
| | Allophycocyanin | 654 |

With the increasing number of remote sensing studies in the marine environment, information available on the spectral signatures of various seaweed species are similarly increasing, globally. However, there is no published spectral information on native and invasive seaweed species in New Zealand. Collecting spectral signatures of various seaweed species is an important step towards mapping them from various water depths.

1.3.3 Challenges of mapping submerged/emerged seaweeds from remote sensing data

Glint

The factors that impede object identification underwater are mainly sun glitter, subsurface illumination, shadowing and surface glare (the reflection of diffuse light) (Mount, 2005). Sun glint is dependent on viewing geometry, sun elevation, azimuth, illumination conditions, wind speed and direction (Kutser et al., 2013). According to Mount (2005), images with wider Field of Views (FOVs) are subjected to greater glitter. While Mount (2005) discusses ways to avoid sun glint in data capture, Kutser et al. (2013) discuss a simple glint removal procedure for field radiometer data without any requirement for auxiliary data. This method is explained in detail in Chapter 4. However, this method does not work for areas shallower than 0.4m or if there is large coverage of high order plants on the water surface where the water-leaving radiance is not zero at 900nm. Glint removal is not possible when NIR values are higher than Ultraviolet (UV) values (Kutser et al., 2016). Other glint removal techniques are presented by Gould et al. (2001) where the remote sensing reflectance at 750nm is subtracted across the spectrum to remove sun glint; Hedley et al. (2005) where they assume NIR reflectance over water is caused by sun glint and their magnitudes are linearly related, the glint spectrum can be derived from NIR reflectance and subtracted from each pixel to obtain glint free values. Mount (2005) states that sun angle, reflection and refraction exaggerate subsurface illumination. Sun angle affects the amount of energy received by earth surface for a given square meter. Consequently, the lower the sun angle, lesser the illumination leading to a lower response from the seafloor.

Water depth and turbidity

The main challenge of remote sensing of submerged aquatic plants is to isolate plant signal from the overall water column interference (Silva et al., 2008). Reflectance can be measured in-water or above the water surface and they both have problems associated with them. The above-water reflectance of an object is influenced by two components – surface reflectance and water leaving signal (Gould et al., 2001). Not all wavelengths of the electromagnetic spectrum are useful for mapping submerged/emerged aquatic vegetation. In an aquatic environment wavelengths between 450 – 550 nm are desirable as these wavelengths pass through the water column (Kieleck et al., 2001). Water absorbs red and infrared/NIR and scatters blue light which makes vegetation mapping in aquatic ecosystem challenging just using the visible region for discriminating species. The spectral range between 500 and 600 nm is useful for kelp detection at various depths as two suitable spectral features ($528 \pm 18\text{nm}$ and $570 \pm 10\text{nm}$) are located in this region (Uhl, Bartsch, and Oppelt, 2016).

Turbidity, determined by the constituents in the water column such as phytoplankton, suspended organic and inorganic matter, promotes spectral scattering thereby affecting the spectral reflectance properties of submerged vegetation (Pu, Bell, Baggett, Meyer, and Zhao, 2012). Cho and Lu (2010), Lu and Cho (2011) and Washington, Kirui, Cho, and Wafo-Soh (2012) used experimentally driven algorithms to determine the water absorption or volumetric scattering of the water column in varying levels of turbidity and improved the reflectance values in NIR region. Zoffoli, Frouin, and Kampel (2014) compared various water column correction techniques available but did not conclude with the best method. This is because the methods identified by the authors are applicable for different water types (whether Case I, Case II or Case III), sensor characteristics, mapping purpose and available in-situ data.

1.4 Discrimination of seaweeds

Many remote sensing studies have been conducted globally on seaweed discrimination. Space-borne multispectral sensors like IKONOS have been successful in discriminating seaweed from other surrounding substrates (Sagawa et al., 2012 and Mikami, 2012) and Worldview-2 in discriminating benthic coral habitats (Botha et al., 2013). Dierssen et al (2015) successfully discriminated floating brown seaweed, *Sargassum*, from floating seagrass species, *Syringodium filiforme* using airborne hyperspectral imaging sensor. Kieleck et al. (2001) used laser-induced selective fluorescence imaging to identify thresholds that successfully separated three seaweed species each belonging to the red, green and brown taxonomic group at various depths down to a maximum of 5m even in turbid waters. Gameiro et al (2015) also used laser-induced fluorescence (LIF) technique to partially identify seaweed species to the higher taxonomic level (red, green and brown).

Using field spectroradiometer, some researchers have collected in-situ spectral data for various substrates at different depths (Hochberg and Atkinson, 2000) while some others collected spectral data over seaweed species out of the water and modelled the spectral reflectance at various depth and turbidity levels using radiative transfer model software (Kutser et al., 2006a; Vahtmäe et al., 2006). Both types of spectral libraries were used to identify wavelengths that best discriminated various seaweeds from each other at different taxonomic levels. Most studies like that of Kutser et al (2006b), Vahtmäe et al. (2006), Casal et al (2013), Casal et al (2011), Casal et al (2012), Hochberg et al (2003), Chao Rodríguez et al (2017) used spectral library approach to discriminate seaweeds at broad taxa level. The first three studies even successfully discriminated or assessed the feasibility of discrimination at broad taxa level (red, green and brown) at various water depths which concluded 4 – 5 m as the optimum depth for discrimination at broad taxa level.

There are only a modest number of studies on species-level discrimination of seaweeds mainly due to the interference of water column which absorbs reflectance in NIR region where the subtle differences between species are located. Casal et al (2013) assessed the feasibility of discriminating 17 seaweed species belonging to the three taxonomic groups and was only successful in discriminating three of them. Similarly, Pu et al (2012) and Fyfe (2003) successfully identified optimal wavelengths that discriminated seagrass at the species level. The study by Rossiter et al (2020) uses high spatial and spectral resolution remote sensing data to successfully discriminate between intertidal seaweed species.

Spectral signatures of green, brown and red seaweed are uniquely consistent in different parts of the world (Hochberg et al., 2003; Maritorena et al., 1994), however, there is no such study on NZ seaweeds available at taxa level or species level. To detect and map *U. pinnatifida*, it is important to understand its spectral characteristics and that of other native seaweed species to discriminate *U. pinnatifida* effectively. Kotta et al (2014) state there is significant variation in pigment composition and quantity among broad taxonomic groups and even within species.

1.4.1 Spectral data analysis techniques

This research has identified some of the common techniques used for discriminating aquatic vegetation both at broad taxa level and at species level using field spectroscopy (Table 4).

Table 4: Spectral data analysis techniques

| No | Technique | Function | Reference |
|----|---|---|---|
| 1 | Analysis of Similarity test (ANOSIM) | Provides information about within and between species variability. Does not give information on specific spectral bands where the main differences occur or what species are differentiable from each other | Casal et al. (2013); Fyfe, (2003) |
| 2 | Kruskal-Wallis test | Determine significant differences between seaweed species at each wavelength | Casal et al., (2013) |
| 3 | Kruskal-Wallis post-hoc test | Shows seaweed pairs that are significantly different at each wavelength band | Casal et al., (2013) |
| 4 | Non-metric multidimensional scaling (nMDS) | | Casal et al., (2013)(Fyfe, (2003) |
| 5 | t-tests | Showed a statistically significant difference in absorption features of two invasive seaweed species | Kišević et al., (2011) |
| | | Identified 5 optimal bands to discriminate 3 seagrass species | Pu et al., (2012) |
| 6 | Wilks' lambda, F-value / Stepwise selection | Lower Wilks' Lambda combined with high F-value helps identify the narrow bands that discriminate different classes | Manjunath et al., (2011) Hochberg and Atkinson, (2000) |
| 7 | Derivative analysis | Detects subtle features in the raw reflectance spectra and reduces the large datasets into smaller useful information | Hochberg and Atkinson, (2000); Louchard et al., (2003); Chao Rodríguez et al., (2017) |
| | | Removes the effect of illumination variation in spectral reflectance of the target | Pu et al., (2012) |
| 8 | Linear discriminant analysis | Identifies linear combination of wavelengths that separate the seaweed species at broad taxa level | Hochberg and Atkinson, (2000) |

| | | | |
|----|--|--|---|
| 9 | True Skill Statistics Optimal Bands (TSS-OB) | Identifies the optimal boundary separation between two taxonomic groups | Chao Rodríguez et al., (2017); Kotta et al., (2014) |
| 10 | RGB (Red Green Blue) Colorimetry | Performs linear classification of three seaweed taxonomic groups based on the sample colours | Chao Rodríguez et al., (2017) |

1.4.2 Image classification approach for seaweed mapping

This research looked at various classification techniques employed by researchers for submerged aquatic vegetation studies (Table 5). Although there were some classification studies using band indices/band ratios (e.g. Dierssen et al. (2015)) and unsupervised (e.g. Casal et al. (2011)) only those that used supervised or unsupervised techniques were considered. Most studies used supervised classification technique like Maximum Likelihood Classification (MLC) which derives training and validation dataset from the images used for classification. Studies also used Spectral Angle Mapper (SAM) classifier which used spectral data collected a) in-situ without water column interference, b) in-situ with water column interference, c) spectral signatures derived from images, d) modelled spectral signatures of a) to various water column properties based on the study site, to classify images. However, SAM technique using a spectral library is advantageous as the spectra do not have to be collected at the time of data acquisition and the existing spectral library can be modified to suit sensors with different spectral resolution (Kutser et al., 2006a).

Table 5: A literature review of some of the image classification approaches relevant to the study. SAM - Spectral Angle Mapper, MLC - Maximum Likelihood Classifier, ACE - Adaptive Cosine Estimator, MDis - Mahalanobis Distance classifier, MD - Minimum Distance classifier, FD – Feature detection processor, LSU – Linear Spectral Unmixing classifier, SVM – Support Vector Machine and WV2 – WorldView-2 satellite imagery with eight multispectral bands.

| No | Reference | Technique | Accuracy | Platform/Sensor | Classes |
|----|--|-------------------|--|----------------------------------|---|
| 1 | Flynn and Chapra (2014) | SAM ACE | 92% (OA) 90% (OA) | UAV/GoPro3 RGB camera | Green algae (<i>Cladophora</i>), background |
| 2 | Reshitnyk, Costa, Robinson, and Dearden (2014) | MLC | 75% (OA) | WV-2 | At <3m depth, eelgrass, brown, green, unvegetated surface |
| 3 | Hoang, Garcia, O'Leary, and Fotedar (2016) | MDis MD SAM | 94% (OA) 97% (OA) 88% (OA) | WV-2 | Canopy algae, seagrass, algal turf, mixed submerged aquatic vegetation, sand, limestone, unclassified |
| 4 | Johnsen, Ludvigsen, Sørensen, and Sandvik Aas (2016) | SAM | n/a | Underwater Hyperspectral Imager | Three coral species and sponge |
| 5 | Uhl, Bartsch, and Oppelt (2016) | FD MLC | 80% (OA) 57% (OA) | Airborne hyperspectral AisaEAGLE | Submerged kelp down to 6m depth |
| 6 | Uhrin and Townsend (2016) | LSU | >85% (OA) | 3 band RGB aerial imagery | Seagrass |
| 7 | Kutser et al. (2006a) | SAM | Unavailable due to insufficient field data | Hyperion | Coral, dead coral/rubble, green algae, brown algae, red algae, sand and deep water |
| 8 | Casal et al. (2011) | MLC | >90% (OA) | CHRIS – Proba mode 2 | Shallow and deep submerged sand, seaweeds in less |

| | | | | | |
|----|-----------------------------------|------|--------------------------------------|--------------------------------------|--|
| | | | | | than 5m water depth and seaweeds in water depths between 5 -10m |
| | | SAM | Insufficient field data | | Red, green and brown seaweeds |
| 9 | O'Neill, Costa, and Sharma (2011) | MD | 63% (OA) on all wavelength bands | Airborne hyperspectral AisaEAGLE | Shallow and deep eelgrass, shallow and deep sand, shallow green algae, exposed sea asparagus and exposed brown algae |
| | | MLC | 83% (OA) on reduced wavelength bands | | |
| 10 | Casal et al. (2012) | MLC | >95% (OA) | Airborne hyperspectral scanner (AHS) | Shallow and deep sand, emerged rock, emerged and submerged seaweed |
| | | MD | n/a | | |
| | | MDis | n/a | | |
| | | SAM | Insufficient field data | | Red, green, brown seaweeds and sand down to 5m water depth |
| 11 | Vahtmäe and Kutser (2013) | MLC | 77.5% | CASI | From areas of water depth < 2m, Dense high order vegetation, dense <i>Charophytes</i> , hard bottom with filamentous green algae, sparse vegetation on the soft bright bottom and optically deep water (>2m) |
| | | | 71.6% | WV-2 | |
| | | SAM | 70.8% | CASI | |
| | | | 64.6% | WV-2 | |
| 12 | Tait et al. (2019) | SVM | 79 – 90% | UAV multispectral | Ten exposed habitat classes – including three brown seaweed species, Ulva, red |

| | | | | | |
|----|------------------------|-----------------------------|-------|------------------------------------|---|
| | | | | | seaweed |
| 13 | Rossiter et al. (2020) | MLC | 94.7% | UAV hyperspectral pushbroom sensor | Five brown seaweed species (emerged), green seaweed (emerged), submerged seaweed and substratum |
| | | SAM (image-derived spectra) | 81.1% | | |
| | | SAM (in-situ spectra) | 71.4% | | |

1.5 Remote sensing scale of mapping emerged/submerged seaweed

Depending on the characteristics of target features and project goals, different types of remote sensing data are utilised, from aerial photos to multi- and hyperspectral satellite, airborne or UAV data (Skowronek et al., 2016) for various application at different spatial, spectral and temporal resolution (Jensen, 2016). Early remote sensing used various platforms like kites and balloons (Estes, 1985), aircraft (Chiang and Meyer, 1974) and satellite (Driscoll, Francis, Smith, and Mead, 1974) for a variety of environmental applications.

The basic characteristic of remote sensing data is spatial resolution and it is analogous to the scale of observation (Woodcock and Strahler, 1987). For example, Hyperion data with spatial resolution of 30m were used successfully to map broadleaved evergreen and conifer forest species in Western Himalayas (George et al., 2014). Whereas, it was a challenge in the floristic mapping of rainforests due to complex vegetation canopies and a 30 x 30m pixel of Hyperion usually contained a mixture of other canopy species that can reduce the accuracy (Somers and Asner, 2014). Mixed pixel is a pixel that contains a mixture of spectral reflectances from various endmembers. Endmember is the spectra of a target object. Precision agriculture needs detailed crop parameters to assess crop growth and yield amongst a variety of other applications and the data requirements depend on the intended application (Gevaert,

Suomalainen, Tang, and Kooistra, 2015). For example, crop biomass or yield estimation demands a relatively fine-scale spatial (1-3m), temporal and spectral resolution whereas for variable rate application of fertilizer the scale of information could be coarser (5-10m) and 0.5-1m for weed control applications (Mulla, 2013). For such applications, satellite sensors are inadequate in providing the required spatial, spectral and temporal resolution (Gevaert et al., 2015).

Kelp monitoring using Satellite Pour l'Observation de la Terre (SPOT) data (20m) was challenging as it did not resolve kelp beds smaller than 10 ha due to the low spatial resolution (Deysher, 1993). Vahtmäe and Kutser (2013) showed that benthic habitat mapping needs to be done at high spatial resolution due to the small-scale heterogeneity of these habitats. Submerged aquatic vegetation or seaweed patches greater than the pixel size will be resolved clearly in remote sensing data. For example, pixel size or spatial resolution of 2m can resolve homogenous seaweed patches of size 4m² or more. In the current satellite remote sensing scenario, the higher the temporal resolution requirement, the lower the spatial requirement and vice versa (Jensen, 2016). There are trade-offs associated with different resolutions when acquiring a satellite data due to technical limitation in attaining high spatial and spectral resolution all in one data in addition to high temporal resolution (Ashraf et al., 2012; Gevaert et al., 2015).

Although there have been many studies conducted using conventional field surveying techniques, highlighting the morphological characteristics, habitat preferences of *U. pinnatifida* in different parts of New Zealand, however, there have been no studies conducted using remote sensing techniques. Given the characteristics of *U. pinnatifida* in section 1.1, it is important to identify the best spatial resolution to detect *U. pinnatifida*.

1.5.1 UAV seaweed mapping

While seaweeds at broad taxa level and a homogenous cover of same seaweed species have been mapped accurately, there are not many classification studies mapping seaweeds at the species level, especially within a taxonomic group (Rossiter et al., 2020). Such studies are limited due to non-availability of remote sensing data with high spatial and spectral resolution. Recently, unmanned aerial vehicle (UAV) is evolving to be a popular platform to obtain remote sensing data of high spatial, spectral and temporal resolution (von Bueren et al., 2015) due to advancement in miniature sensors (Flynn and Chapra, 2014) and the ability to fly them anytime anywhere given the right weather conditions. The study by Rossiter et al. (2020) is the first that has discriminated seaweeds at species level using UAV hyperspectral data. However, these hyperspectral sensors are disadvantageous for the following reasons: a) they produce high dimensional voluminous data (Adão et al., 2017; Dye, Mutanga, and Ismail, 2011; O'Neill et al., 2011), b) they make UAV integration difficult due to weight (Jakob, Zimmermann, and Gloaguen, 2016) and c) they are very expensive expensive. In order to keep it cost- and time- effective, this study analysed the use of ultra-high spatial resolution multispectral remote sensing data for species-level discrimination of seaweed.

1.5.2 Challenges of processing UAV borne multispectral images

There are four basic steps to process remote sensing data ready for further analysis – radiometric calibration, geometric correction, georeferencing and mosaicking.

Radiometric calibration is the conversion of raw data that contain digital numbers (DN) for pixel values into reflectance. Digital numbers of each pixel in an image represent the intensity values and radiometric resolution of an image is expressed in bits. For example, 8-bit imagery consists of DN values between 0 – 255 (2^8-1) or 16-bit imagery consists of DN value between 0 – 65535 ($2^{16}-1$). Geometric correction is the process of

correcting distortions due to camera lens or camera orientation or the terrain below to assign correct positional values to each pixel. For an image over the aquatic environment, the effect of the terrain is assumed to be nil due to lack of relief features. Most commercial satellite imagery is supplied after geometric correction and can be radiometrically corrected if need be. Georeferencing is the process of aligning an image to a coordinate system to do simple observations such as measuring area or distance or advanced analysis such as estimating biomass of vegetation or feature classification. This is usually achieved by identifying ground control points (GCPs) in the study area with known coordinates. Mosaicking is the process of aligning multiple georeferenced images of a study area into one image.

The above process is applicable for most satellite images, however, UAV image processing is made easy by specialised software such as Pix4D Mapper or Agisoft professional scan that automatically perform radiometric calibration, geometric corrections, georeferencing and mosaicking. Such software employ a Structure for Motion (SfM) (Ullman and Brenner, 1979) technique that uses photogrammetric methods to calculate the orientation of various images by collecting matching keypoints in multiple images. It created a three-dimensional scene of the study area and georeferenced them using GCPs. Keypoints matching relies heavily on the feature identified on all images to remain static. However, in a dynamic aquatic environment finding such keypoints can be tricky especially if there are no static features in all the images. Also, such image processing software does not allow single image processing since the process is all built-in as one. A bespoke flowline needs to be developed for processing and direct-georeferencing the images to the ground.

1.6 Rationale and significance of the study

The Japanese kelp, *Undaria pinnatifida*, is a highly invasive opportunistic seaweed that could potentially displace native seaweed, animal species and alter existing trophic relationships (Jiménez et al., 2015; MPI, 2016). Therefore this seaweed is of particular interest to New Zealand's Ministry of Primary Industries (MPI); it is classed as an unwanted organism and has been subjected to extensive research to understand its biology, ecology and occurrence, especially in New Zealand (Chen, 2012; Forrest et al., 2000; Hay and Luckens, 1987; James and Shears, 2016b; Parsons, 1995; Russell et al., 2007). Previous research efforts to map aquatic vegetation have been conducted using conventional methods such as snorkel or SCUBA, which are time-consuming and expensive (Flynn and Chapra, 2014). Therefore, there is a need to detect *U. pinnatifida* and map the extent effectively, non-invasively and at less cost. Remote sensing has been identified as a potential tool for this research (Cho, Mishra, and Wood, 2012) as aquatic plants can be digitally identified using their spectral reflectance (Silva et al., 2008 and Costa, 2008). Spectral reflectance is the digital signature unique to individual plant species (Kieleck et al., 2001 and Cariou, 2001) collected using lab or field-based spectroradiometer. A repository of spectral reflectances is called a spectral library and can be used to classify remote sensing data to detect and map the extent of a species of interest (Shanmugam and SrinivasaPerumal, 2014). There are no remote sensing studies relating to detection of *U. pinnatifida*. This research will fill this knowledge gap by, firstly, creating a spectral library with spectral reflectance of *U. pinnatifida*, and other commonly found seaweed species and substrates associated with *U. pinnatifida*. This library will be the reference to conduct further feasibility studies in the detection of *U. pinnatifida* using remote sensing data from a platform such as an unmanned aerial vehicle (UAV). This research will also develop a methodology to map *U. pinnatifida*

using remote sensing data. A potential species level mapping solution at such a high resolution would be of interest to relevant parties such as MPI.

While there have been significant advances in the remote sensing of terrestrial vegetation, remote sensing of submerged aquatic vegetation has been challenging due to the effect of water and the constituents of the water column (Cho et al., 2012). This research aims to understand these effects of water on *U. pinnatifida* by experimental and observational methods.

1.7 Research questions

This research aims to address the following questions:

1. What are the best spectral bands for discriminating *U. pinnatifida* from other seaweed species?
2. Does season and/or location affect the spectral signatures of seaweeds?
3. Do depth and turbidity affect spectral signature of *U. pinnatifida* and *E. radiata*?
4. To what depth, and in what water clarity conditions, can *U. pinnatifida* be detected using spectral reflectance data?
5. Can *U. pinnatifida* be reliably detected and discriminated at ultra-high spatial resolution multispectral data?

1.8 Thesis structure

Chapter 1 introduced the importance of the aquatic ecosystem and the threats faced, followed by a focus on a particular threat by invasive seaweed species, *U. pinnatifida*. It also reviews the literature on remote sensing techniques for mapping seaweeds and other substrates in general while identifying the knowledge gaps.

Chapter 2 describes the data collection of spectral signatures of common seaweeds for New Zealand, identifies wavelengths that discriminate *U. pinnatifida* from other NZ seaweed species using two classification techniques for multidimensional data. It will also analyse the spectral library for discrimination between seaweed species at a broad taxonomic level and species level and review how this compares to other studies around the world.

Chapter 3 analyses the spectral data of two common habitat-forming seaweeds, *E. radiata* and *C. maschalocarpum*, to examine the effect of location and season on spectral reflectance and identify the wavelengths affected. It also identifies the likely causes for the variation.

Chapters 2 and 3 have been developed into manuscripts and submitted for peer-reviewed publication.

Chapter 4 analyses the spectral data of *U. pinnatifida* and *E. radiata* for the effect of depth and turbidity on the spectral reflectance of the two seaweed species. It studied the feasibility of discriminating both the seaweed species using wavelengths identified in Chapter 1 and using wavelengths matching multispectral Micasense RedEdge-M sensor. This chapter studied the accuracy of discrimination using an experimental method and implemented the method on data collected along the rocky reef in Waiheke Island.

Chapter 5 summarises the findings of the study, proposes further improvements to the study and identifies further relevant research applications.

Chapter 2. Discrimination of common New Zealand native seaweeds from the invasive *Undaria pinnatifida* using hyperspectral data



Chapter 2 cover picture. *Undaria pinnatifida* fouling a dropper line in a mussel farm in Marlborough Sounds, South Island, New Zealand.

This chapter is published in a peer-reviewed journal

In this chapter, I collected spectral signatures of common NZ native and invasive seaweed species to analyse discrimination of an invasive seaweed species, *U. pinnatifida* from the native seaweed species. This is the first step towards understanding the spectral differences of seaweeds in NZ at species level within a taxonomic group and discriminate *U. pinnatifida* from the rest. This chapter aimed to identify wavelengths that achieve discrimination of *U. pinnatifida* from other co-occurring seaweed species.

This study collected 198 spectral signatures of seaweeds belonging to red, green and brown taxonomic group. Out of which 110 were selected for training models and 88 were used for validating the trained models. Despite mixed conclusion on species-level studies in the past, interestingly, the analysis in this chapter revealed species-level discrimination was achievable within a taxonomic group.

2.1 Introduction

Seaweed communities around the world are threatened by various factors (James, 2016; Martínez et al., 2018; Nelson, 2019; Nicastro et al., 2013) but invasive species are among the most serious threats (Gallardo et al., 2016; Maggi et al., 2015; Thomsen et al., 2014). Invasive species not only can displace native species and affect biodiversity (James, 2016; Maggi et al., 2015) but can also adversely affect the economy by fouling aquaculture farms (Fitridge et al., 2012).

Undaria pinnatifida (Harvey) Suringar is a prolific invasive species that has established in numerous temperate coastal habitats around the world (Morelissen, et al., 2016). It is one of only two seaweeds listed in the top 100 most invasive species of the world (Lowe et al., 2000). In New Zealand, it was first recorded in Wellington Harbour in 1987 (Hay, 1990) and has since spread throughout much of the country. It spreads by many vectors including via spores in ballast water in recreational and commercial vessels (MPI, 2016), as fragments or whole plants which can drift up to 10 km (Sanderson, 1997) and as a result of mussel farming activities (James et al., 2016). There are aspects of the ecology of *U. pinnatifida* and its relationship with the environment that have yet to be investigated and as a result, the spatial limits of this species are uncertain (South et al., 2017). Thus, methods that can more effectively quantify the distribution and composition of New Zealand's native and invasive seaweed communities would be beneficial from biosecurity, ecology, and commercial perspectives. Current seaweed mapping/monitoring techniques include conventional methods, such as manual SCUBA or snorkel surveys, which are time-consuming and expensive (Flynn et al., 2014). Remote sensing is potentially a very powerful tool for mapping submerged vegetation as it is non-invasive and less time consuming than conventional methods, and can map large extents effectively (Silva et al., 2008).

Traditionally, classification of remote sensing data is image-based i.e., they are specific to a sensor, location and season that make the approach untransferable (Kutser et al., 2003). To overcome this, a common approach to discriminate plant species is to generate a spectral library through which key differences between wavelengths can be identified (Prosper et al., 2014; Kutser et al., 2006a; Vahtmäe et al., 2013). Developing a spectral library for seaweeds in New Zealand would help in differentiating native from invasive species (Bradley, 2013; Skowronek et al., 2016). This spectral library can then inform decisions on the selection of sensors that include the key wavelengths or lead to the design of custom sensors that could detect and record those wavelengths (De Backer et al., 2005) or develop classification algorithms for hyperspectral sensors. While many spectral libraries have been created for terrestrial plants (Manjunath et al., 2013; NASA, 2019), less attention has been paid to aquatic species, including seaweeds (Kutser et al., 2006a; Wolf et al., 2017). There is currently no published spectral information for common New Zealand native and invasive seaweed species, an issue this research addresses.

There have been considerable attempts to map seaweeds using multispectral and hyperspectral data to discriminate dominant, habitat-forming seaweeds. Reshitnyk et al (2014) utilised 8-band multispectral WorldView-2 data to classify two seaweed species each representative of brown and green taxa and eelgrass in Canada with a total accuracy of 75%. Sagawa et al (2012) used IKONOS data to discriminate five different substrates including three species of brown seaweed in Japan with a total accuracy of 97%. Casal et al (2013) created a hyperspectral library of 17 species of seaweed in Spain whilst this study was able to differentiate these species at a broad taxonomic level only three species could be clearly distinguished in reality. Kotta et al (2014) produced a hyperspectral library with 11 species of seaweed and three species of seagrass in the Baltic Sea. They demonstrated significant differences at broad taxonomic levels but not

at the species level. Kišević et al. (2011) is the only study to attempt to distinguish between native and invasive seaweed species in the Adriatic Sea. They identified regions of the electromagnetic spectrum where the invasive *Caulerpa* differed from local species. Hochberg, Atkinson, and Andre'fouet (2003) successfully classified various substrates at 11 locations across the world, including red, green and brown seaweeds with an accuracy greater than 85%. Kieleck, Bousquet, Le Brun, Cariou, and Lotrian (2001) used laser-induced fluorescence imaging technique to identify three seaweed species each belonging to one of three broad taxonomic level (reds, greens and browns). Though it was conducted in a controlled environment, the classification rate was high with the thresholding method, even successful down to a simulated depth of 5m and with turbidity. Chao Rodríguez, Domínguez Gómez, Sánchez-Carnero, and Rodríguez-Pérez (2017) created an extensive 36 seaweed species-rich spectral library and utilised three different methods to discriminate them at broad taxa level successfully with Cohen's kappa more than 0.65. While the highlighted studies have met with some success at broad taxa level, none incorporate common New Zealand species.

U. pinnatifida, a brown seaweed, has been known to compete with native brown seaweeds (Russell, Hepburn, Hurd, and Stuart, 2007) or replace red and green seaweed species at mean low water neap tide level (Parsons, 1995). Previous studies (some of the above mentioned) suggest that it is difficult to see clear separation within a taxonomic group (Casal et al., 2013; Kotta et al., 2014). Depending on the diversity of seaweeds at a location and variable scale of remote sensing surveys, a given dataset may not have red, brown and green seaweed species present to discriminate *U. pinnatifida* from. Therefore, a focused classification strategy targeting each major group could be beneficial. Despite the highly invasive nature of *U. pinnatifida*, there have been no attempts to use the spectral signature of this seaweed to map its spread or prevalence to

date. Before a full survey, it is prudent to assess the feasibility to discriminate *U. pinnatifida* from common New Zealand seaweed species.

In this study, we created a spectral library consisting of *U. pinnatifida* and habitat-forming and/or common New Zealand seaweeds and discriminated between higher taxonomic levels (red, brown and green). We also evaluated discrimination of *U. pinnatifida* from common New Zealand browns, reds and greens by each taxonomic group or all species combined.

2.2 Materials and Methods

2.2.1 Seaweed collection and spectral measurements

Five to ten individuals of common low intertidal and subtidal seaweed species were collected between May 2017 and December 2018, either at low tide or on snorkel, from the Hauraki Gulf and West Coast of northern New Zealand and Pelorus Sound in South Island (Figure 6). Most of the habitat-forming, common seaweeds of New Zealand were found within these identified locations. These species were, the brown seaweeds (Class Phaeophyceae) *Ecklonia radiata* (C. Agardh) J. Agardh., *Carpophyllum maschalocarpum* (Turner) Grev., *Carpophyllum plumosum* (A. Rich), J. Agardh, *Carpophyllum flexuosum* (Esper) Grev., *Cystophora retroflexa* (Labill.) J. Agardh, *Cystophora torulosa* (R.Br.) J. Agardh, *Dictyota ocellata* J. Agardh, *Hormosira banksii* (Turner) Decne., *Xiphophora chondrophylla* (Turner) Mont. ex Harv.; the reds (Phylum Rhodophyta): *Pterocladia lucida* (Turner) J. Agardh, *Corallina officinalis* Linnaeus, *Melanthalia abscissa* (Turner) J.D.Hooker and Harvey, *Cladhymenia oblongifolia* J.D.Hooker and Harvey, *Gigartina alveata* (Turner) J. Agardh, *Pachymenia lusoria* (Grev.) J. Agardh, *Gigartina circumcincta* J. Agardh, *Gigartina atropurpurea* (J. Agardh) J. Agardh, *Pyropia plicata* W.A.Nelson; the greens (Phylum Chlorophyta) seaweed: *Ulva spp.* and the invasive brown and green seaweeds, *U. pinnatifida* and

Codium fragile (Suringar) Harvey, respectively. All individuals were collected from rocky reef habitats, except for *U. pinnatifida*, which was also collected from mussel farms in Awakiriapa Bay in the North Island and Pelorus Sound in the South Island (Figure 6) since they were found in large numbers in mussel farms and were easier to acquire for sampling.

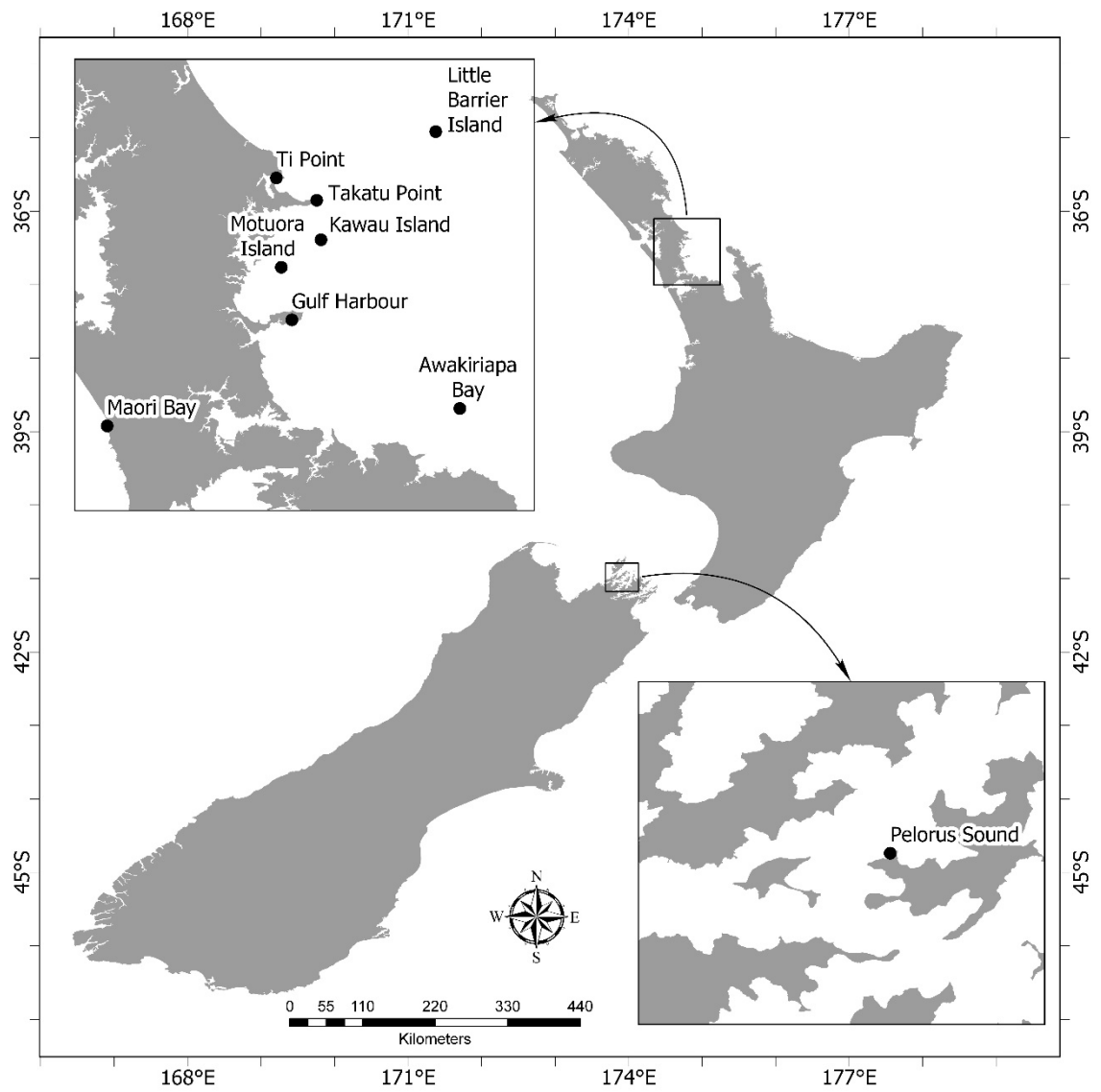


Figure 6: The North Island sites were mainly located near Auckland, in the Hauraki Gulf in the east and one off the western coast. The South Island sites were in Pelorus sound in Marlborough Sounds.

Individuals were removed from the water for the spectral readings as water absorbs red and infrared/Near Infrared (NIR) and scatters blue light (Kieleck, Lotrian, Bousquet, Le Brun, and Cariou, 2001), and NIR is the main component for discriminating vegetation (Cho, Mishra, and Wood, 2012). Each individual was placed on a black mat (Figure 7) to avoid background noise. Only slight differences in true reflectance are found when seaweeds are removed from the water for spectral readings and positioning of the blades only marginally affects the reflectance spectra (Kotta et al., 2014). However, depending on the thickness of the seaweed, the black background could affect the measured reflectance (i.e., light transmitted through the tissue is absorbed rather than reflected from the substrate back through the tissue). Measurements were taken using an ASD Handheld2 VNIR spectroradiometer with a spectral range of 325-1075 nm and a sampling interval of 1 nm and a fibre optic input (FOV 25 deg). This was calibrated against a Spectralon® panel.



Figure 7: Seaweed species, *Xiphophora chondrophylla*, *Carpophyllum maschalocarpum* and *Pterocladia lucida* (left to right), placed against a black mat for measurement of spectral reflectance to minimise any background noise

The spectrometer was held approximately 10 cm directly above the individual and ten measurements were taken over the blade, stipe, and holdfast, where possible the black background was avoided in the field of view (FOV). All measurements were taken within two hours of solar noon.

2.2.2 Data analysis

The data set, created from 198 seaweed individuals, comprised 350 numeric wavelengths of the reflectance values between 400 – 750 nm and the categorical variable “seaweed species”. These wavelengths were selected to encompass the expected transmission window range in water (450–550 nm) (Kieleck et al., 2001) and to expand the field of investigation to wavelengths in the NIR region that have been shown by others to result in the greatest discrimination between species (Casal et al., 2013; Cho et al., 2012; Fyfe, 2003; Laba et al., 2005).

Two supervised analysis techniques, suited to handle multi-dimensional collinear data with a low number of samples such as spectral data, were adopted to discriminate seaweed species at a broad taxonomic level and species level. The broad taxonomic level is the grouping of seaweed species at a higher level as red, green and brown seaweeds. Firstly, a partial least square discriminant analysis (PLS-DA) model was implemented to check for variability between seaweed taxa or between target and non-target species and to identify influential wavelengths using a backward variable selection method. PLS-DA discriminates high dimensional and highly collinear data into classes by the projection of original predictors as latent variables (uncorrelated linear combination of original variables) to explain variance in the response variable (Gold et al., 2019). It was implemented in R using the ‘mdatools’ package, version 0.9.4 (Kucheryavskiy, 2018). PLS-DA method in ‘mdatools’ package performs one-class modelling implicitly. One class PLS-DA is defined as a method where one target class is discriminated from the rest of the classes (Pomerantsev and Rodionova, 2018). For example, in a dataset with three classes for discrimination, pls-da method implicitly performs three models (class-1 vs (class-2 + class-3), class-2 vs (class-1 + class-3), class-3 vs (class-1 + class-2)). This method performs better for three or less number of classes. If there are more than three classes, it is better to explicitly define the model to

discriminate a class of interest against the rest. Discriminant methods are usually unable to classify new samples that do not belong to any of the predefined classes, however, a one-class PLS-DA method corrects for these inabilities (Pomerantsev and Rodionova, 2018). Sensitivity, specificity and accuracy of calibration, cross-validation and external validation were used to measure the performance of the PLS-DA model. Sensitivity is defined as the true positive rate, i.e., seaweed individuals correctly identified to respective broad taxonomic group. Specificity is defined as the true negative rate, i.e., seaweed individuals that do not belong to a particular taxonomic group correctly identified as not belonging to it. Secondly, a ‘random forest’ classification approach, was used to validate the influential wavelengths extracted from the optimal PLS-DA model. Random forest model uses multiple decision trees to classify data accurately due to randomness in feature selection and is better suited for spectral data (Breiman, 2001). This was performed using the ‘randomForest’ package (Liaw and Wiener, 2002) in R. Sensitivity, specificity and kappa were the three random forest model performance statistics. Kappa measured the performance of the classifier especially on an unbalanced dataset and values greater than 0.6 meant the accuracy is substantially agreeable and the model performed very well (Hartling, 2012). While PLS-DA is better suited for feature selection (Peerbhay et al., 2013; Möckel et al., 2014) and random forest for higher classification accuracies (Dye et al., 2011), they are comparable because they capture the interaction between predictors directly or indirectly (Gold et al., 2019).

A total of 198 spectral signatures of red, brown and green seaweeds were collected, out of which 110 spectral signatures were selected as the “training” dataset (collected in May, June, August, October of 2017 and August, December of 2018) while the remaining 88 spectral signatures were the “testing” dataset for external validation (collected in April, August and December 2018 with dates in August and December not overlapping with that of training dataset).

2.2.2.1 Pre-processing

Five individuals of each native seaweed species and ten individuals of *U. pinnatifida* were used for model calibration, cross-validation and external validation as the variation among individuals was low across the wavelengths used in the analysis. The spectrum of each seaweed individual used for analysis was a mean of ten readings taken across different parts of each individual. Raw spectra were standardised by subtracting the mean of values at all the wavelengths, for each individual, from each spectral value and dividing the difference by standard deviation of values of the individual spectrum following Kotta et al. (2014). Data were downloaded, read and compiled into a database in R software (R Core Team, 2019).

2.2.2.2 Discrimination of common seaweeds at a broad taxonomic level

A full PLS-DA model, including all wavelengths considered for investigation, was built using the standardised spectral dataset with 110 observations (55 brown, 10 green and 45 red seaweed individuals) and leave-one-out cross-validation was used. ‘mdatools’ package in R allowed integration of component selection based on a parameter ($ncomp.selcrit = 'min'$ or ‘wold’) within the model. ‘min’ method used in the model is the point at which the root mean squared error (RMSE) of calibration is minimum. Subsequently, an optimal model was built by eliminating wavelengths with variable importance of projection (VIP) scores of less than 1 from full and interim models. VIP is defined as a variable’s importance to a PLS-DA model. An optimal model is defined as a model that discriminates the seaweed species at broad taxa level with accuracy similar to the full model but with lesser wavelengths. Component selection for the optimal model was further refined by visually selecting the number of components that had minimum RMSE from cross-validation curve in the RMSE plot. The optimal model was validated using a testing dataset with 88 observations (43 brown, 10 green and 35 red seaweed individuals) from different dates and/or locations that were not included in

model calibration and cross-validation. During validation, any new observations that were not identified by the optimal model as belonging to any of the specified classes were classified as 'None'. The influential wavelengths identified from the optimal model were chosen using VIP scores for further validation using random forest technique.

A random forest model was built using the influential wavelengths identified above. The model gave an "out-of-bag" error estimate, which was a prediction error estimated using bootstrapped cross-validation. The model was run with a default parameter setting for the number of trees (ntree) built and wavelengths tried at each point where the tree splits (mtry). The model's error rate was plotted to prune the forest. 'tuneRF' method was used to find the optimal 'mtry' with least out-of-bag error and the model was rerun. The same training and testing datasets used for building and validating the PLS-DA model were used for random forest classification. Multidimensional scaling (MDS) plots, using a proximity matrix from the random forest model, were used to visualise grouping of the classes. Proximity was measured as the proportion of times, across the trees in the forest, where two individuals were found to be similar and fell in the same terminal node; two individuals with a value of 1 indicated they were similar whereas 0 indicated two dissimilar individuals (Quach, 2012). MDS mapped this proximity matrix of 'n' objects into an abstract co-ordinate space of (n-1) dimensions.

2.2.2.3 Discrimination of *Undaria pinnatifida* from native seaweed species

The analysis techniques to discriminate *U. pinnatifida* from native brown or red or green or all seaweed groups together were similar to those described in the previous sections. Firstly, four full explicitly defined one-class PLS-DA models were built using standardised data for discriminating *U. pinnatifida* from the three seaweed groups (*U.*

pinnatifida (n = 10) vs browns (n = 45), *U. pinnatifida* (n = 10) vs greens (n = 10), *U. pinnatifida* (n = 10) vs reds (n = 45)) and from all groups combined together (*U. pinnatifida* (n = 10) vs browns + greens + reds (n = 110)). For each full model, the optimal model with similar accuracy to full model but reduced suite of wavelengths was identified. The optimal models were externally validated with testing dataset (*U. pinnatifida* (n = 10) vs browns (n = 33), *U. pinnatifida* (n = 10) vs greens (n = 10), *U. pinnatifida* (n = 10) vs red (n = 35)) and from all groups combined together (*U. pinnatifida* (n = 10) vs browns + greens + reds (n = 78)). Component selection for each of the four models was performed as explained in section 2.2.2.3. The influential wavelengths from each of the four optimal models were chosen using VIP scores for further validation using random forest technique. Random forest classification was carried out as above.

2.3 Results

The spectral data of brown seaweed has reflectance peaks at 600 and 650 nm and a shoulder at 580nm (Figure 8). Most of the red seaweeds had clear peaks at 600 and 650nm, however, there was another peak at 525nm for *Gigartina atropurpurea*, *Gigartina circumcincta* and *Pyropia plicata*. Green seaweeds such as *Codium fragile* had a peak reflectance at 568 nm and an absorption feature at 650 nm while *Ulva* spp. had a peak reflectance at 554 nm and an absorption feature at 670 nm. Chlorophyll absorption was apparent near 675 nm in all the seaweed species.

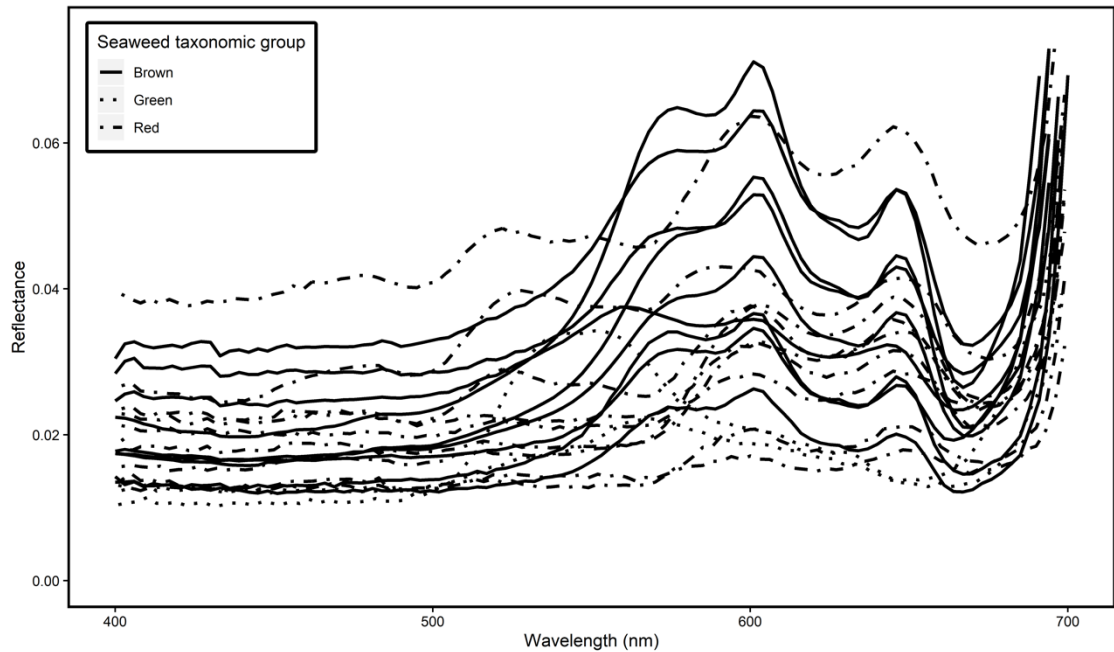


Figure 8: Reflectance spectra of all the common New Zealand seaweed species used in this study grouped at a broad taxa level - brown, red and green.

2.3.1 Discrimination between seaweed taxa (brown, green and red) and influential wavelengths

Extraction of influential wavelengths

The full PLS-DA model performed with 100% sensitivity and specificity in classifying the seaweed species as belonging correctly to each taxon. The optimal model achieved a 100% sensitivity and specificity in both calibration and cross-validation for all three taxa, except for brown, which had a specificity of 98.2% (cross-validation) using ten components. External validation of the optimal model using the testing data set resulted in the following by using ten components (Figure 9); brown taxa had the lowest sensitivity (74.4%) compared to the green (80%) and red (100%), and green taxa had the highest specificity (100%) compared to brown (97.8%) and red (96.2%). Some *Ulva spp.* and brown individuals were classified as ‘None’. 25 influential wavelengths were identified for discriminating all three taxa using the optimal PLS-DA model –572, 633–635, 640, 657, 658, 660, 661, 687, 704–714, 741, 742, 749, 750 nm (Figure 10).

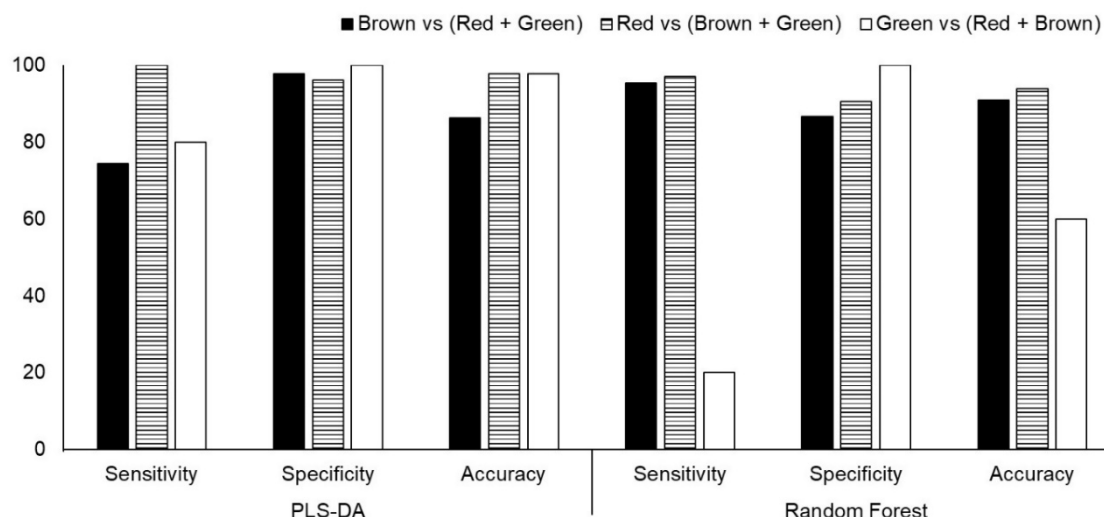


Figure 9: Performace statistics of external validation of models built using PLS-DA and random forest techniques. Sensitivity is defined as the true positive rate, i.e., *U. pinnatifida* individuals correctly identified as *U. pinnatifida*. Specificity is defined as the true negative rate, i.e., non-*U. pinnatifida* individuals correctly identified as non-*U. pinnatifida* individuals. Accuracy is defined as the total number of true positive and true negative out of the total number of samples. Solid, shaded and no fills represent the classification statistics for brown, red and green seaweeds, respectively.

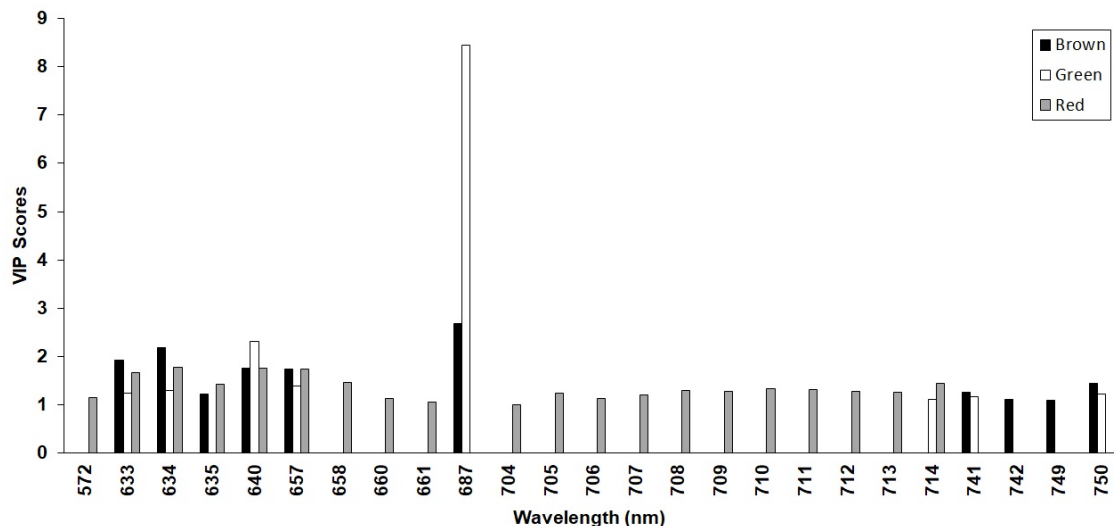


Figure 10: The graph shows the influential wavelengths that discriminate each seaweed taxon (brown seaweed taxa represented in black, green seaweed taxa represented by white and red seaweed taxa represented by grey) from the other two taxa. Wavelengths with VIP scores >1 are classified as influential. Higher the VIP scores, more influential the wavelengths are in the model.

Validation of the influential wavelengths extracted from the PLS-DA model

The random forest classification model (ntree = 300, mtry = 5) built using the training dataset and 25 influential wavelengths identified in the above process resulted in an estimated out-of-bag error of 3.64%. Classification errors for brown, green and red were 3.64%, 20% and 0%, respectively. The random forest model was validated with the testing dataset. The ability to classify seaweed individuals to correct seaweed taxa in the testing dataset was relatively strong, with 87.5% accuracy and kappa of 0.7769. While 95.4% of brown and 97% of red seaweeds were classified correctly only 20% of green seaweeds were correctly classified (Figure 10). All three seaweed taxa were grouped with little overlap between classes in a multidimensional scaling plot (MDS) (Figure 11).

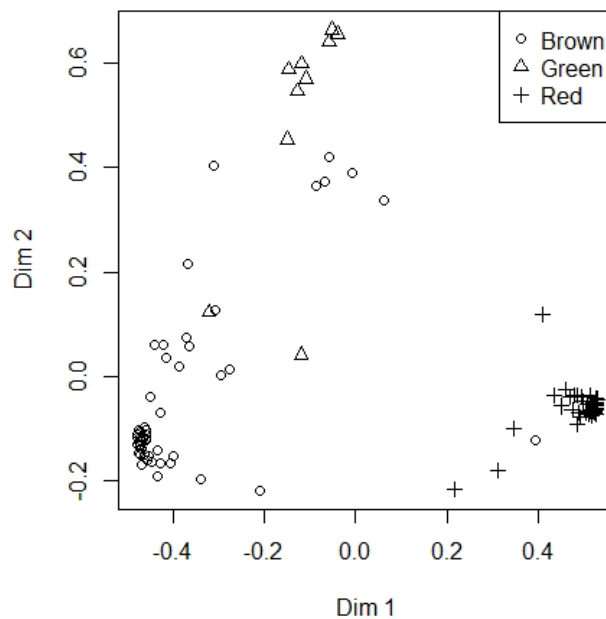


Figure 11: Multidimensional Scaling (MDS) plot using a proximity matrix of n=110 individuals from the between-taxa random forest classification model for brown, green and red seaweeds. X- and Y- axes are first and second dimension, respectively, in 109 (n-1) dimensional cartesian space.

2.3.2 Classification of *Undaria pinnatifida* relative to New Zealand native seaweed species

Extraction of influential wavelengths

Optimal models were obtained for all the four PLS-DA models (*U. pinnatifida* vs browns, *U. pinnatifida* vs greens, *U. pinnatifida* vs reds and *U. pinnatifida* vs browns + greens + reds). Each of these four optimal models produced 100% sensitivity and specificity in both calibration and cross-validation.

The optimal model was subjected to external validation using the testing data and the results are as follows (Table 6): *U. pinnatifida* was discriminated from both brown and green seaweed individuals with 100 % sensitivity and specificity using five and six components, respectively. While discriminating *U. pinnatifida* from red seaweed individuals, all *U. pinnatifida* individuals were correctly classified using 15 components. However, only 83% of red seaweed individuals were correctly classified as not belonging to *U. pinnatifida* and all *P. plicata* individuals were misclassified as *U. pinnatifida*. When *U. pinnatifida* was discriminated against all three seaweed individuals combined (including red, green and brown individuals), sensitivity and specificity were 90% and 75.6%, respectively, using 14 components.

Influential wavelengths that discriminated *U. pinnatifida* from common brown seaweeds, obtained from VIP scores (Figure 12), were in the green (574 nm) and the NIR spectral region (716-718, 720-721, 750 nm). Green seaweeds were discriminated from *U. pinnatifida* by 17 wavelengths in green (541, 547, 548 nm), red (601–604 nm) and NIR (717, 718, 724–731 nm) region with wavelengths in the red region being highly influential. Red seaweeds were discriminated from *U. pinnatifida* by 11 wavelengths in green (567–569 nm), red (698 nm) and NIR (703, 704, 716, 717, 720,

721, 750 nm) region. 22 influential wavelengths discriminated *U. pinnatifida* from all seaweed groups combined (Figure 12).

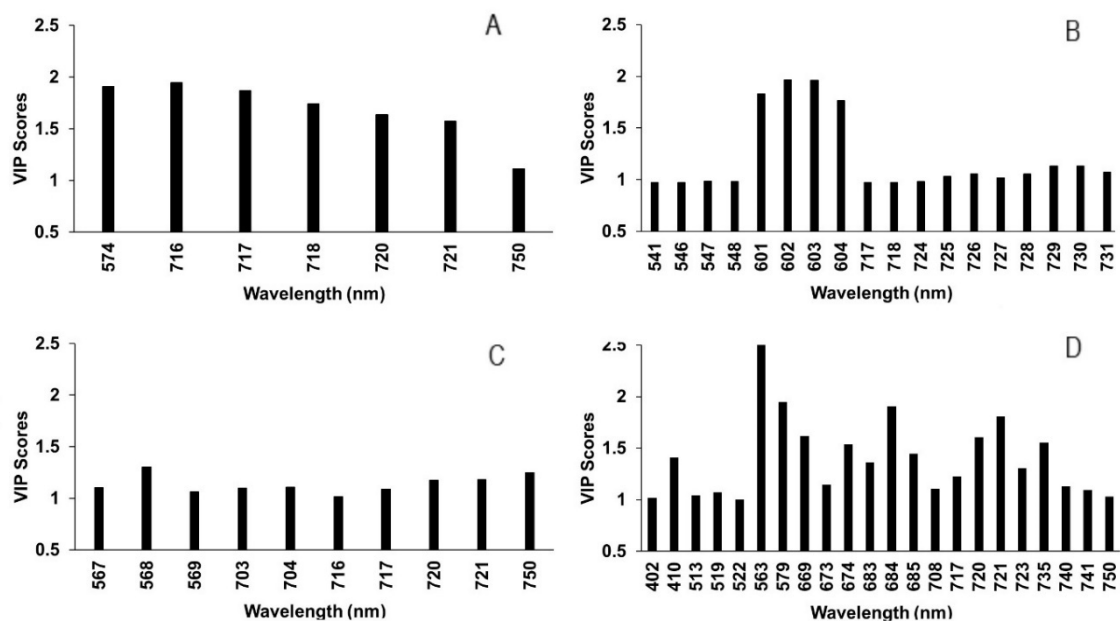


Figure 12: Influential wavelengths discriminating *Undaria pinnatifida* from other seaweed species in each of the four PLS-DA models – *U. pinnatifida* vs (A) brown, (B) green, (C) red and (D) all seaweed species. Each subplot shows the influential wavelengths in the X-axis and the degree of influence represented as VIP scores on the Y-axis.

Validation of the influential wavelengths extracted from the PLS-DA model

Standardised data were subjected to further validation using random forest classification with the wavelengths chosen from PLS-DA modelling. Random forest model out-of-bag error rates were 1.82% (*U. pinnatifida* vs all), 5.45% (*U. pinnatifida* vs brown), 3.64% (*U. pinnatifida* vs red) and 0% (*U. pinnatifida* vs green) (Table 6). The sensitivity of the random forest model remained the same as that of the PLS-DA model but the specificity of *U. pinnatifida* vs red random forest model increased by 2.8% and that of *U. pinnatifida* vs all model increased by 15.4% (Table 7). However, the specificity of *U. pinnatifida* vs brown random forest model decreased by 3% compared to that of the PLS-DA model, nevertheless, it remained high. Multidimensional Scaling (MDS) plot from the random forest models suggested clear grouping of the two classes in each

model, except for the *U. pinnatifida* vs all seaweed groups combined model (Figure 13) which has some individuals from the ‘None’ class overlapping the group of *U. pinnatifida* individuals.

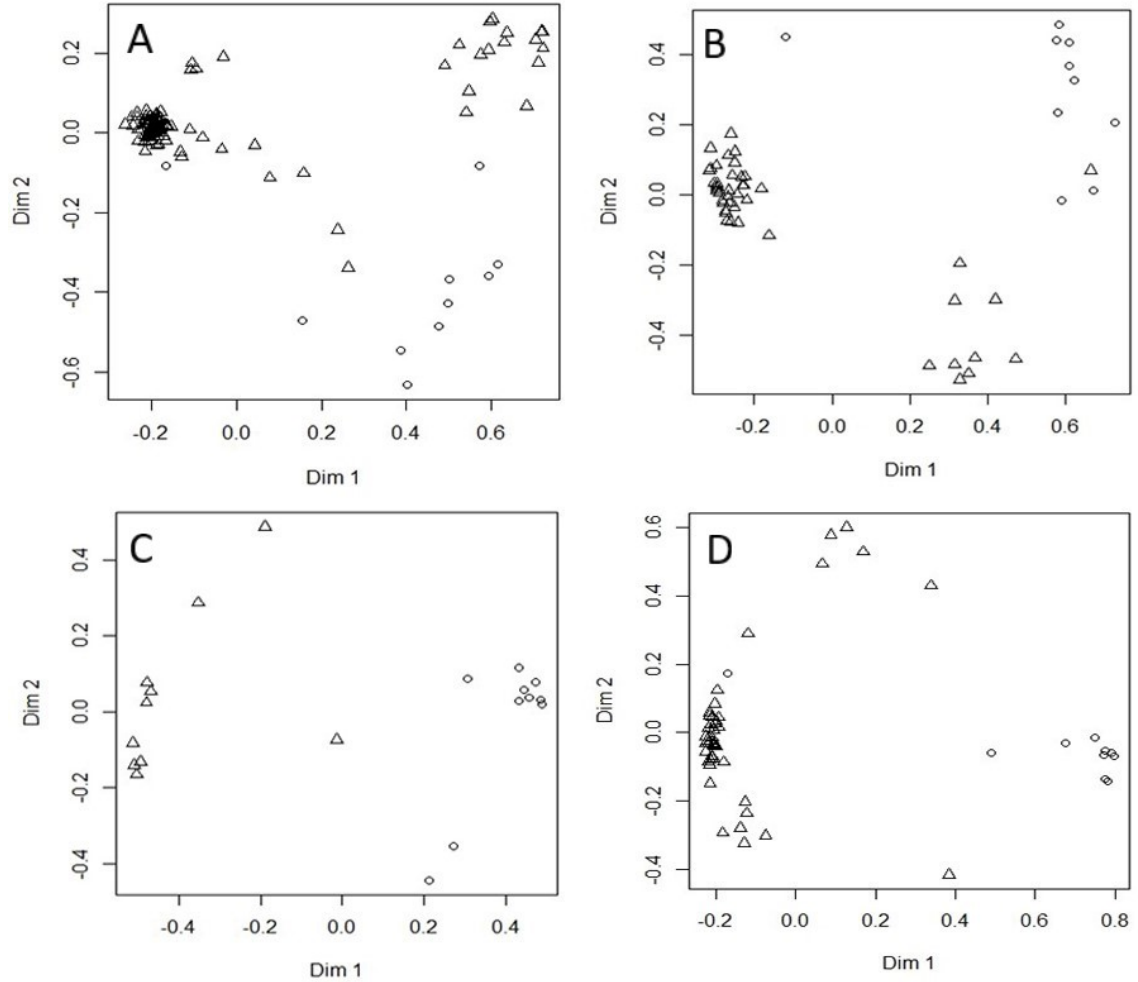


Figure 13: Multidimensional Scaling plots of two class random forest models – *U. pinnatifida* (circle) vs (A) all seaweed groups combined (triangle), vs (B) brown (triangle), vs (C) green (triangle), vs (D) red (triangle). X- and Y- axes are first and second dimension, respectively, in (n-1) dimensional cartesian space. ‘n’ is the total number of samples used in each model.

Table 6: Random forest model calibration parameter settings and performance statistics.

| U. pinnatifida vs | Brown | Green | Red | All |
|--|-----------------------------|--------------|------------|------------|
| Number of trees | 80 | 100 | 120 | 100 |
| Number of wavelengths tried at each split | 2 | 4 | 3 | 4 |
| OOB estimate of error rate | 5.45% | 0% | 3.64% | 1.82% |
| Class | Classification error | | | |
| None | 0.02 | 0 | 0.02 | 0 |
| UP | 0.2 | 0 | 0.1 | 0.2 |

Table 7: Model performance statistics from external validation using both random forest and PLS-DA techniques. Acc is accuracy, Sens is sensitivity, Spec is specificity, K is kappa, ncomp is the number of components selected for PLS-DA models and UP is *U. pinnatifida*.

| Model performance statistics – External validation of optimal models | | | | | | | | |
|---|------------|----------|-------------|-------------|---------------|-------------|-------------|--------------|
| Random Forest | | | | | PLS-DA | | | |
| | Acc | K | Sens | Spec | Acc | Sens | Spec | ncomp |
| UP Vs Brown | 0.977 | 0.937 | 1 | 0.969 | 0.907 | 1 | 0.879 | 5 |
| UP Vs Green | 1 | 1 | 1 | 1 | 1 | 1 | 1 | 6 |
| UP Vs Red | 0.889 | 0.727 | 1 | 0.857 | 0.822 | 1 | 0.771 | 15 |
| UP Vs All | 0.909 | 0.616 | 0.8 | 0.923 | 0.773 | 0.9 | 0.756 | 14 |

2.4 Discussion

This study provides the first detailed investigation of the spectral reflectance of New Zealand native seaweed species and their spectral differences from the wide-spread invasive seaweed *Undaria pinnatifida*. In the terrestrial environment, spectral libraries have been useful in investigative studies such as discriminating tropical wetland species (Prospere et al., 2014), mangrove species (Vaiphasa et al., 2007), and invasive wetland species (Laba et al., 2005). This study adds to some of the studies that have been

conducted on aquatic vegetation, particularly seaweeds (Casal et al., 2013; Fyfe, 2003; Kotta et al., 2014).

Species-level discrimination using remote sensing in aquatic or marine environments has been rarely successful (Fyfe, 2003), especially between species within a broad taxon (Casal et al., 2013; Kotta et al., 2014). However, this work demonstrated that it is possible to distinguish *U. pinnatifida*, a brown seaweed species, from other brown seaweeds with high accuracy and most of the discriminating wavelengths are in the NIR region. Casal et al (2013) found that not all species within a broad taxon showed discrimination but those that did, had differences at wavelengths in the NIR region. This clustering of influential wavelengths in the NIR region possibly explains the reason for discrimination of *U. pinnatifida* from other browns using lesser components compared to other models in PLS-DA. This is most likely because brown seaweeds have similar pigment composition and are mainly different in the NIR part of the spectrum which is affected by the blade structure (Cho et al., 2012). This clustering of wavelengths in one part of the electromagnetic spectrum would likely mean less confusion in discrimination comparatively. It is promising to note that there is a wavelength in the visible region of the spectrum (574 nm), which will not be attenuated as much with increasing water depth, that distinguishes *U. pinnatifida* from other native brown seaweed species. This was not detected in other species-level discrimination studies. This study offers a start to a deeper understanding of the spectral differences underpinning *U. pinnatifida* and other common native seaweed species for remote sensing applications.

Our research showed that discrimination of common native and invasive seaweed species in New Zealand at a broad taxonomic level (red, brown and green) is possible and the results concur with similar studies conducted globally (Casal et al.,

2013; Hochberg, 2003; Kieleck et al., 2001; Kutser et al., 2003). The MDS plots from the random forest models here suggest that red seaweed individuals may be more-readily discriminated from brown and green seaweeds. Although there was a clustering of brown and green seaweed groups, there is some degree of overlap in spectral qualities in multidimensional space. Red and brown seaweeds have similar, unique pigments such as phycoerythrin and chlorophyll-c that have absorption peaks at around 570 and 633 nm, respectively (Casal et al., 2012; Hedley and Mumby, 2002). Our results corroborate this with two of the influential wavelengths (571 and 634 nm) identified as influential in discriminating reds from browns and greens (Figure 9) and, browns from reds and greens (Figure 9). Kutser et al (2003) found similar results where red seaweeds were discriminated from browns (at 570 nm) and greens (at 550 nm). Other influential wavelengths identified in this study e.g. 567, 572, 657 and 658 nm are the same as those identified by Kotta et al (2014). Although these results are not surprising because the pigment composition is diagnostic for algal groups, it shows the algorithms used in the study are fit for further exploration such as discrimination at the species level.

Sensitivity and specificity of class '*U. pinnatifida*' during external validation was high for all PLS-DA models except for *U. pinnatifida* compared to browns + greens + reds where sensitivity and specificity were 90% and 75.6%, respectively. In applications such as mapping invasive species, sensitivity is more important than specificity even at the cost of little specificity. Misclassification can be expensive and uneconomical but the consequences of missing the invasive species can be disastrous (Pyšek et al., 2012; Schmidt et al., 2012). Across our models, the sensitivity and specificity of the random forest models were better than that of PLS-DA, suggesting that PLS-DA may be better-suited for feature/wavelength selection than classification. Of some of the plant species discrimination studies using PLS-DA techniques on

hyperspectral imagery in a terrestrial environment, Peerbhay et al (2013) and Möckel et al (2014) both achieved better classification accuracies for predictive models using variables selected via PLS-DA. On the other hand, using the same selected features, the random forest models classified the testing data better than PLS-DA. This is consistent with the conclusions drawn by Dye et al (2011) that, regardless of the number of wavelengths selected, the classification accuracy remained high with the random forest model.

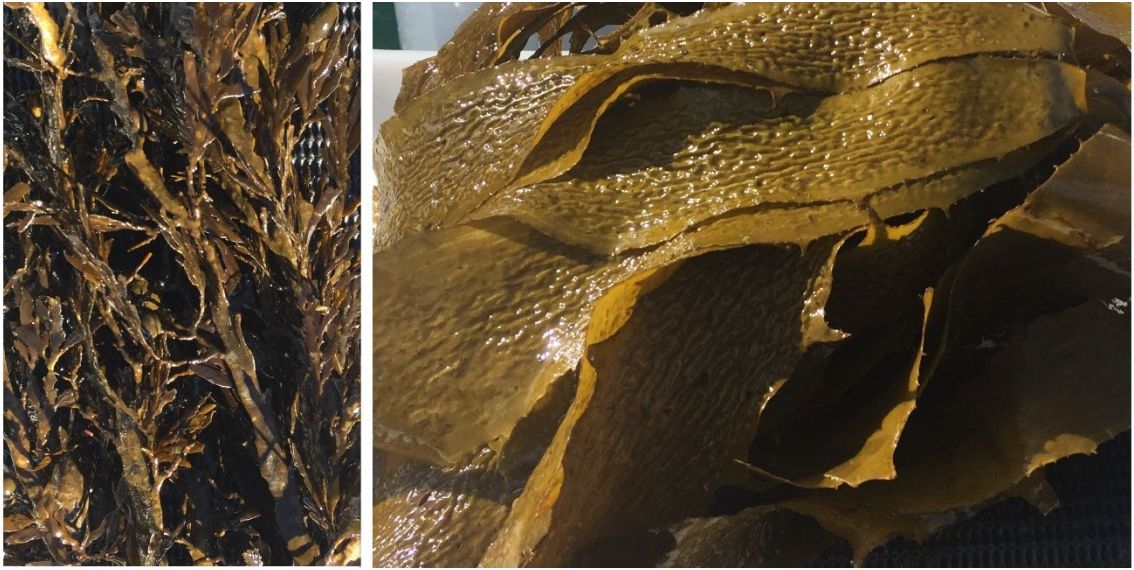
It was expected that *U. pinnatifida* would be discriminated from green and red seaweed species based on the difference in colour. However, it was unclear whether *U. pinnatifida* could be discriminated from common brown seaweeds since there are not many studies supporting successful intra-taxon separation. Results from PCA, PLS-DA and random forest at fine-scale, confirm it is possible to discriminate *U. pinnatifida* from green and red and indeed from other brown seaweed species with high accuracy. Results also indicate that *U. pinnatifida* can be distinguished from each broad seaweed taxa separately with greater accuracy than from all combined. Such a fine-scale approach proved successful in other aquatic applications and some of these studies scaled high-resolution spectral reflectance down to commercially available imaging sensors to assess the suitability for aquatic vegetation mapping (Casal et al., 2013; Fyfe, 2003; Vahtmäe and Kutser, 2013). *U. pinnatifida*, a classified unwanted organism by the New Zealand Ministry of Primary Industries, needs constant monitoring to stop its invasion into pristine environments such as Fiordland (MPI, 2019). These results give promise to the possibility of developing a remote sensing survey solution for mapping *U. pinnatifida*. A tailored solution to identify *U. pinnatifida* specifically would not only be accurate but also quicker and cost-effective to map and, cover larger areas in a short time compared to conventional methods.

The wavelengths used for this study were expanded to include the NIR region of the spectrum even though water strongly absorbs those wavelengths. Studies in a controlled setting have shown that algorithms can be developed to improve the reflectance in the NIR region of the spectrum (Cho and Lu, 2010; Lu and Cho, 2011). However, this retrieval depends on the sensor's signal-to-noise at those wavelengths along with environmental conditions. Since most of the wavelengths that discriminate *U. pinnatifida* from other common native brown seaweeds lie in NIR region, and *U. pinnatifida* is usually found in low intertidal/sub-tidal zones (James and Shears, 2016b; MPI, 2016) where water absorption is high in NIR region, further studies accounting for depth and turbidity would help understand the possibility of discrimination in a real-world scenario.

2.5 Conclusions

This study is the first step towards discriminating seaweed species at all levels with high accuracy, including within brown taxa. Further steps include investigation of differences due to location, season, water depth, and water clarity. Ultimately, spectral discrimination of *U. pinnatifida* will require integration of all these factors into operational retrieval algorithms that can utilize existing or forthcoming remote sensing systems.

Chapter 3. Effects of location and season on seaweed spectral signatures



Chapter 3 cover picture. Two seaweed species used in this study, *Carpophyllum maschalocarpum* (left) and *Ecklonia radiata* (right).

This chapter is published in a peer-reviewed journal. In this chapter, spectral signatures of two common NZ native seaweed species were collected across four different locations in the Hauraki Gulf in different seasons. This is the first comprehensive study on the effect of season and location on spectral signatures of seaweed. The results of the study will help make decisions on remote sensing data acquisition or using appropriate spectral signatures for data already acquired.

Spectral readings from 224 seaweed individuals (*E. radiata* and *C. maschalocarpum*) across four locations and over four seasons were acquired and analysed. Both the seaweed species showed separation from each other with little overlap. The study also showed season affected the spectral reflectance significantly.

3.1 Introduction

Remote sensing surveys use multispectral and hyperspectral sensors to map vegetation based on the unique spectral signature of the individual plant species. Typically for healthy plants, there is low spectral reflectance in the visible region and high reflectance in the near-infrared region of the spectrum attributed to its biochemical and biophysical properties (Clark et al., 2005). Effects of physiological stress due to disease, insects or drought change the plant's spectral signature and such characteristic spectral features can be exploited (using remote sensing) to address mass scale outbreaks by early detection (Abdullah et al., 2018; Kanemasu, 1974; Silva et al., 2008). However, in the terrestrial environment, there is also spectral variability within a single healthy plant due to natural variations such as season, substrate features, illumination or phenological stages (Bue et al., 2015; Silva et al., 2008) which if accounted for, can improve mapping accuracy (Somers and Asner, 2014).

Anthropogenic activities such as urbanisation, deforestation and farming directly impact the coastal environment globally (Seers and Shears, 2015), especially benthic seaweed communities (Benedetti-Cecchi et al., 2001), by reducing the amount of light that these communities receive for photosynthesis. These effects are of growing concern to fast urbanising New Zealand, particularly in the Hauraki Gulf located on the northeast of North Island (Blain and Shears, 2019). The Hauraki Gulf is home to riverine estuaries, sheltered harbours, coastal beaches and open-coast shores with recreational, cultural and economic importance (Seers and Shears, 2015) and high impacts of sedimentation on the coastal environment makes it essential to monitor the health of its benthic habitats (Kelly, 2014). Besides, seaweeds are affected by other natural factors such as season, varying growth cycle in different seasons, nutrient flow or environment conditions (Fung et al., 2013; Kotta et al., 2014). While spectral variability due to natural variations are being explored in terrestrial environment and

seaweeds are being mapped using satellite/aerial data around the world (Uhrin and Townsend, 2016), very little research has investigated the variability of spectral characteristics of seaweeds.

Reflectance properties of a species of marine vegetation can vary spatially and seasonally (Fyfe, 2003). There is little information on reflectance properties of a single marine vegetation species at different seasons (Casal et al., 2013). Researchers who have undertaken studies on eelgrass mapping in shallow waters in Canada (O'Neill et al., 2011), discrimination of invasive seaweed *Caulerpa* species in the Mediterranean (Kišević et al., 2011) and seaweeds in Baltic Sea (Kotta et al., 2014) have all recommended more research on reflectance properties of individual species across different seasons and locations for wide-scale mapping applicability, accurate characterising of the discriminating spectral features of the species in question or true representation of training dataset for spectral library classification approach.

Spectral signatures from hyperspectral data enable us to identify the subtle differences in plant species better than multispectral datasets despite the common chemical composition within species (Cochrane, 2000; George et al., 2014). Therefore, in this study, using hyperspectral data, we analyse the effects of location and season on spectral characteristics of two commonly found, dominant, habitat-forming seaweed species, *Ecklonia radiata* (C. Agardh) J. Agardh. and *Carpophyllum maschalocarpum* (Turner) Grev. in the Hauraki Gulf.

3.2 Materials and Methods

3.2.1 Seaweed collection and spectral measurements

Seven individuals of each species, *Ecklonia radiata* and *Carpophyllum maschalocarpum*, were collected from each of four locations (Figure B-1) located approximately 10km apart from Te Haruhi Bay (174° 49' 2" E, 36° 37' 5" S) north to

Motuora Island (174° 47' 36.59" E, 36° 30' 30.31" S), Kawau Island (174° 52' 33.02" E, 36° 27' 3.93" S), and Takatu Point (174° 51' 59.89" E, 36° 22' 12.18" S) in Autumn (October 2017), Spring (April 2018), Winter (June 2018) and Summer (December 2018). Seasons were chosen as December to February (summer), March to May (autumn), June to August (winter), September to November (spring). Spectral readings of seaweed individuals, taken out of the water and placed on a black mat, were measured using ASD Handheld-2 field spectrometer with a wavelength range of 325 – 1075 nm and 1 nm sampling interval. The spectrometer was held at 10 cm above the individuals looking at nadir and ten readings of each seaweed individual over blade and stipe were recorded. Several calibration readings were taken depending on the cloud conditions using the Spectralon® panel. Readings in each location were recorded within an hour of taking the samples out of water. Every effort was taken to collect the readings within 2 hours of solar noon but some were collected beyond the range and the location description was recorded (Table B-1).

3.2.2 Data analysis

3.2.2.1 Data pre-processing

The spectral data set from seven individuals of each seaweed species from four seasons and four locations comprised: 1120 readings for *C. maschalocarpum*, 1119 readings for *E. radiata*, 350 numeric wavelengths of the reflectance values between 400–750 nm and the categorical variables “seaweed species”, “season” and “location”. There is a missing data point for *E. radiata* due to an erroneous reading. The wavelengths included those that lie within the water transmission window (450–550 nm) (Kieleck et al., 2001) as well as the NIR region that shows the greatest discrimination between species (Fyfe, 2003). The data were standardised using the Standard Normal Variate (SNV) technique. SNV scaling was performed on the data across the columns for each row to remove multiplicative noise from each spectrum (Wehrens, 2011). It was performed by

subtracting the mean of values at all wavelengths, for each spectral signature, from the reflectance values at each wavelength and dividing the difference by standard deviation of the spectrum (Kotta et al., 2014).

3.2.2.2 *Qualitative separation of seaweed species*

Principal Component Analysis (PCA) was performed to qualitatively assess the separation between *E. radiata* and *C. maschalocarpum*. In case of good separation of the two species, the seaweeds were assessed for spatial and seasonal effect, separately. R statistical software package was used for the analysis (Team, 2019).

3.2.2.3 *Spatial and seasonal variability in spectral reflectance*

Due to the high dimensionality of the data, it was decomposed to a few principal components (PCs) that encompassed the variation from influential wavelengths. This was implemented using PCA on the standardised data for the two seaweed species, separately. Principal component (PC) with most variance was chosen and the wavelengths that influenced this PC were selected based on the loading values using ‘factoextra’ package in R software (Kassambara and Mundt, 2017). For each seaweed species, to identify a significant difference in spectral reflectance across various locations and seasons, a linear mixed-effect model was built with each contributing PC as the response variable, location and season as fixed effects, and seaweed individuals as the random effect. The difference between the individuals due to any in-plant variation in each location and season was modelled by the random effect. The linear mixed model separates the variance due to random sampling from the fixed effect (Zuur et al., 2009). The explanatory variables location, season and seaweed individuals were factor variables with four, four and seven levels, respectively. The full model was built including both location, season and the interaction between the two using maximum likelihood (ML) method which was compared against a model with a term dropped

(Table B-2). The best model was selected using Akaike Information Criterion Vaiphasa, Skidmore, de Boer, and Vaiphasa (2007) and the full model was run with all the terms included using the method Restricted Maximum Likelihood (REML). ‘nlme’ package in R was used for this analysis (Pinheiro et al., 2018). The final model prediction plot with +/- 2 Standard deviations at 95% confidence interval was plotted using ‘AICcmodavg’ package in R software (Mazerolle, 2019). The goodness-of-fit of the model was assessed using marginal and conditional R^2 value suited for the mixed-effects model (Nakagawa et al., 2013) and implemented using ‘MuMIn’ package in R software (Barton, 2018). Marginal R^2 value explains the variance due to fixed effects, conditional R^2 value explains the total variance due to fixed and random effects.

3.3 Results

3.3.1 Data pre-processing and PCA

PCA on SNV data of the two seaweed species combined showed clear grouping of *E. radiata* and *C. maschalocarpum* with the maximum variance of 86.5% on the first PC. The two seaweed species were separated (Figure 14) for further analysis of the effect of location and season on spectral reflectance using a linear mixed-effects model.

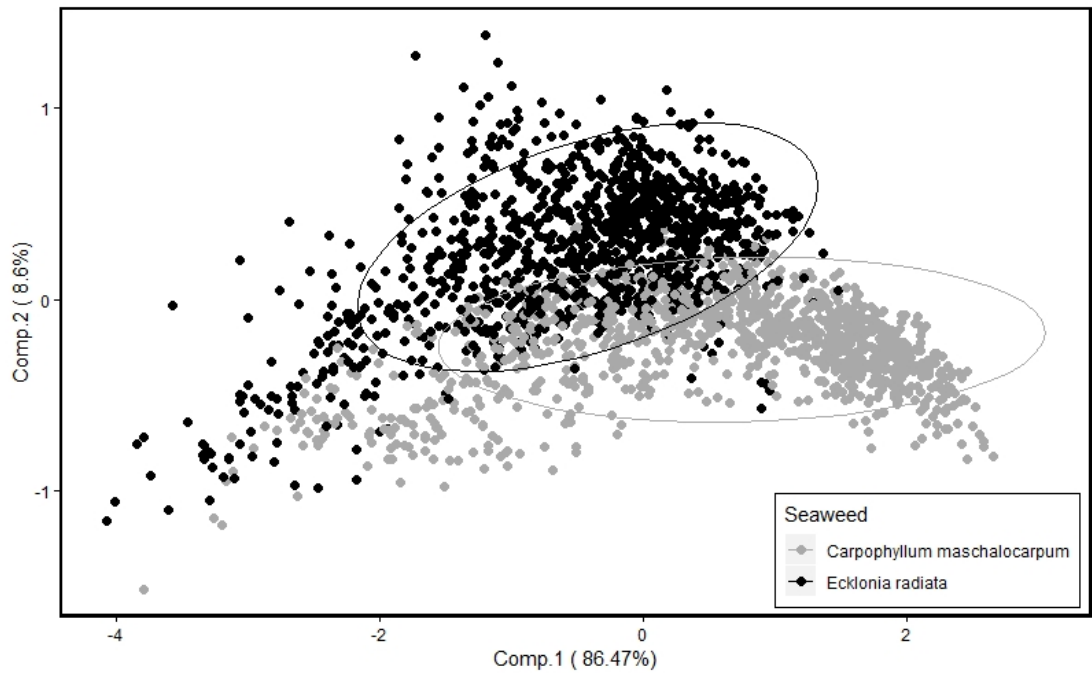


Figure 14: Principal component analysis of *Ecklonia radiata* and *Carpophyllum maschalocarpum* showing the separation of the two seaweed species

3.3.2 Spatial and seasonal variation on the spectral reflectance of *Carpophyllum maschalocarpum* using linear mixed modelling

PCA on standardised spectral data of *C. maschalocarpum* resulted in the maximum variance in the first PC (93.4%).

3.3.2.1 Variables contributing to PC1

Based on loading values, wavelengths that contributed to the variation in PC1 were 597–608 nm, 693–718 nm and 733–750 nm (Figure B-2). The spectral reflectance values of influential wavelengths between 733–750 nm were positively correlated to PC1 scores while that between 597–608 nm and 693–718 nm are negatively correlated and the latter has a higher magnitude.

3.3.2.2 Effect of season and location on PC1

The results of mixed effects modelling on PC1, using likelihood ratio test, showed that location, season and the interaction between them had significant effect on standardised spectral reflectance of *C. maschalocarpum*. Data is more likely under model A than it is

under model B ($L = 197.02$ ($df = 9$, $p < 0.001$)) or model C ($L = 1433.19$ ($df = 12$, $p < 0.001$)) or model D ($L = 423.77$ ($df = 12$, $p < 0.001$)). The final model A performed well with marginal and conditional R^2 of 0.735 and 0.741, respectively.

Winter and spring affect spectral reflectance at wavelengths between 733 – 750 nm but there was no significant difference between the two seasons at each location (Figure 15). However, in summer, spectral reflectance between 693–718 nm described *C. maschalocarpum* in Motuora Island and was significantly different compared to the rest of the locations. The spectral reflectance between 597–608 nm described the seaweed in Autumn across all locations.

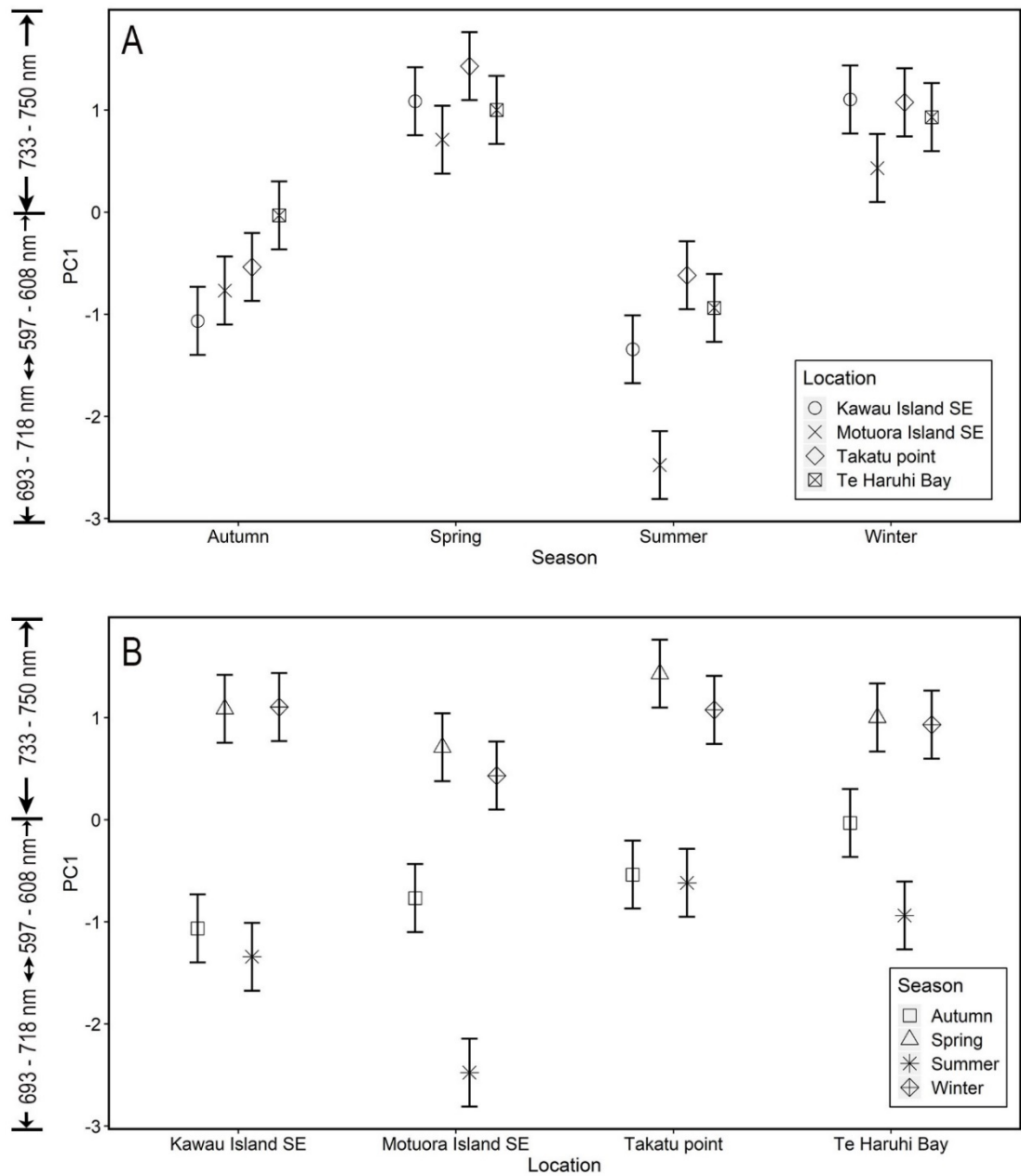


Figure 15: (A) Model predictions plot with two standard deviations (and 95% confidence interval) of PC1 for *Carpophyllum maschalocarpum* in different locations within each season, X-axis represents seasons and Y-axis represents PC1 scores and the interpretation of wavelengths contributing to PC1 axis (B) Model predictions plot with two standard deviations (and 95% confidence interval) of PC1 for *Carpophyllum maschalocarpum* in different seasons within each location, X-axis represents locations and Y-axis represents PC1 scores and the interpretation of wavelengths contributing to PC1 axis.

3.3.3 Spatial and seasonal variation on the spectral reflectance of *Ecklonia radiata* using linear mixed modelling

PCA on standardised spectral data of *E. radiata* resulted in the maximum variance of 83.4 % in first PC and variance of 9.3% in the second PC.

3.3.3.1 Important variables contributing to components PC1 and PC2

Based on loading values, wavelengths that contributed to the variation in PC1 were 572–613 nm, 693–715 nm and 730–750 nm (Figure B-3). The spectral reflectance values in wavelengths between 730–750 nm are positively correlated to PC1 scores while that between 572–613 nm and 693–715 nm are negatively correlated and the latter has a higher magnitude.

3.3.3.2 Effect of season and location on PC1

The results of mixed-effects modelling on PC1, using the likelihood ratio test, showed that location, season and the interaction between them had a significant effect on wavelengths that contributed to PC1. The test revealed that data is more likely under model A with AIC of 2522.54 than it is under model B ($L = 479.82$ ($df = 9$, $p < 0.001$)) with AIC of 2984.36 or model C ($L = 616.35$ ($df = 12$, $p < 0.001$)) with AIC of 3114.89 or model D ($L = 570.21$ ($df = 12$, $p < 0.001$)) with AIC of 3068.75. The final model A performed well with marginal and conditional R^2 of 0.457 and 0.465, respectively.

Autumn and spring had a similar effect pattern on the spectral reflectance values in wavelengths 572–613 nm in all locations (Figure B-4A). There was no seasonal effect on spectral reflectance values in wavelengths 730–750 nm that described the *E. radiata* in Kawau Island (Figure B-4B).

In summer, the wavelengths that described *E. radiata* in Motuora Island and Te Haruhi Bay were 693–715 nm and, in Kawau Island and Takatu point were 730–750 nm (Figure B-4A). Location does not have a significant effect on the spectral reflectance of *E. radiata* in winter and the seaweed was described by wavelengths between 730–750 nm.

3.4 Discussion

This study provides the first detailed investigation into the influence of season and location on the spectral signatures of *E. radiata* and *C. maschalocarpum* and addresses the shortcomings of past research that did not account for natural variations. Season and location were expected to affect the spectral reflectance of the two commonly found New Zealand native seaweed species. This study has found that wavelength regions describing *E. radiata* and *C. maschalocarpum* varies with season within each location which is indicated by significant location and season interaction in the mixed-effects modelling. The result of this study is consistent with other studies that account for temporal and spatial variation in terrestrial (Somers and Asner, 2014) and marine environments (Fyfe, 2003).

The season affects spectral reflectance of *E. radiata*. The wavelengths that describe *E. radiata* varies in summer but remains the same in winter (730–750 nm) across all locations. This indicates that the lowest irradiance level is in winter and the subsequent increase in Chlorophyll-a pigment (Blain and Shears, 2019) levels remain the same across all locations. Photosynthetic pigments such as Chlorophyll-a and accessory pigments such as Chlorophyll-c and Fucoxanthin present in brown seaweeds such as *E. radiata* and *C. maschalocarpum* are responsible for the unique spectral signatures depending on the pigment concentration levels (Casal et al., 2012). Although it is reported that the wavelengths correlated to Chlorophyll-a are in green (550–560 nm) and red edge (680–750 nm) region, it is difficult to quantify the concentration levels of individual pigments remotely (Huang et al., 2015). In summer, the wavelengths that describe *E. radiata* in Motuora Island and Te Haruhi Bay is different from that in Takatu point and Kawau Island. This is likely due to the high irradiance levels in summer (Blain and Shears, 2019) and varying wave exposure levels in different locations, for example, sites in Te Haruhi Bay and Motuora Island are

sheltered while that in Kawau Island and Takatu point are very exposed. Variations in the degree of water movement around plants among other factors influence photosynthesis (Hillman et al., 1989) and in turn, affects the spectral response of seaweed.

There is a very different seasonal pattern exhibited in spectral data of *C. maschalocarpum* across all locations compared to *E. radiata* despite both species being collected from the same locations. *C. maschalocarpum* individuals were spectrally similar across all locations in winter and spring and were described by wavelengths 733 – 750 nm. This is likely due to the lower irradiance levels during those seasons and no chlorophyll production. However, in summer, the wavelengths (597–608 nm and 693–718 nm) that described *C. maschalocarpum* varied significantly from those in spring and winter. Expectedly high photosynthetic activity in summer may likely cause some variation in wavelengths describing *C. maschalocarpum* in different locations (Figure 15A). The spectral reflectance values of both seaweed species in summer is significantly different in Motuora Island compared to other locations (Figure 15B and Figure B-4B). This could be due to the nature of the location (Table B-1) enabling higher photosynthetic activity.

Multispectral and hyperspectral sensors have the capability of capturing high resolution (spatially and spectrally) data that could resolve individual seaweeds. Due to the nature of the water current and movement of seaweed underwater, it is important to understand the within plant spectral variation across various parts of the seaweed individual such as blade and stipe. This study accounts for that variation and has found very low spectral variation within each sample indicated by the minimal difference between marginal and conditional R^2 values of mixed modelling for both species.

Detecting within species spectral variation due to factors such as season and location using remote sensing imaging sensors could be difficult. When combined with other factors such as water column properties, depth and turbidity, detecting these inherent within-species differences could prove more difficult. Modelled spectral signatures have been used for distinguishing three seaweeds belonging to each broad taxon at different turbidity levels and depths (Vahtmäe et al., 2006), classifying seaweeds at a broad taxa level from hyperspectral images (Casal et al., 2013). However, spectral signatures from this study could be modelled for various water column properties using radiative transfer models or approached empirically for further research.

Chapter 4. Discrimination of *Undaria pinnatifida* from *Ecklonia radiata* using multispectral unmanned aerial vehicle (UAV) images and hyperspectral data: Role of depth and turbidity

4.1 Introduction

Undaria pinnatifida, an invasive seaweed in New Zealand (NZ) but native to Japan, has spread all over the coast and human-made structures in NZ. Biosecurity NZ has it classed as ‘under management’ (NIWA, 2020). Along the Otago coastline, Russell et al. (2007) found that in wave-dominated shores *U. pinnatifida* extends into habitats of *Lessonia variegata* and *Marginariella boryana*; in deeper sheltered subtidal areas *U. pinnatifida* invaded *Macrocystis pyrifera* forests and competed with *Ecklonia radiata* and *Landsburgia quercifolia*.

Current seaweed monitoring/management techniques include manual SCUBA surveys which can be time-consuming and expensive (Flynn and Chapra, 2014). Remote sensing is a powerful tool to map such invasive plant species over a large extent in both terrestrial and aquatic environments (Bradley, 2013; Kišević et al., 2011). Previous research used high spatial resolution (0.5m to 2.5m) multispectral data such as IKONOS, QuickBird, SPOT and WorldView to map substrates such as coral, emerged and submerged seaweed classes, floating seagrass or seaweed wrack, sand and rock in the aquatic environment at a broad level due to the width of multispectral bands (Casal et al., 2011a; Deysher, 1993; Lekan and Coney, 1982; Reshitnyk et al., 2014; Sagawa et al., 2012; Wezernak and Lyzenga, 1975). Hyperspectral sensors have found detailed terrestrial applications such as the derivation of various indices to study water and chlorophyll content (Haboudane, 2002; Penuelas, 1997), identification of markers for plant diseases (Mahlein, 2013) and even discrimination of spectrally similar crops (Manjunath et al., 2011) or tree species (Peerbhay et al., 2013; Somers and Asner,

2014). Whereas in the marine environment, hyperspectral sensors such as CHRIS PROBA and Airborne Hyperspectral Scanner have been able to discriminate seaweeds at taxa level and from other substrates underwater (Casal et al., 2012; Casal et al., 2011). Although the spectral resolution is very high (>18 spectral bands), sometimes the taxa level discrimination does not yield high accuracy due to heterogeneity of the seaweed patch and insufficient spatial resolution (Ashraf et al., 2010; Casal et al., 2011). Also, the collection and processing of hyperspectral imagery can be quite expensive, depending on the size of the area to be studied (Cho et al., 2012).

A multispectral or hyperspectral sensor carried on a UAV, a popular low-cost remote sensing platform, presents a promising solution for seaweed mapping as it offers a high spatial, temporal and spectral resolution. Rossiter et al. (2020) utilized a hyperspectral imaging sensor onboard UAV to assess an intertidal seaweed community, especially an ecologically important brown seaweed species, *Ascophyllum nodosum*, and is the only study of this kind. However, such hyperspectral imaging sensors produce high dimensional voluminous data (Adão et al., 2017; Dye et al., 2011; O'Neill et al., 2011), make UAV integration difficult due to weight (Jakob et al., 2016) and the sensors are very expensive making it disadvantageous for such applications. There are miniature hyperspectral spot spectrometers and ever-evolving multispectral imaging sensors such as Micasense's Rededge-m that are lightweight and lower-cost solutions. von Bueren et al (2015) compared four different sensors (Infrared camera, RGB camera, multispectral camera and STS miniature spot spectrometer) onboard a UAV platform for correlation of reflectance across the wavelengths between sensors and ASD field spectrometer over the grassland. He found that STS and ASD reflectances were similar but different in magnitude, the multispectral sensor showed a low correlation with STS and ASD in green and red bands. Doughty and Cavanaugh (2019) used a RedEdge sensor onboard UAV to study the variation in saltmarsh biomass and productivity at

fine spatial and temporal scale. Taddia et al (2019) used a RedEdge-m sensor to detect submerged seaweed in shallow water over some time. These multispectral sensors are purpose-built for terrestrial vegetation mapping, with many studies on terrestrial vegetation, but they have not been extensively used for mapping submerged aquatic vegetation such as seaweeds especially at species level at fine spatial scales.

Traditional satellite- and air-borne images used for marine habitat mapping have large footprints, and the study area may not need a lot of images to cover the area of interest. Also, the images will include some land features which will be used for collecting keypoints between scenes to match and mosaic into single geo-rectified image in a semiautomated fashion. Whereas, the need for ultra-high spatial resolution often results in smaller UAV footprint (due to reduced flight height) and therefore increases the number of images needed to cover the study area. Proprietary software such as Pix4D Mapper pro or Agisoft PhotoScan professional automates UAV image processing by converting raw digital numbers (DNs) to reflectance and employing a structure from motion (SfM) method to match several keypoints in multiple images to build a point cloud of the study area. They often use ground control points (GCPs) to create an accurately georeferenced ortho-rectified image mosaic. This method works well for a terrestrial application where several keypoints can be identified and GCPs located before the survey due to the static nature and accessibility of most of the environment. Unlike terrestrial environment, an aquatic environment is dynamic and harder to obtain enough keypoints from the imagery, especially if the UAV image footprint is covered entirely with water. Georeferencing such images in these circumstances fail. For example, some images in the study by Taddia et al. (2019) failed to align due to lack of keypoints. In such cases where GCPs cannot be obtained, direct georeferencing is the key. Direct georeferencing enables imagery to be georeferenced without GCPs (Turner et al., 2014) and the technique is only as accurate as of the

Global Positioning System (GPS) and Inertial Measurement Unit (IMU) associated with the sensor used. While it is cost-effective to use UAV over traditional airborne platforms for high accuracy surveys, it is crucial to automate or semi-automate image processing to minimise costs (Turner et al., 2014). Currently, there are image processing python libraries that help with converting raw data from RedEdge-m sensor to reflectance (Micasense, 2018). With no software readily available for processing UAV images over the marine environment, a flowline for single image processing and direct-georeferencing would be beneficial.

Previous studies have shown that it is easier to discriminate seaweeds at broad taxa level than at species level but most species within a group showed variability (Casal et al., 2013; Fyfe, 2003). Chapter 2 studied the importance and lack of seaweed spectral library in NZ, discriminated some of NZ seaweeds at taxa level and discriminated *U. pinnatifida* from rest of the brown seaweed species. It also identified key wavelengths suitable for discrimination at both levels. While this discrimination study was using the in-air spectral library (seaweed individuals were taken out of water for spectral measurements), it was important to conduct a similar study with the effect of water depth and turbidity since *U. pinnatifida* is subtidal to over 10m deep. Water absorbs light energy in red and longer wavelengths of the spectrum (Silva et al., 2008) and reflectance in most of the wavelengths useful for discriminating seaweed lie in the red and near-infrared (NIR) region of the spectrum are lost with the increasing water depth (Vahtmäe and Kutser, 2013). Turbidity, determined by the constituents in the water column such as phytoplankton, suspended organic and inorganic matter, promotes spectral scattering thereby affecting the spectral reflectance properties of submerged vegetation (Pu et al., 2012). Casal et al (2013) modelled spectra for many seaweed species belonging to three broad taxa level (red, green and brown) to obtain spectra at various depth levels for defined turbidity level and found that the seaweeds were

separable at taxa level down to 4m depth. Vahtmäe and Kutser (2013) mapped high order vegetation, *charophytes*, filamentous green algae, using CASI and Worldview-2 data with high accuracy down to a depth of 2m. It was optically too deep beyond 2m to map any substrates. The effects of depth and turbidity on spectral reflectance of seaweeds have been widely studied around the world, however, such a study is lacking for seaweeds in New Zealand.

In this study, I created a spectral library of invasive seaweed *U. pinnatifida* and common NZ native seaweed *E. radiata* at five depth levels and two turbidity levels. I also acquired ultra-high spatial resolution multispectral data of the two seaweed species at different depth and turbidity levels using RedEdge-m sensor onboard UAV. I look to answer the following questions using the above-mentioned data:

- Do depth and turbidity affect the spectral signatures of invasive seaweed *U. pinnatifida* and common NZ native seaweed *E. radiata*?
- Is it feasible to discriminate the two seaweed species in a water depth of down to 2m in two turbidity levels using the five bands of RedEdge-m multispectral sensor and wavelengths identified in Chapter 2?
- Can *U. pinnatifida* and *E. radiata* be reliably discriminated using ultra-high spatial resolution multispectral (RedEdge-m) data? If so, up to what depth can it be discriminated?

4.2 Materials and Methods

4.2.1 Spectral data collection and processing

An experiment was designed to collect spectral signatures of *E. radiata* and *U. pinnatifida*. This will be referred to as the ‘depth experiment’. The setup included two frames of 2m and 1m height made of polyvinyl chloride (PVC) pipes that slid into each other. The 2m high frame had a white plate at the base for placing seaweed samples on

and the 1m frame held the spectrometer on the top (Figure 16). A mini-spectroradiometer called STS-VIS (STS-VIS, 2020) with a spectral range of 350-800 nm was used (Figure 17). It was set up with a field of view (FOV) of 3 degrees, the integration time of one second, boxcar width of two and average of five scans for each reading. A green laser (560nm) was attached parallel to the spectroradiometer as a guide to identifying the sampling area. The PVC frame was marked at every 50 cm for easy referencing of depth at the time of measurement. Before the experiment, a Secchi disk was used to get a measure of turbidity. The disc, with black and white marked quarters, was immersed in the water at the study area until the depth at which the disk is not visible anymore. A lower value of Secchi depth indicates higher turbidity level and vice versa.

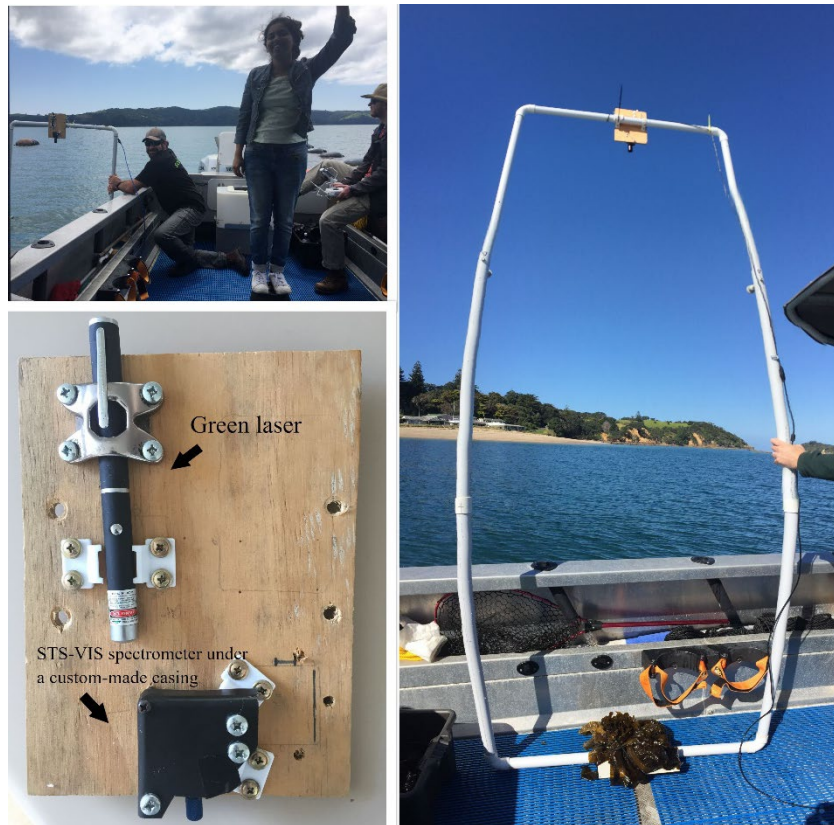


Figure 16: Panoramic shot of depth experiment setup with STS-VIS spectrometer on the top and white base plate for holding seaweed on the bottom (right), team assisting with the depth experiment for moving the setup through the water column, changing the depth and seaweed individual identifiers on top of the boat and flying the UAV at the same time as the experiment while I was validating and collecting spectral readings on the computer (top left), a wooden plate with STS-VIS spectrometer setup that was attached to the top of the PVC setup (bottom left). Bowing of the structure is an artefact of the panoramic shot.



Figure 17: STS-VIS spectroradiometer used for collecting hyperspectral data over the depth experiment.

Five to ten individuals of subtidal seaweeds *U. pinnatifida* and *E. radiata* were used for this experiment over two days (Table 8). Seaweed samples were collected in October and November 2018 from Awakiriapa Bay in Waiheke Island. *U. pinnatifida* and *E. radiata* samples were collected on snorkel from mussel farm and adjacent rocky reefs respectively. The snorkeller observed the abundance of both the seaweed species along the rocky reef. The experiment was carried out near the mussel farm as it was sheltered for calmer water conditions (Figure 18). Dark noise reading of STS-VIS spectrometer was measured by closing the optical fibre with the cap after a 30-minute warm-up time. This set of values were subtracted from all the irradiance measurements. A white base was used for calibration in the field and was later calibrated with a known reference, a Spectralon® panel, separately. This set of values were used for calculating spectral reflectance of the seaweed samples to a known standard. After calibration measurements, each seaweed individual was placed on the base of PVC setup and absolute irradiance was recorded at six different points –just below the surface (<0.1m) (D1), 0.5 m (D2), 1m (D3), 1.5m (D4) and 2m (D5) as the setup went downwards and upwards the water column. This was achieved by immersing the PVC setup and recording the readings at each depth as it went down and came back up the water column. The height of the sensor above the water surface varied at spectral measurements at each depth from ~3m to minimum of 1m. The influence of this variability on the resulting spectral reflectance is assumed to be minimal. Calibration measurements to correct for irradiance conditions were taken every hour or when the conditions change.

Table 8: Information on sample, sea state and sky condition

| Date | Seaweeds | Individuals per seaweed species | Secchi depth (m) | Wind | Sky condition |
|------------|--|---------------------------------|------------------|------------|---|
| 24/10/2018 | <i>U. pinnatifida</i> , <i>E. radiata</i> | 5 | 6 | Very windy | Cloudy to start with and cleared during the day |
| 23/11/2018 | <i>U. pinnatifida</i> , <i>E. radiata</i> | 10 | 3.25 | No wind | Clear sky |

Files from STS-VIS spectrometer were downloaded in ‘.txt’ format. Each file contained irradiance values of seaweed individual for wavelengths between 335 – 822 nm. Text files were processed in the R statistical software package to combine them into one data frame. Details of each spectrum such as the species name, depth, Secchi depth, date, replicate number were added to the data frame. The STS-VIS spectrometer was calibrated with the white base during the experiment, it was later calibrated against Spectralon® using the following formula.

$$\text{Irradiance of Spectralon} = \frac{\text{Irradiance of white base}}{\text{Reflectance of white base}}$$

The irradiance of Spectralon® out of the water at the time of the experiment was calculated using the following parameters. The reflectance of the white base calibrated to Spectralon® is known from a separate experiment and the irradiance of the white base was recorded during each experiment. Irradiance is the amount of light reflected by an object in absolute terms. Reflectance is the amount of light reflected by an object in relation to a known standard. The irradiance of Spectralon® out of the water was used to calculate reflectance of all the seaweed samples using a workflow that was built in R. Spectral data at five depth and two turbidity levels consisted of 150 readings of *E. radiata* and 150 readings of *U. pinnatifida* across wavelength region of 335 – 822 nm.

However, only readings within the wavelength region of 400 – 750 nm were considered for the analysis as water absorbs electromagnetic radiation drastically beyond 750 nm (Kieleck et al., 2001).

Raw spectral data were standardised, following Kotta et al. (2014) for each spectrum, by subtracting the mean of all values at the wavelengths from each spectral value and dividing the difference by standard deviation of values. Standardised hyperspectral data were used for further analysis which is explained in the following data analysis section.

A spectral library of *U. pinnatifida* and *E. radiata* at five depth and two turbidity levels, resampled to Micasense RedEdge-M® sensor bands in R, using both raw and standardised data was created in ENVI. Spectral signatures of a seaweed individual in the library were not averaged to preserve the spectral variability between individuals, following Kotta et al. (2014). The spectral libraries were used for further classification of Unmanned Aerial Vehicle (UAV) borne multispectral data.

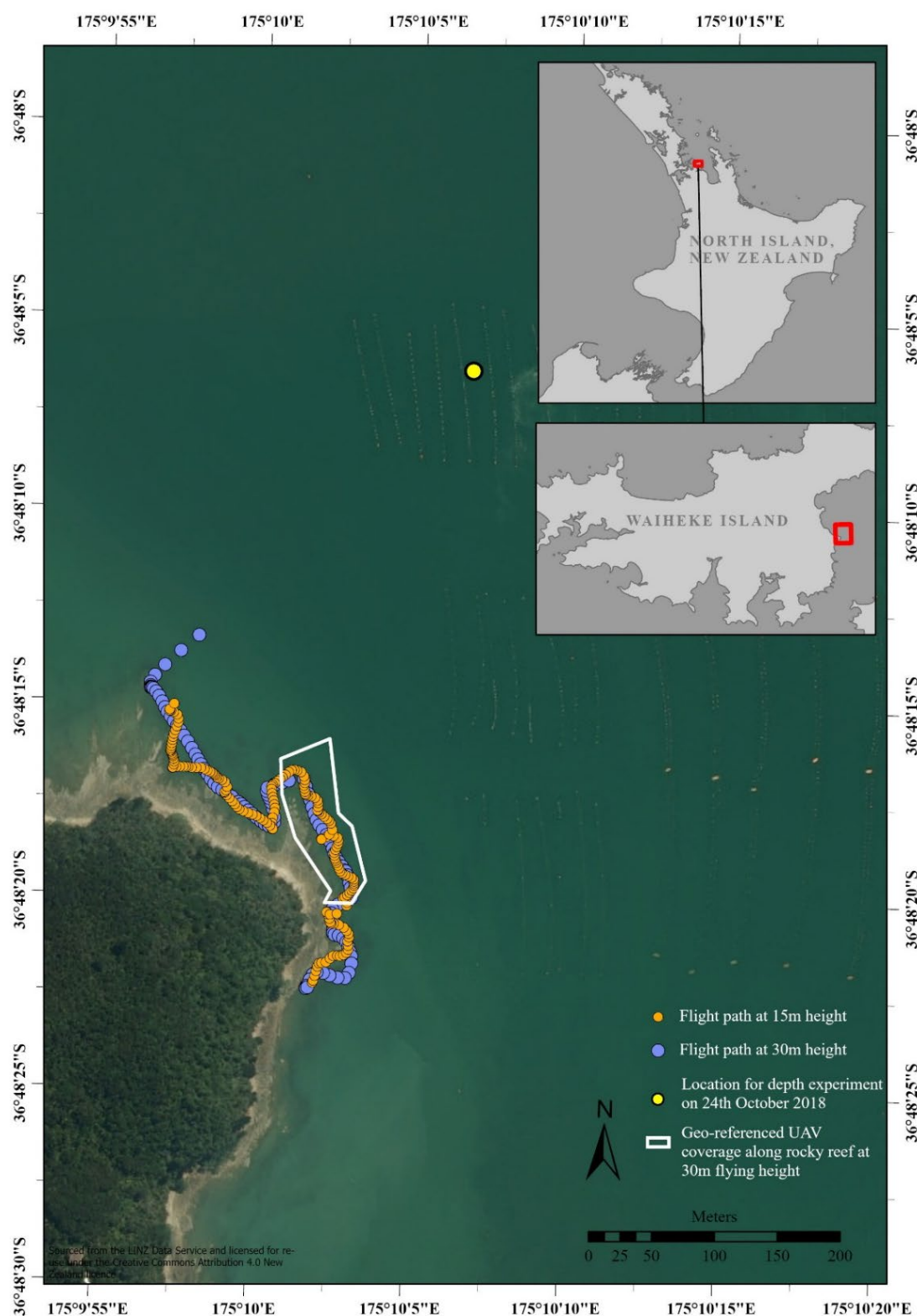


Figure 18: Seaweed sample collection, UAV data collection and experiment location. Orange points represent data collected by UAV multispectral sensor at flight height of 10m, Blue points represent data collected by UAV multispectral sensor at flight height of 30m. Yellow point represents the location where both depth and UAV experiment was conducted on the 24th October 2018.

4.2.2 UAV data collection and image processing

The equipments used for UAV data collection consisted of the following,

Phantom 4 (P4) Pro (UAV)

The DJI Phantom 4 Pro (Figure 19) is a comprehensive off-the-shelf platform that has been seen as a paradigm shift in the field of remote sensing due to its lightweight and high-quality integrated camera. AUT further enhanced the capabilities of the P4 Pro through the development of a customised mounting solution to allow the Rededge-m multispectral camera as an additional payload. It has flight endurance of ~12 minutes with the additional sensor weight, real-time video link, planned flight paths, 4k RGB camera and obstacle avoidance sensors. It uses GPS/GLONASS satellite positioning systems. With GPS positioning it has a horizontal accuracy of +/- 1.5m (DJI, 2020).

Micasense RedEdge-m® and Downwelling Light Sensor (DLS)

Micasense's RedEdge-m (Figure 19) is a multispectral sensor that captures images in five different spectral bands at very high spatial resolution. This sensor has been developed for agriculture and is under-explored for mapping submerged aquatic vegetation. Table 9 lists the specifications for the RedEdge-m used for this research. The DLS (Figure 19) is mounted on the top of the UAV and captures the downwelling irradiance at the time of image capture and accounts for changes in irradiance. This helps improve the radiometric quality of the data by correcting for changes in lighting conditions during the flight.

Table 9: Rededge-M specifications (Micasense, 2020)

| | |
|--|--|
| Weight | 170 grams (6 oz) (includes DLS and cables) |
| Dimensions | 9.4 cm x 6.3 cm x 4.6 cm (3.7 in x 2.5 in x 1.8 in) |
| Spectral Bands (centre wavelength, full width half maximum) | Blue (475, 20) Green (560, 20) Red (668, 10) Rededge (717, 10) Near-InfraRed (840, 40) |
| Ground Sample Distance (GSD) | 8 cm per pixel (per band) at 120 m (~400 ft) AGL |
| Capture rate | 1 capture per second (all bands), 12-bit RAW |
| Field of View | 47.2° HFOV |

Ground control software

Specialised ground control software (UgCS version 3.0) was used to monitor the UAV status. This allowed for optimum endurance per flight and ensured safe operation, providing the pilot with full situational awareness including video, real-time location and telemetry.

Known reflectance panel

Calibration panel with unique ID (RP03-1731212-SC) and known reflectance values at each spectral band (blue -0.55, green - 0.55, red - 0.54, NIR - 0.49, rededge - 0.53) was used for calibration of multispectral images. Images of the reflectance panel were acquired before and after each flight by holding the UAV setup at 1m above the panel. The readings from reflectance panel in conjunction with the measurements from


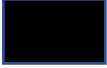








the DLS, improved the radiometric quality of the multispectral images (Taddia et al., 2019).

The DJI Phantom 4 Pro UAV mounted with Micasense Rededge-m sensor and DLS will be referred to as “UAV setup”. To test the suitability of spectral libraries for image classification, on 24th October 2018, two types of UAV data were collected. One type of data captured was where the ‘UAV setup’ was flown at 10m and 30m height obtaining multispectral images of the seaweed samples at each of five depth levels at the same time as the ‘depth experiment’ (Figure 18). The seaweed samples on the base plate are referred to as the reference seaweed To identify the depth and the seaweed species from multispectral images, a set of identifiers (Table 10) were placed on top of the boat. An identifier was not used for identifying seaweed species itself as the order was noted - the spectral readings of *U. pinnatifida* were obtained first followed by *E. radiata*. During this time, the boat was secured in place next to a mussel line. The multispectral data at flight height (FH) of 10m had sub-centimetre spatial resolution and that at FH of 30m had a spatial resolution of ~2.7cm/pixel.



Figure 19: UAV setup including Micasense RedEdge-m sensor on the base, DLS sensor with GPS unit on top of Phantom 4 Pro. Known reflectance panel (bottom right). Photo credit: Graham Hinchliffe.

Table 10: UAV data collection identifiers

| Seaweed individual | | Depth | |
|--------------------|---|-------|---|
| 1 |  | <0.1m |  |
| 2 |  | 0.5m |  |
| 3 |  | 1m |  |
| 4 |  | 1.5m |  |
| 5 |  | 2m |  |

While the snorkeller was collecting *E. radiata* samples for the depth experiment in the rocky reef, the snorkeller identified 20 *U. pinnatifida* locations by show of hand out of the water and the locations were captured by Phantom 4's RGB camera keeping the snorkeller approximately in the centre of the photo. The tide was high during this time. RedEdge-m multispectral data was captured along the same path after the experiment. The UAV setup was first flown south at 30m height and turned around to cover the same area at 15m height. It was ensured that the coverage included *U. pinnatifida* locations identified. The tide was falling during that time.

A flowline was developed for single image processing, direct-georeferencing and mosaicking of UAV images. Image processing included converting raw data to reflectance data with the help of metadata (data about data) stored in each band, aligning individual bands, image stacking and copying metadata over from raw to processed images. Georeferencing is a method of relating camera coordinate system to ground co-ordinate system either by using parameters intrinsic to the images (known as direct georeferencing) or by using pre-planned ground control points (GCPs) in the study area. Direct georeferencing spatially locates an image using altitude, image centre co-ordinates, rotational angles (yaw, pitch and roll) of the UAV, image size and sensor width.

RedEdge-M multispectral data from the depth experiment were sorted based on the identifiers (Table 10) visible on each image and flying height into respective folders. Those images where the identifiers were not visible were not considered. Similarly, multispectral images along the rocky reef were sorted into a respective folder based on the flying height of 15 and 30m. Both types of UAV multispectral images were processed to create raw reflectance and standardised reflectance images but the data over the depth experiment was not georeferenced as it was only to assess the suitability

of the raw reflectance and standardised spectral libraries for classifying *E. radiata* and *U. pinnatifida*. The reflectance converted multispectral images were converted to a standardised image by subtracting the mean of each cell stack from the corresponding cell at each spectral band and dividing by the standard deviation of the cell stack. UAV data over the rocky reef in Awakiriapa Bay were processed, direct geo-referenced and mosaicked. Photo centre points from Phantom 4's RGB camera of 20 *U. pinnatifida* locations were plotted in ArcGIS Pro to approximately locate *U. pinnatifida* positions identified by the snorkeller.

4.2.2.1 Implementation steps - UAV single image processing

The raw images from Micasense RedEdge-m® sensor consisted of five spectral bands (in the order - blue, green, red, NIR, rededge) with digital numbers for pixel values and saved as five separate 16-bit unsigned '.TIF' files. These raw images need to be processed prior to analysis. The routines for processing the images were written using a combination of a) Python and implemented in the Jupyter Notebook, a platform- and language-independent interface (Anaconda Software Distribution) b) Model builder in ArcGIS Pro.

The first step was to convert these raw images to reflectance in conjunction with the Downwelling Light Sensor (fitted to the top of the UAV) and Micasense's calibration panel. DLS's irradiance information at the time of image capture was stored as metadata in each multispectral image. . The conversion of raw digital numbers to reflectance values was performed using libraries in 'micasense/imageprocessing' package (Micasense, 2018).

The second step was the alignment of the individual spectral bands that are slightly offset with each other due to the nature of arrangement of sensors in the RedEdge-m multispectral camera. This was implemented using a feature matching

algorithm called Scale- invariant feature transform or ‘SIFT’ (Lowe, 2004) in Python’s OpenCV package (Bradski and Kaehler, 2008). This algorithm has since been patented.

The third step was to stack the individual aligned bands into a single ‘composite’ image. This was implemented in the ‘ModelBuilder’ environment in ArcGIS Pro. This step was necessary to perform supervised image classification in ENVI version 5.5 (Exelis Visual Information Solutions, Boulder, Colorado). The order of the spectral bands in ‘composite’ images and that in the spectral library used for supervised classification must match. In this case, the order of composite images was – Blue, Green, Red, NIR, Rededge and the spectral library was processed to match this order.

Once the images were processed, the fourth step was to copy the metadata from raw files to processed composite files using ‘exiftool’ (Harvey, 2018).

The fifth step was to georeference the images using direct geo-referencing technique to enable seaweed mapping. Direct geo-referencing of processed images can be achieved by two methods – a) creating control points for image corners and b) creating world files. Method (a) required list of image co-ordinates and their respective projected coordinates in a text file. Method (b) required six parameters as defined by ESRI (2020) – A (pixel size in the x -direction in map units/pixel), D (rotation about the y -axis), B (rotation about the x -axis), E (pixel size in the y -direction in map units, almost always negative), C (x -coordinate of the centre of the upper-left pixel), F (y -coordinate of the centre of the upper-left pixel) in six subsequent lines in the same order in a world file created with extension ‘.tfw’ for each associated image. For both methods, the top left corner of an image was the origin (0,0). Both methods require corner points for the images in the projected coordinate system. To calculate these projected corner points; image centre coordinates, the altitude of UAV, orientation

angles (yaw, pitch, roll), image size (960 x 1280) and sensor width (4.8mm) were required. This information was stored as EXIF or XMP tags in image metadata.

The image centres were in WGS84 (geographic coordinate system) as they were the output from GPS (Global Positioning System) which were converted to NZGD2000/NZTM (projected coordinate system) using ArcPy python package in ArcGIS Pro. To obtain projected corner points, yaw, pitch and roll (orientation angles of the UAV for navigation co-ordinate system) were converted to kappa, phi and omega (orientation angles defining the relationship between image coordinate system and projected coordinate system) using Pix4D companion notes (Pix4D, 2020b).

The multispectral images acquired were nadir (camera pointing straight down). However, the sensor does not always face perfectly straight down due to UAV movement, wind or other factors. Therefore, in addition to the yaw of the UAV, the projected corner point calculation accounted for pitch and roll as well.

Method (a) was implemented in Python in a two-step process where parameters for geo-referencing were calculated and saved as text files in a Jupyter environment and the text files were read as a batch process for all the images in a hosted ArcGIS Notebooks in ArcGIS Pro. It is important to note that the text files were saved in the same location as the images.

The final step was to mosaic the individual geo-referenced images to create a single new image dataset for further analysis. The codes for the above processes are in Appendix C.

4.2.3 Data analysis

4.2.3.1 Field spectroscopy - sun glint removal and data pre-processing

According to Kutser et al. (2013), only 2% of their measurements had above water reflectance close to remote sensing reflectance. It was necessary to remove the glint effects from field radiometry data before analyses. Removal of sun glint from each reading was attempted using the technique described in Kutser et al. (2013) where reflectance values in wavelengths between 350 – 380nm and 890 – 900 nm were used to obtain a glint curve using a power function. This was performed in R software.

4.2.3.2 Effect of depth and turbidity on the spectral reflectance of *Undaria pinnatifida* and *Ecklonia radiata*

High dimensional spectral data was reduced to principal components that capture variation in reflectance across the influential wavelength region. This was performed using PCA (principal component analysis) on the standardised spectral data of *U. pinnatifida* and *E. radiata*, separately. Linear mixed models were built to identify a significant difference in spectral reflectance influenced by depth and turbidity (Table 11). The response variable was the principal component with the highest variance while explanatory variables were turbidity (Secchi depth) and water depth as factors with two and five levels, respectively. The model that best represented the data was chosen based on Akaike Information Criteria (AIC). Model prediction plot with +/- two standard deviations at 95% confidence interval was used to interpret the influence of depth and turbidity on spectral reflectance.

All the analyses were implemented in the R software (R Core Team, 2019). Mixed-effects modelling was performed using ‘nlme’ package (Pinheiro et al., 2018), the prediction plot was built using ‘AICcmodavg’ package (Mazerolle, 2019). Marginal and conditional R^2 values were calculated using ‘MuMIn’ package to assess the goodness-of-fit of the best model (Barton, 2018).

Table 11: Various models used in mixed-effects modelling to test the significance of each term

| Model | Formula | Terms deleted |
|-------------|---|-----------------------------------|
| A (Full) | PC ~ secchiDepth + depth + secchiDepth:depth | None |
| B | PC ~ secchiDepth + depth | secchiDepth:depth |
| C | PC ~ secchiDepth | Depth, secchiDepth:depth |
| D | PC ~ depth | secchiDepth, secchiDepth:depth |

4.2.3.3 Discrimination of Undaria pinnatifida from Ecklonia radiata at various depth and turbidity levels using field spectroscopy data

In addition to understanding the effect of depth and turbidity on spectral reflectance, the hyperspectral data from STS-VIS spectrometer was analysed to see if the two seaweed species, *U. pinnatifida* and *E. radiata*, could be discriminated at various depth and turbidity levels using two sets of spectral band combinations. One was using wavelengths that discriminated *U. pinnatifida* from other browns in Chapter 2 (Dataset A) and the other was the spectral band combination of Micasense Rededge-M sensor (Dataset B). This analysis would help understand usability of existing multispectral sensors compared to a sensor customised for the application. To produce Dataset B, hyperspectral data were resampled to proxy a Micasense RedEdge-m sensor by averaging the raw spectral reflectance values at the wavelength ranges in Table 9. After averaging, Dataset B was standardised following Kotta et al. (2014). Some of seaweed sample readings were duplicated and will be different from that in Table 12. The discrepancy was very small.

Random forest modelling was used to discriminate *U. pinnatifida* from *E. radiata* at five depths and two turbidity levels. ‘randomForest’ package in R was used to build random forest models (Liaw and Wiener, 2002). Starting default parameter settings, the number of trees (ntree) and wavelengths to try at each node (mtry), were

tuned using the ‘tuneRF’ method in ‘randomForest’ package. It was assumed that there was no variation in the turbidity within the study area at the time of acquisition. Two models were built for each dataset (A and B) where each model represents the spectral data of the two seaweed species within the relevant turbidity level using two sets of wavelength information to assess overall discrimination between the two species at all depths down to 2m. While this analysis provides overall accuracy of classification, a further assessment was necessary to determine the accuracy of discrimination at different depths. So, the two datasets were further split to discriminate the two seaweed species at each of five depth levels within a turbidity level and ten models were built for each dataset. Random forest models produced an “out-of-bag” error estimate, which was a prediction error estimated using bootstrapped cross-validation.

Table 12: Spectral data description

| Seaweed Species | Water Depth (m) | Turbidity (Secchi Depth in m) | Readings count per seaweed species (n/species) |
|---|-----------------|-------------------------------|--|
| <i>E. radiata</i> and <i>U. pinnatifida</i> | 0.1 | 6 | 10 |
| <i>E. radiata</i> and <i>U. pinnatifida</i> | 0.5 | 6 | 10 |
| <i>E. radiata</i> and <i>U. pinnatifida</i> | 1 | 6 | 10 |
| <i>E. radiata</i> and <i>U. pinnatifida</i> | 1.5 | 6 | 10 |
| <i>E. radiata</i> and <i>U. pinnatifida</i> | 2 | 6 | 10 |
| <i>E. radiata</i> and <i>U. pinnatifida</i> | 0.1 | 3.25 | 20 |
| <i>E. radiata</i> and <i>U. pinnatifida</i> | 0.5 | 3.25 | 20 |
| <i>E. radiata</i> and <i>U. pinnatifida</i> | 1 | 3.25 | 20 |
| <i>E. radiata</i> and <i>U. pinnatifida</i> | 1.5 | 3.25 | 20 |
| <i>E. radiata</i> and <i>U. pinnatifida</i> | 2 | 3.25 | 20 |

4.2.3.4 Discrimination of Undaria pinnatifida from Ecklonia radiata at various depth levels within a turbidity level using UAV-collected multispectral data

Hyperspectral data (from STS-VIS spectroradiometer) resampled to Micasense

RedEdge-m sensor were used to assess discrimination between *U. pinnatifida* and *E.*

radiata in the section above. In this section, the spectral reflectance data for *U.*

pinnatifida and *E. radiata* at various depth and turbidity levels were assessed for their ability to classify processed multispectral (RedEdge-m) UAV data. The assessment was a two-step process where, in the first step (Figure 20), only those spectral signatures relevant to the seaweed species at a specific depth in the image were used for

classification using both raw and standardised images. For example, a processed image of *E. radiata* ‘individual 1’ at a 50 cm depth (identified using the identifiers visible on the image) was classified using spectral signatures of *E. radiata* at a 50 cm depth. This step was performed to identify the image type (whether raw reflectance or standardised) that best classified the known seaweed pixels while the non-seaweed pixels remained unclassified.

The Spectral Angle Mapper (SAM) supervised classification technique in ENVI was used for classifying multispectral images. This technique classifies a pixel based on the similarity in the shape of the reference spectrum and pixel spectra by calculating the angle between the pair of spectra in n-dimensional space (Kruse et al., 1993). The lower the angle between the reference and classification spectra, the better the accuracy of classification. On a calibrated reflectance data, this technique is insensitive to illumination effects (Vahtmäe and Kutser, 2013). The source of the reference spectrum can be from either the spectrometer or the spectral images. In this case, a maximum angle threshold of 0.2 radians was defined in ENVI for classification. Any pixel with values larger than the threshold value will not be classified. Data used for accuracy assessment was compiled for each of the classified images based on an equalised stratified random sampling technique using 500 random points. The accuracy assessment results were aggregated based on each seaweed species at a specific depth and spatial scale. In this case, five seaweed individuals per species were used in the experiment. Before accuracy assessment, polygon outlines of reference seaweed species were manually mapped in ArcGIS Pro from the processed UAV images and saved to a shapefile along with details of seaweed type, depth, individual number, and flying height. Thus, 250 validation points were randomly distributed within the reference seaweed polygon and the remaining 250 points within the non-seaweed area. There were seaweeds (mostly *U. pinnatifida*) present on the mussel line next to the boat when

the UAV data was collected at a height of 30m; these pixels were considered as a non-seaweed class for simplicity. This will affect the classification but the low coverage of the seaweed laden mussel line in the image at that scale (~14%) compared to non-seaweed area and the low chance of accuracy assessment points falling on the mussel line classification in large numbers reduces the potential impact on the classification accuracy. It is safer to be conservative on the classification accuracy than mislead with errors of commission.

The classification was assessed using four performance statistics: user's accuracy, producer's accuracy, overall accuracy and kappa. User's accuracy suggests the frequency of occurrence of the class on the ground, also known as reliability. Producer's accuracy quantifies the proportion of the class correctly classified. Kappa is a statistical measure of the level of agreement of the reference and the classification corrected by chance, indicating if the classifier performed better than by chance (Oreti et al., 2020). Producer's accuracy was the total number of correct classifications for a class divided by the total number of reference (column) in that class. User's accuracy was the total number of correct classifications for a class divided by the row total. Overall accuracy was the total number of correctly classified values in all classes divided by the total number of reference values in all classes combined. Cohen's kappa (k) was calculated using the formula (Cohen, 1960):

$$k = \frac{p_o - p_e}{1 - p_e}$$

where p_o was the observed accuracy and p_e was the expected accuracy. In this case, classification was assessed based on the producer's accuracy of non-seaweed class and user's accuracy of seaweed class. It is important to note that this depth experiment included one seaweed individual per image classification.

In the second step, the image type (raw reflectance or standardised reflectance) that best classified the seaweed species was utilised for further classification and assessment. Before classification, more reference spectra such as that of boat, buoy, water and glint from one of the multispectral images captured from a flight height of 10m were added to the spectral library. Consequently, the whole spectral library containing image-derived spectra (of boat, buoy, water, glint) and spectrometer-derived spectra (of both seaweeds at all five depth and two turbidity levels); this was the dataset used for classifying the multispectral UAV data of all individuals of both seaweed species at five depth levels at flight heights of 10m and 30m. This classification was performed to assess discrimination between *U. pinnatifida* and *E. radiata* if any. SAM classification technique was implemented in ENVI with maximum angle threshold of 0.2 radians.

Accuracy assessment was performed at three levels in this step – level 1 (collation of individuals), level 2A (collation of each species) and level 2B (collation of both species) (Figure 21). Accuracy for each of the classified images was assessed for classification of reference seaweed species (*U. pinnatifida* or *E. radiata*) at any given depth vs classification of both seaweed species at all five depth levels and unclassified pixels. In addition to those pixels that remained unclassified, water, glint, boat and buoy were reclassified as unclassified pixels since those pixels were not of interest in classification assessment. At level 1, the results from the accuracy assessment were compiled based on the classification of a reference seaweed species at a specific depth across both the seaweed species at five depth levels each, at two spatial scales and unclassified. This includes aggregated values from five seaweed individuals per species. Assessment at this level provides insights into the similarity of spectral signatures of reference seaweed at a specific depth with that of other seaweed species at different depth levels. At level 2A, the results from the accuracy assessment were compiled based

on the classification of a reference seaweed species class across both the seaweed species classes and unclassified class at two spatial scales based on flight heights of 10 and 30m. Based on the results from level 1, this level provides insight into the influence of misclassification of reference seaweed at various depth levels to the classification accuracy. At level 2B, the results from the accuracy assessment were compiled based on the classification of the two reference seaweed species classes across both the seaweed species classes and unclassified class at two spatial scales. To calculate the classification accuracy of *E. radiata* and *U. pinnatifida* combined, *E. radiata* and *U. pinnatifida* classes were aggregated including all points but the unclassified column in the collated tables (Table C-29 and Table C-30) was halved. This step was necessary since the area surrounding the reference seaweed on base plate remains unchanged while the reference seaweed varied between *E. radiata* and *U. pinnatifida*. It was assumed the misclassifications in the unclassified area remained the same in both sets of seaweed species classification images.

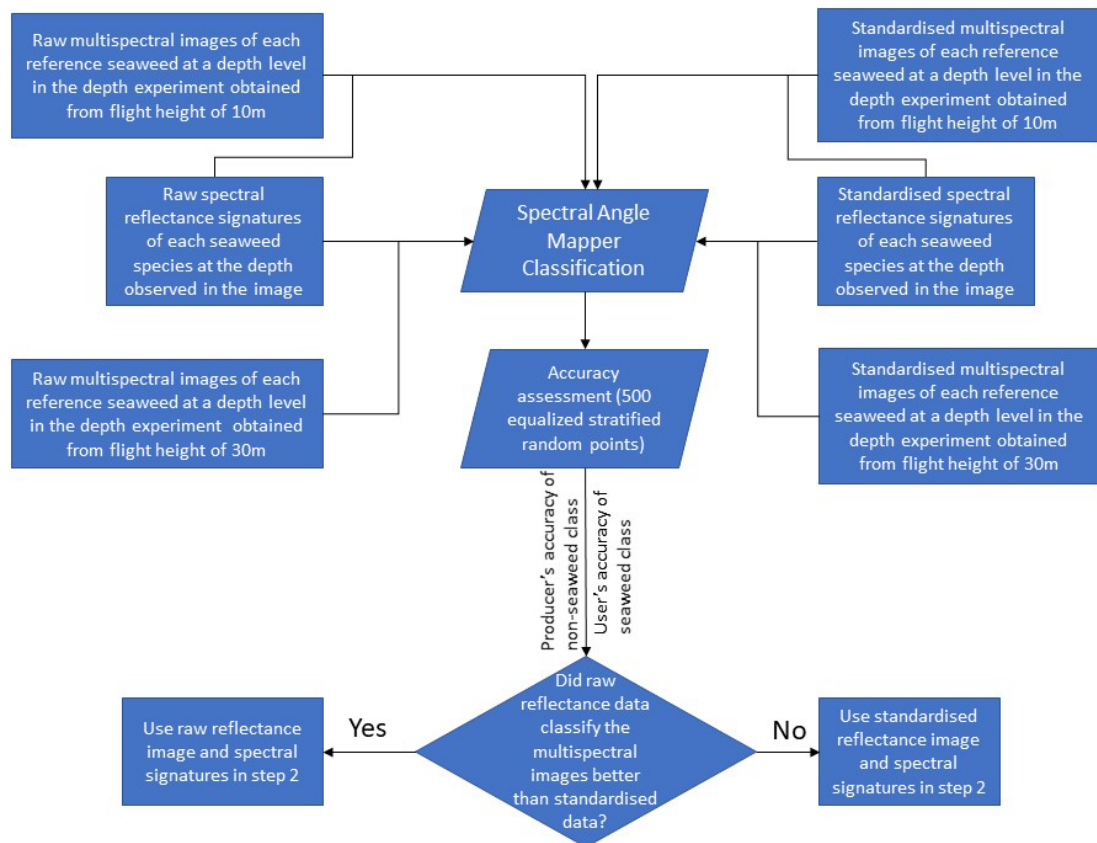


Figure 20: Step 1 in seaweed classification from UAV multispectral data

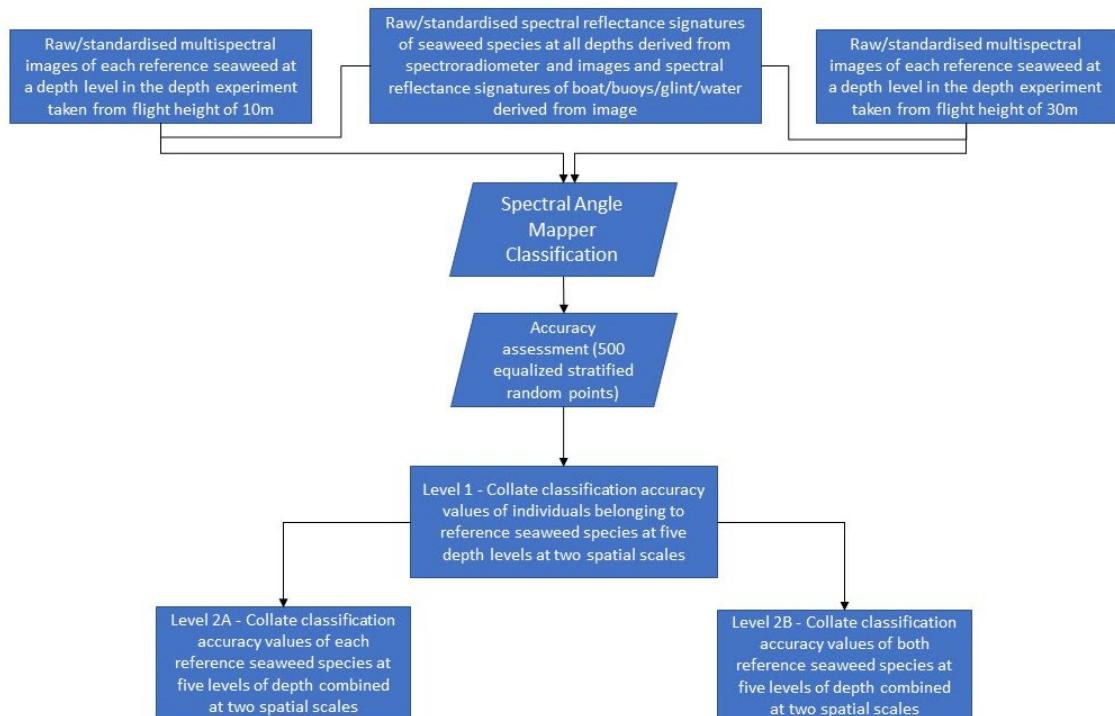


Figure 21: Step 2 in seaweed classification of UAV multispectral data

4.2.4 Application: Classifying *U. pinnatifida* and *E. radiata* along rocky reef using high spatial resolution RedEdge multispectral data

Having classified and analysed *U. pinnatifida* and *E. radiata* at a greater resolution in the depth experiment, the spectral library was used for classifying seaweeds along the rocky reef in Awakiriapa Bay in Waiheke Island. Pixels with reflectance values below 0.08 in NIR band were reclassified as water pixels and the rest were reclassified as land. NIR band absorbs water, therefore, the reflectance values of water pixels are close to zero.. Those shallow water pixels with seaweed or rocks had values slightly more than zero in NIR band, so the threshold value was adjusted to include shallow-water substrates. This was all implemented in model builder in ArcGIS Pro.

The image type (raw reflectance or standardised data) that was used for classification of rocky reef UAV data was determined by the first step in section 4.2.3.4. After masking, spectral library including image-derived and spectrometer-derived spectra of both seaweed species at depths 10cm, 50cm and 1m at two turbidity levels and non-seaweed spectra was used to classify UAV multispectral data over the rocky reef. SAM classification technique with maximum angle threshold of 0.2 radians was implemented in ENVI. The results from initial classification were reorganised to combine all levels of *E. radiata* as one class and those of *U. pinnatifida* as another class. The seaweed individuals measured from the study were in the range of 30 – 50 cm. A 20cm buffer was drawn around the validation points to allow for the detection of blades or stipe of seaweed that may be spread outwards in the classified UAV data. Accuracy of rocky reef classification was assessed two ways. One way was to use level 2B classification accuracy from depth experiment. Another way was to visually assess the presence of *U. pinnatifida* at the 20 validation locations identified by the snorkeller.

4.3 Results

4.3.1 Glint removal and data pre-processing

Raw spectral data (Figure 22) indicate a drop in reflectance values in Red-NIR region of the electromagnetic spectrum as the water depth increases. A similar pattern was observed in the visible region of the electromagnetic spectrum but not as drastic as in Red-NIR region.

The glint removal process yielded negative values in some parts of the spectrum (Figure 22). This was likely caused by the choice of wavelengths used for the correction, especially in the NIR region. Due to extreme noise in the data between 350 – 360 nm only reflectance values in wavelengths between 360 – 380 nm were used instead of the recommended range of 350 – 380 nm. Reflectance at 820 nm was used as the recommended wavelength range (890-900 nm) was beyond the spectral range of STS-VIS spectrometer. Therefore, the glint removal technique was not used for further analysis.

The calibration panel was used to correct for changing illumination and different days, however, these effects were clearly visible on a mixed day (cloudy and clear sky) (Figure 22B) compared to a clear day (Figure 22A). Therefore, the standardisation technique described in section 4.2.3.1 was applied for all of the spectral data so it is comparable and also to enhance the spectral features at various water depth levels (Figure 23).

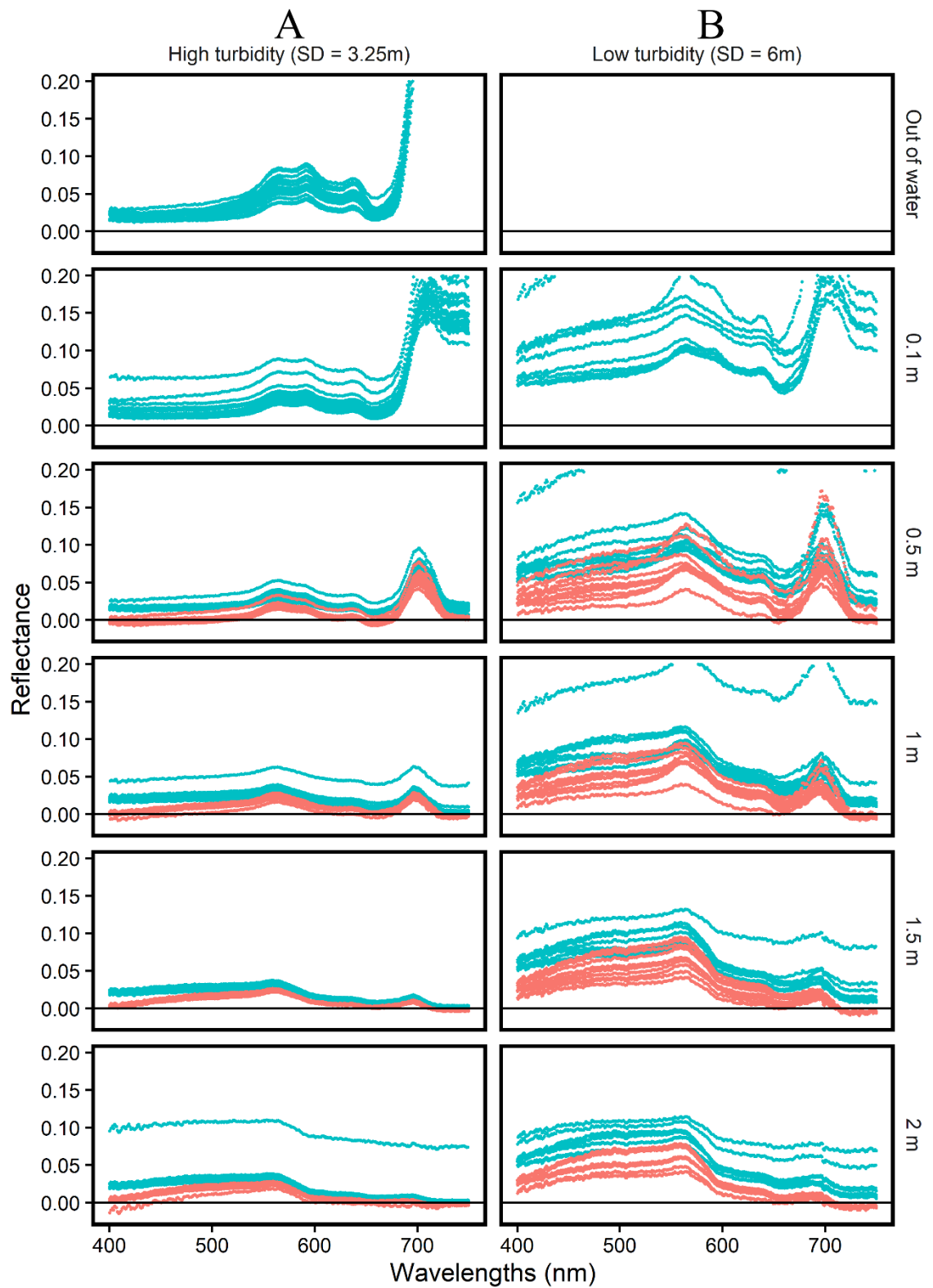


Figure 22: Raw (blue) and glint corrected (orange) spectral reflectance values of *U. pinnatifida* at five depth and two turbidity levels. SD – Secchi depth. “Out of water” spectral readings of the seaweeds were not collected on the 24th October 2018 (data in B).

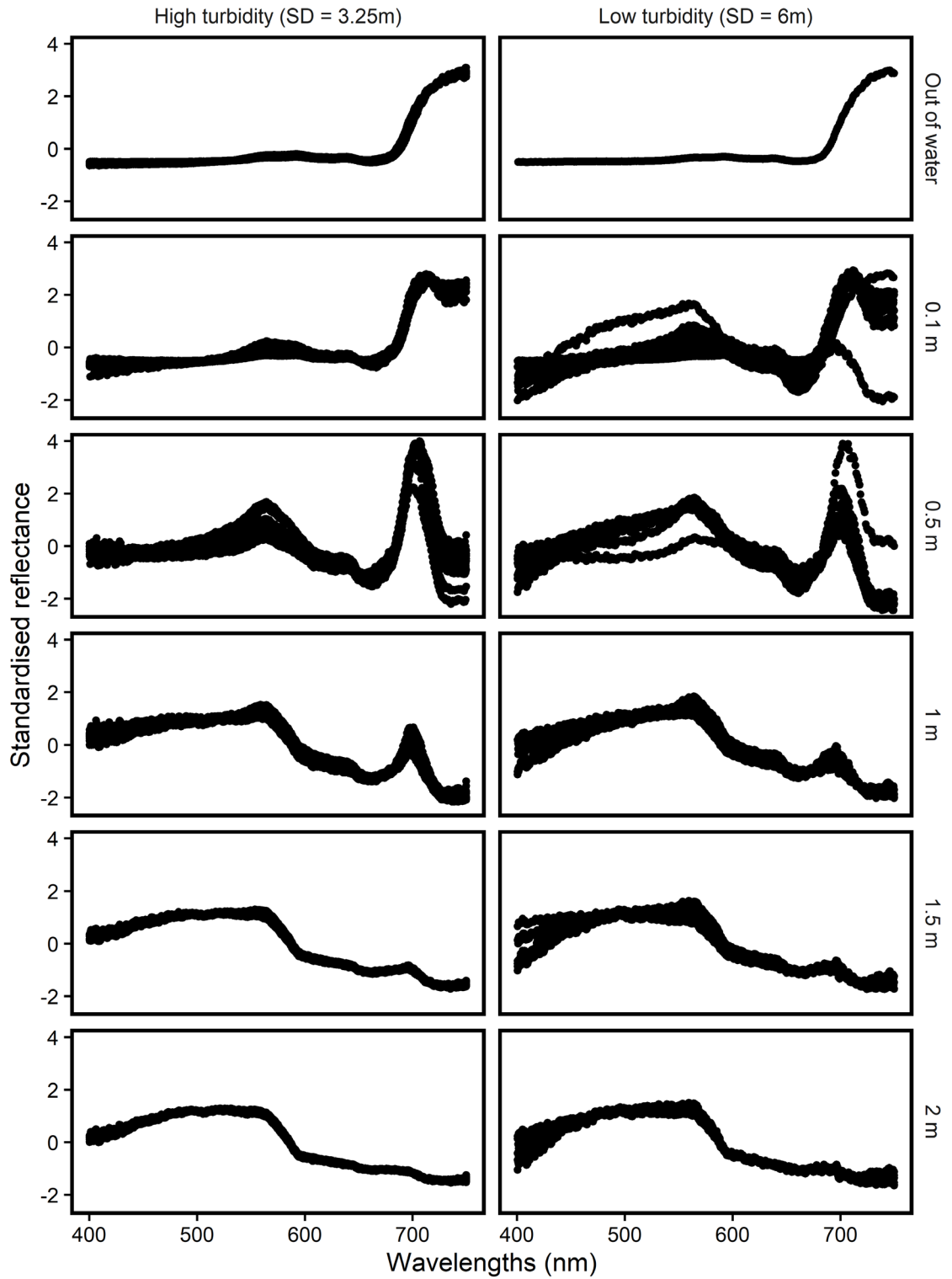


Figure 23: Standardised spectral reflectance values of *U. pinnatifida* at five depth and two turbidity levels. SD – Secchi depth.

4.3.2 UAV data collection and image processing

UAV multispectral data of depth experiment produced five individual spectral bands (Figure 24) with raw digital numbers that were processed and stacked into a single

processed image with raw reflectance values (Figure 25). The edges of the processed file have some noise due to the placement of all five sensors and the variation in image footprint that they capture. This was removed using a mask layer. 60 multispectral images over the depth experiment were processed for further analysis.

Similarly, multispectral images acquired over rocky reef were processed and noisy edges removed. However, direct geo-referencing using orientation angles (yaw, pitch and roll) from image metadata did not produce an accurate result. Near feature in ArcGIS Pro was used to obtain the orientation angles from UAV telemetry points (obtained from the ground control software) closest to the photo centres of the multispectral images. Only 18 of those multispectral images that covered the identified *U. pinnatifida* locations were directly geo-referenced. The image overlap helped remove/reduce the glint in the northern section of each image by reordering the images (Figure 26). While direct geo-referenced images using telemetry from UAV were approximately in its place, they still needed some manually identified tie points between each pair of images to make a seamless mosaic.

Photo centres of 20 UAV RGB images representing *U. pinnatifida* locations that were plotted using metadata (Figure 27) were compared with rocky reef mosaic along with RGB photos (Figure 28, Figure C-1 to C-6). The photo centres were off by 10 – 14m at the ends of the mosaic whereas some locations in the centre were off by 3 – 6m. The photo centres were manually adjusted to represent the true locations of *U. pinnatifida* in the processed multispectral mosaic by comparing with RGB photos (Figure 28). Even though the photo centres were over *U. pinnatifida*, the accuracy of GPS on Phantom 4 pro and that of Rededge-m sensor did not allow for precision in identified *U. pinnatifida* locations. This step is crucial for validating the classification accurately.

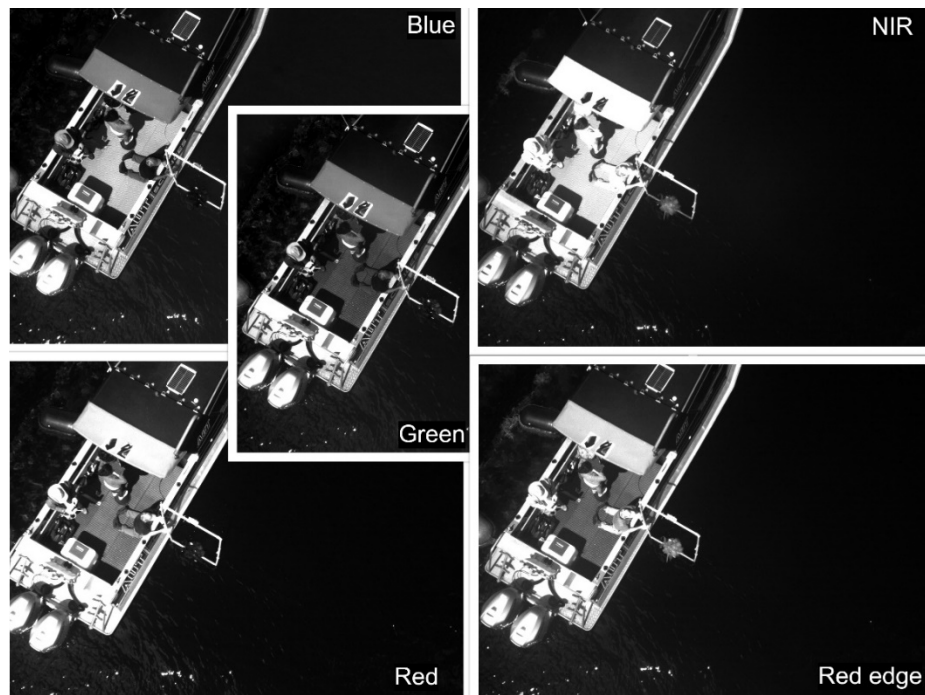


Figure 24: In the depth experiment, *E. radiata* on the base plate immersed in water at <10cm depth was captured in five spectral bands by Rededge-M sensor on Phantom 4 Pro at FH of 10m.

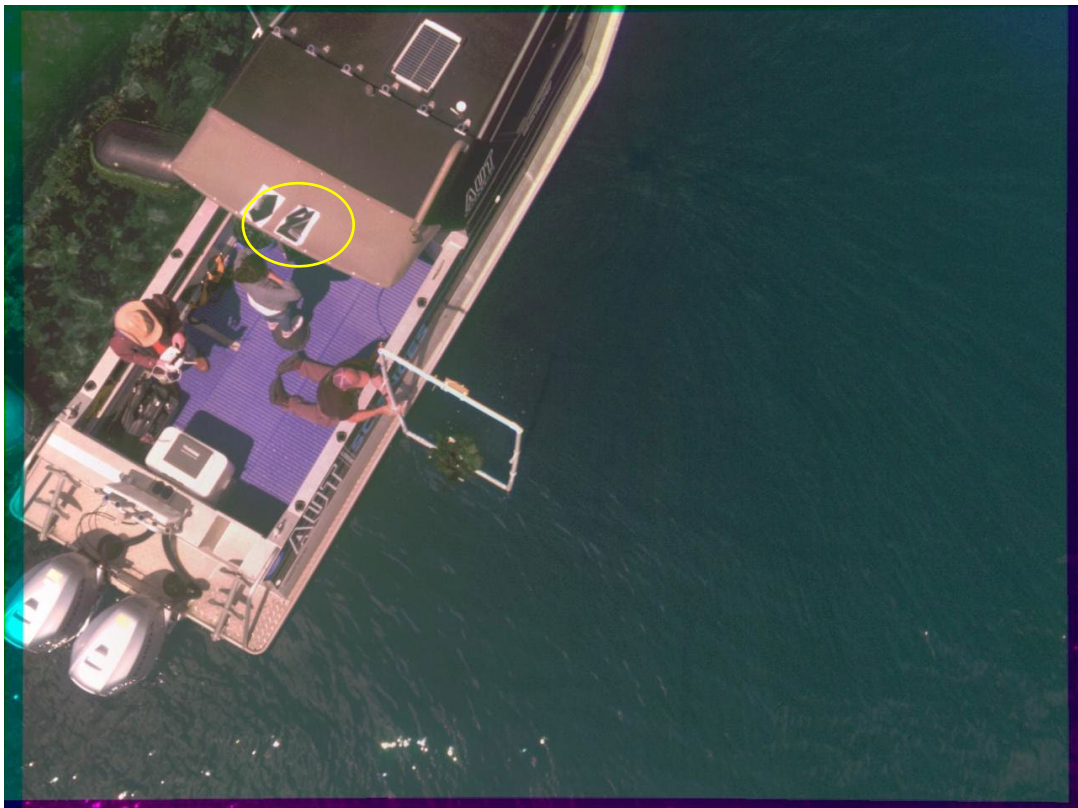


Figure 25: Individual spectral bands of *E. radiata* at <10cm water depth captured on Phantom 4 Pro at FH of 10m were stacked into a single file to create various band combinations, in this case, true colour RGB image. Noise from stacking is visible on the edges. Yellow circle highlights the visible identifiers.

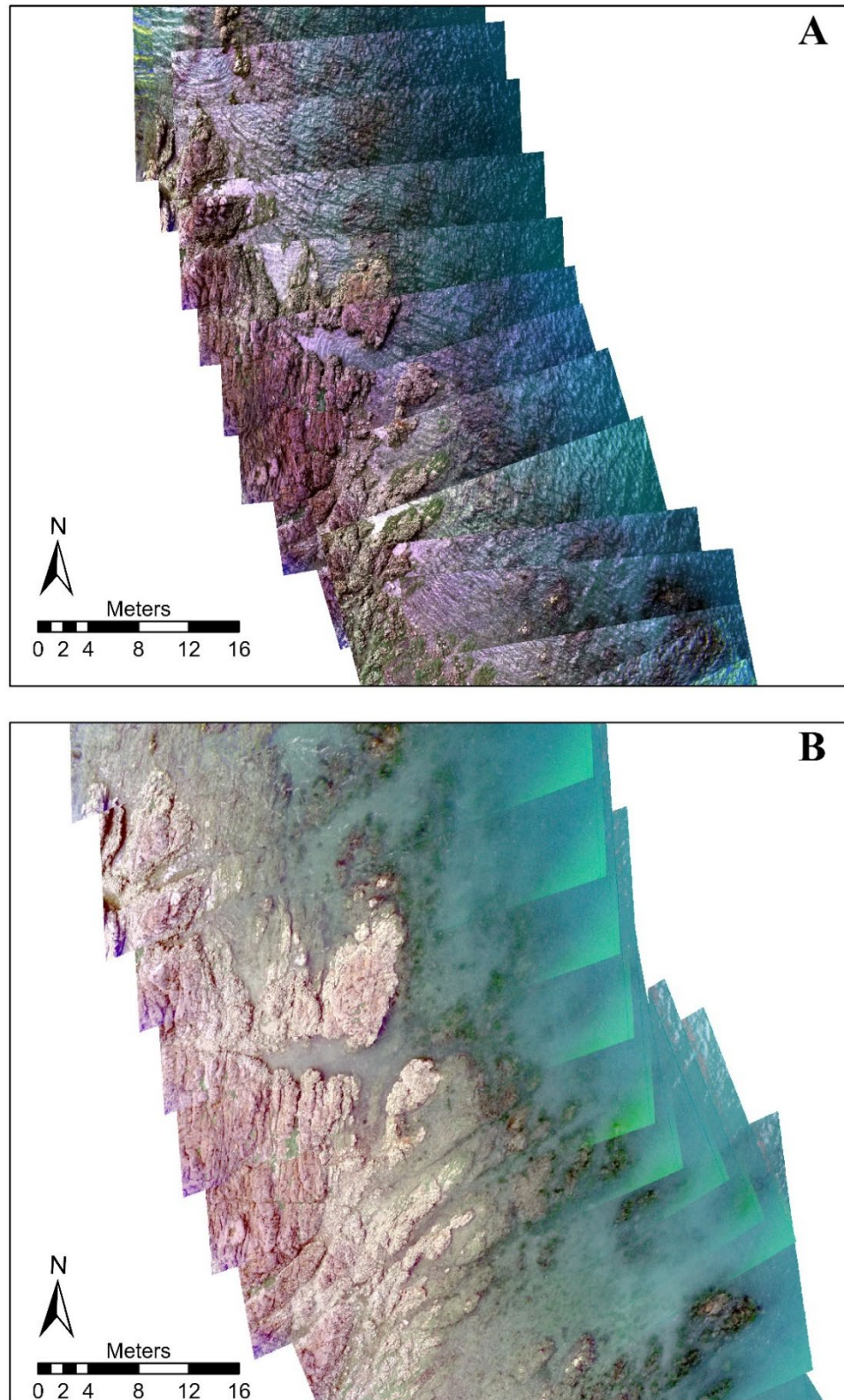


Figure 26: (A) Direct geo-referenced images of the rocky reef at FH of 30m showing glint in the top half of the images, (B) direct georeferenced images with additional tie points to match the locations, reordered to remove glint and mosaicked as a single image.

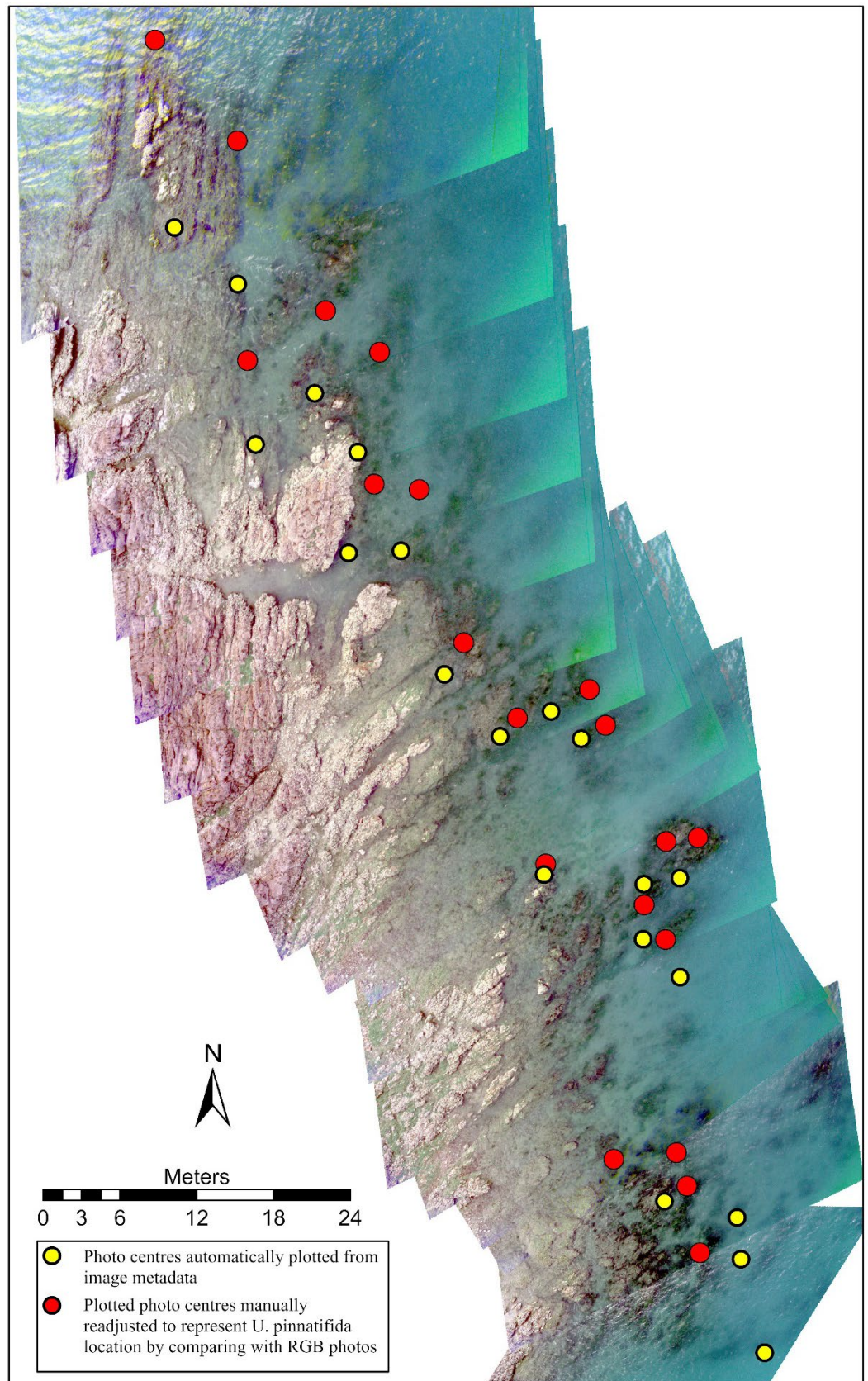


Figure 27: Photo centres automatically plotted from image metadata (represented in yellow), plotted photo centre manually adjusted to represent true *U. pinnatifida* locations by comparing with UAV's RGB photos (represented in red).



Figure 28: Adjusted *U. pinnatifida* locations 6 and 7 on the multispectral mosaic (left) compared to RGB photos (right) with snorkeller in the centre of each photo.

4.3.3 Effect of depth and turbidity on the spectral reflectance of *Undaria pinnatifida*

A PCA on standardised spectral data of *U. pinnatifida* showed a maximum variance of 84.85% explained by the first principal component (PC1). Wavelengths between 690 – and 750 nm were most strongly, and negatively, associated with PC1 (Figure 29).

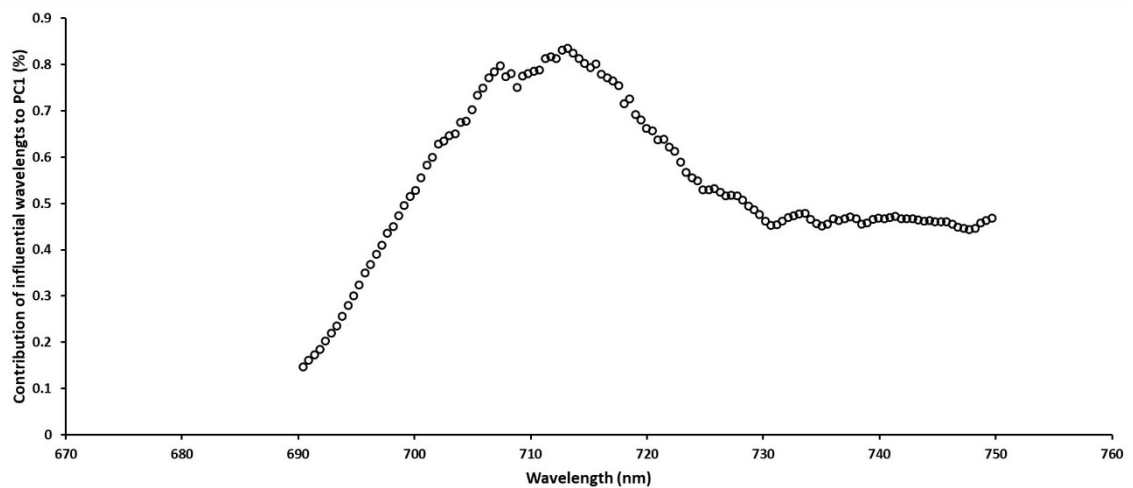


Figure 29: Variables contributing to PC1 for *Undaria pinnatifida*

Linear mixed-effects modelling. A mixed-effects model including depth, turbidity and the interaction between best explained variation in PC1 for *U. pinnatifida*, with marginal and conditional R^2 of 0.946 and 0.946, respectively. A likelihood ratio test revealed that the best model, model A (AIC = 921.28), had more statistical support than the three other alternative models (Table 13).

Table 13: Likelihood ratio test of models explaining difference in spectral signatures of *U. pinnatifida* across four locations and four seasons

| Model | Likelihood ratio test | AIC |
|-------|-------------------------------------|---------|
| B | $L = 83.85$ (df = 8, $p < 0.001$) | 997.13 |
| C | $L = 441.27$ (df = 4, $p < 0.001$) | 1346.55 |
| D | $L = 109.58$ (df = 7, $p < 0.001$) | 1020.87 |

The wavelengths that describe *U. pinnatifida* at depths of 0.1m and 0.5m at turbidity (Secchi depth) of 3.25m and 0.1m water depth at turbidity (Secchi depth) of 6m were between 690 – 750 nm. At depths between 1m and 2m, at both turbidity levels, the wavelengths (based on loading values, they were between 418 – 567 nm) that described *U. pinnatifida* were not significantly different (Figure 30). Turbidity does not significantly affect the spectral reflectance at the wavelengths describing *U. pinnatifida* within each depth except at 0.5m depth (Figure 30).

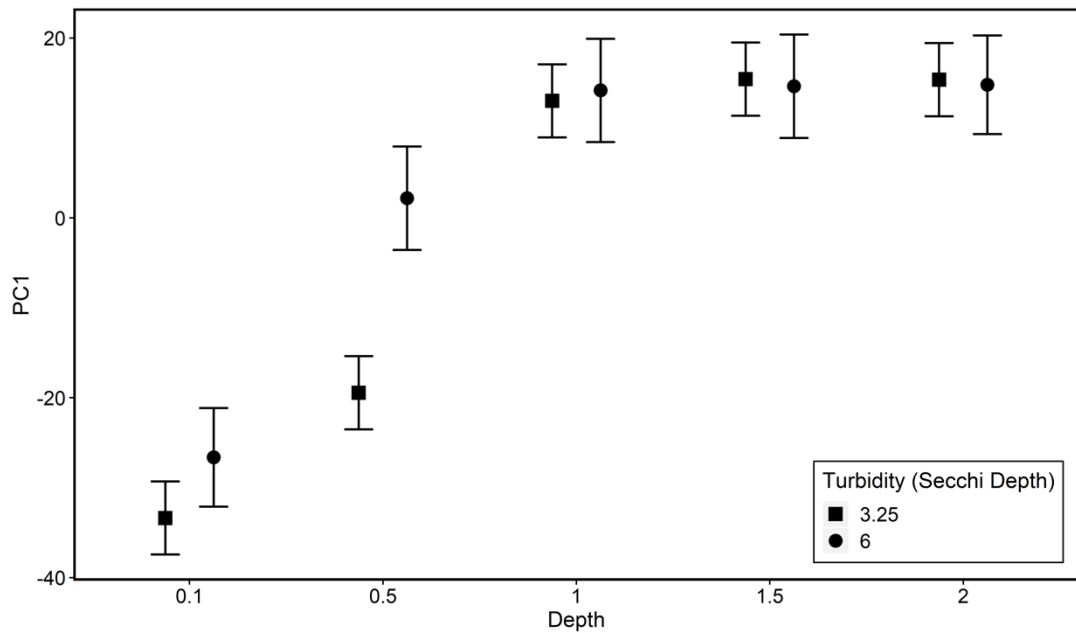


Figure 30: Model predictions plot with two standard deviations (and 95% confidence interval) of PC1 for *Undaria pinnatifida* at different Secchi depth levels (m) within each water depth level (m)

4.3.4 Effect of depth and turbidity on the spectral reflectance of *Ecklonia radiata*

A PCA on standardised spectral data of *E. radiata* showed a maximum variance of 83.49% explained by the first principal component (PC1). Wavelengths between 688 and 750 nm were most strongly, and negatively, associated with PC1 (Figure C-7).

Linear mixed-effect modelling. A mixed-effects model including depth, turbidity and the interaction between best explained variation in PC1 for *E. radiata*, with marginal and conditional R^2 of 0.96 and 0.97, respectively. A likelihood ratio test revealed that the best model, model A (AIC = 850.15), had more statistical support than the three other alternative models (Table C-1).

The wavelengths that describe *E. radiata* at depths of 0.1m and 0.5m at turbidity of 3.25m Secchi depth and 0.1m water depth at turbidity of 6m Secchi depth were between 688 – 750 nm. At depths 1.5m and 2m, at both turbidity levels, the wavelengths (based on loading values, they were between 426 – 567 nm) that described

E. radiata were not significantly different (Figure C-8). Turbidity did not have a significant effect on the spectral reflectance at the wavelengths describing *E. radiata* within each depth except at 0.5m depth (Figure C-8).

4.3.5 Discrimination of *Undaria pinnatifida* from *Ecklonia radiata* at various depth and turbidity levels using field spectroscopy data

Resampling the hyperspectral data to match low spectral resolution Micasense Rededge-m sensor to create Dataset B resulted in a loss of spectral fidelity (Figure 31). Tuned parameter settings for the random forest models produced better accuracy than the one with default parameter settings (Table 14 and Table C-2). At low turbidity, discrimination between the two seaweed species using dataset A is better than dataset B (Figure 32). Dataset A includes spectral reflectance values at wavelengths 571, 716-721 and 750 nm. Dataset B includes spectral reflectance values from hyperspectral data resampled to match Micasense Rededge-m spectral bands. On further assessment, the two seaweed species are discriminated with good accuracy in both datasets (A and B) and the accuracy increases with increasing depth (Figure C-9). At both turbidity levels, discrimination between the two seaweed species was better using Dataset A compared to Dataset B at a depth of 0.1 by 14% (lower turbidity) and 23% (higher turbidity). At depths of 0.5m and 1.5m, discrimination between the two species at lower turbidity was better using dataset A than dataset B by 15% and 5%, respectively. Overall, the discrimination was better at higher turbidity (Secchi depth of 3.25m) compared to lower turbidity (Secchi depth of 6m) at all depth levels for both datasets.

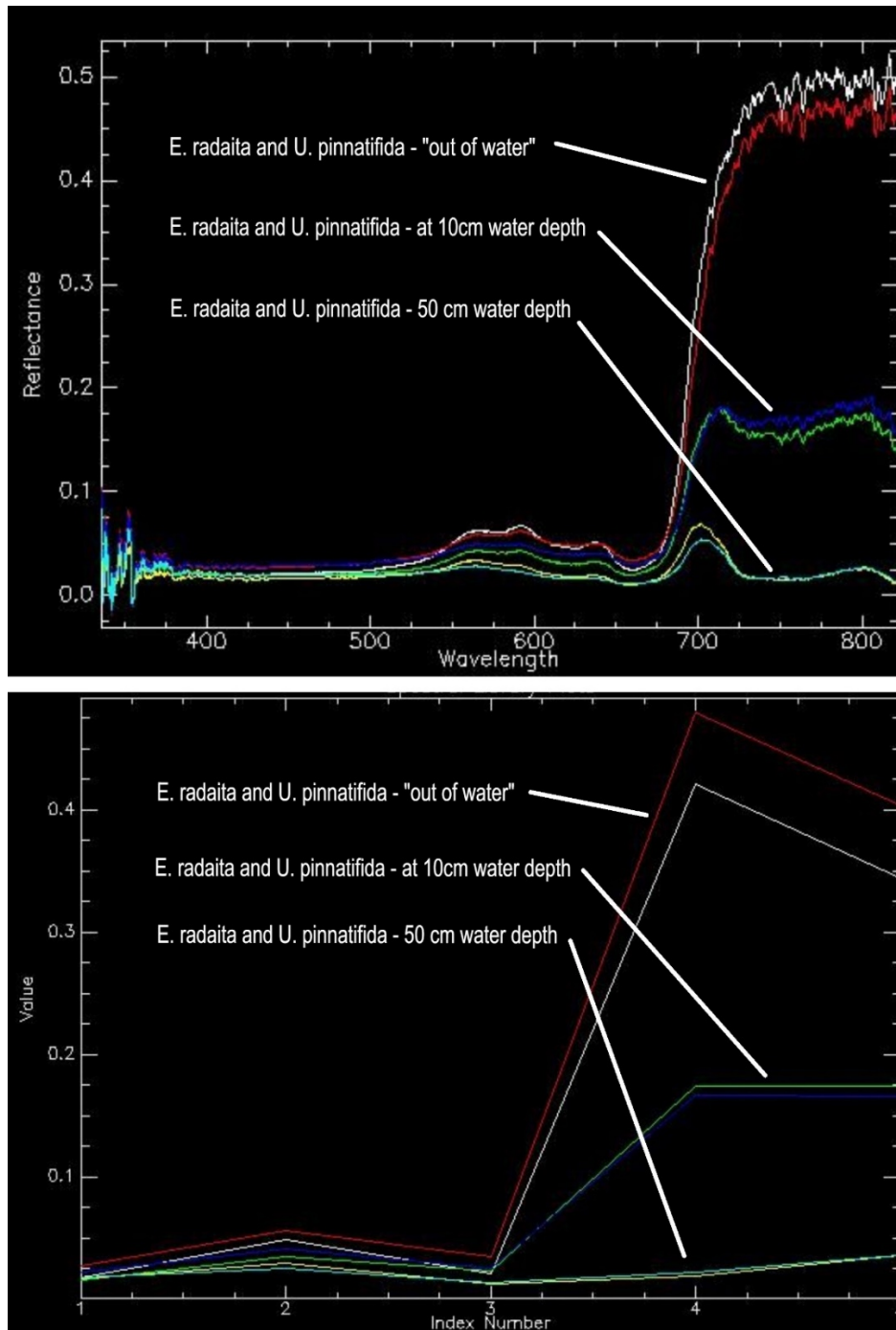


Figure 31: Raw hyperspectral reflectance values (top) and Rededge-m resampled spectral reflectance values (bottom) of *E. radiata* and *U. pinnatifida*. The x-axis represent wavelengths in nm (top) and index numbers 1, 2, 3, 4 and 5 represent blue, green, red, NIR and rededge, respectively (bottom). The y-axis represent the reflectance values and it ranges between 0 – 1.

Table 14: Parameter settings for each of the random forest models across all depths within a turbidity level. ‘ntree’ is the number of trees created in the model, mtry is the number of wavelengths tried at each split. Dataset A includes wavelengths 517, 716 – 721, 750 nm while dataset B includes wavelengths resampled to Micasense RedEdge sensor.

| Dataset | Turbidity (Secchi depth in m) | ntree | mtry |
|---------|-------------------------------|-------|------|
| A | 6 | 280 | 1 |
| | 3.25 | 300 | 5 |
| B | 6 | 500 | 2 |
| | 3.25 | 500 | 2 |

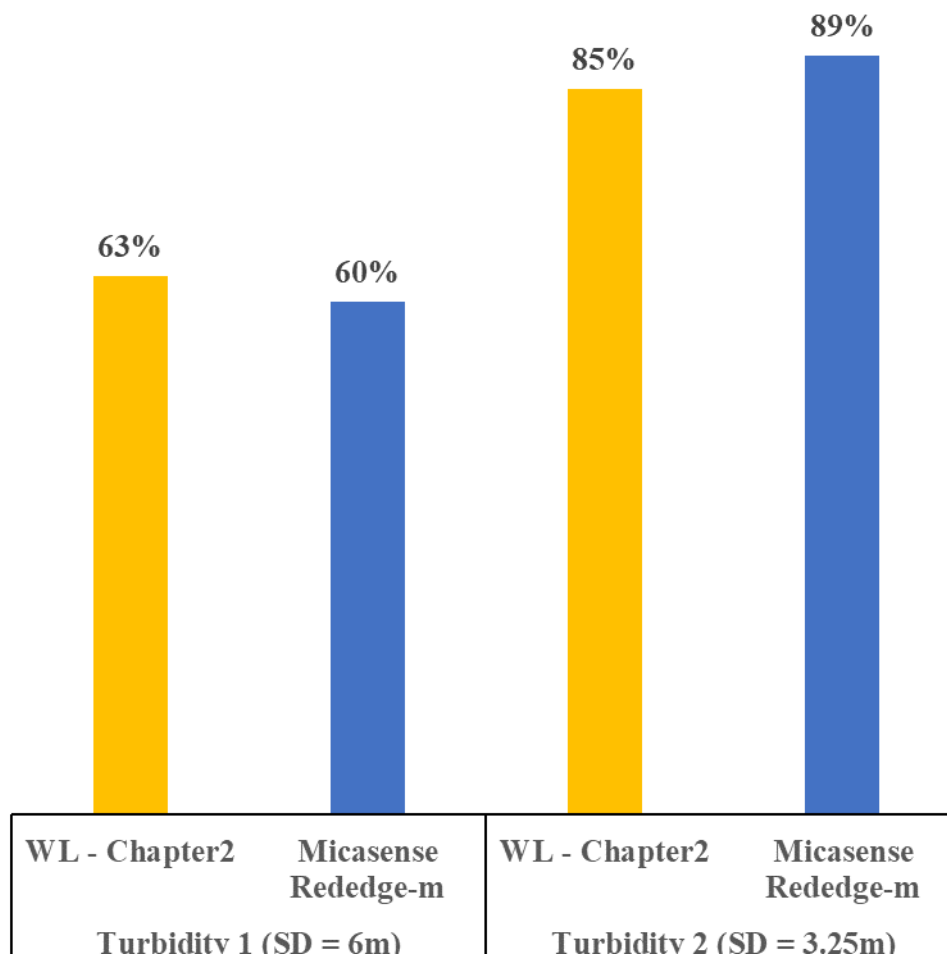


Figure 32: Comparison of the overall accuracy of random forest model classification using two types of datasets for two turbidity levels across all depths. Dataset A includes spectral reflectance values at wavelengths 571, 716-721 and 750 nm (represented in yellow). Dataset B includes spectral reflectance values from hyperspectral data resampled to match Micasense Rededge-M spectral bands (represented in blue). WL – wavelengths.

4.3.6 Discrimination of *Undaria pinnatifida* from *Ecklonia radiata* at various depth and turbidity levels using UAV-collected multispectral data

After sorting the processed multispectral images to respective folders using the identifiers visible on top of the boat, only three out of five individuals each of *U. pinnatifida* and *E. radiata* could be verified to images. For the first step of determining the image type that best classified both the seaweed species, there was a total of 60 multispectral UAV images each of raw reflectance and standardised image type over the depth experiment that were classified using raw reflectance and standardised spectral libraries resampled to Micasense RedEdge-m sensor, respectively.

Visual assessment of 132 classified images of both seaweed species at five depth levels was conducted. While raw reflectance spectral library on raw reflectance multispectral image classified both seaweed species better than that of standardised data, it classified many non-seaweed areas as seaweed pixels (Figure 33 and Figure C-10) – error of commission. The level of such noise only increased with depth (Figure 34). However, noise in classified images of standardised multispectral data and the coverage of correctly classified reference seaweed individuals were less.

Spectrometer-derived spectra of both seaweed species at depths 1m, 1.5m and 2m did not classify the reference seaweed pixels in standardised data with high accuracy and large areas of non-seaweed pixels were being misclassified as seaweed. To overcome this issue, spectra samples over reference seaweed individuals of both species were derived from standardised images. This procedure was performed on images captured at FH of 10m as the pixels were pure at such a high spatial resolution.

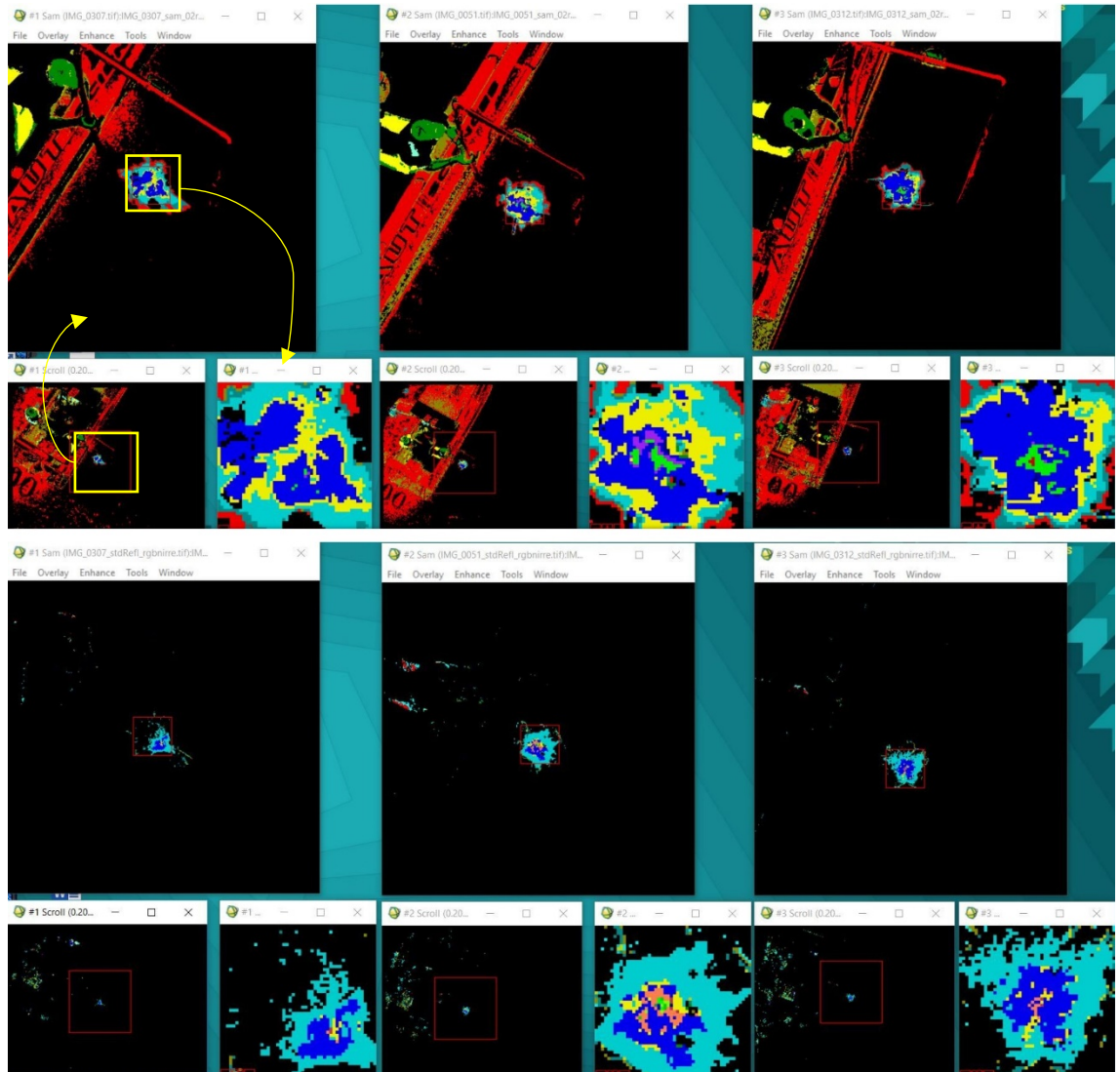


Figure 33: Screenshot of images of three different *E. radiata* individuals at 10cm below water surface classified using raw reflectance spectral signature of *E. radiata* at 10cm water depth on raw reflectance multispectral data (top set of 9 images) and standardised reflectance spectral signature of *E. radiata* at 10cm water depth on standardised multispectral data (bottom set of 9 images). The data was captured at FH of 10m.

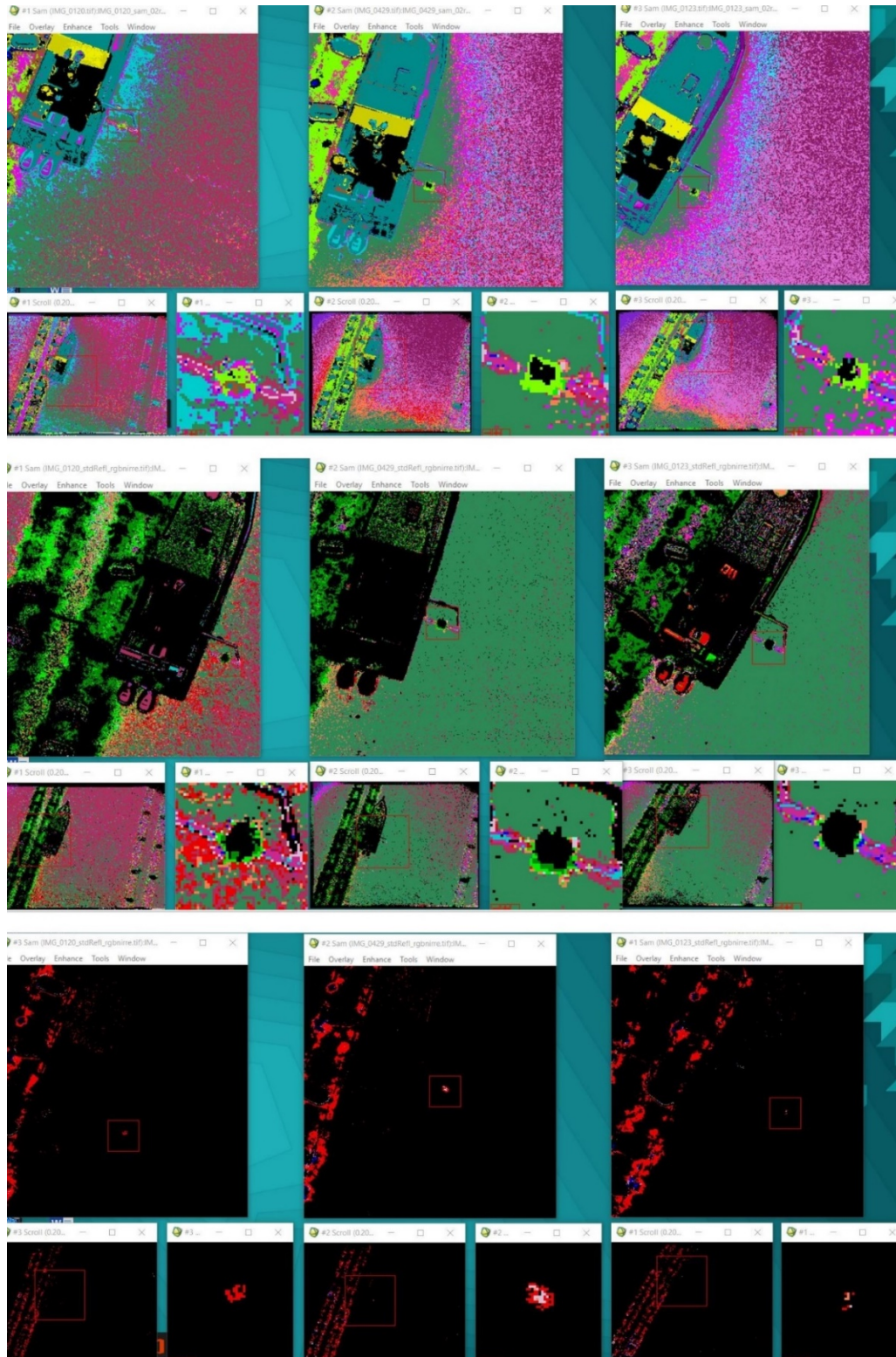


Figure 34: Screenshot of images of three different *U. pinnatifida* individuals at 1m below water surface classified using spectrometer-derived raw reflectance spectral signature of *U. pinnatifida* at 1m water depth (top set of 9 images), the spectrometer-derived standardised spectral signature of *U. pinnatifida* at 1m water depth (middle set of 9 images), the image-derived standardised spectral signature of *U. pinnatifida* at 1m water depth (bottom set of 9 images). The data was captured at FH of 30m.

Based on the producer's accuracy of non-seaweed class and user's accuracy of seaweed class, classification of standardised UAV data using the standardised spectrometer-derived spectral library for both seaweed species at depths 10 cm and 50 cm produced better results than raw reflectance data (Figure 35). Whereas for reference seaweeds at depths 1m, 1.5m and 2m, classification of standardised reflectance UAV data using image-derived spectra yielded good results (Figure 35). For detailed classification accuracy assessment refer to Tables C-5 to C14 in Appendix C.

For the second step of classification, a modified standardised spectral library including spectrometer-derived spectra of both seaweed species at depths 10cm, 50cm and image-derived spectra of the boat, buoy, water, glint and both seaweed species at depths 1m, 1.5m, 2m was created. All the spectral signatures were utilised to classify 60 standardised UAV multispectral images of *U. pinnatifida* and *E. radiata* at five depth levels captured at FH of 10m and 30m.

Visual assessment of these classified images showed some misclassification between the two seaweed species at shallow depths such as 10cm, 50cm and 1m within the reference seaweed area (Figures C-11 to C-13 and C-16 to C-18). However, on images captured at FH of 30m, most of the reference seaweed pixels at depths 1.5m and 2m remained unclassified (Figures C-14, C-15, C-19 and C-20). At FH of 10m where the spatial resolution was very high, the shadow of the boat was being classified as *E. radiata* or *U. pinnatifida* at depths 1.5m and 2m. *U. pinnatifida* at depths of 10cm and 50cm remained mostly unclassified with the threshold value of 0.2 radians on images acquired at FH of 30m. The values were increased to 0.4 radians for better classification.

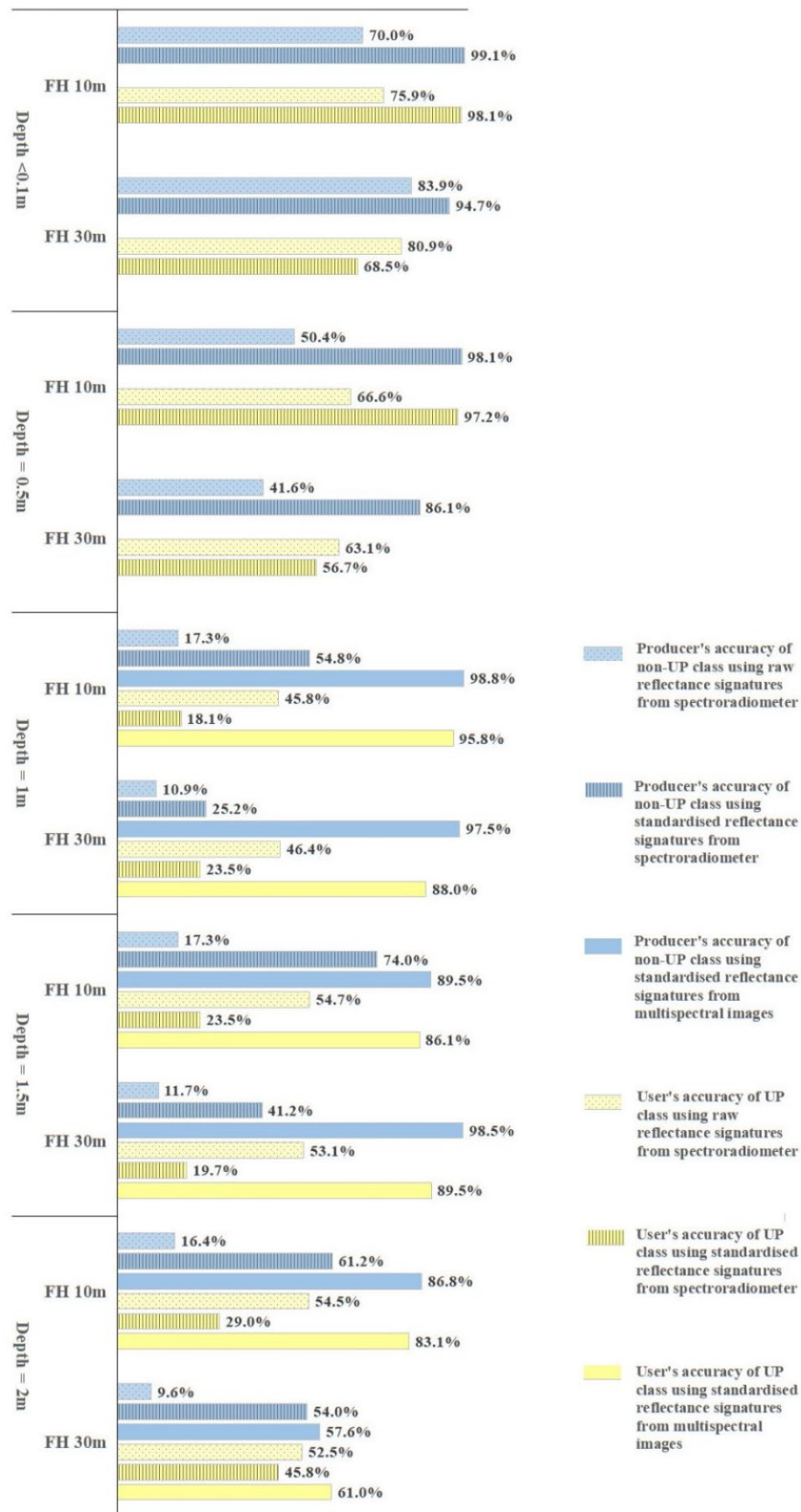


Figure 35: Classification accuracy assessment of *U. pinnatifida* at five depth levels and two spatial scales at FH 10 and 30m. FH – flight height. Shades of blue represent the producer's accuracy of non-seaweed class and shades of yellow represent the user's accuracy of seaweed class. Dots and vertical lines represent accuracy using raw and standardised reflectance signature from spectroradiometer, solid fill represents standardised reflectance signature from multispectral image.

At level 1 (collation of individuals), producer's accuracy of the reference seaweed class at each depth varied between 21 – 38% and 3 – 39% for *E. radiata* on images acquired at FH of 10m and 30m, respectively. Whereas the producer's accuracy varied widely for *U. pinnatifida* at FH 10m (12 – 55%) and FH 30m (0.01 – 31%). The depth level classification accuracy assessments of reference seaweed classes are provided in tables C-15 to C-24.

At level 2A (collation of each species), the low producer's accuracy and kappa value of both seaweed species at depths of 1.5m and 2m from images collected at FH of 30m (Tables C-18, C-19, C-23, C-24) decreased the overall accuracy and kappa values (Figure 36)., As a result, only accuracy values of both seaweed species at depths 10cm, 50cm and 1m were considered for next level of classification. Detailed classification accuracy assessment results are presented in Tables C-25 to C-28 in Appendix C.

Accuracy assessment at level 2B (collation of both species) revealed the two seaweed species were discriminated from each other better in data acquired at FH of 30m than at FH of 10m (Figure 37). Detailed classification accuracy values are presented in Tables C-29 and C-30.

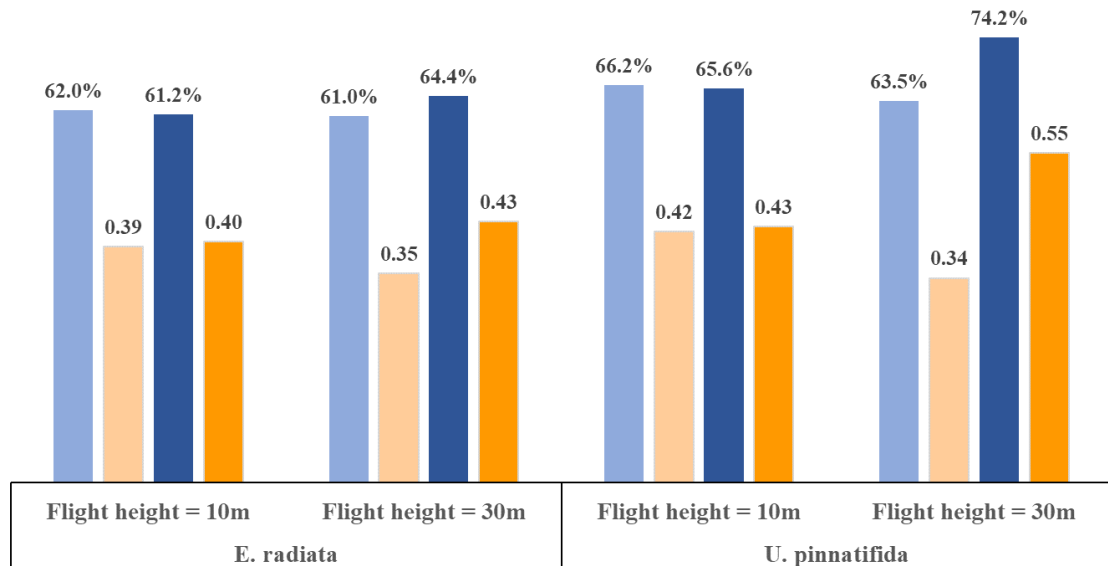


Figure 36: Classification accuracy assessment of *Ecklonia radiata* and *Undaria pinnatifida* collated across depth levels at two spatial scales. Shades of blue represent overall accuracy (OA) and shades of yellow represent kappa (K) values. The lighter shade of both colours represents OA and K where assessment is collated at five depth levels combined. The darker shade of both colours represents OA and K where assessment is collated at depths 10cm, 50cm and 1m.

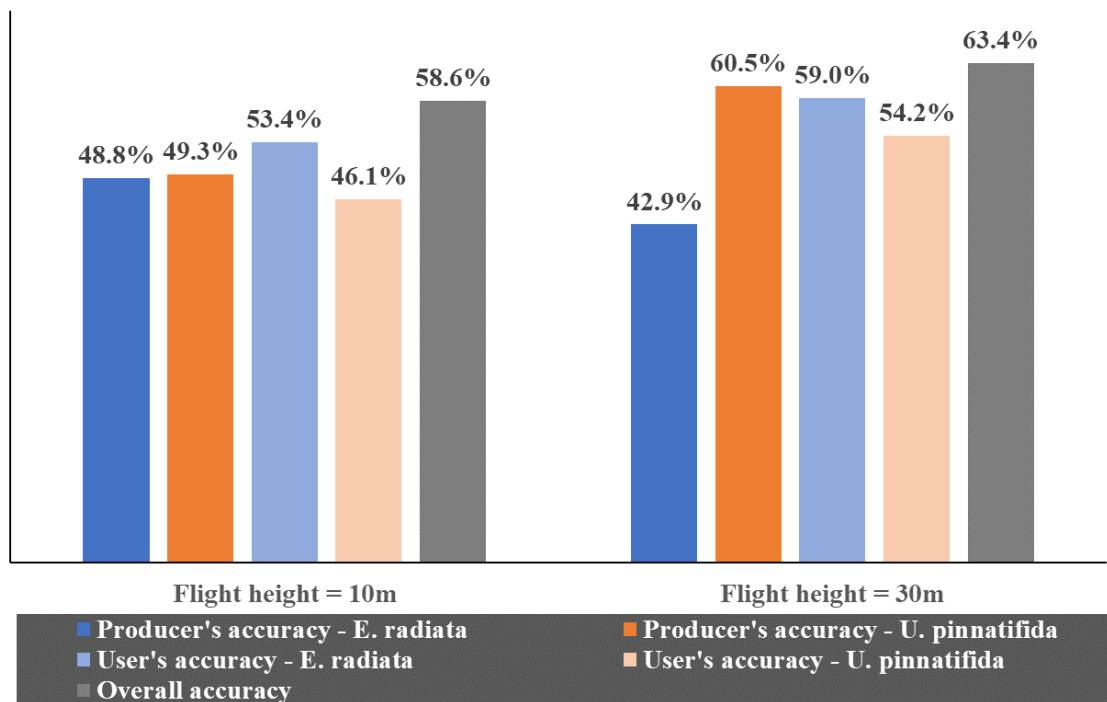


Figure 37: Collated classification accuracy assessment of both seaweed species at all depth levels combined at two spatial scales.

4.3.7 Application: Classifying *Undaria pinnatifida* and *Ecklonia radiata* along rocky reef using high spatial resolution Rededge-m multispectral UAV data

True colour RGB image created from the multispectral bands using red, green and blue bands in the red, green and blue channels, respectively, represents what our eyes see (Figure 38A). Whereas certain combinations of these spectral bands in the red, green and blue channels in the software enhance features of interest depending on the combination – the image is called false colour composite. For example, a combination of NIR, red and green in red, green and blue channels respectively enhances the vegetation which appears in red (Figure 38B). This helped in visual assessment of classification where the seaweed classification can seem misleading in certain areas in true colour RGB.

The multispectral rocky reef mosaic was standardised since this technique reduced the noise in classification (based on the analysis in step 1 (Figure 20)). The land was masked before the SAM classification (Figure 39). The rocky reef AOI was classified using a Spectral Angle Mapper (SAM) classification technique using the standardised spectral library that includes a) spectrometer-derived spectral signatures of both seaweed species from two turbidity and two depth levels (10cm and 50cm) and b) image-derived spectral signatures of glint, water and both seaweed species at a depth of 1m.

While rocky reef classification produced both seaweed species at five depth levels, all classes of *E. radiata* were combined into one *E. radiata* class and all classes of *U. pinnatifida* were combined into one *U. pinnatifida* class. From the classification, areas covered by *U. pinnatifida* and *E. radiata* within the rocky reef AOI were 76 sqm and 108 sqm, respectively (Figure 40). The classification accuracy aggregated at level 2B from depth experiment translates to the rocky reef classification since the area was

mostly covered by *E. radiata* and *U. pinnatifida* (from diver's observation) and the data was acquired on the same day as depth experiment. On data acquired at FH of 30m over depth experiment, 60% of *U. pinnatifida* was classified correctly, however, only 54% of classified *U. pinnatifida* pixels were reliable. Whereas, 43% of *E. radiata* was classified correctly and 59% of classified *E. radiata* pixels were reliable. Overall classification accuracy was 63% with a kappa of 0.45 indicating moderate agreement. Additionally, the classification was visually assessed for the presence of *U. pinnatifida* within the 20cm buffer of each of the 20 validation points (Figure 41).

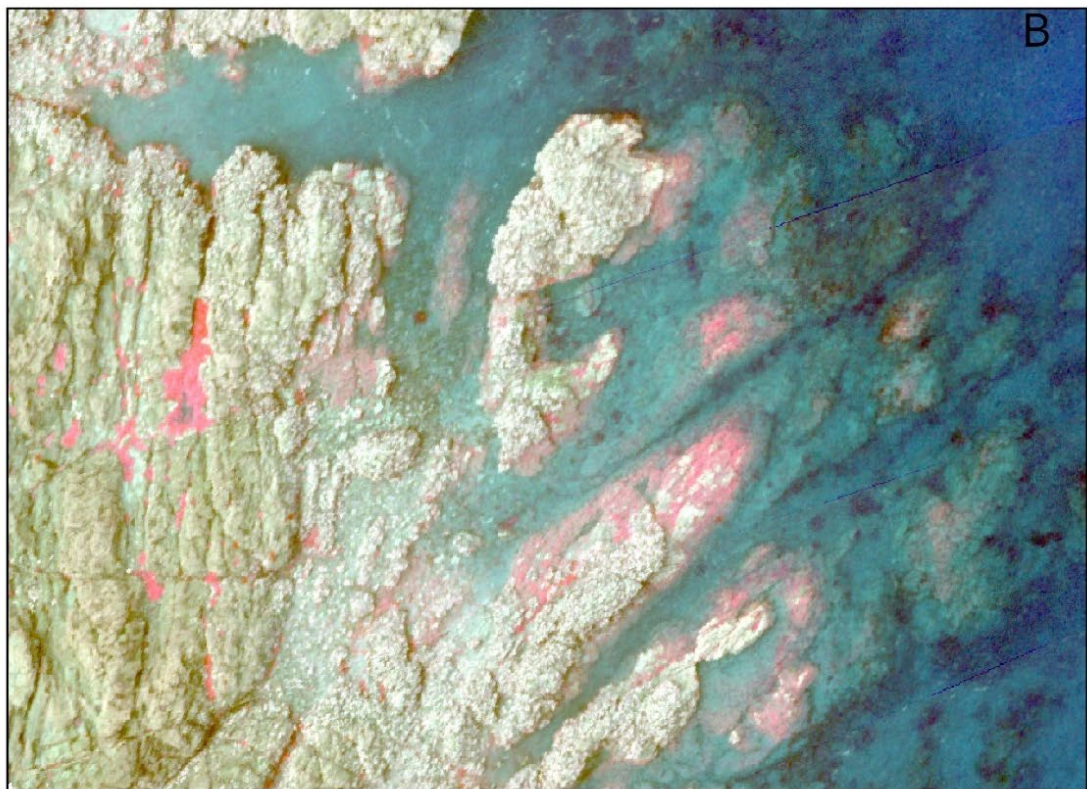


Figure 38: (A) True colour RGB image of a section of the AOI, (B) False colour composite enhancing vegetation of the same area.

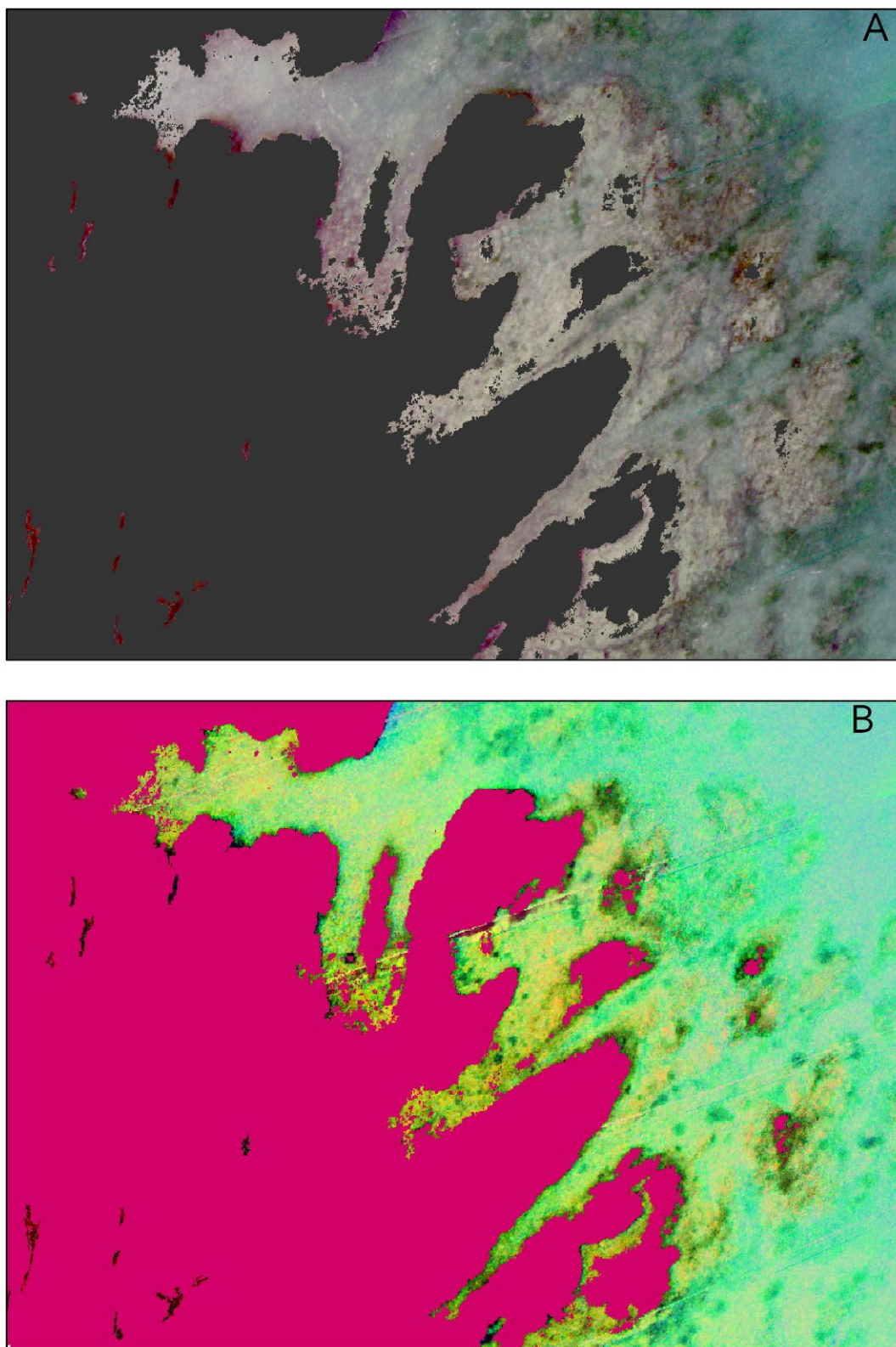


Figure 39: (A) True colour RGB image of a section of the AOI with the land area masked (in black), (B) standardised RGB image of the same area with the land masked (in red).

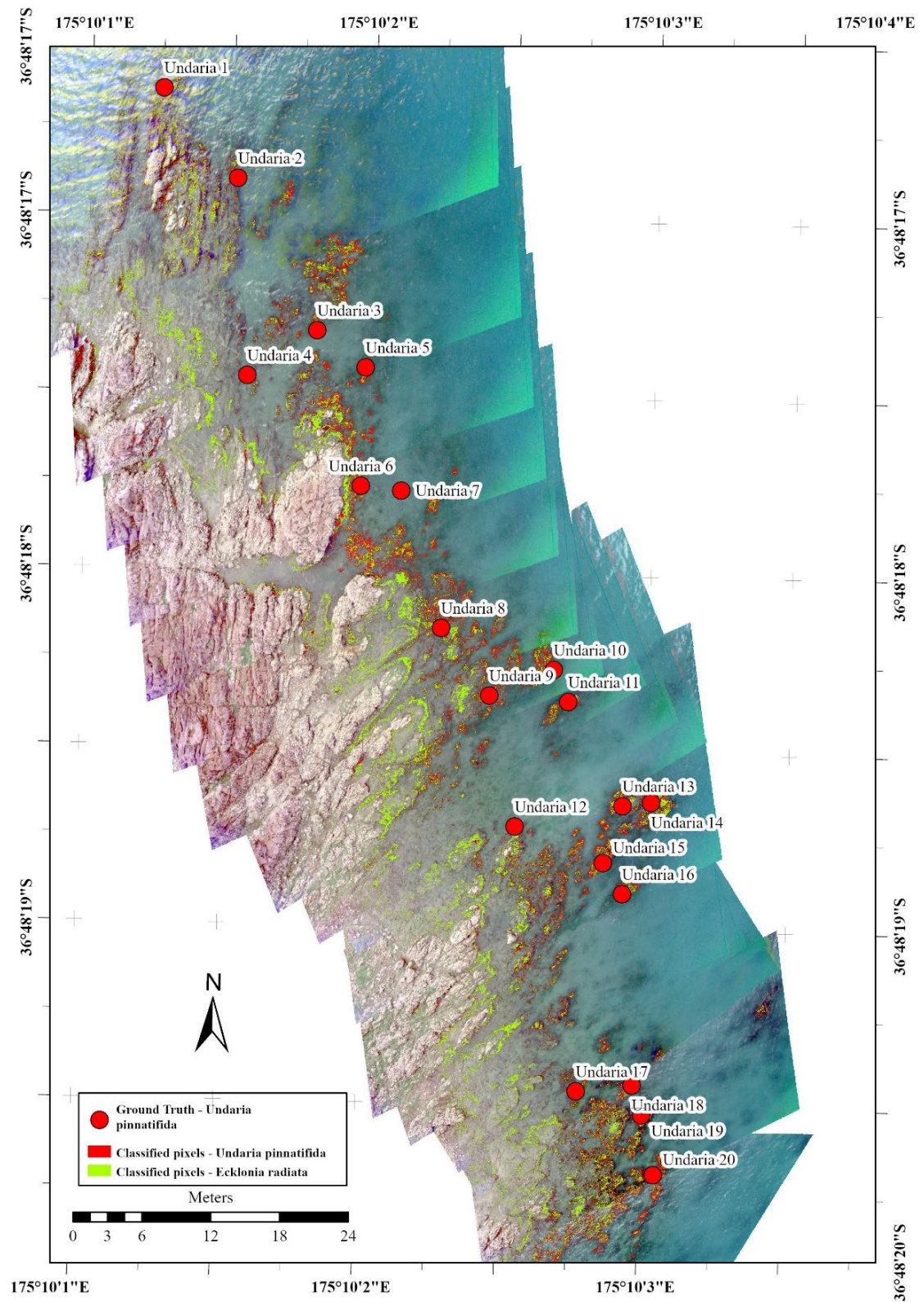


Figure 40: Rocky reef classification. Classification of *U. pinnatifida* is in red and that of *E. radiata* is in green.

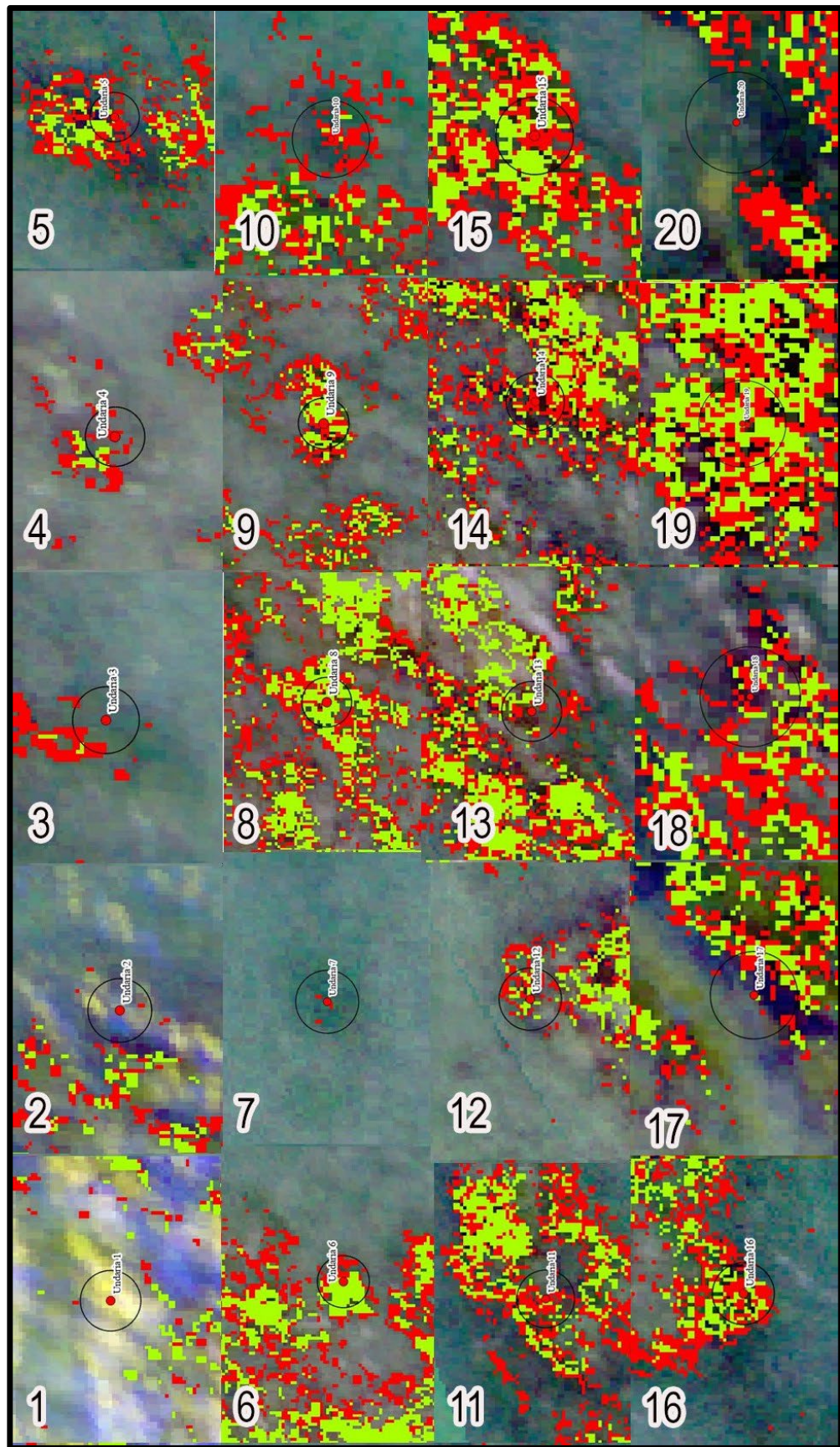


Figure 41: Screenshot of classification of *U. pinnatifida* (red) and *E. radiata* (green) within a buffer of 20cm radius (black circle) at 20 validation locations in the rocky reef

4.4 Discussion

U. pinnatifida is a prolific invasive seaweed in NZ. In order to apply remote sensing techniques to map these seaweed species, it is crucial to understand its spectral reflectance characteristics and the ability to discriminate it from other spectrally similar commonly found NZ native seaweed species such as *E. radiata*. This is the first detailed empirical study to assess various remote sensing aspects of *E. radiata* and *U. pinnatifida* from assessing its hyperspectral signatures to discriminating the two seaweed species on multispectral ultra-high spatial resolution images. The study shows that depth has a significant impact on the spectral variability irrespective of the turbidity levels and the discrimination of spectrally similar seaweed species, *E. radiata* and *U. pinnatifida*, is feasible from both field-spectroscopy and multispectral ultra-high resolution UAV images.

Depth affects the spectral reflectance values of both *E. radiata* and *U. pinnatifida* down to 1m depth, however, deeper than 1.5m there is no significant effect. This result is consistent with other submerged vegetation studies around the world (O'Neill et al., 2011; Uhl et al., 2016) and vegetation signal rapidly decreases within the first 2m of water depth (Vahtmäe and Kutser, 2013). However, turbidity did not influence spectral reflectance within each depth (0.1m, 1m, 1.5m and 2m) except at 0.5m depth. The effect of reduced turbidity (i.e. where 6m Secchi depth) on spectral reflectance values at 0.5m water depth was relatively similar to that at 1m water depth (Figure C-8 and Figure 30). It is expected to be similar to the effect at 0.1m water depth as there was still some reflectance from rededge (~700nm) region of the spectrum (Figure 31). Therefore, the difference in the effect of turbidity at 0.5m depth could likely be due to the composition of the water column particles at that depth. This in turn causes higher reflectance in the visible region. In addition to the sky conditions and glint, the effects could likely be confounded. The glint removal technique on

hyperspectral readings from spectrometer did not perform very well due to the insufficient wavelength regions to model the glint spectrum.

This study used hyperspectral readings of the two seaweeds to assess the feasibility of using available low-cost remote sensing technology such as Micasense Rededge-m sensor on UAV for ultra-high spatial resolution mapping. Since both *U. pinnatifida* and *E. radiata* belong to the Phaeophyceae taxonomic group (brown seaweeds), the feasibility of using wavelengths that discriminated *U. pinnatifida* from other brown seaweed species which was identified in Chapter 2 was assessed. The accuracy of discriminating the two seaweeds varied with turbidity and depth. The overall accuracy at 10cm water depth was 43% in relatively clear waters (turbidity 6m) and actually improved to 65% in more turbid waters (turbidity 3.25m) when using Micasens Rededge-m sensor. However, the overall accuracy could be increased to 57% (turbidity 6m) and 87.5% (turbidity 3.25m) when using the target wavelengths identified in this study. Although accuracy increased with the increasing water depth, the water constituents (CDOM, TSM, Chl-a) at depths of 1m and deeper will contribute more towards the spectral signatures of these seaweed species, depending on its composition in the water column. These water constituents can increase the reflectance in the visible region.

The UAV borne multispectral reflectance images were standardised before image classification. This standardisation technique enabled the use of all the spectral signatures in the spectral library from the depth experiment for classification. It reduced a lot of noise (Wehrens, 2011) which in turn reduced misclassification of non-seaweed pixels. Image classification using reflectance values classified all of the seaweed individual but that was not the case with standardised reflectance values (Figure 33).

However, for applications such as biomass estimation, it is crucial to have the entire individual classified, if possible.

Although the overall accuracy of classification of *U. pinnatifida* and *E. radiata* remained similar between the two spatial scales at which multispectral images were acquired (i.e. FH 10m and FH 30m), classification of data acquired at FH of 30m performed slightly better than that at FH of 10m. Classification accuracy of *E. radiata* and *U. pinnatifida* on data acquired at FH 30m improved with the exclusion of accuracy values at depths 1.5m and 2m. This is likely due to the presence of the shadow of the boat in the image-derived (FH of 10m) spectral data of *E. radiata* and *U. pinnatifida* at depths 1.5m and 2m. On data acquired at FH of 30m, some areas of both seaweed species at 1.5m water depth were being classified by spectra associated with both seaweed species at depths between 0.1m to 1m (Tables C-18 and C-23, Figures C-14 and C-19).

On the rocky reef classification data that was acquired on the same day as the depth experiment, some of the points were directly over *U. pinnatifida* pixels such as points 4, 5, 10, 11, 14 and 15 (Figure 41). Classification at validation point 7 was different from the rest of the points due to the absence of *E. radiata* class within the buffer and the presence of adjacent sand substrate. There have not been many intra-taxon studies on seaweeds at ultra-high spatial resolution multispectral data. However, the accuracy of SAM classification was comparable to a study by Rossiter et al. (2020) that used ultra-high spatial resolution hyperspectral data to also classify various brown seaweed species using an in-situ spectral library. It is important to note that the brown seaweed species in the study area for that study were not submerged in water, nevertheless, the accuracy was 71%. Taddia et al. (2019) also used ultra-high spatial

resolution Rededge-m data to map submerged green seaweed with high accuracy (the exact number was not mentioned in the study).

Direct georeferencing process in the study needs further work to georeference images of various orientations correctly. It works for images with yaw angle of 180 degrees but not for that of 0 degrees. Also, the use of Real-Time Kinematic (RTK) or similar high-accuracy GPS solutions co-mounted onboard the UAV and connected to the multispectral imaging sensor would improve the locational accuracy. This is a correction technique that corrects the location of data in real-time (Pix4D, 2020a). This would be particularly beneficial in applications where GCPs are difficult to obtain and high accuracy is vital such as change detection studies over aquatic habitat, especially identifying invasive species from baseline data.

Chapter 5. Conclusion

This research aimed to evaluate remote sensing techniques and technology for discriminating seaweeds in NZ, with a focus on the separability of invasive species *U. pinnatifida* from other common native seaweed species. It is the first study to investigate the key wavelengths that discriminated *U. pinnatifida* from other common habitat forming NZ native seaweed species; analyse the effect of season and location on NZ native seaweed species, *C. maschalocarpum* and *E. radiata*; discriminate submerged seaweeds, *U. pinnatifida* and *E. radiata*, using multispectral ultra-high resolution UAV images. This chapter will discuss the findings from chapters 2, 3 and 4 and provide future research ideas.

5.1 Insights from the study

The hyperspectral library of common NZ native and invasive seaweeds created for the study is the first in NZ for seaweeds. This library has allowed the following: discrimination of seaweeds at species level (*U. pinnatifida* from rest of red, brown and green seaweeds) with >70% overall; conclude season and depth influences the spectral reflectance of the seaweed species; discrimination of *U. pinnatifida* and *E. radiata* from ultra-high spatial resolution multispectral images with >60% overall accuracy. Using hyperspectral field spectroscopy, it was possible to discriminate seaweed species at broad taxonomic levels (red, green and brown seaweeds) which concurs with studies around the world where the seaweeds were discriminated at broad taxa level with high accuracy. The wavelengths that discriminate the seaweed species at broad taxa level are coincident with absorption features of pigments unique to each taxonomic group. The findings from this study concludes hyperspectral discrimination could be applicable to other species beyond those in the current study. Fucoxanthin content changes for *U. pinnatifida* (Fung et al., 2013) and it was reported to vary significantly with season and

life cycle of the algae, peaking between the winter and spring (mature phase of sporophyte) and lowest during summer (senescence phase) (Terasaki et al., 2009). Once the spectral signature associated with a particular pigment profile is ascertained then the variability could be used to identify species or seasonal variability or even relative “health” of populations. Conclusions of previous studies are conflicting on species-level discrimination of submerged aquatic vegetation where some report difficulty in finding differences at the species level (e.g., Casal et al. (2013)) while some are successful (e.g., Rossiter et al. (2020)). This current study is a step forward where *U. pinnatifida*, a brown seaweed, is discriminated from other brown seaweeds successfully. Most of the wavelengths that were influential in discrimination were in the NIR region of the spectrum, similar to the findings by Casal et al (2013). It also identified a wavelength in the visible region (574 nm) that will not be attenuated by the water column as much as the NIR region. For remote sensing surveys mapping subtidal (submerged) seaweeds, presence of discriminatory wavelengths in the visible region of the EM spectrum rather than in the NIR region facilitates better chance of information retrieval since much of the information is lost due to water absorption in NIR region. The discrimination techniques were evaluated and found that PLS-DA and random forest were better suited for variable reduction and classification, respectively.

The PCA revealed a partial overlap between brown and red seaweeds but green was separate from browns and reds. Within browns, *Hormosira banksii*, *Ecklonia radiata*, *Dictyota ocellata*, *Cystophora torulosa*, *Carpophyllum maschalocarpum* and *Xiphophora chondrophylla* could be most clearly differentiated (Figure A-1). However, *Carpophyllum plumosum*, *Cystophora retroflexa* and *Carpophyllum flexuosum* could not be differentiated. Within reds, all species showed total separation from each other, except *Cladhymenia oblongifolia* and *Corallina officinalis* that could not be clearly differentiated, and *Pyropia plicata* could not be differentiated from *Melanthalia*

abscissa. These results concur with a study by Tait et al. (2019), where spectrally similar *H. banksii* and *C. maschalocarpum* were easily separable from the spectrally rich dataset and red seaweed species had unique spectral signatures. Most of the species in this group were separated due to wavelengths in the NIR region (702–749 nm). Among greens, both *Ulva spp.* and *Codium fragile* both showed total separation from each other. This would mean that using imaging sensors that have the wavelengths that discriminate the two species it is possible to map the two green seaweed species from UAV remote sensing survey.

The accuracy of mapping across different dates and locations depends highly on accurate spectral reflectance data. It is important to understand the impact of main factors such as season, location, water depth and turbidity. Although the focus was on *U. pinnatifida*, two NZ native seaweed species (*E. radiata* and *C. maschalocarpum*) were used to understand the effect of season and location. *E. radiata* and *C. maschalocarpum* were considered for the study of the effect of season and location since it co-occurs with *U. pinnatifida*. Without prior knowledge, it was harder to ascertain the presence of *U. pinnatifida* and *E. radiata* at the same location across all seasons. Season affects the spectral reflectance compared to location for both species. Wavelengths describing *C. maschalocarpum* were not significantly different in winter or spring across all locations. Wavelengths describing *E. radiata* were not significantly different in winter across all locations. This means any remote sensing data collected for both seaweed species during winter across all locations would be comparable. A detailed discussion of the effect of season and location is presented in section 3.4.

In addition to season and location, water depth and turbidity also affect the spectral reflectance of submerged seaweeds significantly. Since *U. pinnatifida* is usually found at high densities at 0-3 m below mean low water in the shallow subtidal or very

low intertidal zone, it was crucial to understanding the effect of water depth and turbidity on its spectral reflectance across these depth zones. *E. radiata* is one of the commonly found brown seaweeds that also co-occurs with *U. pinnatifida*. Analysis of the spectral data of both seaweed species at five depth and two turbidity levels revealed that depth has a significant effect in different parts of the electromagnetic spectrum from 10cm down to 1m. However, between the two turbidity levels, there was no significant difference in wavelengths describing both seaweed species at each depth. Using hyperspectral data from field campaign, *U. pinnatifida* and *E. radiata* were discriminated from each other successfully at each depth within a turbidity level and the accuracy increased with depth. This study used low-cost multispectral sensor onboard UAV to map two brown seaweed species at an overall accuracy of 63% and kappa of 0.45 (moderately agreeable). Along with the direct georeferencing technique implemented in this study, it makes mapping of submerged seaweed at species level in relatively clear waters affordable and quick.

Standardization of data from field spectroscopy and UAV multispectral sensor improved the quality of classification by reducing noise in the data. This technique can be applied out of this study. To the author's knowledge, there are no studies that use standardisation technique on multispectral or hyperspectral images before image classification.

5.2 Future research

With the availability of the spectral library of seaweeds from various locations and seasons obtained out of the water from this research, a radiative transfer model such as Hydrolight can be used to model spectral signatures of seaweed for various water condition and depth. The modelled spectra can then be used for further studies such as the feasibility of discriminating these seaweed species at different depths for various

sensors, classifying a submerged habitat and biomass estimation. With classified images of earlier years as the base map, further applications are numerous such as habitat change analysis over time and impact analysis of invasive seaweed species like *U. pinnatifida*.

The out-of-water NZ seaweed spectral library can be used as is for mapping those seaweed species that are exposed during tidal change. Although multispectral UAV images have produced fair classification accuracy, a higher spectral resolution of the imaging sensor could potentially yield better classification accuracy at the species level.

The limitation of the UAV image classification study is the use of spectra of both seaweed species at depths 1.5m and 2m derived from UAV data obtained at FH 10m for classification. This resulted in poor classification at those depths which is likely due to shadowing of the boat. It would be recommended to obtain spectral signatures from UAV data at FH 30m. Correcting the image for glint would also be advantageous before spectra collection. The images from the depth experiment were not glint corrected due to software issues while attempting the correction following Hedley et al. (2005). Despite the limitations, the UAV image classification performed well for the rocky reef. Due to the limited number of validation points for *U. pinnatifida* and lack of validation points for *E. radiata*, only visual analysis of presence or absence of *U. pinnatifida* was performed. Further improvements include cleaning the spectral library using the multispectral images of depth experiment as validation. For example, only those spectral signatures that classified the reference seaweed pixels be used for further classification. This will likely improve the user's accuracy of the two seaweed species. Also, masking the seaweed-laden mussel line before classification would also increase the user's accuracy of both seaweed species.

Lack of static ground control features has limited the area for exploration to nearshore using UAV remote sensing. With the single image direct georeferencing workflow in this research, the study area does not need any GCPs and will process the images only using parameters intrinsic to the imaging sensor. Current process needs some manually identified tie points between images to improve mosaic results but adding high accuracy RTK GPS and IMU units to the sensor on UAV will potentially automate the image processing method. Further improvements and testing of the current process is needed to identify errors for various input for each parameter.

This research used similar remote sensing technology to that in the study by Zeng, King, Richardson, and Shan (2017). They fused data from a multispectral imaging sensor and hyperspectral spot spectroradiometer onboard UAV to estimate a hyperspectral data for each image pixel in multispectral data. Although there were numerous uncertainties in the fusion, the study had a significant impact due to the use of low-cost sensors and platform to produce a rich dataset. While their research was for precision farming applications on land, it would be beneficial to try this method for submerged habitat mapping despite the challenges of an aquatic environment. Especially since part of the challenge of image georeferencing has been addressed by this research.

The depth experiment in this research was near a mussel farm that was infested with *U. pinnatifida*. Though classified *U. pinnatifida* pixels from adjacent mussel line was not accounted for in the accuracy assessment, nevertheless all *U. pinnatifida* pixels were classified as either *U. pinnatifida* or *E. radiata* from the visual assessment. This indicates that use of the spectral library for classifying submerged seaweed is achievable with accuracy comparable to other marine habitat classification studies.

5.3 Summary

This research has contributed significantly towards understanding the spectral difference between the invasive seaweed species, *U. pinnatifida* and other native seaweed species for successfully discriminating and mapping the invasive seaweed. The research successfully studied the spectral variability of some of the NZ native seaweed species due to season and location which was not studied until now. This will help in the decision-making process on the best time to conduct remote sensing survey of seaweeds. This research also identified the challenges in processing and georeferencing multispectral remote sensing images from the UAV in an aquatic environment and developed a workflow to address the issues. A novel image pre-processing technique that reduced noise in the classified images was implemented and compared against conventional technique. The study is also the first to use 5-band multispectral ultra-high resolution UAV image to classify two submerged spectrally similar brown invasive and native seaweed species of New Zealand.

References

- Abdullah, H., Skidmore, A. K., Darvishzadeh, R., Heurich, M., Pettorelli, N., & Disney, M. (2018). Sentinel-2 accurately maps green-attack stage of European spruce bark beetle (*Ips typographus*, L.) compared with Landsat-8. *Remote Sensing in Ecology and Conservation*, 5(1), 87-106. DOI:10.1002/rse2.93
- Adão, T., Hruška, J., Pádua, L., Bessa, J., Peres, E., Morais, R., & Sousa, J. (2017). Hyperspectral Imaging: A Review on UAV-Based Sensors, Data Processing and Applications for Agriculture and Forestry. *Remote Sensing*, 9(11). <https://doi.org/10.3390/rs9111110>
- Anaconda Software Distribution. *Conda*. Version 2-2.4.0, Anaconda, Nov. 2016. Computer Software. *Anaconda*, www.anaconda.com
- Aneece, I., & Epstein, H. (2016). Identifying invasive plant species using field spectroscopy in the VNIR region in successional systems of north-central Virginia. *International Journal of Remote Sensing*, 38(1), 100-122. <https://doi.org/10.1080/01431161.2016.1259682>
- ASD Inc. (2017). *HandHeld 2: Hand-held VNIR Spectroradiometer*. Retrieved from <https://www.asdi.com/products-and-services/fieldspec-spectroradiometers/handheld-2-portable-spectroradiometer>
- Ashraf, S., Brabyn, L., & Hicks, B. J. (2012). Image data fusion for the remote sensing of freshwater environments. *Applied Geography*, 32(2), 619-628. <https://doi.org/10.1016/j.apgeog.2011.07.010>
- Ashraf, S., Brabyn, L., Hicks, B. J., & Collier, K. (2010). Satellite remote sensing for mapping vegetation in New Zealand freshwater environments: A review. *New Zealand Geographer*, 66(1), 33-43. <https://doi.org/10.1111/j.1745-7939.2010.01168.x>
- Barton, K. (2018). MuMIn: Multi-Model Inference.
- Benedetti-Cecchi, L., Pannacciulli, F., Bulleri, F., Moschella, P. S., Airoidi, L., Relini, G. & Cinelli, F. (2001). Predicting the consequences of anthropogenic disturbance: large-scale effects of loss of canopy algae on rocky shores. *Marine Ecology Progress Series*, 214, 137-150.
- Blackburn, G. A. (2007). Hyperspectral remote sensing of plant pigments. *Journal of Experimental Botany*, 58(4), 855-867. <https://doi.org/10.1093/jxb/erl123>
- Blain, C. O., & Shears, N. T. (2019). Seasonal and spatial variation in photosynthetic response of the kelp *Ecklonia radiata* across a turbidity gradient. *Photosynth Res*, 140(1), 21-38. DOI:10.1007/s11120-019-00636-7
- Botha, E. J., Brando, V. E., Anstee, J. M., Dekker, A. G., & Sagar, S. (2013). Increased spectral resolution enhances coral detection under varying water conditions. *Remote Sensing of Environment*, 131, 247-261. <https://doi.org/10.1016/j.rse.2012.12.021>
- Bradley, B. A. (2013). Remote detection of invasive plants: a review of spectral, textural and phenological approaches. *Biological Invasions*, 16(7), 1411-1425. <https://doi.org/10.1007/s10530-013-0578-9>
- Bradski, G. R., & Kaehler, A. (2008). *Learning OpenCV: Computer vision with the OpenCV library*. Sebastopol, CA: O'Reilly.

- Breiman, L. (2001). Random Forests. *Machine Learning*, 40, 5-32.
- Bue, B. D., Thompson, D. R., Sellar, R. G., Podest, E. V., Eastwood, M. L., Helmlinger, M. C., . . . Morgan, J. D. (2015). Leveraging in-scene spectra for vegetation species discrimination with MESMA-MDA. *ISPRS Journal of Photogrammetry and Remote Sensing*, 108, 33-48. <https://doi.org/10.1016/j.isprsjprs.2015.06.001>
- Cacabelos, E., Olabarria, C., Incera, M., & Troncoso, J. S. (2010). Effects of habitat structure and tidal height on epifaunal assemblages associated with macroalgae. *Estuarine, Coastal and Shelf Science*, 89(1), 43-52. <https://doi.org/10.1016/j.ecss.2010.05.012>
- Casal, G., Domínguez-Gómez, J. A., Kutser, T., Freire, J., & Sánchez-Carnero, N. (2012). Assessment of AHS (Airborne Hyperspectral Scanner) sensor to map macroalgal communities on the Ría de vigo and Ría de Aldán coast (NW Spain). *Marine Biology*, 159(9), 1997-2013. <https://doi.org/10.1007/s00227-012-1987-5>
- Casal, G., Kutser, T., Domínguez-Gómez, J. A., Sánchez-Carnero, N., & Freire, J. (2011). Mapping benthic macroalgal communities in the coastal zone using CHRIS-PROBA mode 2 images. *Estuarine, Coastal and Shelf Science*, 94(3), 281-290. <https://doi.org/10.1016/j.ecss.2011.07.008>
- Casal, G., Kutser, T., Domínguez-Gómez, J. A., Sánchez-Carnero, N., & Freire, J. (2013). Assessment of the hyperspectral sensor CASI-2 for macroalgal discrimination on the Ría de Vigo coast (NW Spain) using field spectroscopy and modelled spectral libraries. *Continental Shelf Research*, 55, 129-140. <https://doi.org/10.1016/j.csr.2013.01.010>
- Casal, G., Sánchez-Carnero, N., Sánchez-Rodríguez, E., & Freire, J. (2011a). Remote sensing with SPOT-4 for mapping kelp forests in turbid waters on the south European Atlantic shelf. *Estuarine, Coastal and Shelf Science*, 91(3), 371-378. <https://doi.org/http://dx.doi.org/10.1016/j.ecss.2010.10.024>
- Chao Rodríguez, Y., Domínguez Gómez, J. A., Sánchez-Carnero, N., & Rodríguez-Pérez, D. (2017). A comparison of spectral macroalgae taxa separability methods using an extensive spectral library. *Algal Research*, 26, 463-473. <https://doi.org/10.1016/j.algal.2017.04.021>
- Chen, W. W. (2012). *Distribution, abundance and reproduction of Undaria pinnatifida (Harvey) Suringar from the Marlborough Sounds, New Zealand* (Masters thesis). Auckland University of Technology (AUT), Auckland.
- Chiang, H. C., & Meyer, M. P. (1974). Remote Sensing Applications to Agricultural Monitoring1. *EPPO Bulletin*, 4(3), 309-315. <https://doi.org/10.1111/j.1365-2338.1974.tb02369.x>
- Cho, H. J., & Lu, D. (2010). A water-depth correction algorithm for submerged vegetation spectra. *Remote Sensing Letters*, 1(1), 29-35. <https://doi.org/10.1080/01431160903246709>
- Cho, H. J., Mishra, D., & Wood, J. (2012). *Remote Sensing of Submerged Aquatic Vegetation*. Retrieved from <http://www.intechopen.com/books/remote-sensing-applications/remote-sensing-of-submerged-aquatic-vegetation>
- Christie, H., Fredriksen, S., & Rinde, E. (1998). Regrowth of kelp and colonization of epiphyte and fauna community after kelp trawling at the coast of Norway. *Hydrobiologia*, 49 - 58.

- Clark, M. L., Roberts, D. A., & Clark, D. B. (2005). Hyperspectral discrimination of tropical rain forest tree species at leaf to crown scales. *Remote Sensing of Environment*, 96(3), 375-398. doi:<https://doi.org/10.1016/j.rse.2005.03.009>
- Cochrane, M. A. (2000). Using vegetation reflectance variability for species level classification of hyperspectral data. *International Journal of Remote Sensing*, 21(10), 2075-2087. DOI:10.1080/01431160050021303
- Cohen, J. (1960). A Coefficient of Agreement for Nominal Scales. *Educational and Psychological Measurement*, 20(1), 37-46. <https://doi.org/10.1177/001316446002000104>
- Corporation, S. I. *Pleiades-1A Satellite Sensor*. Retrieved 13/02/2017, from <http://www.satimagingcorp.com/satellite-sensors/pleiades-1/>
- Davenport, A. C., & Anderson, T. W. (2007). Positive indirect effects of reef fishes on kelp performance: The importance of mesograzers. *Ecology*, 88(6), 1548-1561. <https://doi.org/10.1890/06-0880>
- Dean, P. R., & Hurd, C. L. (2007). Seasonal growth, erosion rates, and nitrogen and photosynthetic ecophysiology of *Undaria pinnatifida* (Heterokontophyta) in southern New Zealand. *Journal of Phycology*, 43(6), 1138-1148. <https://doi.org/10.1111/j.1529-8817.2007.00416.x>
- De Backer, S., Kempeneers, P., Debruyne, W., & Scheunders, P. (2005). A band selection technique for spectral classification. *IEEE Geoscience and Remote Sensing Letters*, 2(3), 319-323. <https://doi.org/10.1109/LGRS.2005.848511>
- Dehouck, A., Lafon, V., Baghdadi, N., & Marieu, V. (2012, 2012). Use of optical and radar data in synergy for mapping intertidal flats and coastal salt-marshes (Arcachon lagoon, France) Retrieved from <http://www.scopus.com/inward/record.url?eid=2-s2.0-84873108453&partnerID=40&md5=8d9114135e07bb0bd4154aeef30f448c>
- Deysher, L. E. (1993). Evaluation of remote sensing techniques for monitoring giant kelp populations. *Hydrobiologia*, 260(1), 307-312.
- Dierssen, H. M., Chlus, A., & Russell, B. (2015). Hyperspectral discrimination of floating mats of seagrass wrack and the macroalgae *Sargassum* in coastal waters of Greater Florida Bay using airborne remote sensing. *Remote Sensing of Environment*, 167, 247-258. <https://doi.org/http://dx.doi.org/10.1016/j.rse.2015.01.027>
- DJI. (2020). *Phantom 4 Pro Specs*. Retrieved 22/07/2020, from <https://www.dji.com/nz/phantom-4-pro/info>
- Dörnhöfer, K., & Oppelt, N. (2016). Remote sensing for lake research and monitoring – Recent advances. *Ecological Indicators*, 64, 105-122. <https://doi.org/10.1016/j.ecolind.2015.12.009>
- Doughty, C., & Cavanaugh, K. (2019). Mapping Coastal Wetland Biomass from High Resolution Unmanned Aerial Vehicle (UAV) Imagery. *Remote Sensing*, 11(5). <https://doi.org/10.3390/rs11050540>
- Driscoll, R. S., Francis, R. E., Smith, J. A., & Mead, R. A. (1974). ERTS-1 Data for Classifying native plant communities - Central Colorado. 2, 1195-1211.
- Dye, M., Mutanga, O., & Ismail, R. (2011). Examining the utility of random forest and AISA Eagle hyperspectral image data to predict *Pinus patula* in KwaZulu-

- Natal, South Africa. *Geocarto International*, 26(4), 275-289.
<https://doi.org/10.1080/10106049.2011.562308>
- EarthData. (2020). *Remote Sensors*. Retrieved 29/07/2020, from
<https://earthdata.nasa.gov/learn/remote-sensors>
- ESRI. (2020, 6/16/2020). *FAQ: What is the format of the world file used for georeferencing images?* Retrieved from <https://support.esri.com/en/technical-article/000002860>
- Estes, J. E. (1985). Geographic Applications of Remotely Sensed Data. *Proceedings of the IEEE*, 73(6), 1097-1107. <https://doi.org/10.1109/PROC.1985.13240>
- Fitridge, I., Dempster, T., Guenther, J., & de Nys, R. (2012). The impact and control of biofouling in marine aquaculture: a review. *Biofouling*, 28(7), 649-669.
<https://doi.org/10.1080/08927014.2012.700478>
- Flynn, F. K., & Chapra, C. S. (2014). Remote Sensing of Submerged Aquatic Vegetation in a Shallow Non-Turbid River Using an Unmanned Aerial Vehicle. *Remote Sensing*, 6, 12815-12836. <https://doi.org/10.3390/rs61212815>
- Forrest, B. M., Brown, S. N., Taylor, M. D., Hurd, C. L., & Hay, C. H. (2000). The role of natural dispersal mechanisms in the spread of *Undaria pinnatifida* (Laminariales, Phaeophyceae). *Phycologia*, 39, 547-553.
- Fung, A., Hamid, N., & Lu, J. (2013). Fucoxanthin content and antioxidant properties of *Undaria pinnatifida*. *Food Chemistry*, 136(2), 1055-1062.
<https://doi.org/10.1016/j.foodchem.2012.09.024>
- Fyfe, S. K. (2003). Spatial and temporal variation in spectral reflectance: Are seagrass species spectrally distinct? *Limnology and Oceanography*, 48(1), 464 - 479.
- Gallardo, B., Clavero, M., Sanchez, M. I., & Vila, M. (2016). Global ecological impacts of invasive species in aquatic ecosystems. *Glob Chang Biol*, 22(1), 151-163.
<https://doi.org/10.1111/gcb.13004>
- Gameiro, C., Utkin, A. B., & Cartaxana, P. (2015). Characterisation of estuarine intertidal macroalgae by laser-induced fluorescence. *Estuarine Coastal and Shelf Science*, 167, 119-124. <https://doi.org/10.1016/j.ecss.2015.11.010>
- George, R., Padalia, H., & Kushwaha, S. P. S. (2014). Forest tree species discrimination in western Himalaya using EO-1 Hyperion. *International Journal of Applied Earth Observation and Geoinformation*, 28, 140-149.
<https://doi.org/10.1016/j.jag.2013.11.011>
- Gevaert, C. M., Suomalainen, J., Tang, J., & Kooistra, L. (2015). Generation of Spectral - Temporal Response Surfaces by Combining Multispectral Satellite and Hyperspectral UAV Imagery for Precision Agriculture Applications. *IEEE Journal of Selected Topics in Applied Earth Observations and Remote Sensing*, 8(6), 3140-3146. <https://doi.org/10.1109/JSTARS.2015.2406339>
- Giri, C., Pengra, B., Zhu, Z., Singh, A., & Tieszen, L. L. (2007). Monitoring mangrove forest dynamics of the Sundarbans in Bangladesh and India using multi-temporal satellite data from 1973 to 2000. *Estuarine, Coastal and Shelf Science*, 73(1-2), 91-100. <https://doi.org/10.1016/j.ecss.2006.12.019>
- Gold, K. M., Townsend, P. A., Herrmann, I., & Gevens, A. J. (2019). Investigating potato late blight physiological differences across potato cultivars with spectroscopy and machine learning. *Plant Science*.
<https://doi.org/10.1016/j.plantsci.2019.110316>

- Gould, R. W. J., Arnone, R. A., & Sydor, M. (2001). Absorption, scattering, and remote-sensing reflectance relationships in coastal waters: Testing a new inversion algorithm. *Journal of Coastal Research*, 17(2), 328-341.
- Haboudane, D., Miller, J. R., Tremblay, N., Zarco-Tejada, P. J., Dextraze, L. (2002). Integrated narrow-band vegetation indices for prediction of crop chlorophyll content for application to precision agriculture. *Remote Sensing of Environment*, 81(13), 416 - 426.
- Hartling, L., Hamm, M., Milne, A., et al. (2012). *Validity and Inter-Rater Reliability Testing of Quality Assessment Instruments [Internet]*. Retrieved from <https://www.ncbi.nlm.nih.gov/books/NBK92295/table/methods.t2/>
- Harvey, P. (2018). ExifTool. Ontario, Canada. Retrieved from <https://exiftool.org/>
- Hay, C., & Gibbs, W. (1996). *A practical manual for culturing the Asia sea vegetable 'Wakame' (Undaria pinnatifida): 1: Gametophytes*. Nelson, New Zealand.
- Hay, C. H. (1990). The dispersal of sporophytes of *Undaria pinnatifida* by coastal shipping in New Zealand, and implications for further dispersal of *Undaria* in France. *British Phycological Journal*, 25(4), 301-313. <https://doi.org/10.1080/00071619000650331>
- Hay, C. H., & Villouta, E. (1993). Seasonality of the Adventive Asian Kelp *Undaria pinnatifida* in New Zealand. *Botanica Marina*, 36(5), 461-476. <https://doi.org/10.1515/botm.1993.36.5.461>
- Hedley, J. D., & Mumby, P. J. (2002). Biological and remote sensing perspectives of pigmentation in coral reef organisms. In *Advances in Marine Biology* (Vol. 43, pp. 277-317): Academic Press. Retrieved from <http://www.sciencedirect.com/science/article/pii/S0065288102430064>. [https://doi.org/https://doi.org/10.1016/S0065-2881\(02\)43006-4](https://doi.org/https://doi.org/10.1016/S0065-2881(02)43006-4)
- Hedley, J. D., Harborne, A. R., & Mumby, P. J. (2005). Technical note: Simple and robust removal of sun glint for mapping shallow-water benthos. *International Journal of Remote Sensing*, 26(10), 2107-2112. <https://doi.org/10.1080/01431160500034086>
- Hillman, K., Walker, D. I., Larkum, A. W. D., & McComb, A. J. (1989). Productivity and nutrient limitation. In A. W. D. Larkum, A. J. McComb, & S. A. Shephard (Eds.), *Biology of seagrasses: a treatise on the biology of seagrasses with special reference to the Australian region* (pp. 635-685). Amsterdam, The Netherlands: Elsevier Science.
- Hoang, T., Garcia, R., O'Leary, M., & Fotedar, R. (2016). Identification and Mapping of Marine Submerged Aquatic Vegetation in Shallow Coastal Waters with WorldView-2 Satellite Data. *Journal of Coastal Research*, 75(sp1), 1287-1291. <https://doi.org/10.2112/si75-258.1>
- Hochberg, E., Atkinson, M. J., & Andre'foue't, S. (2003). Spectral reflectance of coral reef bottom-types worldwide and implications for coral reef remote sensing. *Remote Sensing of Environment*, 85(2), 159-173. [https://doi.org/10.1016/s0034-4257\(02\)00201-8](https://doi.org/10.1016/s0034-4257(02)00201-8)
- Hochberg, E. J., & Atkinson, M. J. (2000). Spectral discrimination of coral reef benthic communities. *Coral Reefs*, 19(2), 164-171. <https://doi.org/10.1007/s003380000087>

- Hu, C., Feng, L., Hardy, R. F., Hochberg, E. J. (2015). Spectral and spatial requirements of remote measurements of pelagic Sargassum macroalgae. *Remote Sensing of Environment*, **167**: p. 229-246.
- Huang, J., Wei, C., Zhang, Y., Blackburn, G. A., Wang, X., Wei, C., & Wang, J. (2015). Meta-Analysis of the Detection of Plant Pigment Concentrations Using Hyperspectral Remotely Sensed Data. *PLOS ONE*, *10*(9), e0137029. <https://doi.org/10.1371/journal.pone.0137029>
- Jakob, S., Zimmermann, R., & Gloaguen, R. (2016, 21-24 Aug. 2016). Processing of drone-borne hyperspectral data for geological applications Symposium conducted at the meeting of the 2016 8th Workshop on Hyperspectral Image and Signal Processing: Evolution in Remote Sensing (WHISPERS) <https://doi.org/10.1109/WHISPERS.2016.8071689>
- James, K. (2016). *A review of the impacts from invasion by the introduced kelp Undaria pinnatifida* Hamilton. Retrieved from https://www.researchgate.net/publication/313429187_A_review_of_the_impacts_from_invasion_by_the_introduced_kelp_Undaria_pinnatifida
- James, K., Kibele, J., & Shears, N. T. (2015). Using satellite-derived sea surface temperature to predict the potential global range and phenology of the invasive kelp *Undaria pinnatifida*. *Biological Invasions*, *17*(12), 3393-3408. <https://doi.org/10.1007/s10530-015-0965-5>
- James, K., & Shears, N. T. (2016a). Population ecology of the invasive kelp *Undaria pinnatifida* towards the upper extreme of its temperature range. *Marine Biology*, *163*(11). <https://doi.org/10.1007/s00227-016-2993-9>
- James, K., & Shears, N. T. (2016b). Proliferation of the invasive kelp *Undaria pinnatifida* at aquaculture sites promotes spread to coastal reefs. *Marine Biology*, *163*(2), 34-34. <https://doi.org/10.1007/s00227-015-2811-9>
- Jensen, J. R. (2016). *Introductory digital image processing: A remote sensing perspective*: Pearson Education Inc.
- Jiménez, M., & Díaz-Delgado, R. (2015). Towards a Standard Plant Species Spectral Library Protocol for Vegetation Mapping: A Case Study in the Shrubland of Doñana National Park. *ISPRS International Journal of Geo-Information*, *4*(4), 2472-2495. <https://doi.org/10.3390/ijgi4042472>
- Johnsen, G., Ludvigsen, M., Sørensen, A., & Sandvik Aas, L. M. (2016). The use of underwater hyperspectral imaging deployed on remotely operated vehicles - methods and applications. *IFAC-PapersOnLine*, *49*(23), 476-481. <https://doi.org/10.1016/j.ifacol.2016.10.451>
- Kanemasu, E. T. (1974). Seasonal canopy reflectance patterns of wheat, sorghum, and soybean. *Remote Sensing of Environment*, *3*(1), 43-47. doi:[http://dx.doi.org/10.1016/0034-4257\(74\)90037-6](http://dx.doi.org/10.1016/0034-4257(74)90037-6)
- Kassambara, A., & Mundt, F. (2017). factoextra: Extract and Visualize the Results of Multivariate Data Analyses.
- Kelly, S., Sim-Smith, C., Faire, S., Pierre, J., Hikuroa, D. (2014). *State of our Gulf 2014 Hauraki Gulf - Tikapa Moana/ Te Moananui a Toi State of the Environment Report 2014*. Retrieved from <http://hdl.handle.net/2292/25449>
- Kieleck, C., Bousquet, B., Le Brun, G., Cariou, J., & Lotrian, J. (2001). Laser induced fluorescence imaging: application to groups of macroalgae identification.

Journal of Physics D-Applied Physics, 34(16), 2561-2571. <https://doi.org/Doi10.1088/0022-3727/34/16/324>

- Kišević, M., Smailbegović, A., Gray, K. T., Andričević, R., Craft, J. D., Petrov, V., . . . Dragičević, I. (2011, 2011). Spectral reflectance profile of *Caulerpa racemosa* var. *cyllindracea* and *Caulerpa taxifolia* in the Adriatic Sea Retrieved from <http://www.scopus.com/inward/record.url?eid=2-s2.0-84255166982&partnerID=40&md5=ca21a813b84810c06bc48c86dbc6a294>
- <http://ieeexplore.ieee.org/ielx5/6071746/6080842/06080960.pdf?tp=&arnumber=6080960&isnumber=6080842>
<https://doi.org/10.1109/WHISPERS.2011.6080960>
- Kotta, J., Remm, K., Vahtmäe, E., Kutser, T., & Orav-Kotta, H. (2014). In-air spectral signatures of the Baltic Sea macrophytes and their statistical separability. *Journal of Applied Remote Sensing*, 8(1), 083634. <https://doi.org/10.1117/1.jrs.8.083634>
- Krecker, F. H. (1939). A Comparative Study of the Animal Population of Certain Submerged Aquatic Plants [research article](4), 553. Retrieved from <http://ezproxy.aut.ac.nz/login?url=http://search.ebscohost.com/login.aspx?direct=true&db=edsjsr&AN=edsjsr.10.2307.1930445&site=eds-live>
- Kruse, F. A., Lefkoff, A. B., Boardman, J. W., Heidebrecht, K. B., Shapiro, A. T., Barloon, P. J., & Goetz, A. F. H. (1993). The spectral image processing system (SIPS)—interactive visualization and analysis of imaging spectrometer data. *Remote Sensing of Environment*, 44(2), 145-163. [https://doi.org/https://doi.org/10.1016/0034-4257\(93\)90013-N](https://doi.org/https://doi.org/10.1016/0034-4257(93)90013-N)
- Kucheryavskiy, S. (2018). mdatools: Multivariate Data Analysis for Chemometrics.
- Kutser, T., Dekker, A. G., & Skirving, W. (2003). Modelling spectral discrimination of Great Barrier Reef benthic communities by remote sensing instruments. *Limnology and Oceanography*, 48(1 II), 497-510.
- Kutser, T., Miller, I., & Jupp, D. L. B. (2006a). Mapping coral reef benthic substrates using hyperspectral space-borne images and spectral libraries. *Estuarine, Coastal and Shelf Science*, 70(3), 449-460. <https://doi.org/10.1016/j.ecss.2006.06.026>
- Kutser, T., Vahtmäe, E., & Metsamaa, L. (2006b). Spectral library of macroalgae and benthic substrates in Estonian coastal waters. *Proc. Estonian Acad. Sci. Biol. Ecol.*, 55(4), 329-340.
- Kutser, T., Vahtmäe, E., Paavel, B., & Kauer, T. (2013). Removing glint effects from field radiometry data measured in optically complex coastal and inland waters. *Remote Sensing of Environment*, 133, 85-89. <https://doi.org/10.1016/j.rse.2013.02.011>
- Laba, M., Tsai, F., Ogurcak, D., Smith, S., & Richmond, M. E. (2005). Field determination of optimal dates for the discrimination of invasive wetland plant species using Derivative Spectral Analysis. *Photogrammetric Engineering & Remote Sensing*, 71(5), 603-611.
- Lekan, J. F., & Coney, T. A. (1982). The Use of Remote Sensing to Map the Areal Distribution of *Cladophora Glomerata* at a Site in Lake Huron. *Journal of Great Lakes Research*, 8(1), 144-152. [https://doi.org/http://dx.doi.org/10.1016/S0380-1330\(82\)71952-5](https://doi.org/http://dx.doi.org/10.1016/S0380-1330(82)71952-5)

- Liaw, A., & Wiener, M. (2002). Classification and Regression by randomForest. *R News*, 2(3), 18-22.
- Lillesand, T. M., Kiefer, R. W., & Chipman, J. W. (2004). *Remote Sensing and Image Interpretation* (fifth ed.). New York, NY
- Lorentsen, S. H., Grémillet, D., & Nymoen, G. H. (2004). Annual variation in diet of breeding Great Cormorants: Does it reflect varying recruitment of Gadoids? *Waterbirds*, 27(2), 161-169.
- Louchard, E. M., Reid, R. P., Stephens, F. C., Davis, C. O., Leathers, R. A., & Downes, T. V. (2003). Optical remote sensing of benthic habitats and bathymetry in coastal environments at Lee Stocking Island, Bahamas: A comparative spectral classification approach [Article]. *Limnology and Oceanography*, 48(1 II), 511-521.
- Lowe, D. G. (2004). Distinctive Image Features from Scale-Invariant Keypoints. *International Journal of Computer Vision*, 60(2), 91-110.
- Lowe, S., Browne, M., Boudjekas, S., & De Poorter, M. (2000). 100 of the World's Worst Invasive Alien Species. *The Invasive Species Specialist Group (ISSG) a specialist group of the Species Survival Commission (SSC) of the World Conservation Union (IUCN)*, 11.
- Lu, D., & Cho, H. J. (2011). An improved water-depth correction algorithm for seagrass mapping using hyperspectral data. *Remote Sensing Letters*, 2(2), 91-97. <https://doi.org/10.1080/01431161.2010.502152>
- Maggi, E., Benedetti-Cecchi, L., Castelli, A., Chatzinikolaou, E., Crowe, T. P., Ghedini, G., . . . MacIsaac, H. (2015). Ecological impacts of invading seaweeds: a meta-analysis of their effects at different trophic levels. *Diversity and Distributions*, 21(1), 1-12. <https://doi.org/10.1111/ddi.12264>
- Mahlein, A. K., Rumpf, T., Welke, P., Dehne, H. W., Plümer, L., Steiner, U., Oerke, E.-C. (2013). Development of spectral indices for detecting and identifying plant diseases. *Remote Sensing of Environment*, 128, 21 - 30.
- Manjunath, K. R., Ray, S. S., & Panigrahy, S. (2011). Discrimination of Spectrally-Close Crops Using Ground-Based Hyperspectral Data. *Journal of the Indian Society of Remote Sensing*, 39(4), 599-602. <https://doi.org/10.1007/s12524-011-0099-x>
- Maritorena, S., Morel, A., & Gentili, B. (1994). Diffuse reflectance of oceanic shallow waters: Influence of water depth and bottom albedo. *Limnology and Oceanography*, 39(7), 1689-1703. <https://doi.org/10.4319/lo.1994.39.7.1689>
- Martínez, B., Radford, B., Thomsen, M. S., Connell, S. D., Carreño, F., Bradshaw, C. J. A., . . . Lahoz-Monfort, J. (2018). Distribution models predict large contractions of habitat-forming seaweeds in response to ocean warming. *Diversity and Distributions*, 24(10), 1350-1366. <https://doi.org/10.1111/ddi.12767>
- Mazerolle, M. J. (2019). AICcmodavg: Model selection and multimodel inference based on (Q)AIC(c).
- Micasense. (2018). *Micasense Image Processing*. Retrieved 2018, from <https://github.com/micasense/imageprocessing>
- Micasense. (2020). *RedEdge-M User Manual (PDF)*. Retrieved from <https://support.micasense.com/hc/en-us/articles/115003537673-RedEdge-M-User-Manual-PDF->

- Möckel, T., Dalmayne, J., Prentice, H., Eklundh, L., Purschke, O., Schmidtlein, S., & Hall, K. (2014). Classification of Grassland Successional Stages Using Airborne Hyperspectral Imagery. *Remote Sensing*, 6(8), 7732-7761. <https://doi.org/10.3390/rs6087732>
- Morelissen, B., Dudley, B. D., & Phillips, N. E. (2016). Recruitment of the invasive kelp *Undaria pinnatifida* does not always benefit from disturbance to native algal communities in low-intertidal habitats. *Marine Biology*, 163(12). <https://doi.org/10.1007/s00227-016-3014-8>
- Mount, R. (2005). Acquisition of Through-water Aerial Survey Images. *Photogrammetric Engineering & Remote Sensing*, 71(12), 1407-1415. <https://doi.org/10.14358/PERS.71.12.1407>
- MPI. (2016, 9/6/2016). *Pests and Diseases – Undaria*. Retrieved from <http://www.biosecurity.govt.nz/pests/undaria>
- MPI. (2019, 26 Jul 2019). *Fiordland marine biosecurity*. Retrieved 2019, from <https://www.biosecurity.govt.nz/protection-and-response/long-term-pest-management/fiordland-marine-biosecurity/>
- MPI. (2020). *Commercial Harvest of Undaria pinnatifida - Application Form*. Retrieved from <https://www.biosecurity.govt.nz/dmsdocument/15964/direct>
- Mulla, D. J. (2013). Twenty five years of remote sensing in precision agriculture: Key advances and remaining knowledge gaps. *Biosystems Engineering*, 114(4), 358-371. <https://doi.org/10.1016/j.biosystemseng.2012.08.009>
- Nakagawa, S., Schielzeth, H., & O'Hara, R. B. (2013). A general and simple method for obtaining R² from generalized linear mixed-effects models. *Methods in Ecology and Evolution*, 4(2), 133-142. DOI:10.1111/j.2041-210x.2012.00261.x
- NASA. (2019). *EcoSIS Spectral Library*. Retrieved 08/06/2019, from <https://ecosis.org/>
- Nelson, W. (2019). *Seaweeds: sustaining habitats and harvest*. Retrieved 28/02/2019, 2019, from <https://www.niwa.co.nz/sites/niwa.co.nz/files/import/attachments/Nelson.pdf>
- Nicastro, K. R., Zardi, G. I., Teixeira, S., Neiva, J., Serrão, E. A., Pearson, G. A. (2013). Shift happens: Trailing edge contraction associated with recent warming trends threatens a distinct genetic lineage in the marine macroalga *Fucus vesiculosus*. *BMC Biology*, 11(6). [https://doi.org/https://doi.org/10.1186/1741-7007-11-6](https://doi.org/10.1186/1741-7007-11-6)
- NIWA. (2020). *Wakame Asian Kelp*. Retrieved 26/07/2020, from <https://marinebiosecurity.niwa.co.nz/undaria-pinnatifida-harvey-suringar/>
- O'Neill, J. D., Costa, M., & Sharma, T. (2011). Remote Sensing of Shallow Coastal Benthic Substrates: In situ Spectra and Mapping of Eelgrass (*Zostera marina*) in the Gulf Islands National Park Reserve of Canada. *Remote Sensing*, 3(12), 975-1005. <https://doi.org/10.3390/rs3050975>
- Ollinger, S. V. (2011). Sources of variability in canopy reflectance and the convergent properties of plants. *New Phytol*, 189(2), 375-394. <https://doi.org/10.1111/j.1469-8137.2010.03536.x>
- Oreti, L., Barbati, A., Marini, F., & Giularelli, D. (2020). Very high-resolution true color leaf-off imagery for mapping *Taxus baccata* L. and *Ilex aquifolium* L. understory population. *Biodiversity and Conservation*, 29(8), 2605-2622. <https://doi.org/10.1007/s10531-020-01991-x>

- Pallas, A., Garcia-Calvo, B., Corgos, A., Bernardez, C., & Freire, J. (2006). Distribution and habitat use patterns of benthic decapod crustaceans in shallow waters: A comparative approach. *Marine Ecology Progress Series*, 324, 173-184. <https://doi.org/10.3354/meps324173>
- Parsons, M. J. (1995). *Status of the introduced brown seaweed Undaria in New Zealand* (112). Department of Conservation, Wellington.
- Peerbhay, K. Y., Mutanga, O., & Ismail, R. (2013). Commercial tree species discrimination using airborne AISA Eagle hyperspectral imagery and partial least squares discriminant analysis (PLS-DA) in KwaZulu-Natal, South Africa. *ISPRS Journal of Photogrammetry and Remote Sensing*, 79, 19-28. <https://doi.org/10.1016/j.isprsjprs.2013.01.013>
- Penuelas, J., Pinol, J., Ogaya, R., Filella, I. (1997). Estimation of plant water concentration by the reflectance water index WI (R900/R970). *International Journal of Remote Sensing*, 18, 2869–2875.
- Perreault, M.-C., Borgeaud, I. A., & Gaymer, C. F. (2014). Impact of grazing by the sea urchin *Tetrapygus niger* on the kelp *Lessonia trabeculata* in Northern Chile. *Journal of Experimental Marine Biology and Ecology*, 453, 22-27. <https://doi.org/10.1016/j.jembe.2013.12.021>
- Persson, A., Ljungberg, P., Andersson, M., Götzman, E., & Nilsson, P. A. (2012). Foraging performance of juvenile Atlantic cod *Gadus morhua* and profitability of coastal habitats. *Marine Ecology Progress Series*, 456, 245-253. <https://doi.org/10.3354/meps09705>
- Pinheiro, J., Bates, D., DebRoy, S., Sarkar, D., & Team, R. C. (2018). nlme: Linear and Nonlinear Mixed Effects Models.
- Pix4D. (2020a). *Do RTK/PPK drones give you better results than GCPs?* Retrieved 27/07/2020, from <https://www.pix4d.com/blog/rtk-ppk-drones-gcp-comparison>
- Pix4D. (2020b). *Yaw, Pitch, Roll and Omega, Phi, Kappa angles*. Retrieved 2020, from <https://support.pix4d.com/hc/en-us/articles/202558969-Yaw-Pitch-Roll-and-Omega-Phi-Kappa-angles#How%20to%20convert%20Yaw,%20Pitch,%20Roll%20to%20Omega,%20Phi,%20Kappa>
- Pomerantsev, A. L., & Rodionova, O. Y. (2018). Multiclass partial least squares discriminant analysis: Taking the right way-A critical tutorial. *Journal of Chemometrics*, 32(8), e3030. <https://doi.org/10.1002/cem.3030>
- Prospere, K., McLaren, K., & Wilson, B. (2014). Plant Species Discrimination in a Tropical Wetland Using In Situ Hyperspectral Data. *Remote Sensing*, 6(9), 8494-8523. <https://doi.org/10.3390/rs6098494>
- Pyšek, P., Jarošík, V., Hulme, P. E., Pergl, J., Hejda, M., Schaffner, U., & Vilà, M. (2012). A global assessment of invasive plant impacts on resident species, communities and ecosystems: the interaction of impact measures, invading species' traits and environment. *Global Change Biology*, 18(5), 1725-1737. <https://doi.org/10.1111/j.1365-2486.2011.02636.x>
- Pu, R., Bell, S., Baggett, L., Meyer, C., & Zhao, Y. (2012). Discrimination of Seagrass Species and Cover Classes within situ Hyperspectral Data. *Journal of Coastal Research*, 285, 1330-1344. <https://doi.org/10.2112/jcoastres-d-11-00229.1>

- Quach, A. T. (2012). *Interactive Random Forests Plots*: Utah State University. Retrieved from <https://digitalcommons.usu.edu/gradreports/134>
- R Core Team (2019). R: A Language and Environment for Statistical Computing: R Foundation for Statistical Computing.
- Reshitnyk, L., Costa, M., Robinson, C., & Dearden, P. (2014). Evaluation of WorldView-2 and acoustic remote sensing for mapping benthic habitats in temperate coastal Pacific waters. *Remote Sensing of Environment*, 153, 7-23. <https://doi.org/10.1016/j.rse.2014.07.016>
- Rossiter, T., Furey, T., McCarthy, T., & Stengel, D. B. (2020). UAV-mounted hyperspectral mapping of intertidal macroalgae. *Estuarine, Coastal and Shelf Science*, 242. <https://doi.org/10.1016/j.ecss.2020.106789>
- Russell, L. K., Hepburn, C. D., Hurd, C. L., & Stuart, M. D. (2007). The expanding range of *Undaria pinnatifida* in southern New Zealand: distribution, dispersal mechanisms and the invasion of wave-exposed environments. *Biological Invasions*, 10(1), 103-115. <https://doi.org/10.1007/s10530-007-9113-1>
- Sagawa, T., N. Aoki, M., Komatsu, T., & Mikami, A. (2012). Mapping seaweed forests with IKONOS image based on bottom surface reflectance (Vol. 8525 85250).
- Saito, G., Seki, H., Uto, K., Kosugi, Y., & Komatsu, T. (2014, 2014). Development of hyperspectral imaging sensor, which mounted on UAV for environmental study at coastal zone. *Asian Association on Remote Sensing*. Retrieved from <http://www.scopus.com/inward/record.url?eid=2-s2.0-84925433505&partnerID=40&md5=730ffa0b3deced58b2dd060b7f12010b>
- Saito, Y. (1975). *Undaria*. In J. Tokida & H. Hirose (Eds.), *Advance in phycology in Japan* (pp. 304-320). The Hague
- Sanderson, J. C. (1997). *Survey of Undaria pinnatifida in Tasmanian coastal waters*: Tasmanian Department of Marine Resources, Tasmania.
- Schmidt, J. P., Springborn, M., & Drake, J. M. (2012). Bioeconomic forecasting of invasive species by ecological syndrome. *Ecosphere*, 3(5), art46. <https://doi.org/10.1890/es12-00055.1>
- Seers, B. M., & Shears, N. T. (2015). Spatio-temporal patterns in coastal turbidity – Long-term trends and drivers of variation across an estuarine-open coast gradient. *Estuarine, Coastal and Shelf Science*, 154, 137-151. <https://doi.org/https://doi.org/10.1016/j.ecss.2014.12.018>
- Shanmugam, S., & SrinivasaPerumal, P. (2014). Spectral matching approaches in hyperspectral image processing. *International Journal of Remote Sensing*, 35(24), 8217-8251. <https://doi.org/10.1080/01431161.2014.980922>
- Silva, T. S. F., Melack, J. M., Novo, E. M. L. M., & Costa, M. P. F. (2008). Remote sensing of aquatic vegetation: theory and applications. *Environmental Monitoring and Assessment*, 140(1), 131-145. <https://doi.org/10.1007/s10661-007-9855-3>
- Sinner, J., Forrest, B., & Taylor, M. (2000). *A strategy for managing the Asian kelp Undaria: final report*.
- Skowronek, S., Ewald, M., Isermann, M., Van De Kerchove, R., Lenoir, J., Aerts, R., . . . Feilhauer, H. (2016). Mapping an invasive bryophyte species using hyperspectral remote sensing data. *Biological Invasions*, 19(1), 239-254. <https://doi.org/10.1007/s10530-016-1276-1>

- Smith, S. D. A. (2000). Evaluating stress in rocky shore and shallow reef habitats using the macrofauna of kelp holdfasts. *Journal of Aquatic Ecosystem Stress and Recovery*, 7(4), 259-272. <https://doi.org/10.1023/A:1009993611262>
- Somers, B., & Asner, G. P. (2014). Tree species mapping in tropical forests using multi-temporal imaging spectroscopy: Wavelength adaptive spectral mixture analysis. *International Journal of Applied Earth Observation and Geoinformation*, 31, 57-66. <https://doi.org/10.1016/j.jag.2014.02.006>
- South, P. M., Floerl, O., Forrest, B. M., & Thomsen, M. S. (2017). A review of three decades of research on the invasive kelp *Undaria pinnatifida* in Australasia: An assessment of its success, impacts and status as one of the world's worst invaders. *Mar Environ Res*, 131, 243-257. <https://doi.org/10.1016/j.marenvres.2017.09.015>
- STS-VIS (2020). *STS-VIS-L-25-400-SMA*. Retrieved from <https://www.oceaninsight.com/products/spectrometers/microspectrometer/sts-series/sts-vis-l-25-400-sma/?qty=1>
- Taddia, Y., Russo, P., Lovo, S., & Pellegrinelli, A. (2019). Multispectral UAV monitoring of submerged seaweed in shallow water. *Applied Geomatics*, 12(S1), 19-34. <https://doi.org/10.1007/s12518-019-00270-x>
- Tait, L., Bind, J., Charan-Dixon, H., Hawes, I., Pirker, J., & Schiel, D. (2019). Unmanned Aerial Vehicles (UAVs) for Monitoring Macroalgal Biodiversity: Comparison of RGB and Multispectral Imaging Sensors for Biodiversity Assessments. *Remote Sensing*, 11(19). <https://doi.org/10.3390/rs11192332>
- Thompson, G. A., & Schiel, D. R. (2012). Resistance and facilitation by native algal communities in the invasion success of *Undaria pinnatifida*. *Marine Ecology Progress Series*, 468, 95–105.
- Thomsen, M. S., Byers, J. E., Schiel, D. R., Bruno, J. F., Olden, J. D., Wernberg, T., & Silliman, B. R. (2014). Impacts of marine invaders on biodiversity depend on trophic position and functional similarity. *Marine Ecology Progress Series*, 495, 39-47. <https://doi.org/10.3354/meps10566>
- Turner, D., Lucieer, A., & Wallace, L. (2014). Direct Georeferencing of Ultrahigh-Resolution UAV Imagery. *IEEE Transactions on Geoscience and Remote Sensing*, 52(5), 2738-2745. <https://doi.org/10.1109/tgrs.2013.2265295>
- Uhl, F., Bartsch, I., & Oppelt, N. (2016). Submerged Kelp Detection with Hyperspectral Data. *Remote Sensing*, 8(6), 487. <https://doi.org/10.3390/rs8060487>
- Uhrin, A. V., & Townsend, P. A. (2016). Improved seagrass mapping using linear spectral unmixing of aerial photographs. *Estuarine, Coastal and Shelf Science*, 171, 11-22. <https://doi.org/http://dx.doi.org/10.1016/j.ecss.2016.01.021>
- Ullman, S., & Brenner, S. (1979). The interpretation of structure from motion. *Proceedings of the Royal Society of London. Series B. Biological Sciences*, 203(1153), 405-426. <https://doi.org/10.1098/rspb.1979.0006>
- Ünsalan, C., & Boyer, K. L. (2011). *Multispectral Satellite Image Understanding*: Springer London Dordrecht Heidelberg New York. <https://doi.org/10.1007/978-0-85729-667-2>
- USGS. (2017, December 13, 2011). *Earth Observing-1, Sensors - Hyperion*. Retrieved 22/01/2017, from <https://eo1.usgs.gov/sensors/hyperion>

- Vahtmäe, E., & Kutser, T. (2013). Classifying the Baltic Sea Shallow Water Habitats Using Image-Based and Spectral Library Methods. *Remote Sensing*, 5(5), 2451-2474. <https://doi.org/10.3390/rs5052451>
- Vahtmäe, E., Kutser, T., Martin, G., & Kotta, J. (2006). Feasibility of hyperspectral remote sensing for mapping benthic macroalgal cover in turbid coastal waters—a Baltic Sea case study. *Remote Sensing of Environment*, 101(3), 342-351. <https://doi.org/10.1016/j.rse.2006.01.009>
- Vaiphasa, C., Skidmore, A. K., de Boer, W. F., & Vaiphasa, T. (2007). A hyperspectral band selector for plant species discrimination. *ISPRS Journal of Photogrammetry and Remote Sensing*, 62(3), 225-235. <https://doi.org/10.1016/j.isprsjprs.2007.05.006>
- Vásquez, J. A., Zuñiga, S., Tala, F., Piaget, N., Rodríguez, D. C., & Vega, J. M. A. (2014). Economic valuation of kelp forests in northern Chile: values of goods and services of the ecosystem. *Journal of Applied Phycology*, 26(2), 1081-1088. <https://doi.org/10.1007/s10811-013-0173-6>
- von Bueren, S. K., Burkart, A., Hueni, A., Rascher, U., Tuohy, M. P., & Yule, I. J. (2015). Deploying four optical UAV-based sensors over grassland: challenges and limitations. *Biogeosciences*, 12(1), 163-175. <https://doi.org/10.5194/bg-12-163-2015>
- Washington, M., Kirui, P., Cho, H. J., & Wafo-Soh, C. (2012). Data-driven correction for light attenuation in shallow waters. *Remote Sensing Letters*, 3(4), 335-342. <https://doi.org/10.1080/01431161.2011.597791>
- Wehrens, R. (2011). *Chemometrics with R*: Springer. <https://doi.org/10.1007/978-3-642-17841-2>
- Wezernak, C. T., & Lyzenga, D. R. (1975). Analysis of Cladophora distribution in Lake Ontario using remote sensing. *Remote Sensing of Environment*, 4, 37-48. [https://doi.org/http://dx.doi.org/10.1016/0034-4257\(75\)90004-8](https://doi.org/http://dx.doi.org/10.1016/0034-4257(75)90004-8)
- White, L., Lu, J., & White, W. L. (2014). *Scoping assessment of the economic viability of harvesting Undaria pinnatifida from NZ mussel lines and potential uses of the collected material*. Applied Ecology New Zealand Report14/01. 76p
- White, L. N., & White, W. L. (2020). Seaweed utilisation in New Zealand. *Botanica Marina*(0), 000010151520190089. <https://doi.org/https://doi.org/10.1515/bot-2019-0089>
- White, W. L., & Wilson, P. (2015). Chapter 2 - World seaweed utilization. In B. K. Tiwari & D. J. Troy (Eds.), *Seaweed Sustainability* (pp. 7-25). San Diego: Academic Press. Retrieved from <http://www.sciencedirect.com/science/article/pii/B9780124186972000027>. <https://doi.org/https://doi.org/10.1016/B978-0-12-418697-2.00002-7>
- Wolf, P., Rößler, S., Schneider, T., & Melzer, A. (2017). Collecting in situ remote sensing reflectances of submersed macrophytes to build up a spectral library for lake monitoring. *European Journal of Remote Sensing*, 46(1), 401-416. <https://doi.org/10.5721/EuJRS20134623>
- Woodcock, C. E., & Strahler, A. H. (1987). The factor of scale in remote sensing. *Remote Sensing of Environment*, 21(3), 311-332. doi:[http://dx.doi.org/10.1016/0034-4257\(87\)90015-0](http://dx.doi.org/10.1016/0034-4257(87)90015-0)

- Zeng, C., King, D. J., Richardson, M., & Shan, B. (2017). Fusion of Multispectral Imagery and Spectrometer Data in UAV Remote Sensing. *Remote Sensing*, 9(7), 696. <https://doi.org/10.3390/rs9070696>
- Zoffoli, M. L., Frouin, R., & Kampel, M. (2014). Water column correction for coral reef studies by remote sensing. *Sensors (Basel)*, 14(9), 16881-16931. <https://doi.org/10.3390/s140916881>
- Zuur, A., Ieno, E. N., Walker, N., Saveliev, A. A., & Smith, G. M. (2009). *Mixed Effects Models and Extensions in Ecology with R* (1 ed.): Springer-Verlag New York. DOI:10.1007/978-0-387-87458-6

Appendix A. Chapter 2 Appendices

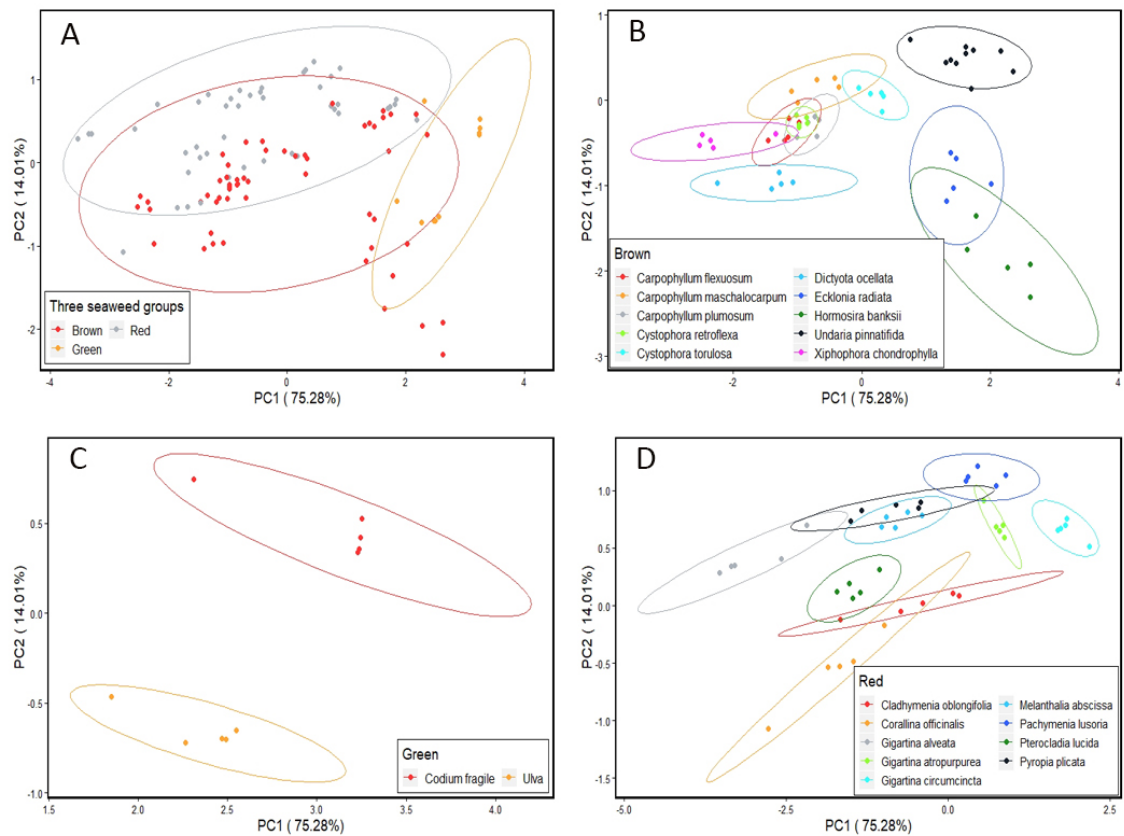


Figure A-1: PCA plots of seaweed grouping at (A) taxa level, (B) grouping of seaweed species within brown, (C) within green and (D) within red using standardised data

Appendix B. Chapter 3 Appendices

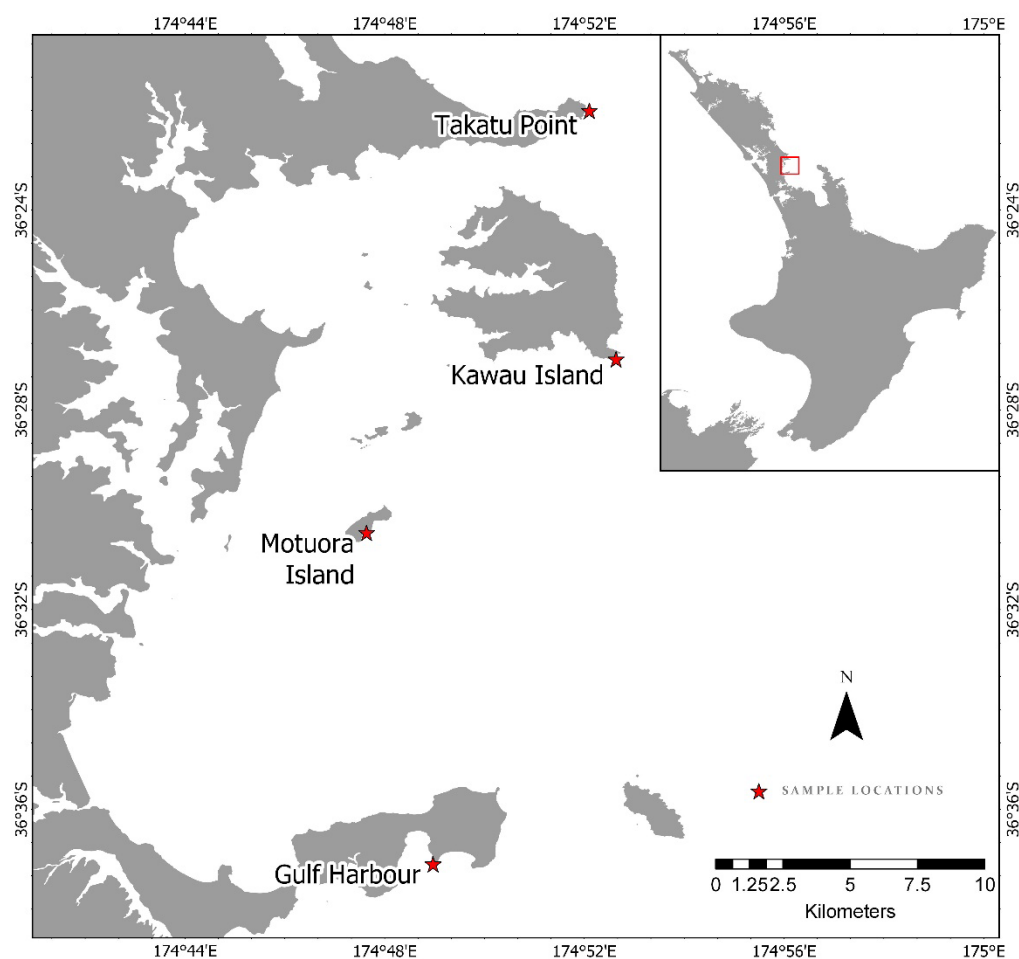


Figure B-1: Seaweed sample locations in Hauraki Gulf, North Island, NZ

Table B-1: Description of locations where the seaweed individuals were collected

| Site | Attributes |
|------------------------------|--|
| Kawau Island, Hauraki Gulf | Patches of seaweed. Diverse seaweed communities. Quite exposed. |
| Motuora Island, Hauraki Gulf | Rocky reef. Sheltered site. |
| Takatu Point, Hauraki Gulf | Rocky reef with large swathes of seaweed. Very exposed but less turbid compared to Gulf Harbour. |
| Te Haruhi Bay, Hauraki Gulf | Wreck nearby. Sheltered site but very turbid waters. Less diverse. |

Table B-2: Various models used in mixed-effects modelling to test the significance of each term

| Model | Formula | Term deleted from Model A |
|-------------|--|---------------------------|
| A (Full) | PC ~ location + season + location:season | None |
| B | PC ~ location + season | location:season |
| C | PC ~ season | location, location:season |
| D | PC ~ location | season, location:season |

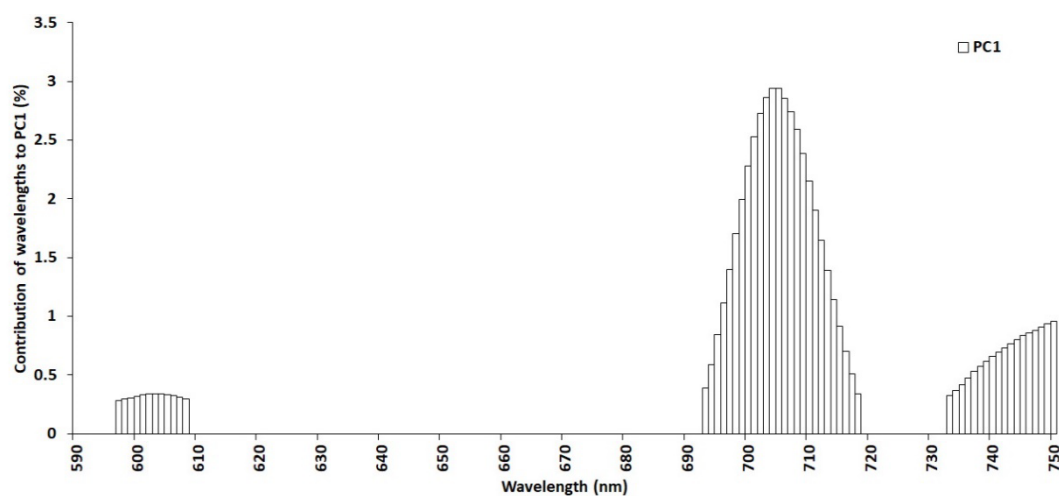


Figure B-2: Variables contributing to variance in PC1 for *Carpophyllum maschalocarpum* in percentage

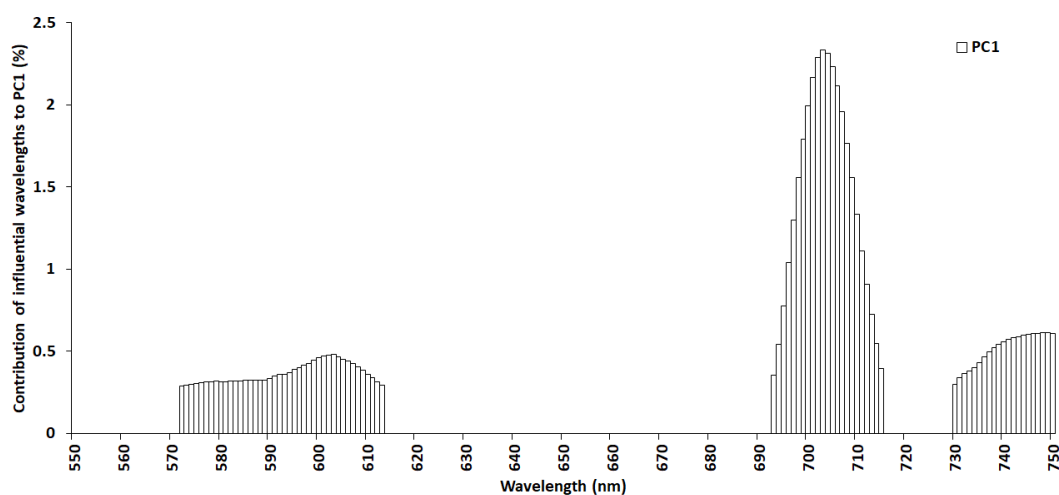


Figure B-3: Variables contributing to variance in PC1 for *Ecklonia radiata* in percentage

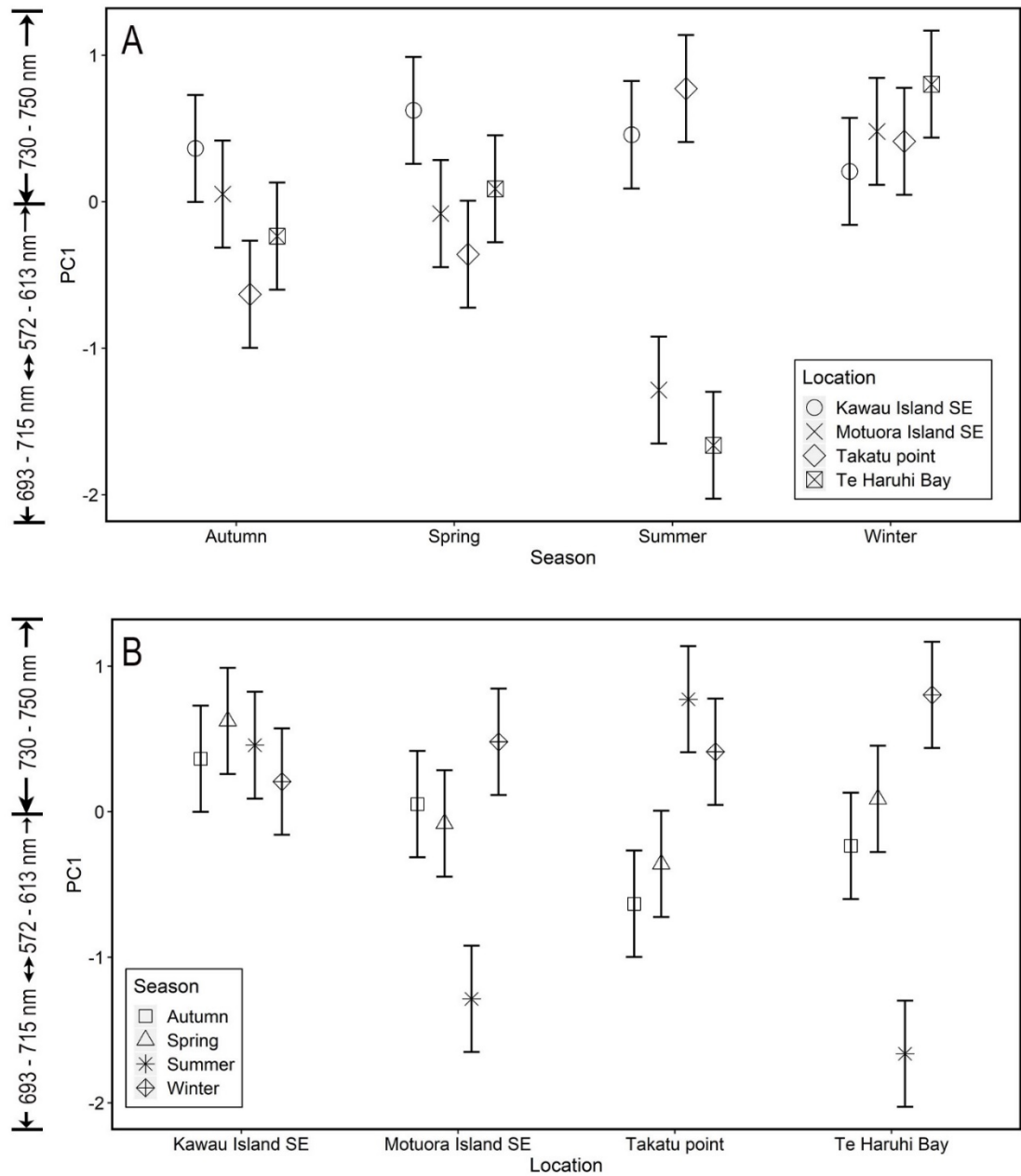


Figure B-4: (A) Model predictions plot with two standard deviations (and 95% confidence interval) of PC1 for *Ecklonia radiata* in different locations within each season, X-axis represents seasons and Y-axis represents PC1 scores and the interpretation of wavelengths contributing to PC1 axis (B) Model predictions plot with two standard deviations (and 95% confidence interval) of PC1 for *Ecklonia radiata* in different seasons within each location, X-axis represents locations and Y-axis represents PC1 scores and the interpretation of wavelengths contributing to PC1 axis.

Appendix C. Chapter 4 Appendices

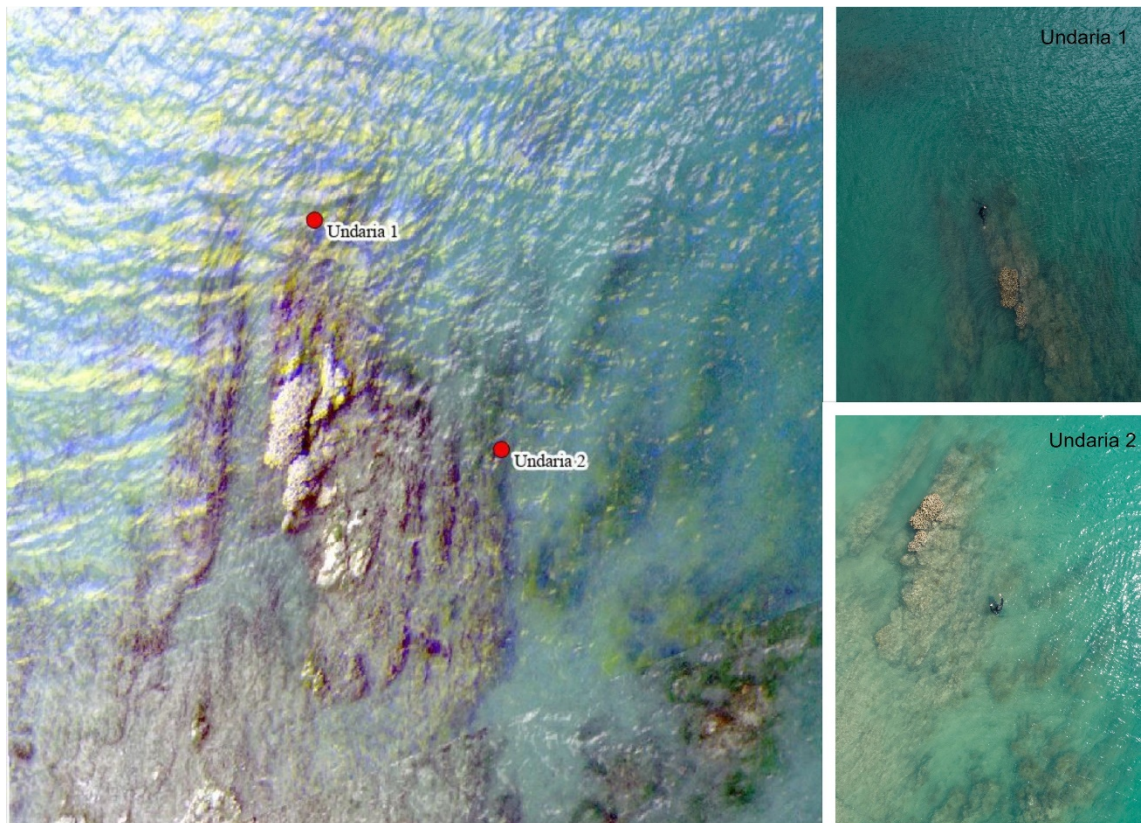


Figure C-1: Adjusted *U. pinnatifida* locations 1 and 2 on the multispectral mosaic (left) compared to RGB photos (right) with snorkeller in the centre of each photo.

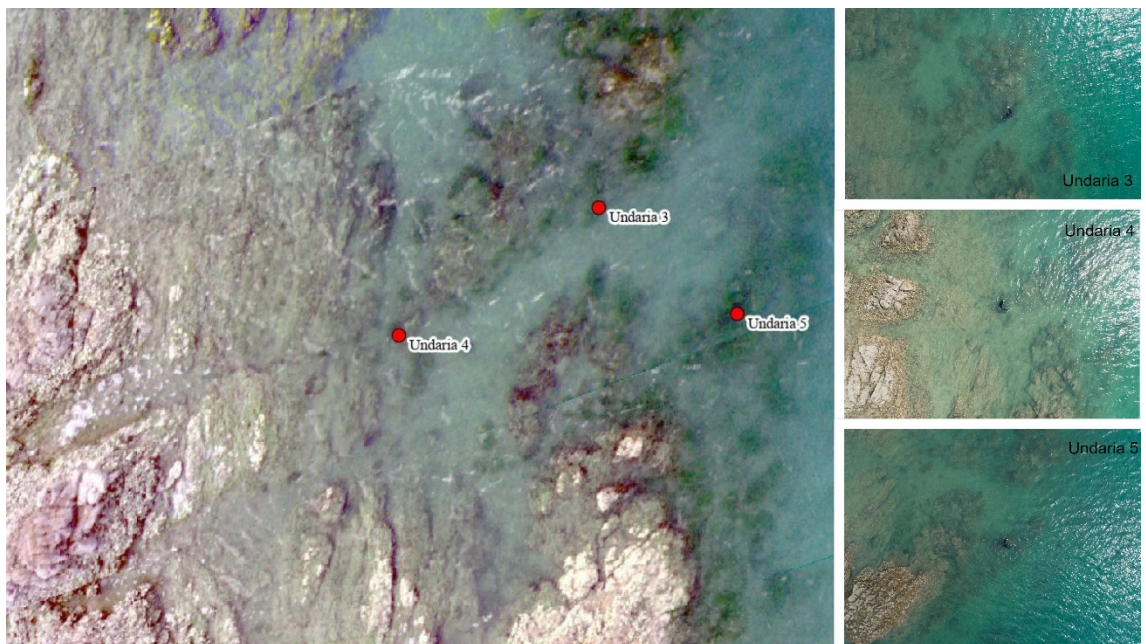


Figure C-2: Adjusted *U. pinnatifida* locations 3, 4 and 5 on the multispectral mosaic (left) compared to RGB photos (right) with snorkeller in the centre of each photo.

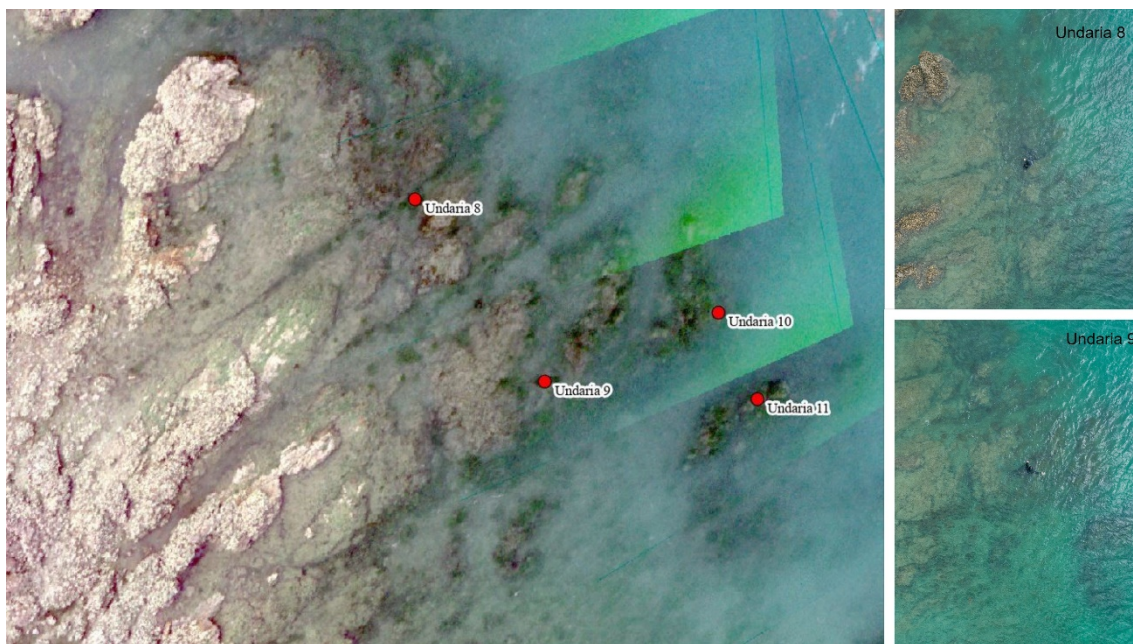


Figure C-3: Adjusted *U. pinnatifida* locations 8 and 9 on the multispectral mosaic (left) compared to RGB photos (right) with snorkeller in the centre of each photo.

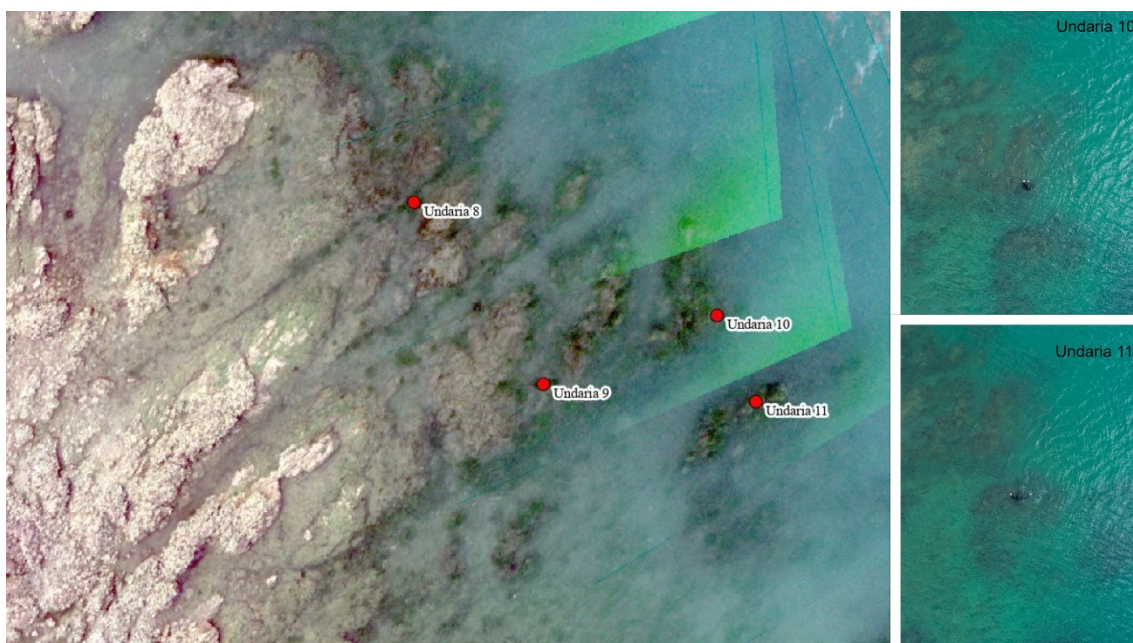


Figure C-4: Adjusted *U. pinnatifida* locations 10 and 11 on the multispectral mosaic (left) compared to RGB photos (right) with snorkeller in the centre of each photo.



Figure C-5: Adjusted *U. pinnatifida* locations 12 to 16 on the multispectral mosaic (top left) compared to RGB photos (bottom and right) with snorkeller in the centre of each photo.

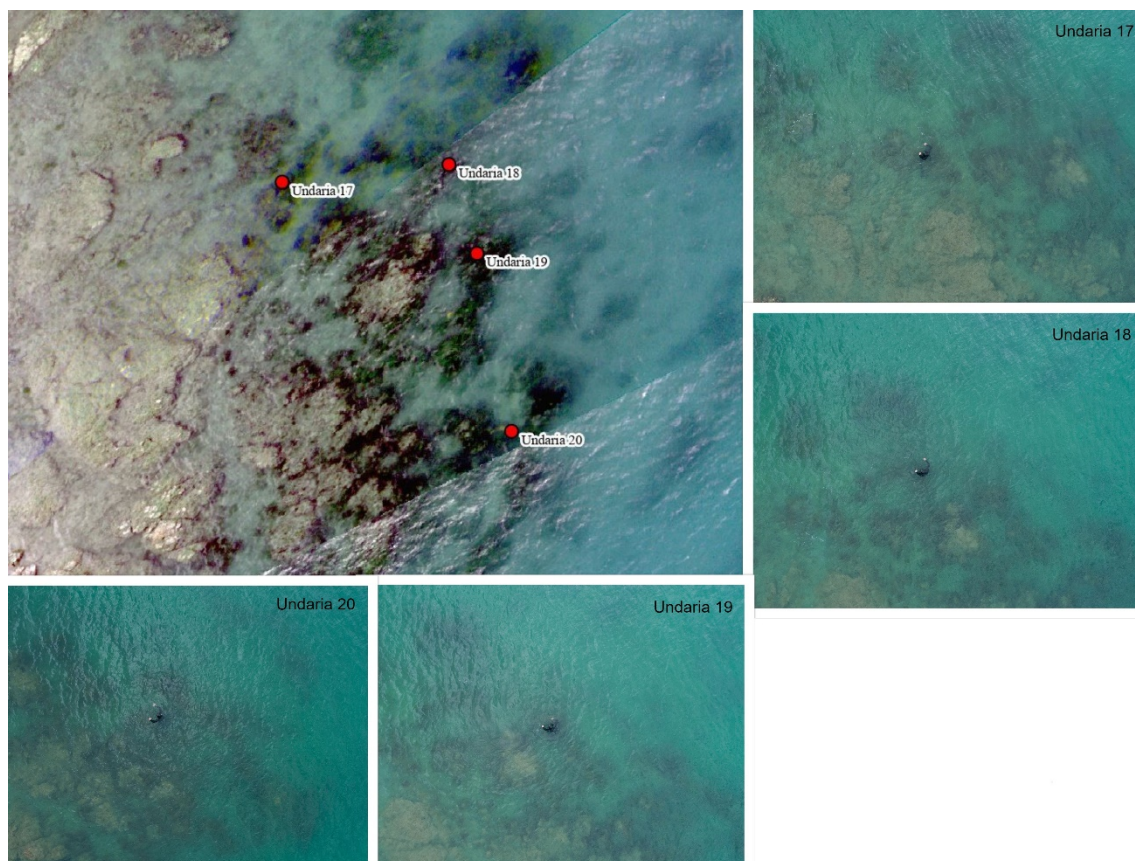


Figure C-6: Adjusted *U. pinnatifida* locations 17 to 20 on the multispectral mosaic (top left) compared to RGB photos (bottom and right) with snorkeller in the centre of each photo.

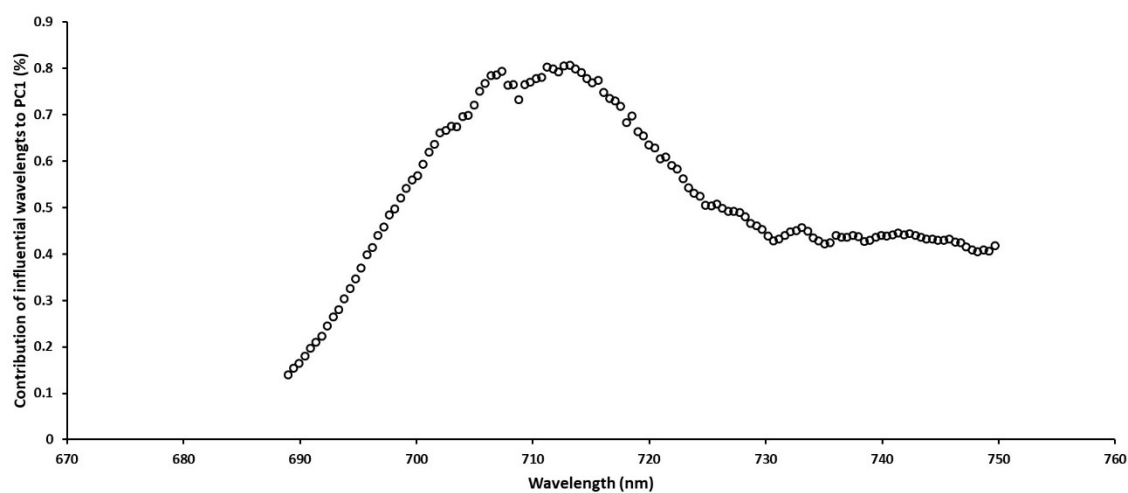


Figure C-7: Variables contributing to PC1 of *Ecklonia radiata*

Table C-1: Likelihood ratio test of models explaining difference in spectral signatures of *E. radiata* across four locations and four seasons

| Model | Likelihood ratio test | AIC |
|-------|-----------------------------------|---------|
| B | $L = 101.6733(df = 8, p < 0.001)$ | 943.82 |
| C | $L = 497.48(df = 4, p < 0.001)$ | 1331.62 |
| D | $L = 140.23(df = 7, p < 0.001)$ | 980.37 |

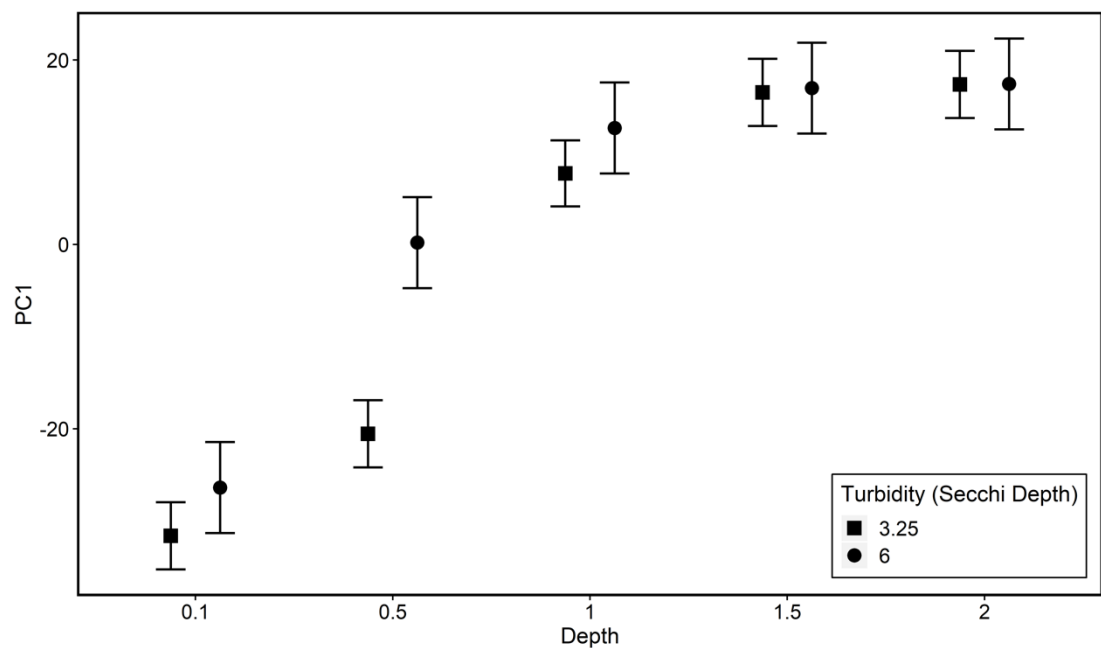


Figure C-8: Model predictions plot with two standard deviations (and 95% confidence interval) of PC1 for *Ecklonia radiata* at different Secchi depth levels (m) within each water depth level (m)

Table C-2: Parameter settings for each of the random forest models at each depth within a turbidity level. ‘ntree’ is the number of trees created in the model, mtry is the number of wavelengths tried at each split. Dataset A includes wavelengths 517, 716 – 721, 750 nm while dataset B includes wavelengths resampled to Micesense RedEdge sensor.

| Dataset | Turbidity (Secchi depth in m) | Depth (m) | Model | ntree | mtry |
|---------|-------------------------------|-----------|-------|-------|------|
| A | 6 | 0.1 | 1 | 130 | 5 |
| | | 0.5 | 2 | 480 | 1 |
| | | 1 | 3 | 100 | 1 |
| | | 1.5 | 4 | 160 | 2 |
| | | 2 | 5 | 200 | 1 |
| | 3.25 | 0.1 | 6 | 500 | 4 |
| | | 0.5 | 7 | 410 | 4 |
| | | 1 | 8 | 300 | 2 |
| | | 1.5 | 9 | 190 | 2 |
| | | 2 | 10 | 500 | 4 |
| B | 6 | 0.1 | 11 | 150 | 4 |
| | | 0.5 | 12 | 400 | 1 |
| | | 1 | 13 | 500 | 2 |
| | | 1.5 | 14 | 200 | 1 |
| | | 2 | 15 | 130 | 1 |
| | 3.25 | 0.1 | 16 | 210 | 1 |
| | | 0.5 | 17 | 450 | 1 |
| | | 1 | 18 | 500 | 2 |
| | | 1.5 | 19 | 500 | 2 |
| | | 2 | 20 | 40 | 2 |

Table C-3: Random forest model classification statistics for discriminating two seaweed species at each depth with two turbidity levels utilising dataset A including wavelengths 517, 716 – 721, 750 nm. E – *Ecklonia radiata*, U – *Undaria pinnatifida*, SD – Secchi depth, OOB – Out-of-bag error, CE – classification error of the classes along each row.

| Depth (m) | Turbidity 1 (SD = 6m) | | | | | Turbidity 2 (SD = 3.25m) | | | | |
|--------------|-----------------------|--------------|---|----|---------|--------------------------|----|----|---------|--|
| | Reference ↓ | Classified → | | | OOB (%) | Classified → | | | OOB (%) | |
| 0.1 | | E | U | CE | 42.9 | E | U | CE | 12.5 | |
| | | E | 6 | 4 | 0.4 | | 19 | 1 | 0.05 | |
| | | U | 5 | 6 | 0.45 | | 4 | 16 | 0.2 | |
| 0.5 | | E | U | CE | 35 | E | U | CE | 15 | |
| | | E | 7 | 3 | 0.3 | | 17 | 3 | 0.15 | |
| | | U | 4 | 6 | 0.4 | | 3 | 17 | 0.15 | |
| 1 | | E | U | CE | 30 | E | U | CE | 14.6 | |
| | | E | 8 | 2 | 0.2 | | 19 | 2 | 0.09 | |
| | | U | 4 | 6 | 0.4 | | 4 | 16 | 0.2 | |
| 1.5 | | E | U | CE | 15 | E | U | CE | 7.5 | |
| | | E | 9 | 1 | 0.1 | | 18 | 2 | 0.1 | |
| | | U | 2 | 8 | 0.2 | | 1 | 19 | 0.05 | |
| 2 | | E | U | CE | 28.6 | E | U | CE | 12.5 | |
| | | E | 6 | 4 | 0.4 | | 18 | 2 | 0.1 | |
| | | U | 2 | 9 | 0.18 | | 3 | 17 | 0.15 | |

Table C-4: Random forest model classification statistics for discriminating two seaweed species at each depth with two turbidity levels utilising wavelengths resampled to Micasense RedEdge-m sensor. E – *Ecklonia radiata*, U – *Undaria pinnatifida*, SD – Secchi depth, OOB – Out-of-bag error, CE – classification error.

| Depth (m) | Reference ↓ | Turbidity 1 (SD = 6m) | | | | Turbidity 2 (SD = 3.25m) | | | |
|--------------|----------------|-----------------------|----|---------|------|--------------------------|----|---------|-----|
| | | Classified → | | OOB (%) | | Classified → | | OOB (%) | |
| 0.1 | | E | U | CE | 57.1 | E | U | CE | 35 |
| | E | 5 | 5 | 0.5 | | 13 | 7 | 0.35 | |
| | U | 7 | 4 | 0.64 | | 7 | 13 | 0.35 | |
| 0.5 | | E | U | CE | 50 | E | U | CE | 5 |
| | E | 5 | 5 | 0.5 | | 19 | 1 | 0.05 | |
| | U | 5 | 5 | 0.5 | | 1 | 19 | 0.05 | |
| 1 | | E | U | CE | 25 | E | U | CE | 0 |
| | E | 7 | 3 | 0.3 | | 21 | 0 | 0 | |
| | U | 2 | 8 | 0.2 | | 0 | 20 | 0 | |
| 1.5 | | E | U | CE | 20 | E | U | CE | 0 |
| | E | 8 | 2 | 0.2 | | 20 | 0 | 0 | |
| | U | 2 | 8 | 0.2 | | 0 | 20 | 0 | |
| 2 | | E | U | CE | 9.5 | E | U | CE | 2.5 |
| | E | 8 | 2 | 0.2 | | 20 | 0 | 0 | |
| | U | 0 | 11 | 0 | | 1 | 19 | 0.05 | |

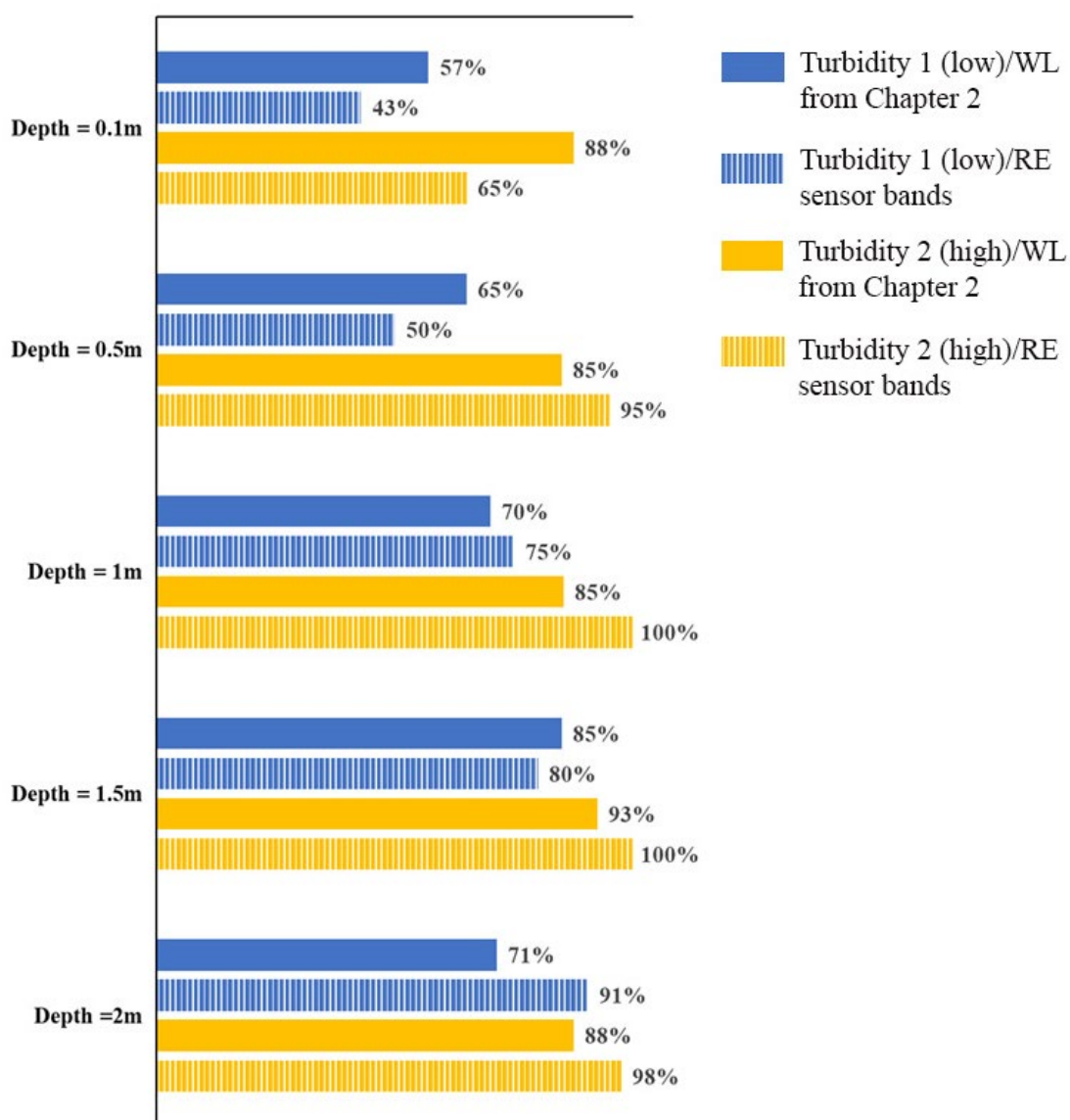


Figure C-9: Comparison of the overall accuracy of random forest model classification using two types of datasets for two turbidity and five depth levels. Dataset A includes spectral reflectance values at wavelengths 571, 716-721 and 750 nm. Dataset B includes spectral reflectance values from hyperspectral data resampled to match Micasense Rededge-m spectral bands. Turbidity 1 (low) - Secchi depth of 6m indicates low turbidity level compared to turbidity 2, Turbidity 2 -Secchi depth of 3.25m indicates higher turbidity level compared to turbidity 1, WL – wavelengths and RE – Micasense Rededge-m sensor. Values for the plot were obtained from Table C-2 and Table C-3 in appendix C.

Table C-5: Collated accuracy assessment of *E. radiata* at a depth of 10 cm from the water surface. NS - non-seaweed, S - seaweed, UA - User accuracy, PA - Producer accuracy, K - kappa.

| | Flight height – 10 m | | | | | | Flight height – 30 m | | | | |
|---------------------------------|----------------------|------|------|-------|------|------|----------------------|------|-------|------|------|
| | Class | NS | S | Total | UA | K | NS | S | Total | UA | K |
| Raw Reflectance | NS | 603 | 43 | 646 | 0.93 | | 685 | 63 | 748 | 0.92 | |
| | S | 147 | 707 | 854 | 0.83 | | 65 | 687 | 752 | 0.91 | |
| | Total | 750 | 750 | 1500 | | | 750 | 750 | 1500 | | |
| | PA | 0.80 | 0.94 | | 0.87 | | 0.91 | 0.92 | | 0.92 | |
| | K | | | | | 0.75 | | | | | 0.83 |
| | | | | | | | | | | | |
| | Class | NS | S | Total | UA | K | NS | S | Total | UA | K |
| Standardised Reflectance | NS | 744 | 367 | 1111 | 0.67 | | 748 | 231 | 979 | 0.76 | |
| | S | 6 | 383 | 389 | 0.98 | | 2 | 519 | 521 | 0.99 | |
| | Total | 750 | 750 | 1500 | | | 750 | 750 | 1500 | | |
| | PA | 0.99 | 0.51 | | 0.75 | | 0.99 | 0.69 | | 0.84 | |
| | K | | | | | 0.5 | | | | | 0.69 |
| | | | | | | | | | | | |

Table C-6: Collated accuracy assessment of *E. radiata* at a depth of 50 cm from the water surface. NS - non-seaweed, S - seaweed, UA - User accuracy, PA - Producer accuracy, K - kappa.

| | Flight height – 10 m | | | | | | Flight height – 30 m | | | | |
|--------------------------|----------------------|------|------|-------|------|------|----------------------|------|-------|------|------|
| | Class | NS | S | Total | UA | K | NS | S | Total | UA | K |
| Raw Reflectance | NS | 209 | 1 | 210 | 0.99 | | 138 | 0 | 138 | 1 | |
| | S | 541 | 749 | 1290 | 0.58 | | 612 | 750 | 1362 | 0.55 | |
| | Total | 750 | 750 | 1500 | | | 750 | 750 | 1500 | | |
| | PA | 0.28 | 0.99 | | 0.64 | | 0.18 | 1 | | 0.59 | |
| | K | | | | | 0.28 | | | | | 0.18 |
| | | | | | | | | | | | |
| | Class | NS | S | Total | UA | K | NS | S | Total | UA | K |
| Standardised Reflectance | NS | 679 | 298 | 977 | 0.69 | | 523 | 416 | 939 | 0.56 | |
| | S | 71 | 452 | 523 | 0.86 | | 227 | 334 | 561 | 0.59 | |
| | Total | 750 | 750 | 1500 | | | 750 | 750 | 1500 | | |
| | PA | 0.91 | 0.6 | | 0.75 | | 0.69 | 0.45 | | 0.57 | |
| | K | | | | | 0.51 | | | | | 0.14 |
| | | | | | | | | | | | |

Table C-7: Collated accuracy assessment of *E. radiata* at a depth of 100 cm from the water surface. NS - non-seaweed, S - seaweed, UA - User accuracy, PA - Producer accuracy, K - kappa.

| | Flight height – 10 m | | | | | | Flight height – 30 m | | | | |
|---|----------------------|------|------|-------|------|------|----------------------|------|-------|------|------|
| | Class | NS | S | Total | UA | K | NS | S | Total | UA | K |
| Raw Reflectance | NS | 205 | 130 | 335 | 0.61 | | 65 | 141 | 206 | 0.32 | |
| | S | 545 | 620 | 1165 | 0.53 | | 685 | 609 | 1294 | 0.47 | |
| | Total | 750 | 750 | 1500 | | | 750 | 750 | 1500 | | |
| | PA | 0.27 | 0.83 | | 0.55 | | 0.08 | 0.81 | | 0.45 | |
| | K | | | | | 0.1 | | | | | -0.1 |
| | | | | | | | | | | | |
| Standardised Reflectance | NS | 707 | 697 | 1404 | 0.5 | | 551 | 533 | 1084 | 0.51 | |
| | S | 43 | 53 | 96 | 0.55 | | 199 | 217 | 416 | 0.52 | |
| | Total | 750 | 750 | 1500 | | | 750 | 750 | 1500 | | |
| | PA | 0.94 | 0.07 | | 0.51 | | 0.73 | 0.29 | | 0.51 | |
| | K | | | | | 0.01 | | | | | 0.02 |
| | | | | | | | | | | | |
| Standardised Reflectance from image-derived spectra | NS | 706 | 384 | 1090 | 0.65 | | 715 | 244 | 959 | 0.75 | |
| | S | 44 | 366 | 410 | 0.89 | | 35 | 506 | 541 | 0.94 | |
| | Total | 750 | 750 | 1500 | | | 750 | 750 | 1500 | | |
| | PA | 0.94 | 0.49 | | 0.71 | | 0.95 | 0.67 | | 0.81 | |
| | K | | | | | 0.43 | | | | | 0.63 |
| | | | | | | | | | | | |

Table C-8: Collated accuracy assessment of *E. radiata* at a depth of 150 cm from the water surface. NS - non-seaweed, S - seaweed, UA - User accuracy, PA - Producer accuracy, K - kappa.

| | Flight height – 10 m | | | | | | Flight height – 30 m | | | | |
|---|----------------------|------|------|-------|------|------|----------------------|------|-------|------|------|
| | Class | NS | S | Total | UA | K | NS | S | Total | UA | K |
| Raw Reflectance | NS | 199 | 29 | 228 | 0.87 | | 94 | 3 | 97 | 0.97 | |
| | S | 551 | 721 | 1272 | 0.57 | | 656 | 747 | 1403 | 0.53 | |
| | Total | 750 | 750 | 1500 | | | 750 | 750 | 1500 | | |
| | PA | 0.27 | 0.96 | | 0.61 | | 0.12 | 0.99 | | 0.56 | |
| | K | | | | | 0.23 | | | | | 0.12 |
| | | | | | | | | | | | |
| Standardised Reflectance | NS | 700 | 750 | 1450 | 0.48 | | 462 | 604 | 1066 | 0.43 | |
| | S | 50 | 0 | 50 | 0 | | 288 | 146 | 434 | 0.34 | |
| | Total | 750 | 750 | 1500 | | | 750 | 750 | 1500 | | |
| | PA | 0.93 | 0 | | 0.47 | | 0.62 | 0.19 | | 0.41 | |
| | K | | | | | -0.1 | | | | | -0.2 |
| | | | | | | | | | | | |
| Standardised Reflectance from image-derived spectra | NS | 737 | 330 | 1067 | 0.69 | | 719 | 358 | 1077 | 0.67 | |
| | S | 13 | 420 | 433 | 0.97 | | 31 | 392 | 423 | 0.93 | |
| | Total | 750 | 750 | 1500 | | | 750 | 750 | 1500 | | |
| | PA | 0.98 | 0.56 | | 0.77 | | 0.96 | 0.52 | | 0.74 | |
| | K | | | | | 0.54 | | | | | 0.48 |
| | | | | | | | | | | | |

Table C-9: Collated accuracy assessment of *E. radiata* at a depth of 200 cm from the water surface. NS - non-seaweed, S - seaweed, UA - User accuracy, PA - Producer accuracy, K - kappa.

| | Flight height – 10 m | | | | | | Flight height – 30 m | | | | |
|---|----------------------|------|------|-------|------|------|----------------------|------|-------|------|------|
| | Class | NS | S | Total | UA | K | NS | S | Total | UA | K |
| Raw Reflectance | NS | 165 | 2 | 167 | 0.98 | | 90 | 0 | 90 | 1 | |
| | S | 585 | 748 | 133 | 0.56 | | 660 | 750 | 1410 | 0.53 | |
| | Total | 750 | 750 | 1500 | | | 750 | 750 | 1500 | | |
| | PA | 0.22 | 0.99 | | 0.61 | | 0.12 | 1 | | 0.56 | |
| | K | | | | | 0.22 | | | | | 0.12 |
| | | | | | | | | | | | |
| Standardised Reflectance | NS | 650 | 692 | 1342 | 0.48 | | 400 | 534 | 934 | 0.43 | |
| | S | 100 | 58 | 158 | 0.37 | | 350 | 216 | 566 | 0.38 | |
| | Total | 750 | 750 | 1500 | | | 750 | 750 | 1500 | | |
| | PA | 0.87 | 0.08 | | 0.47 | | 0.53 | 0.29 | | 0.41 | |
| | K | | | | | -0.1 | | | | | -0.2 |
| | | | | | | | | | | | |
| Standardised Reflectance from image-derived spectra | NS | 650 | 198 | 848 | 0.77 | | 674 | 400 | 1074 | 0.63 | |
| | S | 100 | 552 | 652 | 0.85 | | 76 | 350 | 426 | 0.82 | |
| | Total | 750 | 750 | 1500 | | | 750 | 750 | 1500 | | |
| | PA | 0.87 | 0.74 | | 0.8 | | 0.89 | 0.47 | | 0.68 | |
| | K | | | | | 0.6 | | | | | 0.37 |
| | | | | | | | | | | | |

Table C-10: Collated accuracy assessment of *U. pinnatifida* at a depth of 10 cm from the water surface. NS - non-seaweed, S - seaweed, UA - User accuracy, PA - Producer accuracy, K - kappa.

| | Flight height – 10 m | | | | | | Flight height – 30 m | | | | |
|--------------------------|----------------------|------|------|-------|------|------|----------------------|------|-------|------|------|
| | Class | NS | S | Total | UA | K | NS | S | Total | UA | K |
| Raw Reflectance | NS | 525 | 43 | 568 | 0.92 | | 629 | 236 | 865 | 0.73 | |
| | S | 225 | 707 | 932 | 0.76 | | 121 | 514 | 635 | 0.81 | |
| | Total | 750 | 750 | 1500 | | | 750 | 750 | 1500 | | |
| | PA | 0.7 | 0.94 | | 0.82 | | 0.84 | 0.69 | | 0.76 | |
| | K | | | | | 0.64 | | | | | 0.52 |
| | | | | | | | | | | | |
| | Class | NS | S | Total | UA | K | NS | S | Total | UA | K |
| Standardised Reflectance | NS | 743 | 393 | 1136 | 0.65 | | 710 | 663 | 1373 | 0.52 | |
| | S | 7 | 357 | 364 | 0.98 | | 40 | 87 | 127 | 0.69 | |
| | Total | 750 | 750 | 1500 | | | 750 | 750 | 1500 | | |
| | PA | 0.99 | 0.48 | | 0.73 | | 0.95 | 0.12 | | 0.53 | |
| | K | | | | | 0.47 | | | | | 0.06 |
| | | | | | | | | | | | |

Table C-11: Collated accuracy assessment of *U. pinnatifida* at a depth of 50 cm from the water surface. NS - non-seaweed, S - seaweed, UA - User accuracy, PA - Producer accuracy, K - kappa.

| | Flight height – 10 m | | | | | | Flight height – 30 m | | | | |
|--------------------------|----------------------|------|------|-------|------|------|----------------------|------|-------|------|------|
| | Class | NS | S | Total | UA | K | NS | S | Total | UA | K |
| Raw Reflectance | NS | 378 | 7 | 385 | 0.98 | | 312 | 0 | 312 | 1 | |
| | S | 372 | 743 | 1115 | 0.67 | | 438 | 750 | 1188 | 0.63 | |
| | Total | 750 | 750 | 1500 | | | 750 | 750 | 1500 | | |
| | PA | 0.5 | 0.99 | | 0.75 | | 0.416 | 1 | | 0.71 | |
| | K | | | | | 0.49 | | | | | 0.42 |
| | Class | NS | S | Total | UA | K | NS | S | Total | UA | K |
| Standardised Reflectance | NS | 736 | 270 | 1006 | 0.73 | | 646 | 614 | 1260 | 0.51 | |
| | S | 14 | 480 | 494 | 0.97 | | 104 | 136 | 240 | 0.57 | |
| | Total | 750 | 750 | 1500 | | | 750 | 750 | 1500 | | |
| | PA | 0.98 | 0.64 | | 0.81 | | 0.86 | 0.18 | | 0.52 | |
| | K | | | | | 0.62 | | | | | 0.04 |

Table C-12: Collated accuracy assessment of *U. pinnatifida* at a depth of 100 cm from the water surface. NS - non-seaweed, S - seaweed, UA - User accuracy, PA - Producer accuracy, K - kappa.

| | Flight height – 10 m | | | | | | Flight height – 30 m | | | | |
|---|----------------------|------|------|-------|------|------|----------------------|------|-------|------|------|
| | Class | NS | S | Total | UA | K | NS | S | Total | UA | K |
| Raw Reflectance | NS | 130 | 226 | 356 | 0.37 | | 82 | 171 | 253 | 0.32 | |
| | S | 620 | 524 | 1144 | 0.46 | | 668 | 579 | 1247 | 0.46 | |
| | Total | 750 | 750 | 1500 | | | 750 | 750 | 1500 | | |
| | PA | 0.17 | 0.69 | | 0.44 | | 0.11 | 0.77 | | 0.44 | |
| | K | | | | | -0.1 | | | | | -0.1 |
| | | | | | | | | | | | |
| Standardised Reflectance | NS | 411 | 675 | 1086 | 0.38 | | 189 | 578 | 767 | 0.25 | |
| | S | 339 | 75 | 414 | 0.18 | | 561 | 172 | 733 | 0.23 | |
| | Total | 750 | 750 | 1500 | | | 750 | 750 | 1500 | | |
| | PA | 0.55 | 0.1 | | 0.32 | | 0.25 | 0.23 | | 0.24 | |
| | K | | | | | -0.4 | | | | | -0.5 |
| | | | | | | | | | | | |
| Standardised Reflectance from image-derived spectra | NS | 741 | 546 | 1287 | 0.58 | | 731 | 611 | 1342 | 0.54 | |
| | S | 9 | 204 | 213 | 0.96 | | 19 | 139 | 158 | 0.88 | |
| | Total | 750 | 750 | 1500 | | | 750 | 750 | 1500 | | |
| | PA | 0.99 | 0.27 | | 0.63 | | 0.97 | 0.19 | | 0.58 | |
| | K | | | | | 0.26 | | | | | 0.16 |
| | | | | | | | | | | | |

Table C-13: Collated accuracy assessment of *U. pinnatifida* at a depth of 150 cm from the water surface. NS - non-seaweed, S - seaweed, UA - User accuracy, PA - Producer accuracy, K - kappa.

| | Flight height – 10 m | | | | | | Flight height – 30 m | | | | |
|--|----------------------|------|------|-------|------|------|----------------------|------|-------|------|------|
| | Class | NS | S | Total | UA | K | NS | S | Total | UA | K |
| Raw Reflectance | NS | 130 | 1 | 131 | 0.99 | | 88 | 0 | 88 | 1 | |
| | S | 620 | 749 | 1369 | 0.55 | | 662 | 750 | 1412 | 0.53 | |
| | Total | 750 | 750 | 1500 | | | 750 | 750 | 1500 | | |
| | PA | 0.17 | 0.99 | | 0.59 | | 0.12 | 1 | | 0.56 | |
| | K | | | | | 0.17 | | | | | 0.12 |
| | | | | | | | | | | | |
| Standardised Reflectance | NS | 555 | 690 | 1245 | 0.45 | | 309 | 642 | 951 | 0.32 | |
| | S | 195 | 60 | 255 | 0.24 | | 441 | 108 | 549 | 0.19 | |
| | Total | 750 | 750 | 1500 | | | 750 | 750 | 1500 | | |
| | PA | 0.74 | 0.08 | | 0.41 | | 0.41 | 0.14 | | 0.28 | |
| | K | | | | | -0.2 | | | | | -0.4 |
| | | | | | | | | | | | |
| Standardised Reflectance from image-derived spectra | NS | 671 | 259 | 930 | 0.72 | | 739 | 656 | 1395 | 0.53 | |
| | S | 79 | 491 | 570 | 0.86 | | 11 | 94 | 105 | 0.89 | |
| | Total | 750 | 750 | 1500 | | | 750 | 750 | 1500 | | |
| | PA | 0.89 | 0.65 | | 0.77 | | 0.98 | 0.12 | | 0.55 | |
| | K | | | | | 0.55 | | | | | 0.11 |
| | | | | | | | | | | | |

Table C-14: Collated accuracy assessment of *U. pinnatifida* at a depth of 200 cm from the water surface. NS - non-seaweed, S - seaweed, UA - User accuracy, PA - Producer accuracy, K - kappa.

| | Flight height – 10 m | | | | | | Flight height – 30 m | | | | |
|---|----------------------|------|------|-------|------|------|----------------------|------|-------|------|------|
| | Class | NS | S | Total | UA | K | NS | S | Total | UA | K |
| Raw Reflectance | NS | 123 | 0 | 123 | 1 | | 72 | 0 | 72 | 1 | |
| | S | 627 | 750 | 1377 | 0.54 | | 678 | 750 | 1428 | 0.53 | |
| | Total | 750 | 750 | 1500 | | | 750 | 750 | 1500 | | |
| | PA | 0.16 | 1 | | 0.58 | | 0.09 | 1 | | 0.55 | |
| | K | | | | | 0.16 | | | | | 0.09 |
| | | | | | | | | | | | |
| Standardised Reflectance | NS | 459 | 631 | 1090 | 0.42 | | 405 | 458 | 863 | 0.47 | |
| | S | 291 | 119 | 410 | 0.29 | | 345 | 292 | 637 | 0.46 | |
| | Total | 750 | 750 | 1500 | | | 750 | 750 | 1500 | | |
| | PA | 0.61 | 0.16 | | 0.39 | | 0.54 | 0.39 | | 0.46 | |
| | K | | | | | -0.2 | | | | | -0.1 |
| | | | | | | | | | | | |
| Standardised Reflectance from image-derived spectra | NS | 651 | 262 | 913 | 0.71 | | 432 | 252 | 684 | 0.63 | |
| | S | 99 | 488 | 587 | 0.83 | | 318 | 498 | 816 | 0.61 | |
| | Total | 750 | 750 | 1500 | | | 750 | 750 | 1500 | | |
| | PA | 0.87 | 0.65 | | 0.76 | | 0.58 | 0.66 | | 0.62 | |
| | K | | | | | 0.52 | | | | | 0.24 |
| | | | | | | | | | | | |

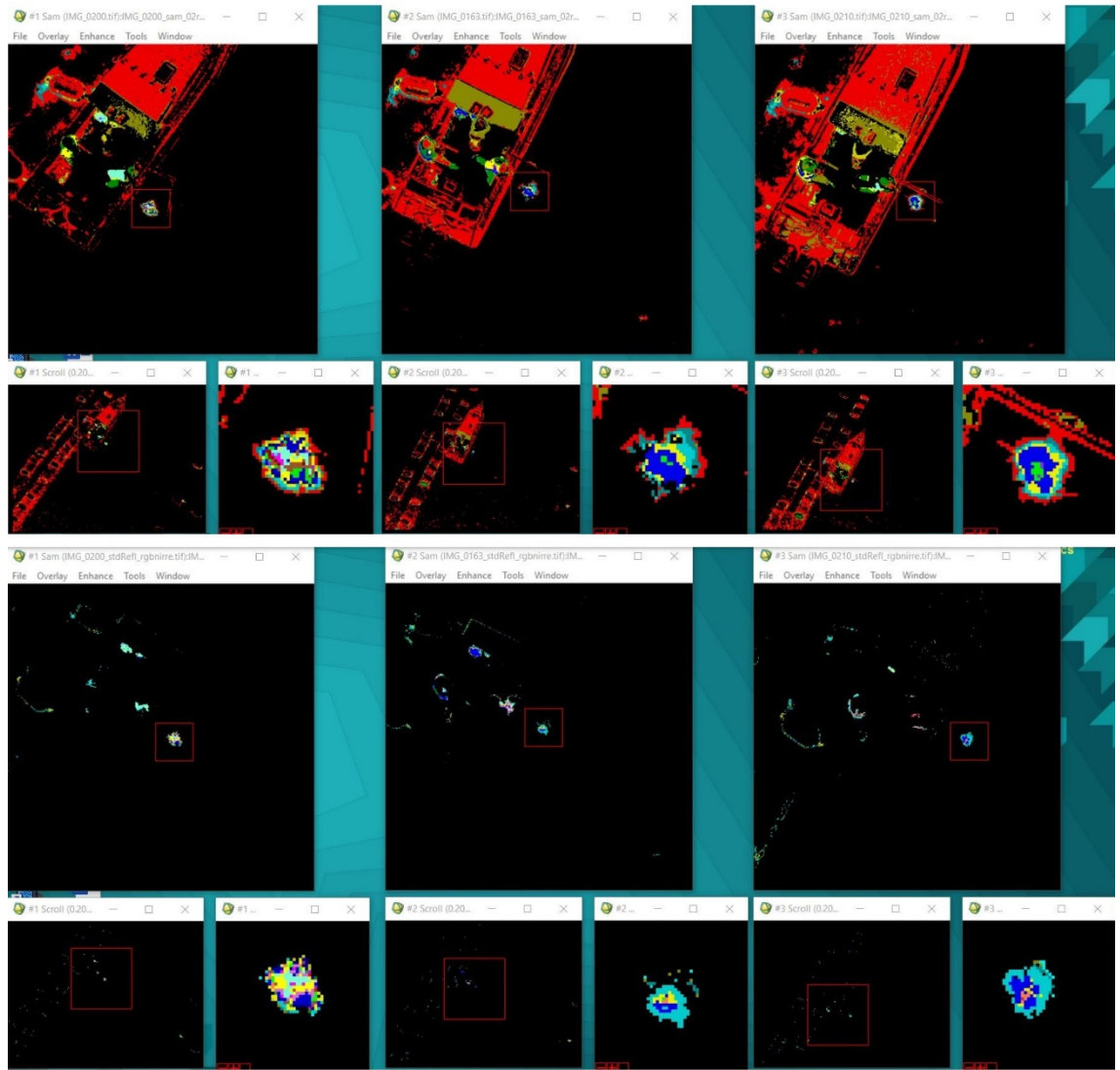


Figure C-10: Screenshot of images of three different *E. radiata* individuals at 10cm below water surface classified using raw reflectance spectral signature of *E.radiata* at 10cm water depth on raw reflectance multispectral data (top) and standardised reflectance spectral signature of *E.radiata* at 10cm water depth on standardised multispectral data (bottom). The data was captured at FH of 30m.

Table C-15: Collated accuracy assessment of *E. radiata* at a depth of 10cm from the water surface. uC - unclassified, UA - User accuracy, PA - Producer accuracy, K – kappa. E – *E. radiata*, U – *U. pinnatifida* and 1,2,3,4,5,6 in the class column represent depth levels at “out-of-water”, <10cm, 50cm, 1m, 1.5m and 2m, respectively.

| Flight height – 10m | | | | | | Flight height – 30m | | | | | |
|---------------------|------|------|-------|------|------|---------------------|------|------|-------|------|------|
| Class | uC | E_2 | Total | UA | K | Class | uC | E_2 | Total | UA | K |
| uC | 568 | 19 | 587 | 0.97 | | uC | 659 | 29 | 688 | 0.96 | |
| E_1 | 0 | 0 | 0 | | | E_1 | 0 | 2 | 2 | | |
| E_2 | 0 | 240 | 240 | 1 | | E_2 | 3 | 290 | 293 | 0.99 | |
| E_3 | 8 | 89 | 97 | | | E_3 | 29 | 50 | 79 | | |
| E_4 | 11 | 1 | 12 | | | E_4 | 8 | 2 | 10 | | |
| E_5 | 8 | 0 | 8 | | | E_5 | 4 | 1 | 5 | | |
| E_6 | 45 | 0 | 45 | | | E_6 | 7 | 0 | 7 | | |
| U_1 | 6 | 0 | 6 | | | U_1 | 1 | 0 | 1 | | |
| U_2 | 2 | 5 | 7 | | | U_2 | 6 | 141 | 147 | | |
| U_3 | 9 | 394 | 403 | | | U_3 | 24 | 217 | 241 | | |
| U_4 | 2 | 1 | 3 | | | U_4 | 2 | 12 | 14 | | |
| U_5 | 12 | 1 | 13 | | | U_5 | 2 | 4 | 6 | | |
| U_6 | 79 | 0 | 79 | | | U_6 | 5 | 2 | 7 | | |
| Total | 750 | 750 | 1500 | | | Total | 750 | 750 | 1500 | | |
| PA | 0.76 | 0.32 | | 0.54 | | PA | 0.88 | 0.39 | | 0.63 | |
| K | | | | | 0.36 | K | | | | | 0.45 |

Table C-16: Collated accuracy assessment of *E. radiata* at a depth of 50cm from the water surface. uC - unclassified, UA - User accuracy, PA - Producer accuracy, K – kappa. E – *E. radiata*, U – *U. pinnatifida* and 1,2,3,4,5,6 in the class column represent depth levels at “out-of-water”, <10cm, 50cm, 1m, 1.5m and 2m, respectively.

| Flight height – 10m | | | | | | Flight height – 30m | | | | | |
|---------------------|------|------|-------|------|------|---------------------|------|------|-------|------|------|
| Class | uC | E_3 | Total | UA | K | Class | uC | E_3 | Total | UA | K |
| uC | 539 | 55 | 594 | 0.91 | | uC | 640 | 105 | 745 | 0.86 | |
| E_1 | 0 | 0 | 0 | | | E_1 | 0 | 0 | 0 | | |
| E_2 | 5 | 0 | 5 | | | E_2 | 0 | 0 | 0 | | |
| E_3 | 14 | 154 | 168 | 0.92 | | E_3 | 38 | 271 | 309 | 0.88 | |
| E_4 | 10 | 130 | 140 | | | E_4 | 9 | 87 | 96 | | |
| E_5 | 19 | 11 | 30 | | | E_5 | 0 | 0 | 0 | | |
| E_6 | 30 | 2 | 32 | | | E_6 | 11 | 0 | 11 | | |
| U_1 | 5 | 0 | 5 | | | U_1 | 0 | 0 | 0 | | |
| U_2 | 4 | 0 | 4 | | | U_2 | 3 | 0 | 3 | | |
| U_3 | 9 | 333 | 342 | | | U_3 | 24 | 199 | 223 | | |
| U_4 | 5 | 63 | 68 | | | U_4 | 9 | 79 | 88 | | |
| U_5 | 15 | 2 | 17 | | | U_5 | 2 | 9 | 11 | | |
| U_6 | 95 | 0 | 95 | | | U_6 | 14 | 0 | 14 | | |
| Total | 750 | 750 | 1500 | | | Total | 750 | 750 | 1500 | | |
| PA | 0.72 | 0.21 | | 0.46 | | PA | 0.85 | 0.36 | | 0.61 | |
| K | | | | | 0.28 | K | | | | | 0.39 |

Table C-17: Collated accuracy assessment of *E. radiata* at a depth of 100cm from the water surface. uC - unclassified, UA - User accuracy, PA - Producer accuracy, K – kappa. E – *E. radiata*, U – *U. pinnatifida* and 1,2,3,4,5,6 in the class column represent depth levels at “out-of-water”, <10cm, 50cm, 1m, 1.5m and 2m, respectively.

| Flight height – 10m | | | | | | Flight height – 30m | | | | | |
|---------------------|------|------|-------|------|------|---------------------|------|------|-------|------|------|
| Class | uC | E_4 | Total | UA | K | Class | uC | E_4 | Total | UA | K |
| uC | 550 | 115 | 665 | 0.83 | | uC | 635 | 135 | 770 | 0.82 | |
| E_1 | 0 | 0 | 0 | | | E_1 | 0 | 0 | 0 | | |
| E_2 | 5 | 9 | 14 | | | E_2 | 3 | 0 | 3 | | |
| E_3 | 19 | 25 | 44 | | | E_3 | 48 | 186 | 234 | | |
| E_4 | 11 | 283 | 294 | 0.96 | | E_4 | 7 | 60 | 67 | 0.89 | |
| E_5 | 16 | 109 | 125 | | | E_5 | 3 | 4 | 7 | | |
| E_6 | 25 | 46 | 71 | | | E_6 | 3 | 12 | 15 | | |
| U_1 | 5 | 0 | 5 | | | U_1 | 1 | 0 | 1 | | |
| U_2 | 6 | 1 | 7 | | | U_2 | 1 | 1 | 2 | | |
| U_3 | 8 | 89 | 97 | | | U_3 | 30 | 282 | 312 | | |
| U_4 | 2 | 45 | 47 | | | U_4 | 6 | 62 | 68 | | |
| U_5 | 23 | 24 | 47 | | | U_5 | 2 | 8 | 10 | | |
| U_6 | 80 | 4 | 84 | | | U_6 | 11 | 0 | 11 | | |
| Total | 750 | 750 | 1500 | | | Total | 750 | 750 | 1500 | | |
| PA | 0.73 | 0.38 | | 0.55 | | PA | 0.85 | 0.08 | | 0.46 | |
| K | | | | | 0.35 | K | | | | | 0.26 |

Table C-18: Collated accuracy assessment of *E. radiata* at a depth of 150cm from the water surface. uC - unclassified, UA - User accuracy, PA - Producer accuracy, K – kappa. E – *E. radiata*, U – *U. pinnatifida* and 1,2,3,4,5,6 in the class column represent depth levels at “out-of-water”, <10cm, 50cm, 1m, 1.5m and 2m, respectively.

| Flight height – 10m | | | | | | Flight height – 30m | | | | | |
|---------------------|------|------|-------|------|------|---------------------|------|------|-------|------|------|
| Class | uC | E_5 | Total | UA | K | Class | uC | E_5 | Total | UA | K |
| uC | 538 | 102 | 640 | 0.84 | | uC | 649 | 355 | 1004 | 0.65 | |
| E_1 | 0 | 0 | 0 | | | E_1 | 0 | 0 | 0 | | |
| E_2 | 5 | 0 | 5 | | | E_2 | 1 | 1 | 2 | | |
| E_3 | 7 | 0 | 7 | | | E_3 | 39 | 84 | 123 | | |
| E_4 | 18 | 4 | 22 | | | E_4 | 3 | 0 | 3 | | |
| E_5 | 9 | 265 | 274 | 0.97 | | E_5 | 2 | 20 | 22 | | |
| E_6 | 32 | 200 | 232 | | | E_6 | 10 | 128 | 138 | | |
| U_1 | 6 | 0 | 6 | | | U_1 | 0 | 0 | 0 | | |
| U_2 | 4 | 0 | 4 | | | U_2 | 6 | 3 | 9 | | |
| U_3 | 7 | 0 | 7 | | | U_3 | 27 | 114 | 141 | | |
| U_4 | 1 | 0 | 1 | | | U_4 | 3 | 0 | 3 | | |
| U_5 | 21 | 73 | 94 | | | U_5 | 4 | 42 | 46 | | |
| U_6 | 102 | 106 | 208 | | | U_6 | 6 | 3 | 9 | | |
| Total | 750 | 750 | 1500 | | | Total | 750 | 750 | 1500 | | |
| PA | 0.72 | 0.35 | | 0.54 | | PA | 0.87 | 0.03 | | 0.45 | |
| K | | | | | 0.33 | K | | | | | 0.16 |

Table C-19: Collated accuracy assessment of *E. radiata* at a depth of 200cm from the water surface. uC - unclassified, UA - User accuracy, PA - Producer accuracy, K – kappa. E – *E. radiata*, U – *U. pinnatifida* and 1,2,3,4,5,6 in the class column represent depth levels at “out-of-water”, <10cm, 50cm, 1m, 1.5m and 2m respectively.

| Flight height – 10m | | | | | | Flight height – 30m | | | | | |
|---------------------|------|------|-------|------|------|---------------------|------|------|-------|------|------|
| Class | uC | E_6 | Total | UA | K | Class | uC | E_6 | Total | UA | K |
| uC | 553 | 290 | 843 | 0.66 | | uC | 640 | 541 | 1181 | 0.54 | |
| E_1 | 0 | 0 | 0 | | | E_1 | 0 | 0 | 0 | | |
| E_2 | 3 | 0 | 3 | | | E_2 | 1 | 0 | 1 | | |
| E_3 | 13 | 2 | 15 | | | E_3 | 46 | 55 | 101 | | |
| E_4 | 8 | 0 | 8 | | | E_4 | 4 | 0 | 4 | | |
| E_5 | 14 | 44 | 58 | | | E_5 | 5 | 9 | 14 | | |
| E_6 | 44 | 288 | 332 | 0.87 | | E_6 | 3 | 91 | 94 | 0.97 | |
| U_1 | 3 | 0 | 3 | | | U_1 | 0 | 0 | 0 | | |
| U_2 | 2 | 0 | 2 | | | U_2 | 2 | 3 | 5 | | |
| U_3 | 10 | 0 | 10 | | | U_3 | 27 | 8 | 35 | | |
| U_4 | 1 | 0 | 1 | | | U_4 | 2 | 0 | 2 | | |
| U_5 | 10 | 16 | 26 | | | U_5 | 3 | 14 | 17 | | |
| U_6 | 89 | 110 | 199 | | | U_6 | 17 | 29 | 46 | | |
| Total | 750 | 750 | 1500 | | | Total | 750 | 750 | 1500 | | |
| PA | 0.73 | 0.38 | | 0.56 | | PA | 0.85 | 0.12 | | 0.49 | |
| K | | | | | 0.28 | K | | | | | 0.11 |

Table C-20: Collated accuracy assessment of *U. pinnatifida* at a depth of 10cm from the water surface. uC - unclassified, UA - User accuracy, PA - Producer accuracy, K – kappa. E – *E. radiata*, U – *U. pinnatifida* and 1,2,3,4,5,6 in the class column represent depth levels at “out-of-water”, <10cm, 50cm, 1m, 1.5m and 2m, respectively.

| Flight height – 10m | | | | | | Flight height – 30m | | | | | |
|---------------------|------|------|-------|------|-----|---------------------|------|-------|-------|------|------|
| Class | uC | U_2 | Total | UA | K | Class | uC | U_2 | Total | UA | K |
| uC | 619 | 28 | 647 | 0.96 | | uC | 671 | 57 | 728 | 0.92 | |
| E_1 | 0 | 0 | 0 | | | E_1 | 0 | 0 | 0 | | |
| E_2 | 0 | 320 | 320 | | | E_2 | 0 | 116 | 116 | | |
| E_3 | 4 | 13 | 17 | | | E_3 | 28 | 44 | 72 | | |
| E_4 | 5 | 3 | 8 | | | E_4 | 9 | 10 | 19 | | |
| E_5 | 7 | 2 | 9 | | | E_5 | 1 | 1 | 2 | | |
| E_6 | 18 | 0 | 18 | | | E_6 | 5 | 0 | 5 | | |
| U_1 | 3 | 0 | 3 | | | U_1 | 1 | 0 | 1 | | |
| U_2 | 0 | 88 | 88 | 1 | | U_2 | 1 | 1 | 2 | 0.5 | |
| U_3 | 7 | 284 | 291 | | | U_3 | 26 | 491 | 517 | | |
| U_4 | 2 | 3 | 5 | | | U_4 | 2 | 23 | 25 | | |
| U_5 | 13 | 5 | 18 | | | U_5 | 1 | 5 | 6 | | |
| U_6 | 72 | 4 | 76 | | | U_6 | 5 | 2 | 7 | | |
| Total | 750 | 750 | 1500 | | | Total | 750 | 750 | 1500 | | |
| PA | 0.83 | 0.12 | | 0.47 | | PA | 0.89 | 0.001 | | 0.45 | |
| K | | | | | 0.3 | K | | | | | 0.27 |

Table C-21: Collated accuracy assessment of *U. pinnatifida* at a depth of 50cm from the water surface. uC - unclassified, UA - User accuracy, PA - Producer accuracy, K – kappa. E – *E. radiata*, U – *U. pinnatifida* and 1,2,3,4,5,6 in the class column represent depth levels at “out-of-water”, <10cm, 50cm, 1m, 1.5m and 2m, respectively.

| Flight height – 10m | | | | | | Flight height – 30m | | | | | |
|---------------------|------|------|-------|------|------|---------------------|------|------|-------|------|------|
| Class | uC | U_3 | Total | UA | K | Class | uC | U_3 | Total | UA | K |
| uC | 631 | 139 | 770 | 0.82 | | uC | 651 | 54 | 705 | 0.92 | |
| E_1 | 0 | 0 | 0 | | | E_1 | 0 | 0 | 0 | | |
| E_2 | 1 | 1 | 2 | | | E_2 | 0 | 0 | 0 | | |
| E_3 | 10 | 83 | 93 | | | E_3 | 33 | 167 | 200 | | |
| E_4 | 8 | 80 | 88 | | | E_4 | 7 | 74 | 81 | | |
| E_5 | 7 | 10 | 17 | | | E_5 | 2 | 0 | 2 | | |
| E_6 | 12 | 10 | 22 | | | E_6 | 6 | 3 | 9 | | |
| U_1 | 0 | 0 | 0 | | | U_1 | 1 | 0 | 1 | | |
| U_2 | 2 | 0 | 2 | | | U_2 | 4 | 0 | 4 | | |
| U_3 | 4 | 413 | 417 | 0.99 | | U_3 | 30 | 235 | 265 | 0.89 | |
| U_4 | 2 | 8 | 10 | | | U_4 | 11 | 209 | 220 | | |
| U_5 | 15 | 5 | 20 | | | U_5 | 1 | 8 | 9 | | |
| U_6 | 58 | 1 | 59 | | | U_6 | 4 | 0 | 4 | | |
| Total | 750 | 750 | 1500 | | | Total | 750 | 750 | 1500 | | |
| PA | 0.84 | 0.55 | | 0.69 | | PA | 0.87 | 0.31 | | 0.59 | |
| K | | | | | 0.49 | K | | | | | 0.39 |

Table C-22: Collated accuracy assessment of *U. pinnatifida* at a depth of 100cm from the water surface. uC - unclassified, UA - User accuracy, PA - Producer accuracy, K – kappa. E – *E. radiata*, U – *U. pinnatifida* and 1,2,3,4,5,6 in the class column represent depth levels at “out-of-water”, <10cm, 50cm, 1m, 1.5m and 2m, respectively.

| Flight height – 10m | | | | | | Flight height – 30m | | | | | |
|---------------------|------|------|-------|------|------|---------------------|------|------|-------|------|------|
| Class | uC | U_4 | Total | UA | K | Class | uC | U_4 | Total | UA | K |
| uC | 591 | 181 | 772 | 0.77 | | uC | 654 | 269 | 923 | 0.71 | |
| E_1 | 0 | 0 | 0 | | | E_1 | 0 | 0 | 0 | | |
| E_2 | 2 | 0 | 2 | | | E_2 | 3 | 0 | 3 | | |
| E_3 | 10 | 3 | 13 | | | E_3 | 44 | 57 | 101 | | |
| E_4 | 6 | 123 | 129 | | | E_4 | 4 | 33 | 37 | | |
| E_5 | 5 | 92 | 97 | | | E_5 | 1 | 2 | 3 | | |
| E_6 | 14 | 52 | 66 | | | E_6 | 4 | 2 | 6 | | |
| U_1 | 6 | 0 | 6 | | | U_1 | 0 | 0 | 0 | | |
| U_2 | 2 | 2 | 4 | | | U_2 | 3 | 0 | 3 | | |
| U_3 | 7 | 29 | 36 | | | U_3 | 26 | 144 | 170 | | |
| U_4 | 4 | 155 | 159 | 0.97 | | U_4 | 6 | 141 | 147 | 0.96 | |
| U_5 | 10 | 76 | 86 | | | U_5 | 1 | 95 | 96 | | |
| U_6 | 93 | 37 | 130 | | | U_6 | 4 | 7 | 11 | | |
| Total | 750 | 750 | 1500 | | | Total | 750 | 750 | 1500 | | |
| PA | 0.79 | 0.21 | | 0.49 | | PA | 0.87 | 0.19 | | 0.53 | |
| K | | | | | 0.27 | K | | | | | 0.27 |

Table C-23: Collated accuracy assessment of *U. pinnatifida* at a depth of 150cm from the water surface. uC - unclassified, UA - User accuracy, PA - Producer accuracy, K – kappa. E – *E. radiata*, U – *U. pinnatifida* and 1,2,3,4,5,6 in the class column represent depth levels at “out-of-water”, <10cm, 50cm, 1m, 1.5m and 2m, respectively.

| Flight height – 10m | | | | | | Flight height – 30m | | | | | |
|---------------------|------|------|-------|------|------|---------------------|------|------|-------|------|------|
| Class | uC | U_5 | Total | UA | K | Class | uC | U_5 | Total | UA | K |
| uC | 610 | 235 | 845 | 0.72 | | uC | 662 | 636 | 1298 | 0.51 | |
| E_1 | 0 | 0 | 0 | | | E_1 | 0 | 0 | 0 | | |
| E_2 | 2 | 0 | 2 | | | E_2 | 1 | 0 | 1 | | |
| E_3 | 8 | 1 | 9 | | | E_3 | 34 | 21 | 55 | | |
| E_4 | 8 | 0 | 8 | | | E_4 | 3 | 0 | 3 | | |
| E_5 | 6 | 19 | 25 | | | E_5 | 0 | 0 | 0 | | |
| E_6 | 18 | 162 | 180 | | | E_6 | 4 | 34 | 38 | | |
| U_1 | 0 | 0 | 0 | | | U_1 | 0 | 0 | 0 | | |
| U_2 | 1 | 2 | 3 | | | U_2 | 5 | 1 | 6 | | |
| U_3 | 8 | 0 | 8 | | | U_3 | 33 | 29 | 62 | | |
| U_4 | 0 | 0 | 0 | | | U_4 | 4 | 0 | 4 | | |
| U_5 | 15 | 119 | 134 | 0.89 | | U_5 | 2 | 21 | 23 | 0.91 | |
| U_6 | 74 | 212 | 286 | | | U_6 | 2 | 8 | 10 | | |
| Total | 750 | 750 | 1500 | | | Total | 750 | 750 | 1500 | | |
| PA | 0.81 | 0.16 | | 0.49 | | PA | 0.88 | 0.03 | | 0.46 | |
| K | | | | | 0.24 | K | | | | | 0.03 |

Table C-24: Collated accuracy assessment of *U. pinnatifida* at a depth of 200cm from the water surface. uC - unclassified, UA - User accuracy, PA - Producer accuracy, K – kappa. E – *E. radiata*, U – *U. pinnatifida* and 1,2,3,4,5,6 in the class column represent depth levels at “out-of-water”, <10cm, 50cm, 1m, 1.5m and 2m, respectively.

| Flight height – 10m | | | | | | Flight height – 30m | | | | | |
|---------------------|------|------|-------|------|------|---------------------|------|------|-------|------|-------|
| Class | uC | U_6 | Total | UA | K | Class | uC | U_6 | Total | UA | K |
| uC | 628 | 257 | 885 | 0.71 | | uC | 667 | 710 | 1377 | 0.48 | |
| E_1 | 0 | 0 | 0 | | | E_1 | 0 | 0 | 0 | | |
| E_2 | 1 | 0 | 1 | | | E_2 | 2 | 0 | 2 | | |
| E_3 | 11 | 3 | 14 | | | E_3 | 33 | 2 | 35 | | |
| E_4 | 7 | 0 | 7 | | | E_4 | 8 | 0 | 8 | | |
| E_5 | 4 | 0 | 4 | | | E_5 | 0 | 0 | 0 | | |
| E_6 | 14 | 48 | 62 | | | E_6 | 10 | 2 | 12 | | |
| U_1 | 1 | 0 | 1 | | | U_1 | 1 | 0 | 1 | | |
| U_2 | 3 | 0 | 3 | | | U_2 | 0 | 0 | 0 | | |
| U_3 | 7 | 2 | 9 | | | U_3 | 16 | 1 | 17 | | |
| U_4 | 0 | 0 | 0 | | | U_4 | 4 | 0 | 4 | | |
| U_5 | 10 | 41 | 51 | | | U_5 | 1 | 0 | 1 | | |
| U_6 | 64 | 399 | 463 | 0.86 | | U_6 | 8 | 35 | 43 | 0.81 | |
| Total | 750 | 750 | 1500 | | | Total | 750 | 750 | 1500 | | |
| PA | 0.84 | 0.53 | | 0.68 | | PA | 0.89 | 0.05 | | 0.47 | |
| K | | | | | 0.43 | K | | | | | -0.01 |

Table C-25: Collated classification accuracy assessment of *E. radiata* at all depths. uC - unclassified, UA - User accuracy, PA - Producer accuracy, K – kappa. E – *E. radiata*, U – *U. pinnatifida*.

| Flight height – 10m | | | | | | Flight height – 30m | | | | |
|---------------------|-------|------|-------|-------|------|---------------------|------|-------|-------|------|
| Class | uC | E | Total | UA | K | uC | E | Total | UA | K |
| uC | 2748 | 581 | 3329 | 0.825 | | 3223 | 1165 | 4388 | 0.735 | |
| E | 379 | 1902 | 2281 | 0.834 | | 287 | 1353 | 1640 | 0.825 | |
| U | 623 | 1267 | 1890 | | | 240 | 1232 | 1472 | | |
| Total | 3750 | 3750 | 7500 | | | 3750 | 3750 | 7500 | | |
| PA | 0.733 | 0.51 | | 0.62 | | 0.86 | 0.36 | | 0.61 | |
| K | | | | | 0.39 | | | | | 0.35 |

Table C-26: Collated classification accuracy assessment of *E. radiata* at all depths excluding 1.5 and 2m. uC - unclassified, UA - User accuracy, PA - Producer accuracy, K – kappa. E – *E. radiata*, U – *U. pinnatifida*.

| Flight height – 10m | | | | | | Flight height – 30m | | | | |
|---------------------|-------|-------|-------|-------|-----|---------------------|------|-------|-------|------|
| Class | uC | E | Total | UA | K | uC | E | Total | UA | K |
| uC | 1657 | 189 | 1846 | 0.898 | | 1934 | 269 | 2203 | 0.878 | |
| E | 226 | 1099 | 1325 | 0.829 | | 173 | 965 | 1138 | 0.848 | |
| U | 367 | 962 | 1329 | | | 143 | 1016 | 1159 | | |
| Total | 2250 | 2250 | 4500 | | | 2250 | 2250 | 4500 | | |
| PA | 0.736 | 0.488 | | 0.612 | | 0.86 | 0.43 | | 0.64 | |
| K | | | | | 0.4 | | | | | 0.43 |

Table C-27: Collated classification accuracy assessment of *U. pinnatifida* at all depths. uC - unclassified, UA - User accuracy, PA - Producer accuracy, K – kappa. E – *E. radiata*, U – *U. pinnatifida*.

| Flight height – 10m | | | | | | Flight height – 30m | | | | |
|---------------------|------|------|-------|-------|-------|---------------------|------|-------|-------|------|
| Class | uC | U | Total | UA | K | uC | U | Total | UA | K |
| uC | 3079 | 840 | 3919 | 0.786 | | 3305 | 1726 | 5031 | 0.657 | |
| E | 188 | 1025 | 1213 | | | 242 | 568 | 810 | | |
| U | 483 | 1885 | 2368 | 0.796 | | 203 | 1456 | 1659 | 0.878 | |
| Total | 3750 | 3750 | 7500 | | | 3750 | 3750 | 7500 | | |
| PA | 0.82 | 0.5 | | 0.661 | | 0.88 | 0.39 | | 0.64 | |
| K | | | | | 0.417 | | | | | 0.34 |

Table C-28: Collated classification accuracy assessment of *U. pinnatifida* at all depths excluding 1.5m and 2m. uC - unclassified, UA - User accuracy, PA - Producer accuracy, K – kappa. E – *E. radiata*, U – *U. pinnatifida*.

| Flight height – 10m | | | | | | Flight height – 30m | | | | |
|---------------------|------|------|-------|-------|-------|---------------------|-------|-------|-------|-------|
| Class | uC | U | Total | UA | K | uC | U | Total | UA | K |
| uC | 1841 | 348 | 2189 | 0.84 | | 1976 | 380 | 2356 | 0.839 | |
| E | 109 | 792 | 901 | | | 147 | 509 | 656 | | |
| U | 300 | 1110 | 1410 | 0.787 | | 127 | 1361 | 1488 | 0.915 | |
| Total | 2250 | 2250 | 4500 | | | 2250 | 2250 | 4500 | | |
| PA | 0.82 | 0.49 | | 0.656 | | 0.878 | 0.605 | | 0.74 | |
| K | | | | | 0.426 | | | | | 0.549 |

Table C-29: Collated accuracy assessment of classification of both seaweed species at depths 10cm, 50cm and 1m from images collected at a flight height of 10m. uC - unclassified, UA - User accuracy, PA - Producer accuracy, K – kappa. E – *E. radiata*, U – *U. pinnatifida*.

| Class | uC | E | U | Total | UA | K |
|-------|-------|------|------|--------|------|------|
| uC | 1749 | 189 | 348 | 2286 | 0.77 | |
| E | 167.5 | 1099 | 792 | 2058.5 | 0.53 | |
| U | 333.5 | 962 | 1110 | 2405.5 | 0.46 | |
| Total | 2250 | 2250 | 2250 | 6750 | | |
| PA | 0.78 | 0.49 | 0.49 | | 0.59 | |
| K | | | | | | 0.38 |

Table C-30: Collated accuracy assessment of classification of both seaweed species at depths 10cm, 50cm and 1m from images collected at a flight height of 30m. uC - unclassified, UA - User accuracy, PA - Producer accuracy, K – kappa. E – *E. radiata*, U – *U. pinnatifida*.

| Class | uC | E | U | Total | UA | K |
|-------|------|------|------|-------|------|------|
| uC | 1955 | 269 | 380 | 2604 | 0.75 | |
| E | 160 | 965 | 509 | 1634 | 0.59 | |
| U | 135 | 1016 | 1361 | 2512 | 0.54 | |
| Total | 2250 | 2250 | 2250 | 6750 | | |
| PA | 0.87 | 0.43 | 0.6 | | 0.63 | |
| K | | | | | | 0.45 |

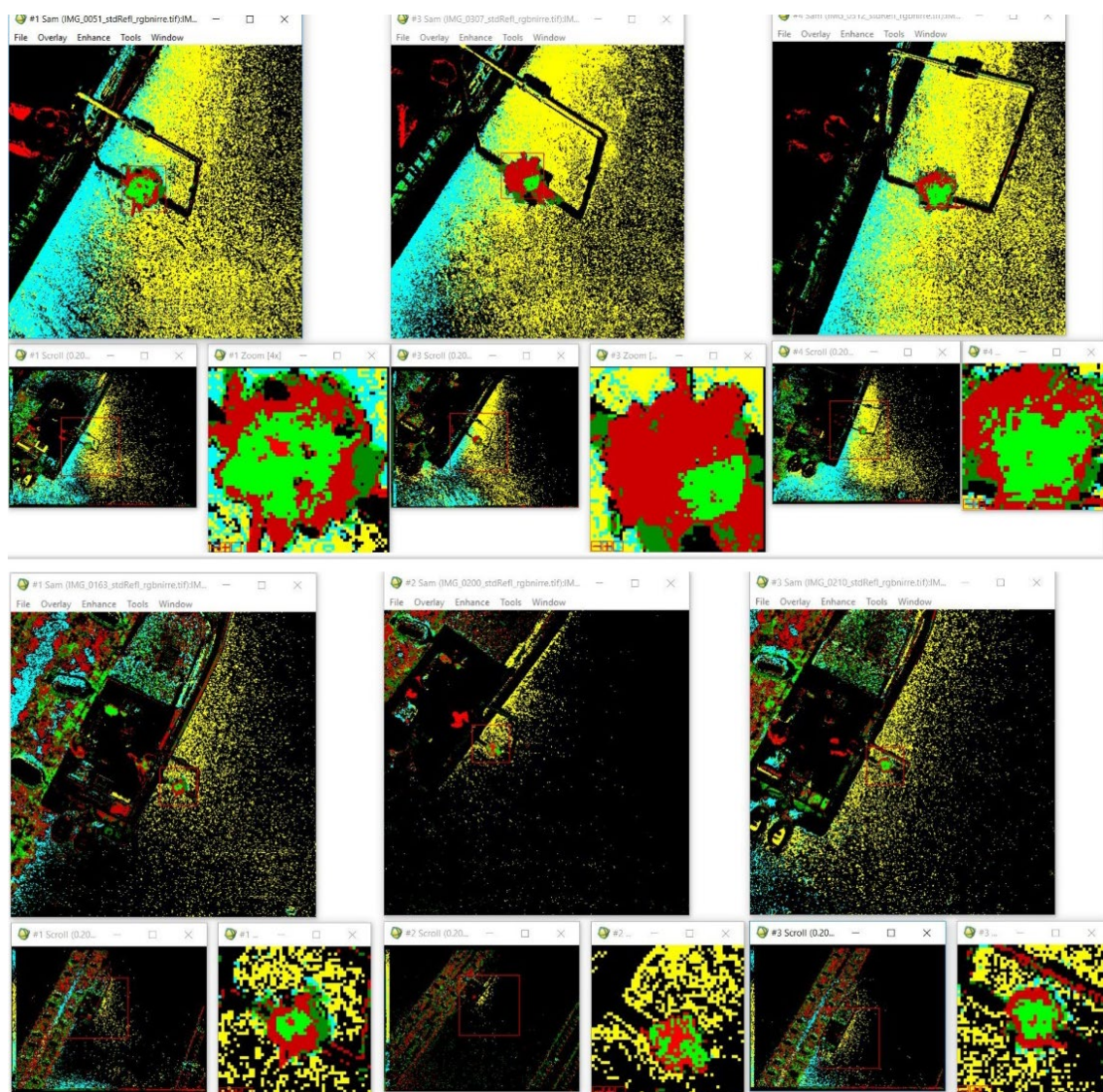


Figure C-11: Classification of *E. radiata* at 10cm water depth from images captured at FH of 10m (top set of 9 images) and FH of 30m (bottom set of 9 images). Shades of red represent *U. pinnatifida* and shades of green represent *E. radiata* at depths between 10cm – 1m. *E. radiata* at depths 1.5m and 2m is represented in cyan and *U. pinnatifida* at depths 1.5m and 2m are represented in yellow.

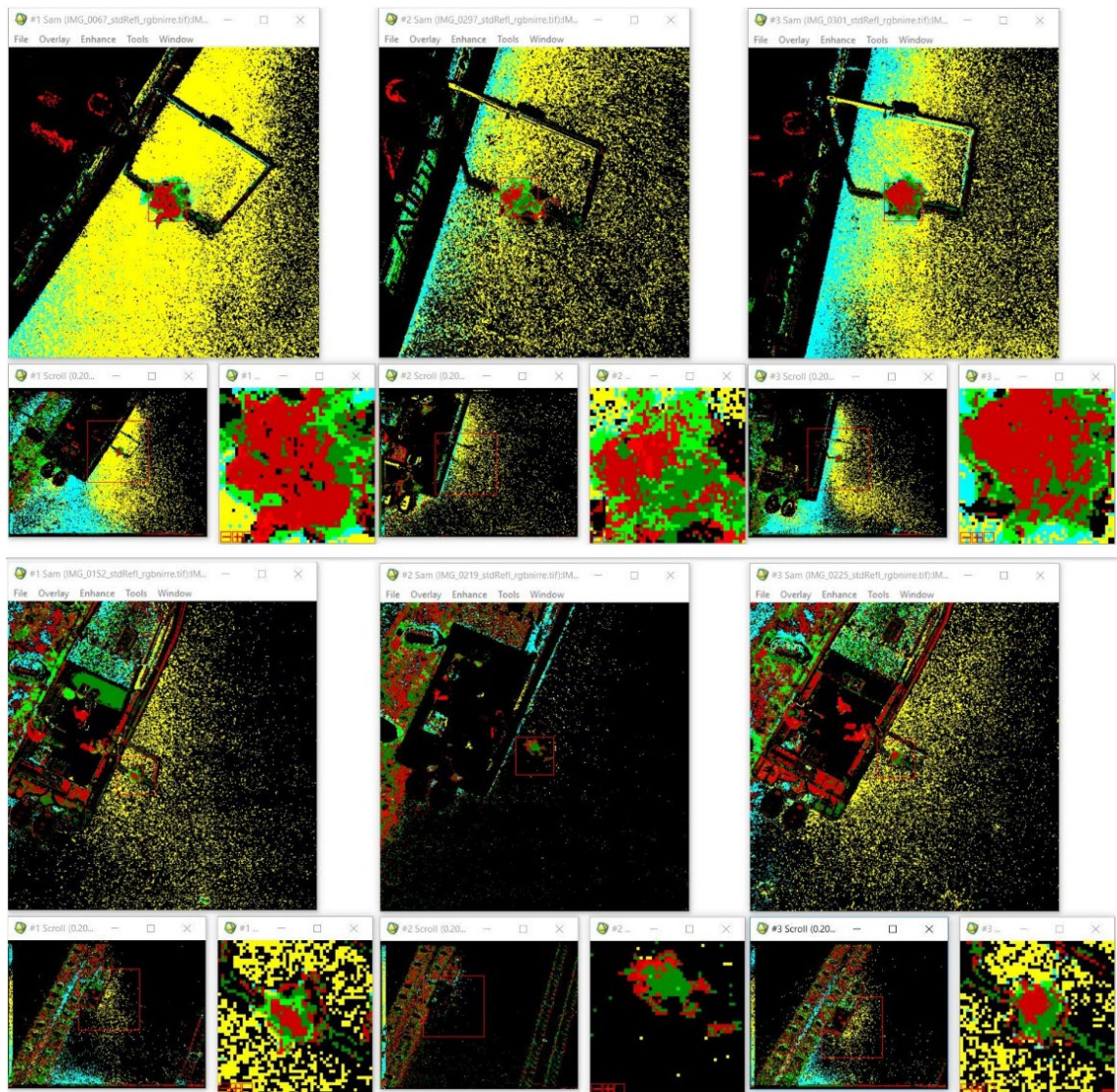


Figure C-12: Classification of *E. radiata* at 50cm water depth from images captured at FH of 10m (top set of 9 images) and FH of 30m (bottom set of 9 images). Shades of red represent *U. pinnatifida* and shades of green represent *E. radiata* at depths between 10cm – 1m. *E. radiata* at depths 1.5m and 2m is represented in cyan and *U. pinnatifida* at depths 1.5m and 2m are represented in yellow.

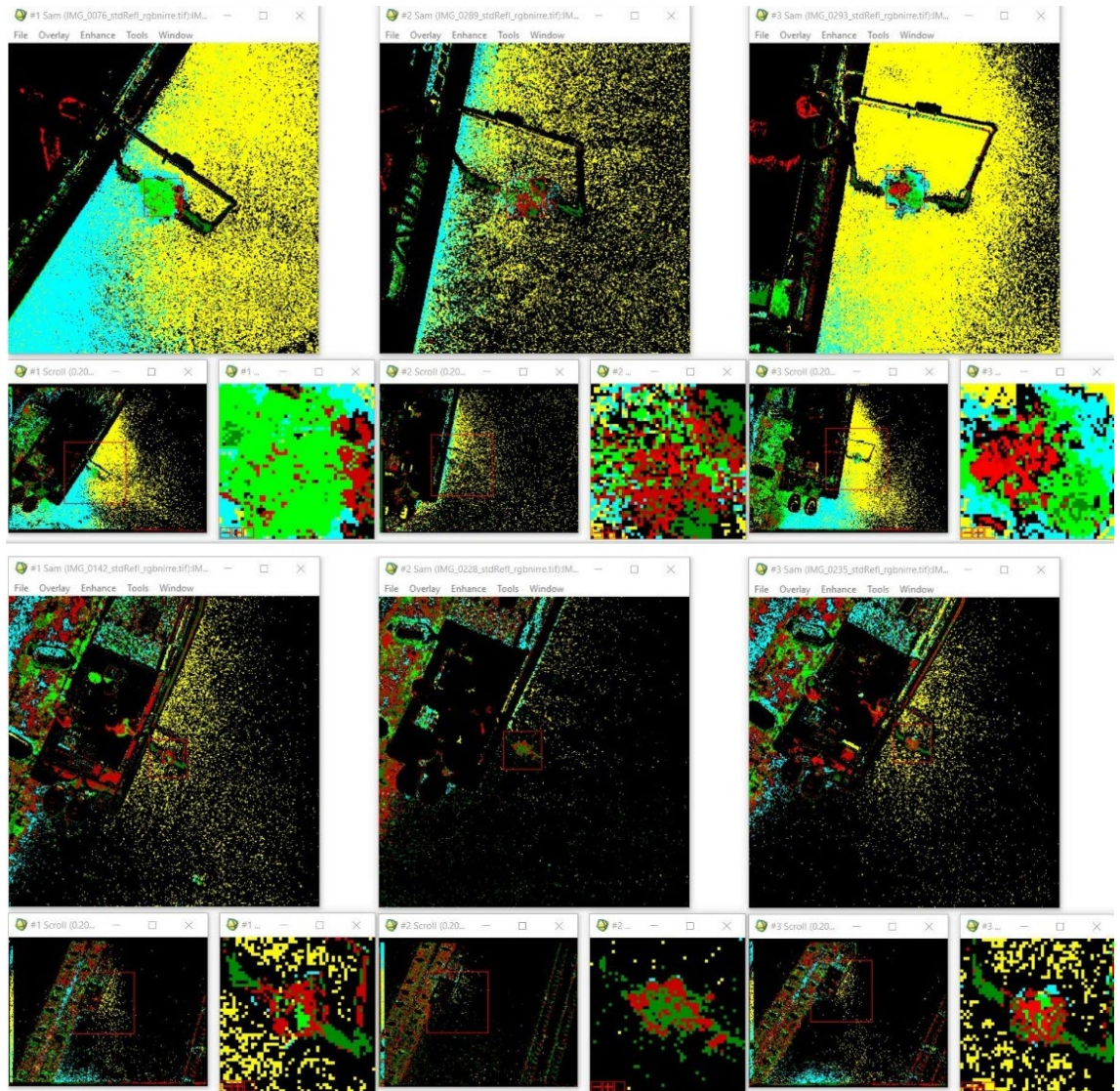


Figure C-13: Classification of *E. radiata* at 1m water depth from images captured at FH of 10m (top set of 9 images) and FH of 30m (bottom set of 9 images). Shades of red represent *U. pinnatifida* and shades of green represent *E. radiata* at depths between 10cm, 50cm and 1m. *E. radiata* at depths 1.5m and 2m is represented in cyan and *U. pinnatifida* at depths 1.5m and 2m are represented in yellow.

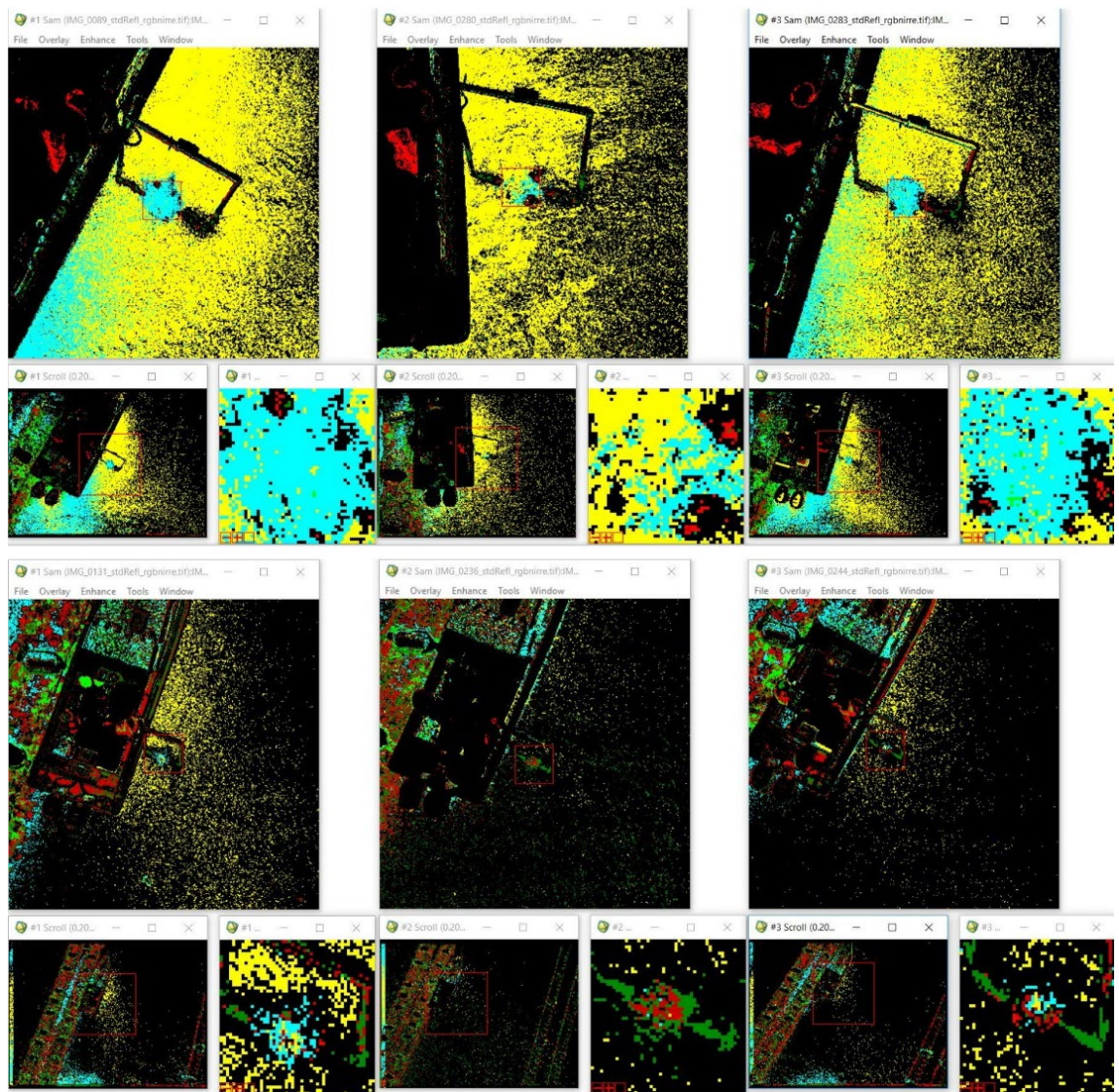


Figure C-14: Classification of *E. radiata* at 1.5m water depth from images captured at FH of 10m (top set of 9 images) and FH of 30m (bottom set of 9 images). Shades of red represent *U. pinnatifida* and shades of green represent *E. radiata* at depths between 10cm, 50cm and 1m. *E. radiata* at depths 1.5m and 2m is represented in cyan and *U. pinnatifida* at depths 1.5m and 2m are represented in yellow.

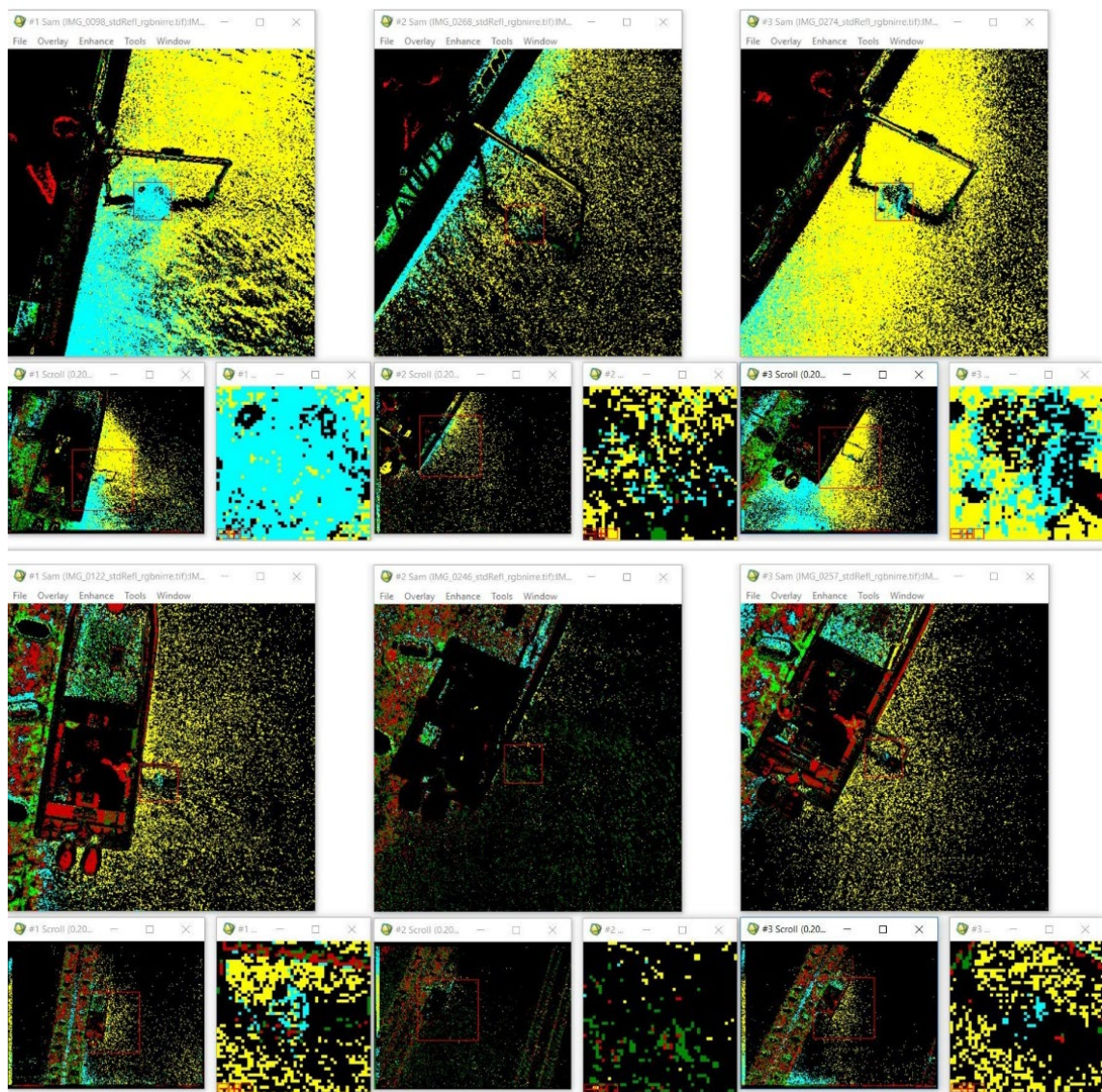


Figure C-15: Classification of *E. radiata* at 2m water depth from images captured at FH of 10m (top set of 9 images) and FH of 30m (bottom set of 9 images). Shades of red represent *U. pinnatifida* and shades of green represent *E. radiata* at depths between 10cm, 50cm and 1m. *E. radiata* at depths 1.5m and 2m is represented in cyan and *U. pinnatifida* at depths 1.5m and 2m are represented in yellow.

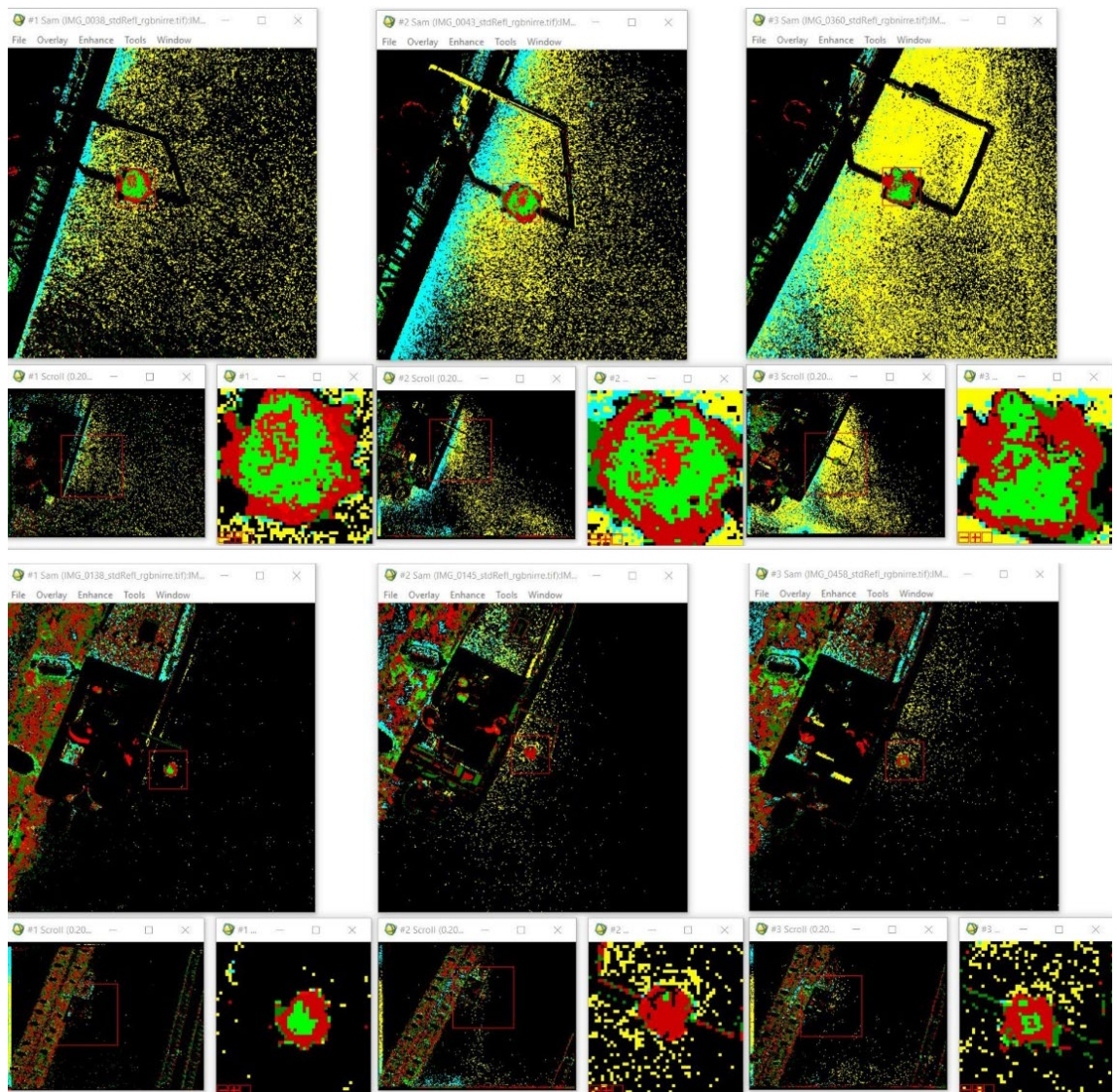


Figure C-16: Classification of *U. pinnatifida* at 10cm water depth from images captured at FH of 10m (top set of 9 images) and FH of 30m (bottom set of 9 images). Shades of red represent *U. pinnatifida* and shades of green represent *E. radiata* at depths between 10cm, 50cm and 1m. *E. radiata* at depths 1.5m and 2m is represented in cyan and *U. pinnatifida* at depths 1.5m and 2m are represented in yellow.

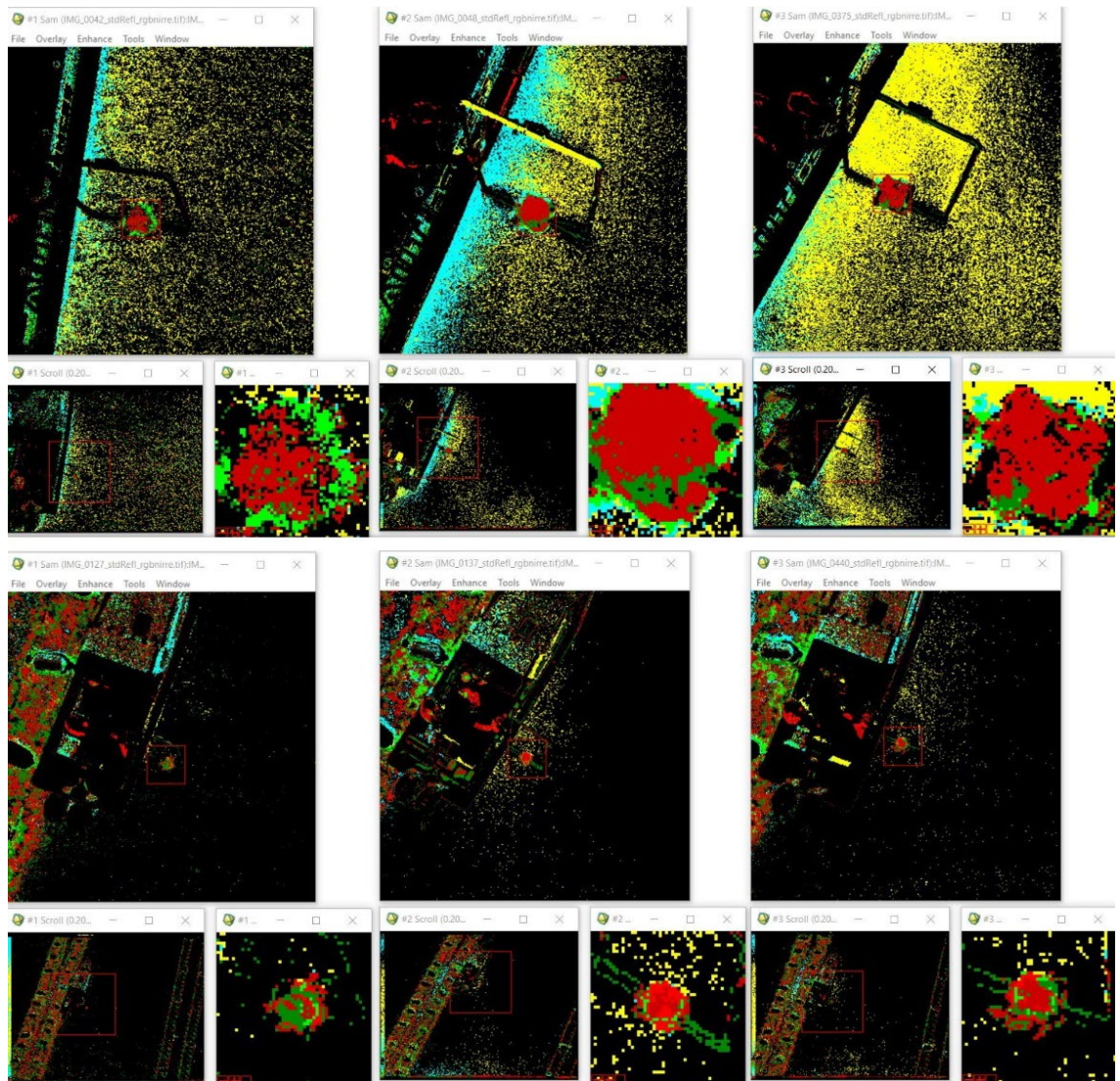


Figure C-17: Classification of *U. pinnatifida* at 50cm water depth from images captured at FH of 10m (top set of 9 images) and FH of 30m (bottom set of 9 images). Shades of red represent *U. pinnatifida* and shades of green represent *E. radiata* at depths between 10cm, 50cm and 1m. *E. radiata* at depths 1.5m and 2m is represented in cyan and *U. pinnatifida* at depths 1.5m and 2m are represented in yellow.

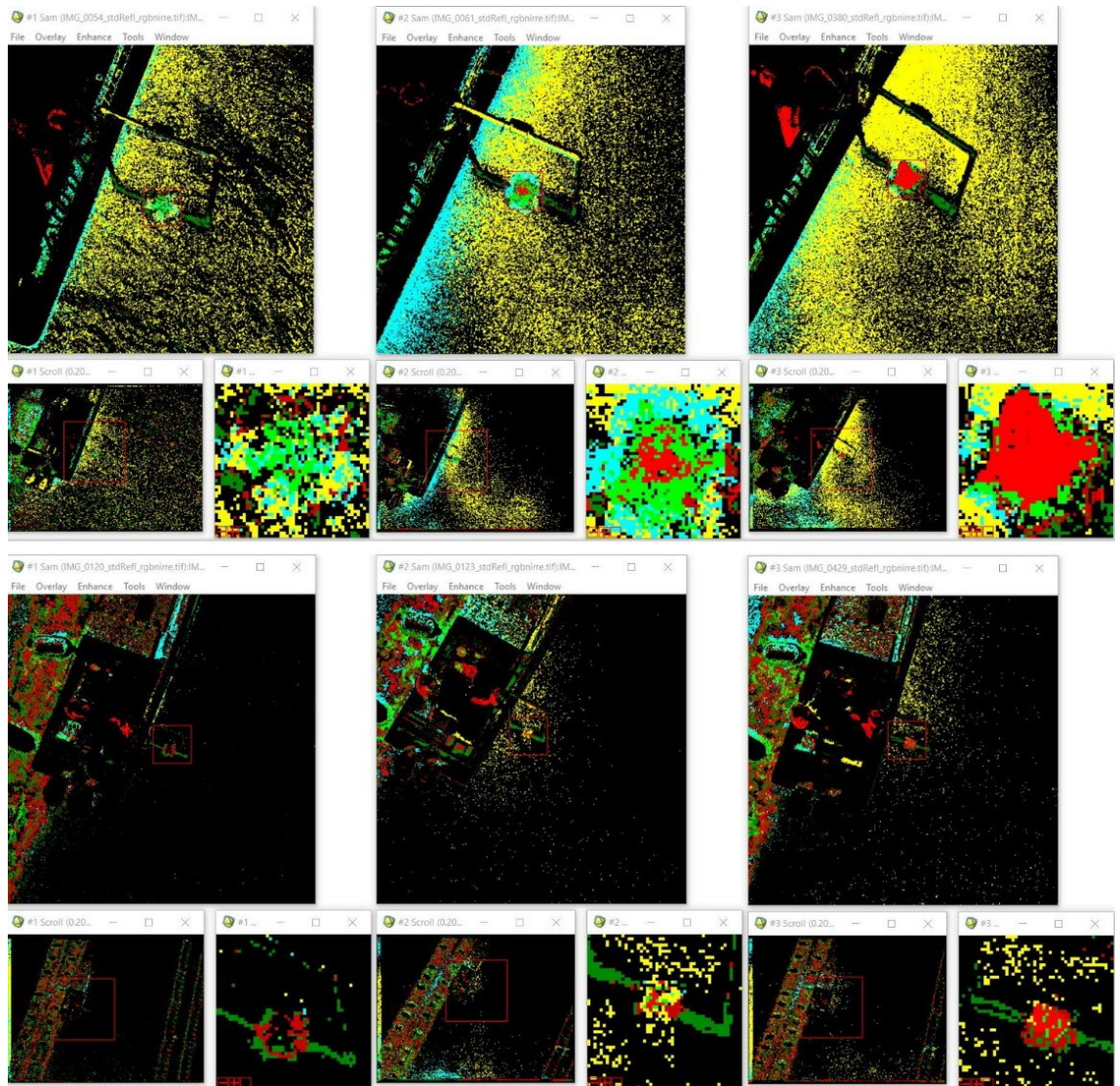


Figure C-18: Classification of *U. pinnatifida* at 1m water depth from images captured at FH of 10m (top set of 9 images) and FH of 30m (bottom set of 9 images). Shades of red represent *U. pinnatifida* and shades of green represent *E. radiata* at depths between 10cm, 50cm and 1m. *E. radiata* at depths 1.5m and 2m is represented in cyan and *U. pinnatifida* at depths 1.5m and 2m are represented in yellow.

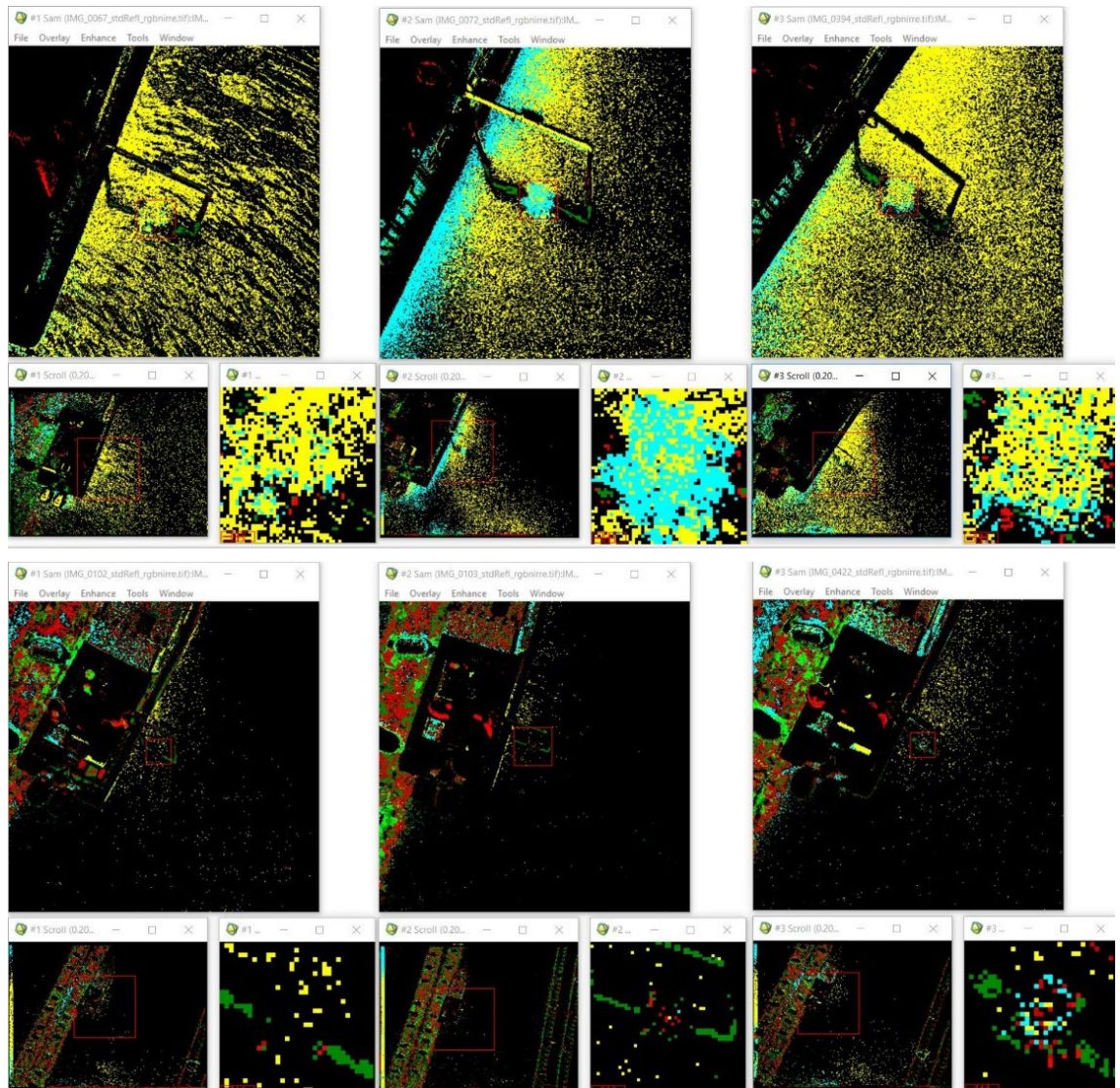


Figure C-19: Classification of *U. pinnatifida* at 1.5m water depth from images captured at FH of 10m (top set of 9 images) and FH of 30m (bottom set of 9 images). Shades of red represent *U. pinnatifida* and shades of green represent *E. radiata* at depths between 10cm, 50cm and 1m. *E. radiata* at depths 1.5m and 2m is represented in cyan and *U. pinnatifida* at depths 1.5m and 2m are represented in yellow.

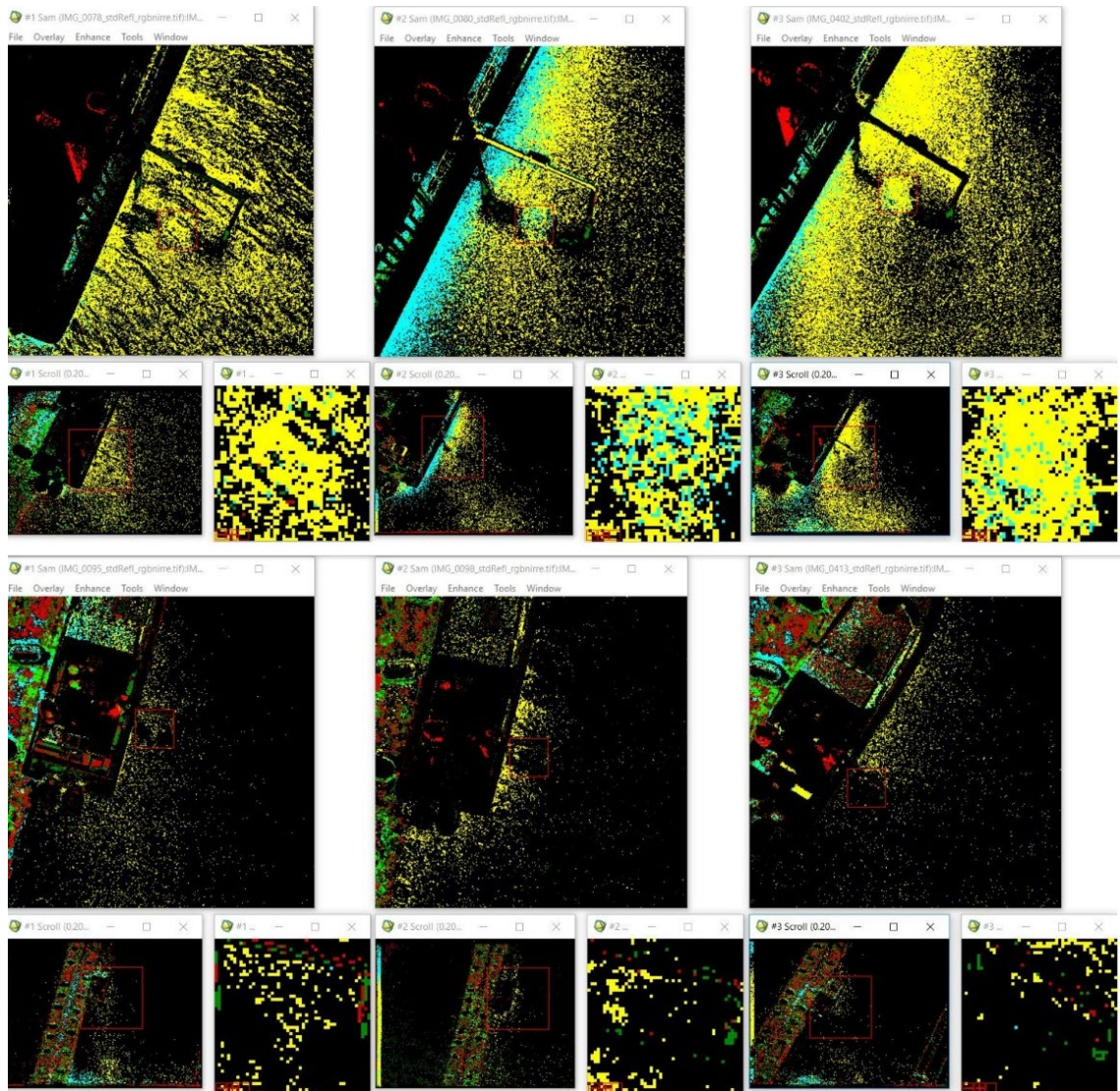


Figure C-20: Classification of *U. pinnatifida* at 2m water depth from images captured at FH of 10m (top set of 9 images) and FH of 30m (bottom set of 9 images). Shades of red represent *U. pinnatifida* and shades of green represent *E. radiata* at depths between 10cm, 50cm and 1m. *E. radiata* at depths 1.5m and 2m is represented in cyan and *U. pinnatifida* at depths 1.5m and 2m are represented in yellow.

Flowline developed for UAV Rededge-M image processing and direct georeferencing of single images can be downloaded from GitHub: <https://github.com/sadsel-AUT/Chapter4-UAV-imageprocessing-directgeoreferencing.git>.